CR 114514

AVAILABLE TO PUBLIC

STUDY TO ADAPT SOLAR ELECTRIC PROPULSION TO THE PIONEER F and G SPACECRAFT

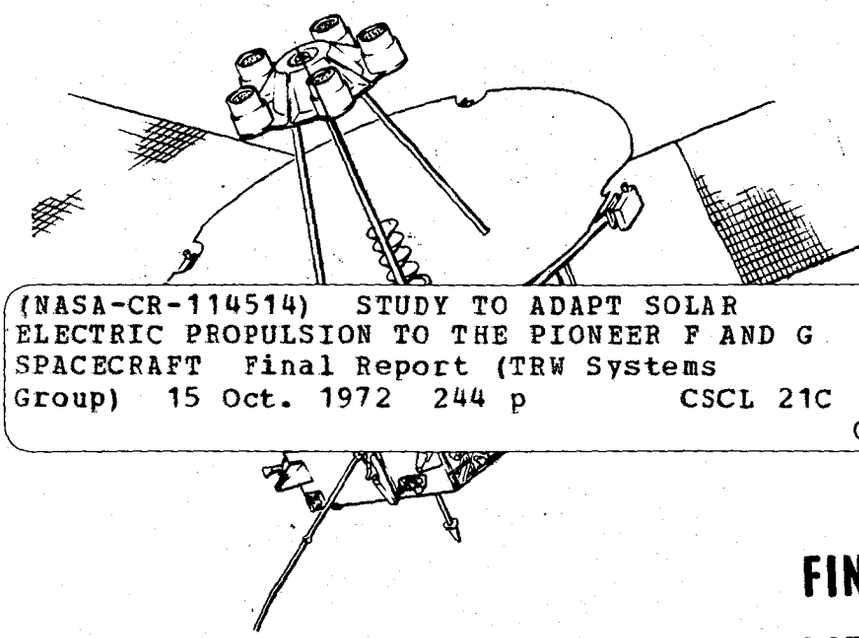

(NASA-CR-114514) STUDY TO ADAPT SOLAR ELECTRIC PROPULSION TO THE PIONEER F AND G SPACECRAFT Final Report (TRW Systems Group) 15 Oct. 1972 244 p CSCL 21C

N73-11798

Unclas

G3/28 46899

FINAL REPORT

OCTOBER 15, 1972

TRW SYSTEMS GROUP

244

STUDY TO ADAPT SOLAR ELECTRIC PROPULSION TO THE PIONEER F and G SPACECRAFT

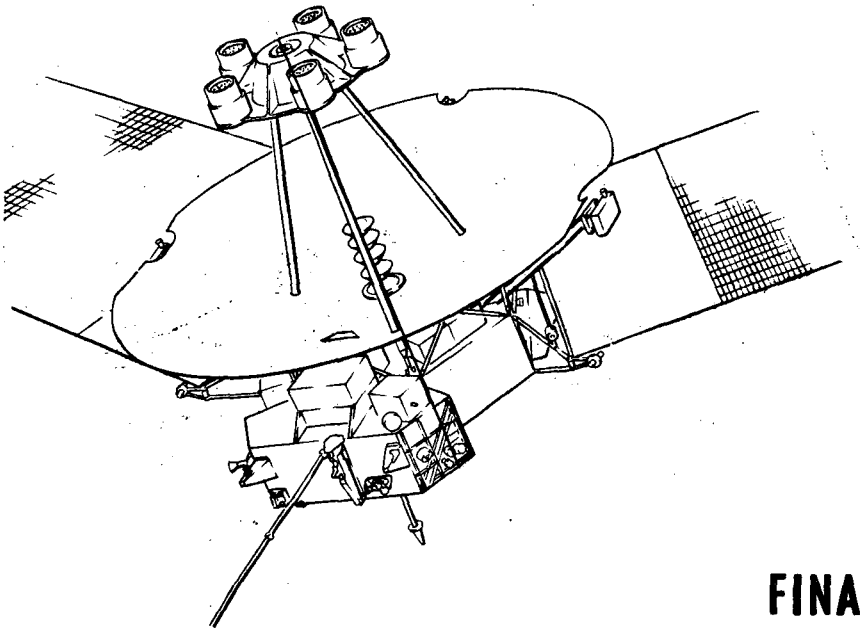

FINAL REPORT

OCTOBER 15, 1972

TRW
SYSTEMS GROUP
Redondo Beach, Calif.

22125-6001-R0-00

STUDY TO ADAPT SOLAR ELECTRIC PROPULSION TO THE PIONEER F AND G SPACECRAFT

FINAL REPORT

OCTOBER 15, 1972

Prepared for NASA/AMES RESEARCH CENTER
under Contract NAS2-6796

TRW
SYSTEMS GROUP

C

CONTENTS

CONTENTS (CONTINUED)

ILLUSTRATIONS

ILLUSTRATIONS (CONTINUED)

ILLUSTRATIONS (CONTINUED)

ILLUSTRATIONS (CONTINUED)

ILLUSTRATIONS (CONTINUED)

ILLUSTRATIONS (CONTINUED)

TABLES

TABLES (CONTINUED)

ABBREVIATIONS

ACS	Attitude control subsystem
ARC	Ames Research Center
A/C/T	Atlas Centaur TE-364-4
AU	Astronomical unit
bps	Bits per second
CDU	Command distribution unit
CEA	Control electronics assembly
cg	Center of gravity
CSP	Conscan signal processor
CTRF	Central transformer rectifier filter
DDU	Digital decoder unit
DSA	Despin sensor assembly
DSN	Deep Space Network
DSU	Data storage unit
DTU	Digital telemetry unit
GFE	Government furnished equipment
IR	Infrared
I_{sp}	Specific impulse
PCU	Power control unit
PPU	Power processing unit
RTG	Radioisotope thermoelectric generator
SAS	Solar aspect sensor
SCT	Spin control thruster
SEP	Solar electric propulsion
SPSG	Spin period sector generator
SRA	Stellar reference assembly
SSA	Sun sensor assembly
TCA	Thruster cluster assembly
T/C/T	Titan Centaur TE-364-4
TRF	Transformer rectifier filter
TWT	Traveling wave tube
TWTA	Traveling wave tube assembly
UV	Ultraviolet
XYZ	Spacecraft body axes

ABSTRACT

This study by TRW Systems under the direction of NASA/Ames Research center has shown that the addition of an electric thrust subsystem to the spin-stabilized Pioneer F and G spacecraft will substantially improve performance capability for certain missions. The evaluation was performed for the Atlas and Titan launch vehicles with Centaur and TE-364-4 stages and for electric thrust stages of 8- and 5-kw with three 30- and five 15-cm thrusters respectively.

The combination of a spinning spacecraft with electric propulsion is a concept only recently evaluated and the penalty from spinning over three-axis stabilized is not as significant as might initally be thought. Indeed there are major gains in weight, cost, and reliability, the disadvantages being lower data rate during the thrust phase and less efficient pointing.

A variety of missions were evaluated from a solar approach mission into 0.14 AU to a flyby mission of Neptune at approximately 30 AU. Performance improvements were present for all missions evaluated. The most significant improvement was for a rendezvous of the comet Tempel II. In fact, there is no other way to perform such a rendezvous mission. Electric propulsion is particularly performance-effective in missions when a major spacecraft maneuver must be performed without the assistance of a large local gravity well. The second most attractive mission was for a Jupiter swingby to out of the ecliptic. For this mission the performance improvement went from 32 to 92 degrees using the Atlas/Centaur/TE-364-4. However, an offloaded Titan/Centaur/TE-364-4 would also allow solar polar passages without electric propulsion augmentation, thereby reducing considerably the probability that this, as an electric propulsion mission, will have high priority.

The necessary hardware to augment the Pioneer spacecraft with electric propulsion was evaluated and satisfactory solutions were found with the exception of providing adequate thermal control for missions approaching closer than 0.7 AU to the sun. These evaluations included the medium-gain off-axis antenna, centrifugally deployed solar arrays, thrust vector pointing sensor, terminal guidance sensor and accommodation of all electric propulsion components.

1. INTRODUCTION AND SUMMARY

1.1 STUDY GROUND RULES AND METHODS

The ARC/TRW study approach has been to investigate the feasibility of augmenting a Pioneer spin-stabilized spacecraft with electric propulsion capability. Three spacecraft configurations and their associated missions have been evaluated individually and in the order shown in the table below.

Environment	Missions
1 to 5 AU	Asteroid Flyby and Comet Rendezvous
	Asteroid Belt Mapper
	Out-of-Ecliptic (Jupiter Swingby)
1 to 30 AU	Saturn, Uranus and Neptune Direct Flybys
1 to ≤0.7 AU	Direct Solar Approach

Each configuration evaluation started with the basic Pioneer F and G spacecraft and minimum necessary modifications have been defined to allow operation in the environment shown. Key considerations in the approach include:

a) Use flight-proven Pioneer F and G structure and subsystems with minimum modification.

b) Use Pioneer F and G science payload as practical for each specific mission.

c) Size the electric power and electric propulsion subsystems to augment boosters. In particular, evaluate a 5-kw solar array with 15-cm thrusters and an 8-kw solar array with 30-cm thrusters.

d) Trade off all missions against two boosters – Atlas/Centaur with a third stage, and the Titan/Centaur with a third stage.

e) Minimize burn time of electric propulsion to reduce development and verification test cost.

f) Evaluate potential electric propulsion byproduct interaction with the spacecraft and science payload, and design to reduce or remove the effects of any problems that arise.

g) Address the thrust vector pointing problems for all missions and the terminal guidance problems involved in asteroid flyby and comet rendezvous, and design an appropriate attitude control system.

h) Design, fabricate and test an off-axis medium-gain antenna for earth coverage during electric propulsion thrusting.

i) Design a centrifugally deployed solar array and compare with previously developed and tested solar array hardware.

An external view of the Pioneer F and G spacecraft is presented in Figure 1-1. The spacecraft is stabilized by spinning about an axis parallel to the high-gain antenna. Four radioisotope thermoelectric generators (RTG's) and the magnetometer science instrument are deployed as three equally-spaced masses in a plane perpendicular to the spin axis. Other external features of the spacecraft include several other scientific instrument sensors, a medium-gain horn antenna forward of the high-gain antenna feed and directed forward, and a low-gain antenna aft of the equipment compartment directed aft. One-pound hydrazine thruster assemblies are located 180 degrees apart at the rim of the dish and are used for velocity correction, precession, and spin control maneuvers. External attitude control subsystem includes a sun sensor mounted near one of the thruster assemblies, and the stellar reference assembly with its external light shield.

The general technical approach included incorporation onto the Pioneer F and G spacecraft of deployable solar arrays, thrusters, power processing units, and an off-axis medium-gain antenna. Placement of the thrusters was evaluated in considerable detail to assure minimum effects to experiments, antennas, and solar array by mercury and molybdenum by-products. Minimum modifications to Pioneer F and G suggested retention of the RTG's and addition of the solar array mounted opposite one another below the RTG plane, as shown in Figure 1-2 for the 1 to 30 AU missions. The inbound and 1 to 5 AU missions allowed removal and replacement of the RTG's by the solar array, thereby allowing 120-degree separation of the solar arrays and improved viewing for the experiments. This configuration is shown in Figure 1-3.

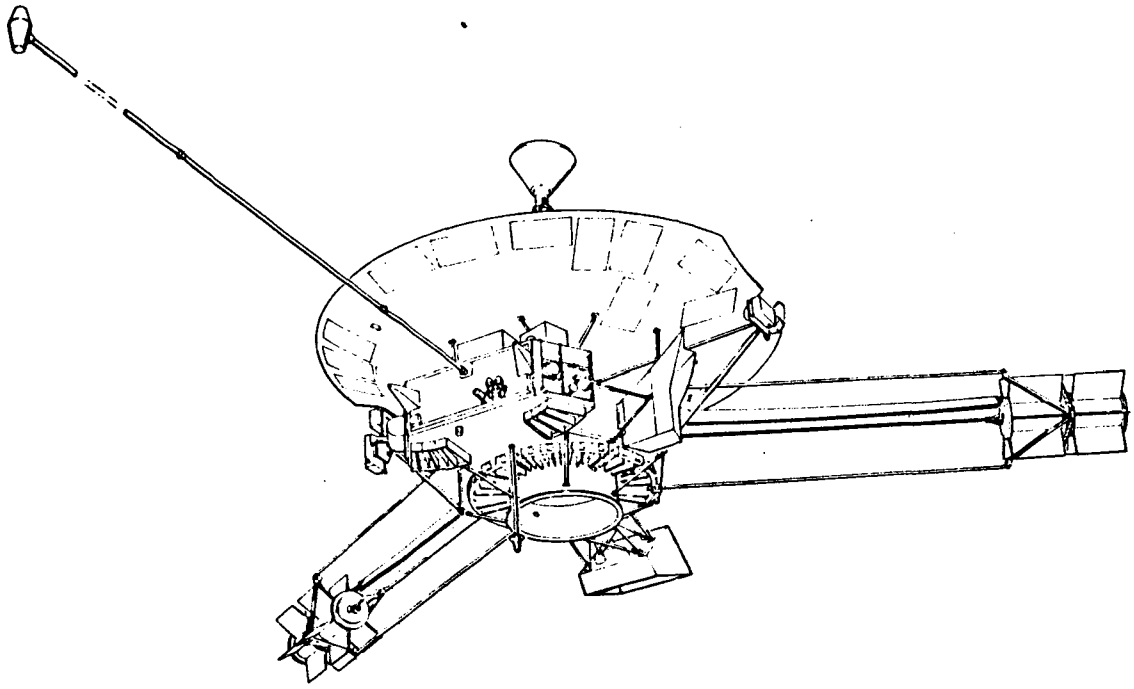

Figure 1-1. Pioneer F and G Spacecraft

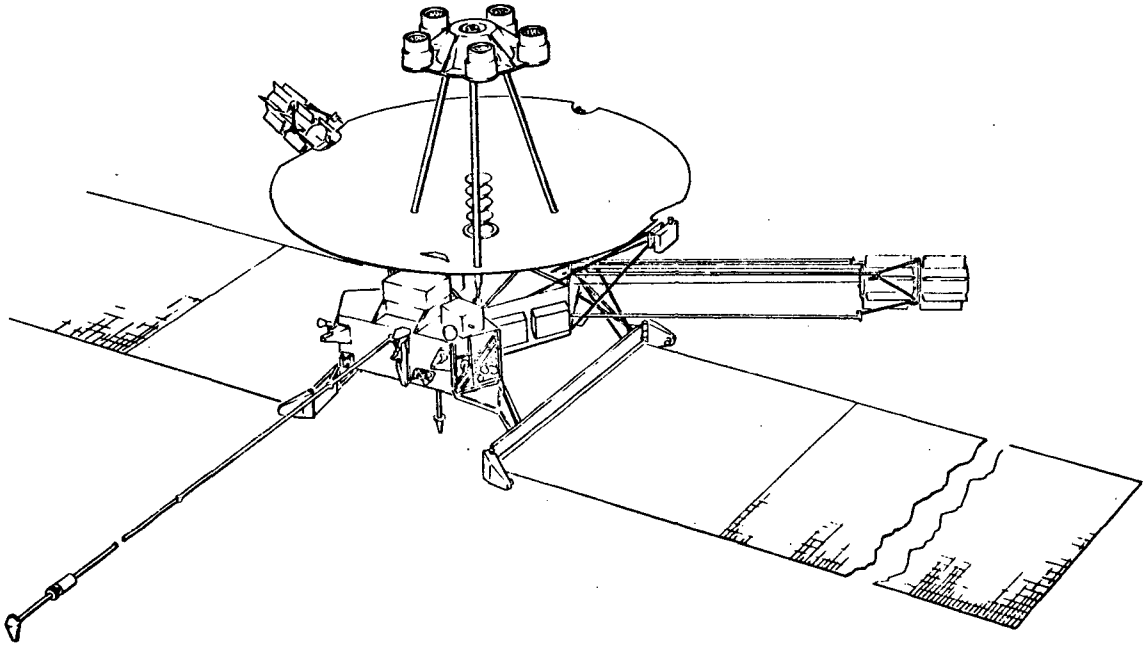

Figure 1-2. Configuration for 1 to 30 AU Missions: 5-kw Array, Five 15-cm Electric Thrusters

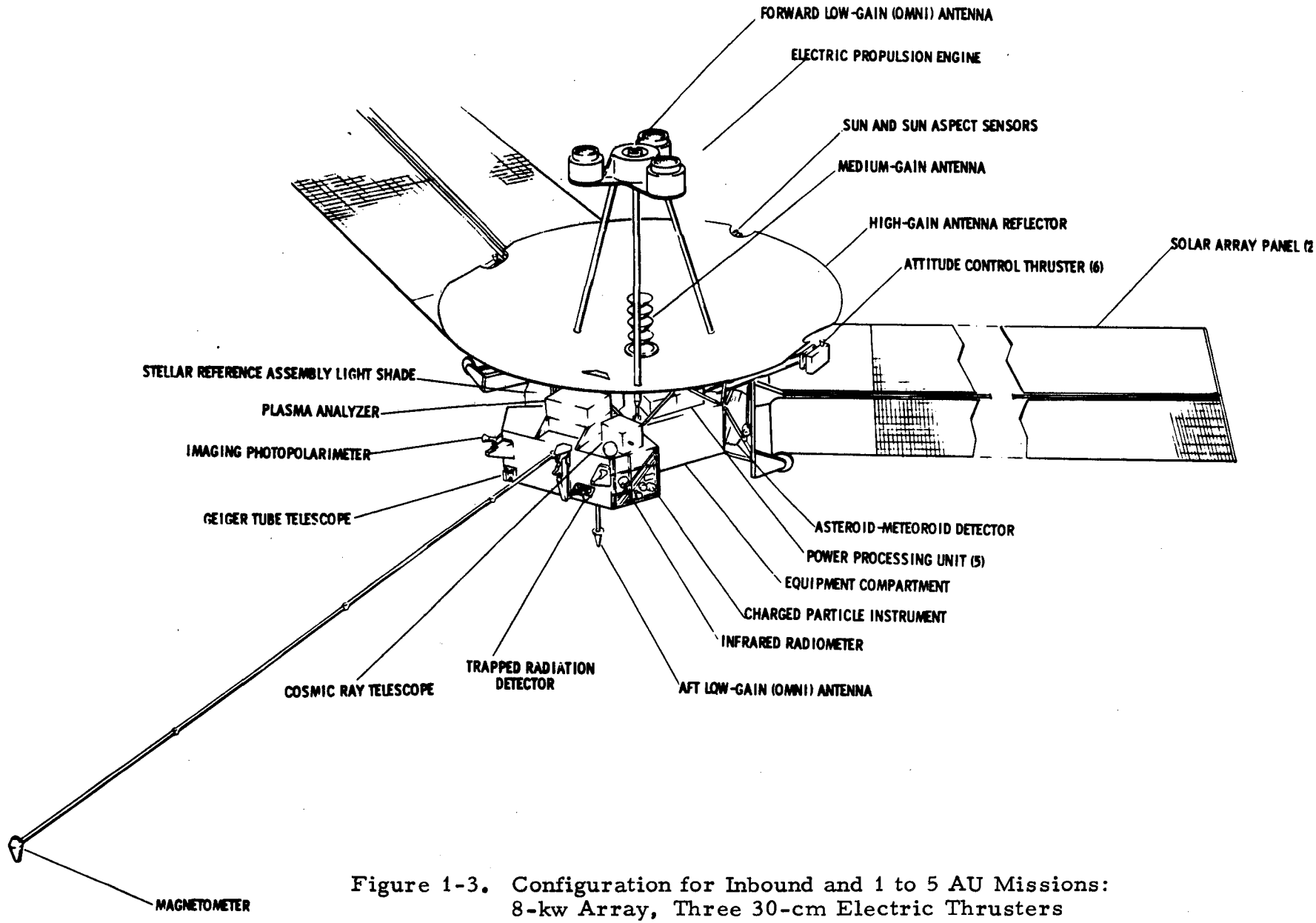

Figure 1-3. Configuration for Inbound and 1 to 5 AU Missions: 8-kw Array, Three 30-cm Electric Thrusters

Figure 1-2 (1 to 30 AU missions) shows a 5-kw solar array with five 15-cm thrusters, and Figure 1-3 (inbound and 1 to 5 AU missions) shows an 8-kw array with three 30-cm thrusters. Either version would be acceptable for all missions and are shown only to illustrate the accommodation of either size system.

In parallel with the general configuration evaluation, all three of the missions were analyzed to determine whether electric propulsion would improve spacecraft performance sufficiently for each mission to justify its incorporation in the spacecraft design. Another consideration was the effect on mission performance of using 30-cm rather than 15-cm thrusters and 85- by 6-foot instead of 53- by 6-foot solar panels.

As the mission analyses and configuration designs were being developed, fabrication and test of the medium-gain off-axis antenna and design definition for the centrifugally deployed array were in progress. Both of these designs were new and, while optimization was not possible within the scope of this contract, sufficient evaluation and development were accomplished to prove feasibility. During this and the previous study* solutions were also found to the thrust vector pointing problem for all missions and to the terminal guidance problem for asteroid flyby and comet rendezvous missions. A detailed discussion of the antenna and solar array designs and the method and accuracy of thrust vector pointing and terminal guidance is found in Section 5.

1.2 BASIC SPINNER CONCEPT

1.2.1 Description

There are two methods of stabilizing unmanned spacecraft, either three-axis or spin. Inclusion of electric propulsion complicates the design of both of these types of spacecraft by adding the requirement for thrust vector pointing. The three-axis stabilized version thrusts with the sun-spacecraft line perpendicular to the solar array and ends up with a gimballed antenna, gimballed solar arrays and gimballed or

*TRW Final Report, "Feasibility Study for a Multi-Mission Electric Propulsion Spacecraft," NASA/ARC Contract NAS2-6287, June 1971.

gimballed/translatable electric propulsion thrusters. The spin-stabilized vehicle thrusts along the spin axis, with the sun-spacecraft line 45 degrees to the array and thereby requires a larger array or longer thrust times to compensate. In addition, for the spin-stabilized version, a special 360-degree off-axis pointing antenna must be provided during the thrust phase to keep the earth in view.

A visual description of the operation of the Pioneer spin-stabilized electric propulsion spacecraft is shown in Figure 1-4. The thrusters are mounted on the tripod over the high-gain antenna dish to remove all serious thruster by-product contamination effects. The special purpose thrust-phase antenna is mounted at the center of the 9-foot parabolic dish to allow 360-degree off-axis viewing free of thruster by-product contaminants. The basic outbound mission is carried out in two phases. The first is an electric propulsion thrust phase of about 180 days. Note that the spin axis is along the thrust vector and the solar array is 45 degrees to the sun line. The second phase is the coast and/or intercept phase after the thrusters are shut down and the spacecraft has been reoriented to operate in the same manner as Pioneer 10,* from the on-axis high-gain antenna system.

Figure 1-5 shows the general pointing and maneuver requirements necessary during the thrust phase using the actual angles established for the Jupiter swingby to out-of-the-ecliptic mission. Following launch, the spacecraft is aligned with earth using the onboard sequencer. After initial checkout of all equipment and experiments, a reorientation is performed using either a star mapper or a sun aspect sensor (not currently available on Pioneer). This maneuver places the solar array at 45 degrees to the sun line and the thrust vector within a few degrees of optimum pointing. Electric propulsion thrusters are turned on and properly throttled and sequenced to utilize available solar energy. At approximately 80 days from launch, the omni will be reaching the limit of its capability and will be switched out. The fan beam will be in view of

*Pioneer F has been called Pioneer 10 since its successful launch in February of 1972.

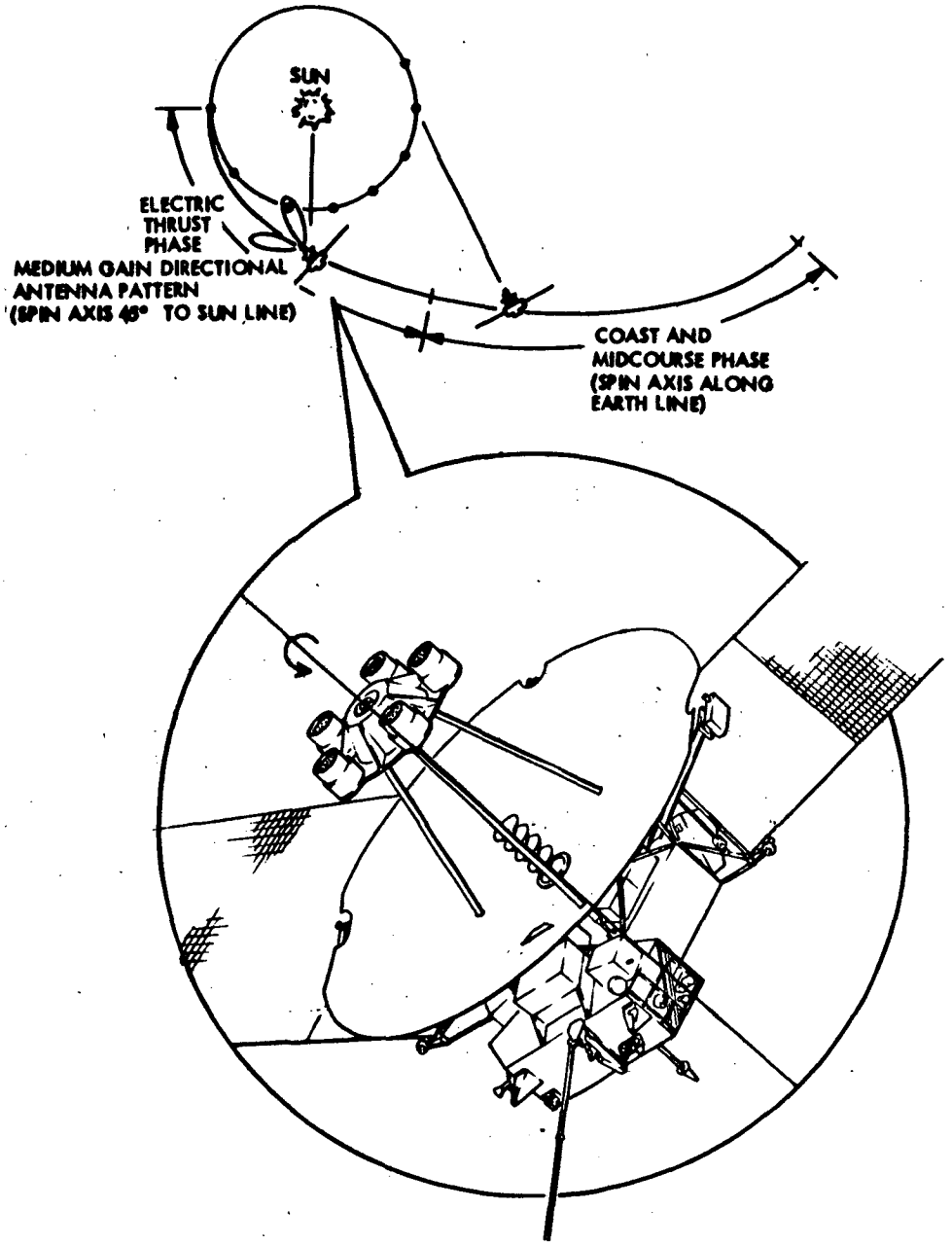

Figure 1-4. Operational Sequence

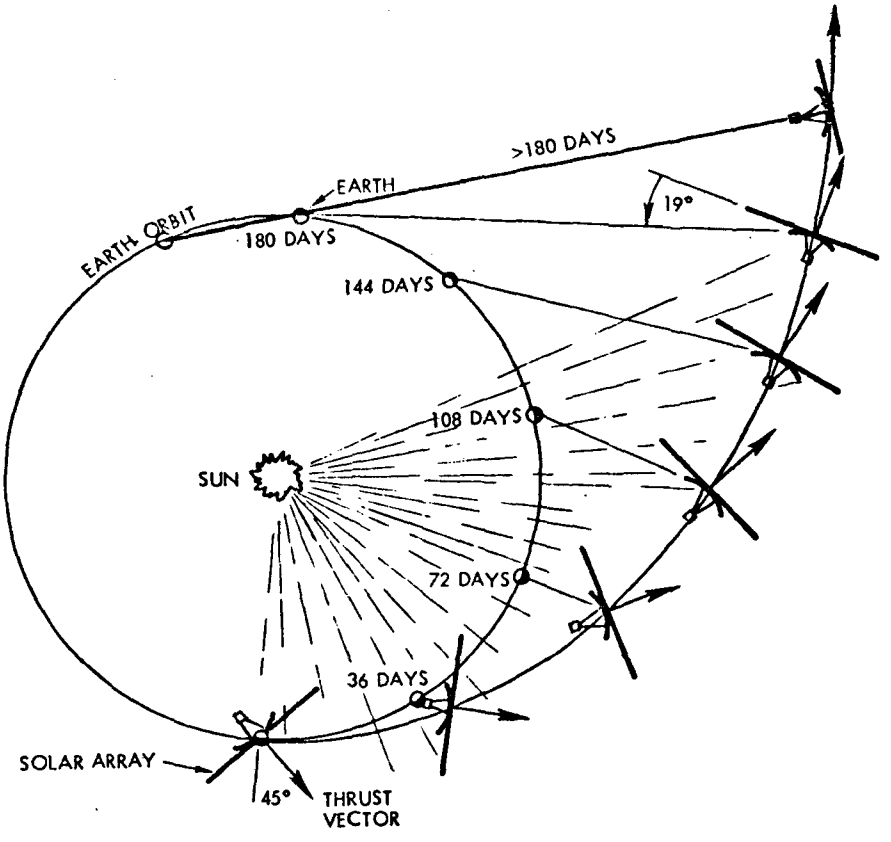

Figure 1-5. Pointing Maneuver Requirements

the earth and will be switched in. At approximately 180 days, using the sun aspect sensor as a reference, the spacecraft is reoriented to operate off the Pioneer 10 high-gain antenna, using conical scan for earth pointing. Following several days of tracking, a small midcourse maneuver may be included in the flight operations sequence to compensate for pointing errors.

1.2.2 Comparison with Three-Axis Stabilized Spacecraft

A representative three-axis stabilized spacecraft configuration, with design features required for the Encke rendezvous mission, is shown in Figure 1-6. This configuration was developed during the JPL/TRW Study of a Comet Rendezvous Mission.*

*Study of a Comet Rendezvous Mission, Contract No. 953247, 12 May 1972.

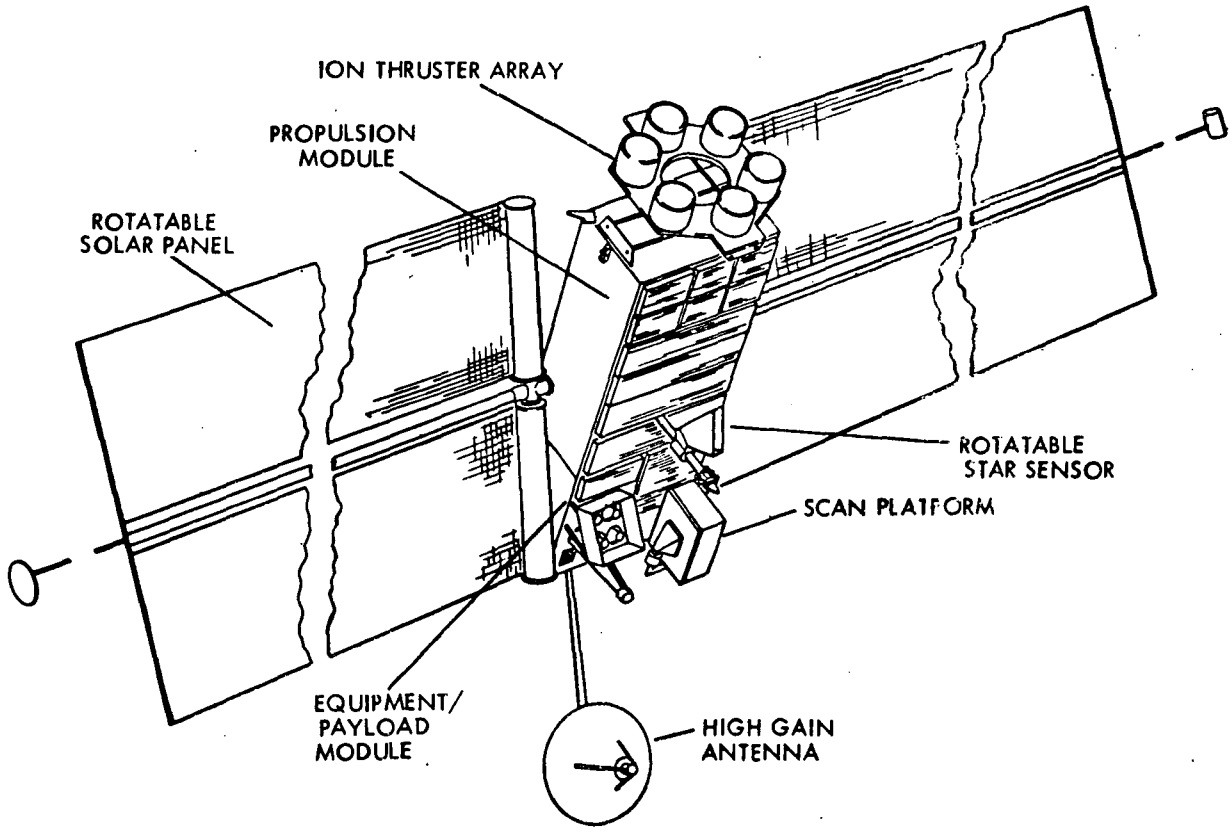

Figure 1-6. Three-Axis Stabilized Spacecraft in Cruise Configuration

The vehicle consists of a flat oblong center body and two boom-deployed solar arrays. The center body is separated into two modules: the electric propulsion module with an articulated array of six growth version 30-cm mercury ion thrusters, power processors, propellant storage and feed system. The entire structure consists of open trusswork for the large overall dimensions of the center body (about 12 by 6 by 3 feet). A 6-foot diameter high-gain antenna is mounted on a deployment arm that is hinged to the bottom of the equipment module. This biaxially rotatable antenna is stowed against the vehicle body during launch. After deployment it can be pointed in all directions in front and rear of the center body for an unobstructed view of earth.

The vehicle's three-axis stabilization system requires the sun and a selected reference star as celestial references. Attitude control functions are performed during thrust periods by the articulated ion engines and

during coast periods by hydrazine thrusters. The hydrazine thrusters are also used during the electric thrust phase (a) to control large attitude excursions and (b) to provide third-axis control capability when only one ion thruster is operating.

The two solar arrays use the motor driven boom rollout deployment principle. A single boom serves as deployment actuator and support structure for each panel. The solar arrays with a deployed length and width of 67.2 by 13.8 feet for each panel generates 17.5 kw of gross power at earth departure.

The solar array panels can be rotated up to ±90 degrees from an orientation parallel to the center body to permit optimal thrust vector pointing relative to the sun line; unconstrained terminal guidance and other maneuvers in the vicinity of the target, and controlled sun exposure at solar distances below 0.68 AU. Out-of-plane thrust vector pointing is achieved by rotating the entire vehicle around the sun line. Such roll maneuvers are facilitated by the one-axis rotatable star seeker mounted on the rear side of the vehicle. Rotation of the star seeker also permits selection and tracking of reference stars that are not obstructed by the solar panels. A double-gimballed scan platform attached to one corner of the payload module carries the TV image system and other optical sensors and spectrometers. This platform can be scanned over a wide range of azimuths and co-elevations without field-of-view obstruction.

The three-axis and spin-stabilized electric propulsion spacecraft have a number of common problems, namely:

a) Solar array stowage and deployment

b) Solar array dynamics

c) Thrust vector pointing

d) Antenna and solar array pointing

e) Experiment viewing

f) Experiment, solar array and antenna contamination.

Thrust vector, antenna, and solar array pointing problems on the three-axis stabilized spacecraft are handled by the added complexity

of gimballing. For the spinner, a special coverage antenna must be provided and a power penalty accepted from the solar array. However, an equivalent payload is achievable with either configuration since the spinning solar array off-optimum pointing weight penalty is cancelled by the three axis-stabilized thrust vector control mechanism weight.

The thrust vector control mechanism is required on a three-axis stabilized vehicle and not on a spin-stabilized vehicle. The reason is that shifts in the cg due to the use of consummables and the shutdown or failure of thrusters, causes thrust vector biases which cannot otherwise be removed. Since the spinner provides a continuous thrust vector couple about the spin axis, it is not similarly affected. Figure 1-7 is a picture of the only developed thrust vector control system; it uses three 20-cm thrusters which can be translated or gimballed. The weight quoted for such a device is 9 lb/kw, and since a flexible harness and mercury lines which translate up to 14 inches feed the thrusters, reliability must be considered a problem area.

Solar array stowage and deployment, either rollout or foldout, have been evaluated in considerable detail; however the dynamic interaction effects occurring during spacecraft maneuvers have previously not been considered in any depth. The problem is common to both spin and three-axis spacecraft and occurs during precession maneuvers. The solar array tends to retain its original position while the spacecraft precesses. This can be overcome in both cases with the incorporation of a damper and a hinged solar array.

There are a variety of potential contaminants in the ion exhaust beam that can act to degrade spacecraft performance if they deposit on critical spacecraft surfaces. Therefore, particular attention must be paid during the design of both the spin- or three-axis stabilized spacecraft so that neither primary or secondary particles can deposit on science windows, solar array, or antennas. An adjunct to this study is currently being performed at TRW on mercury ion bombardment thruster by-product distribution, magnetic cleanliness and RF interferences that

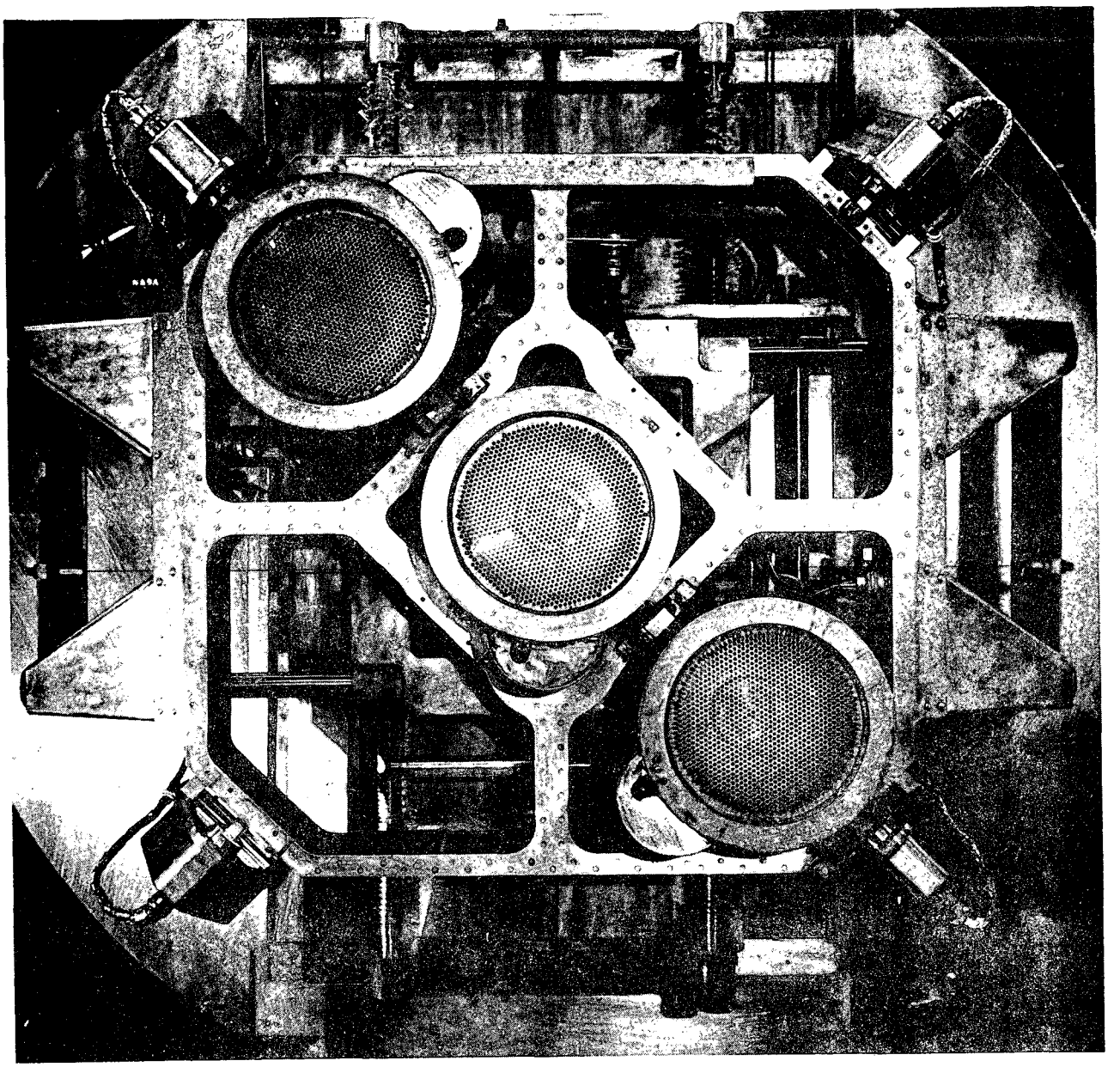

Figure 1-7. Translatable, Gimballed Ion Thruster Array

will be applicable to thruster positioning in the design of electric propulsion spacecraft. Thrusters and their power processing units are inherently magnetically dirty and must be cleaned up if a sensitive magnetometer instrument is to be placed within a reasonable distance, ≤30 feet.

General Electric, under NASA contract, has developed a 5-kw-driven rollout solar array and considerable testing has been performed independent of the effects of spacecraft motion. During this study a much lighter centrifugally deployed rollout array was evaluated theoretically but was rejected in favor of the General Electric version, primarily because of the difficulty in testing such a nonrigidized body.

1.3 ARRAY AND THRUSTER SIZING

The optimum propulsion system power level and burn time depends on the mission profile, booster type, net spacecraft mass, and thruster design parameters including overall efficiency, throttling range and specific impulse. The size and number of thrusters in turn is determined by the mission power level profile and reliability goal.

Five-, 15-, 20- and 30-cm thrusters have been built, currently the only extensive development effort resides with the 5- and 30-cm engines. The 5- and 30-cm engines are being developed for large three-axis stabilized spacecraft where the 5-cm would be used for precession maneuvers. Evaluation shows that three of the 30-cm engines can be accommodated on the Pioneer electric propulsion spacecraft and would be preferable for the rendezvous-type missions. Other missions evaluated indicated a preference based on reliability and performance for five 15-cm engines. The minimum number of thrusters required, exclusive of reliability considerations, is a function of the maximum available power and the thruster power rating. The maximum practical throttling range for these engines is 33 percent, that is, when the beam current reaches one-third of its maximum value.

A single 30-cm thruster requires 4020 watts at the array (assumes solar array 45 degrees to the sun line) and therefore the solar array must be sized in multiples of 4000 watts. With the exception of certain comet rendezvous, two thrusters, approximately 8000 solar array watts, were found adequate to perform the most demanding of the missions evaluated. Based on the probability of mission success versus number of thrusters, an additional thruster was included for reliability. This results in a total increase in weight for the 8 kw three 30-cm systems over the 5-kw five

15-cm system of 125 pounds. By comparison, five 15-cm thrusters at approximately 1000 solar array watts each accomplished the same missions with slightly higher reliability but with longer operating time.

1.4 SYSTEM AND PERFORMANCE CHARACTERISTICS

System and performance characteristics for the Pioneer F and G and Pioneer electric propulsion spacecraft are shown in Table 1-1 for the 1 to 5 AU missions and the less than 1 AU mission. Spacecraft weight varies primarily as a function of the size and number of solar electric components. The quantity of hydrazine is reduced from 60 to 30 pounds for all but the rendezvous mission since the majority of ΔV corrections can be accomplished using electric propulsion. The Saturn, Uranus, and Neptune direct missions require RTG's to support electrical power requirements beyond 6 AU and therefore 140 pounds additional weight must be added for these missions. Total thruster burn time is greatest for the Tempel II rendezvous mission; this mission has a total duration of 1000 days, approximately one-half of this time for thrusting if the 5 kw five 15-cm system is used and approximately one-third if the 8 kw three 30-cm system is used. Outbound missions to swing by Jupiter or fly by Saturn, Uranus, or Neptune directly would thrust for 150 to 200 days before leaving the required amount of solar illumination to support electric propulsion. Inbound missions to maximum solar periapsis are short in duration, the thruster burn times being less than 100 days.

Communications for the Saturn, Uranus and Neptune direct missions will require the addition of X-band which, with an 8-watt transmitter, allows 256 bps at Neptune and 512 and 1024 bps at Uranus and Saturn, respectively. The reduction in data rate between Pioneer F and G and the electric propulsion spacecraft is due to an estimated 1.5 dB loss resulting from the placement of electric propulsion thrusters above the high-gain parabolic reflector. To compare the ballistic Pioneer with the solar electric propulsion (SEP) Pioneer performance on outbound missions, the concept of "available C_3" was developed. The actual C_3 achievable using the 560-pound Pioneer spacecraft and the Atlas/Centaur/TE-364-4 is 88 km^2/sec^2; augmentation of electric propulsion increases

Table 1-1. Pioneer System and Performance Characteristics Comparison (≤5 AU Missions)

Characteristics	Basic Pioneer F and G	5-kw/Five 15-cm Pioneer Electric Propulsion	8 kw/Three 30-cm Pioneer Electric Propulsion
Spacecraft weight, lb	560	649* (without mercury)	759* (without mercury)
Experiment weight, lb	64	64	64
Hydrazine weight, lb	60	30 (nominal)	30 (nominal)
Experiment power, watts	24	24	24
Power available, watts	116	3.8-kw earth, 225 W at 5 AU	5.8-kw earth, 344 W at 5 AU
Spacecraft power consumed, watts	108	137 (thrust phase, experiments off)	137 (thrust phase, experiments off)
Total thruster burn, days max.	---	600	314
Single thruster burn, days max.	---	300	120
Communications	S-band	S-band	S-band
Core storage, kbps	50	50	50**
5 AU data rate, bps	1024	512	512
Transmitter output power, watts	8	24 and 8	24 and 8
Equivalent C_3 (km^2/sec^2) Atlas/Centaur/ TE-364	88	130 (200-day burn)	140 (180-day burn)

*TRW solar array; GE bistem motor deployed array ≈40 pounds weight increase.

**Half-million bit storage recommended for Tempel II mission

the weight from 560 pounds to 649 pounds for the 5 kw five 15-cm system and to 759 pounds for the 8 kw three 30-cm system. The improvement in available energy (C_3, km^2/sec^2) is shown in Figure 1-8 and 1-9 for the Atlas/Centaur, TE-364-4 and the Titan/Centaur/TE-364-4 launch vehicles. Available energy is defined as the sum of the launch vehicle energy for a given payload weight plus the energy derived from the inclusion of an electric propulsion system whose thrusters burn for a specified time. In this case 100 and 200 days.

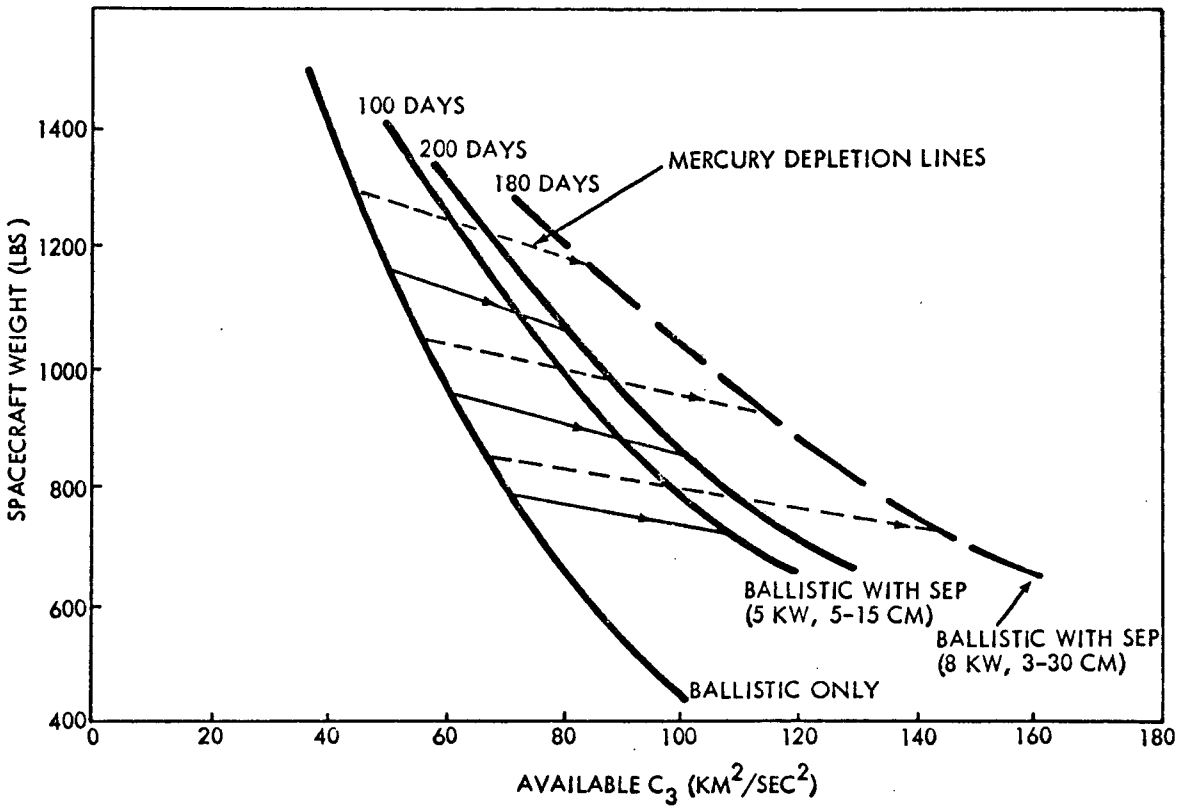

Figure 1-8. Atlas/Centaur/TE-364-4 Energy Curves With and Without Electric Propulsion (8 kw Three 30-cm and 5 kw Five 15-cm Electric Propulsion Systems)

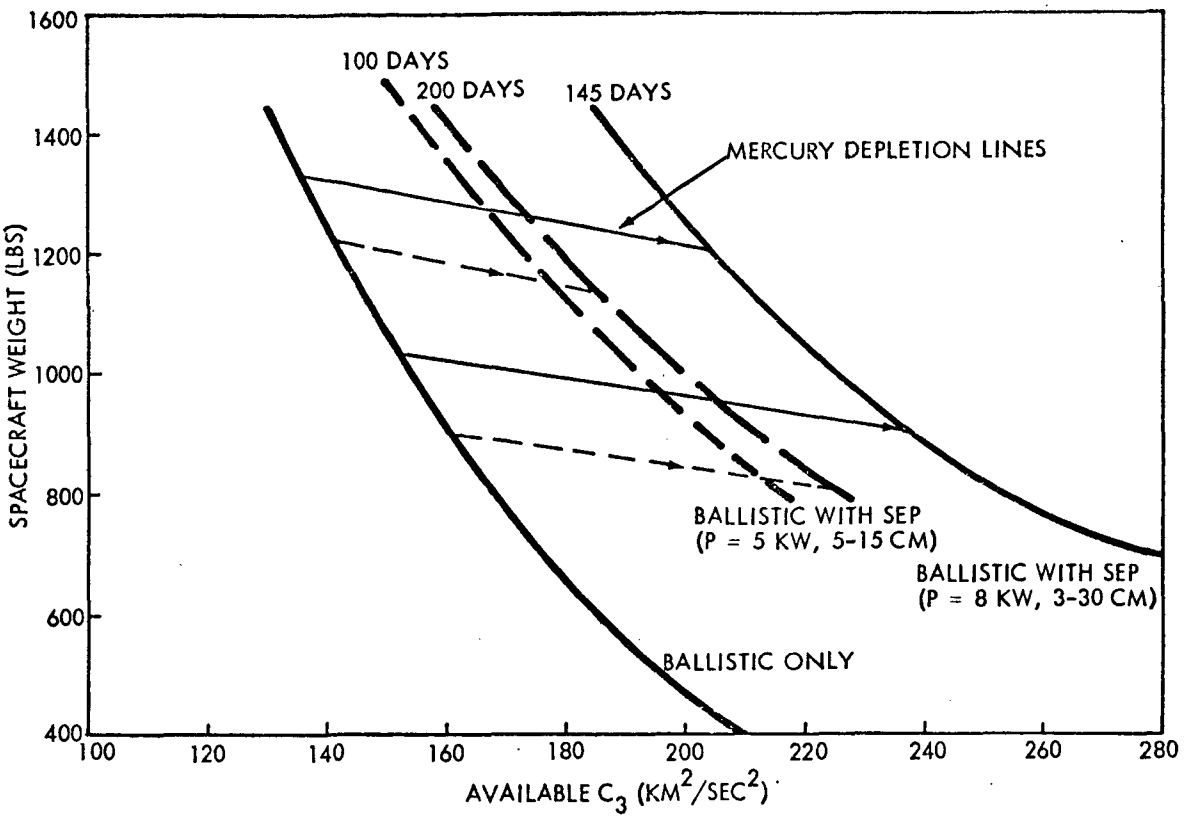

Figure 1-9. Titan IIID(5)/Centaur/TE-364-4 Energy Curves With and Without Electric Propulsion (8 kw Three 30-cm and 5 kw Five 15-cm Electric Propulsion Systems)

Table 1-2 shows the spacecraft design characteristics for each of the missions evaluated using either a 5-kw system with five 15-cm thrusters or an 8-kw system with three 30-cm thrusters. Such things as weight, range, launch vehicle, communications range, and thrust time are summarized for each of the missions evaluated. Neither the asteroid belt mission or the direct solar approach mission were evaluated for the 8 kw three 30-cm thruster case, although the direct solar approach mission was evaluated for both the Titan and Atlas class launch vehicles.

Table 1-2. Summary of Spacecraft Typical Design Requirements

Characteristics	Tempel II Rendezvous		Asteroid Belt Mapper		Out of Ecliptic		Neptune Direct Flyby		Direct Solar* Approach	
Electric propulsion system**	15	30	15	30	15	30	15	30	15	15
Approximate thrust time, days	600	314	65	Not Evaluated	200	150	200	145	70	70
Maximum communication range during thrust, AU	3.6	3.6	0.8		2.7	1.8	2.8	1.9	0.5	0.6
Mission duration, days	1000	1000	1305		450	445	2640	2560	99	84
Maximum communication range at encounter, AU	2.3	2.3	4.5		5.0	5.0	31.2	31.2	1.0	1.05
Launch Vehicle***	A/C/T	A/C/T	A/C/T		A/C/T	A/C/T	T/C/T	T/C/T	A/C/T	T/C/T
Spacecraft launch weight, lb	889	1032	720		752	924	879	1029	660	663
Injected C_3 (available C_3)	64 (NA)	56 (NA)	68 (NA)		73 (130)	62 (140)	162 (230)	152 (239)	80 (106)	180 (218)
Spacecraft burnout weight, lb	662	803	660		649	759	789	899	604	603

*Analyzed only for five 15-cm thruster with 3-kw solar array

**15 refers to 5-kw with five 15-cm thrusters and 30 refers to 8-kw with three 30-cm thrusters

***Launch Vehicle: A/C/T = Atlas/Centaur/TE-364-4; T/C/T = Titan/Centaur/TE-364-4

1.5 MISSION RESULTS

A summary of comparative results for each mission evaluated is presented in Table 1-3. Only the preferred launch vehicle and preferred size of electric propulsion system is given for each mission. These preferences are based on the best showing for electric propulsion. For example, the Jupiter swingby out-of-the-ecliptic is shown for the Atlas using the 8 kw three 30-cm thruster system. If the Titan were used, electric propulsion would not be necessary since the Titan can inject a Pioneer spacecraft anywhere up to 125 degrees inclination to the Jovian orbit plane following Jupiter swingby. The 8 kw three 30-cm electric propulsion system following launch from an Atlas/Centaur/TE-364-4 can achieve 92 degrees to the Jovian orbit plane after Jupiter swingby while the 5 kw five 15-cm electric propulsion system can only achieve 84 degrees.

Direct flyby missions to Saturn, Uranus, and Neptune are all possible during the 1975 to 1980 time frame, and launch opportunities repeat at about 13 months intervals.

Although the heliocentric latitude for all three planets is small, a mid-opportunity launch (1978) for each mission finds Saturn near its maximum latitude. Improved Saturn flyby performance could be expected for launches in other years. Uranus, sometimes as much as 7.7 degrees out-of-the-ecliptic plane, is in the ecliptic plane for a 1978 launch. Neptune stays about 1 degree out-of-the-ecliptic throughout the possible launch opportunities. The highly hyperbolic transfers to the outer planets are shown in Figure 1-10.

For Saturn there is a savings of 0.2 year (10 percent), for Uranus 0.6 year (12 percent), and for Neptune 1.4 years (16 percent). This is probably not a substantial enough savings in transit time to make worthwhile candidate missions for electric propulsion. However if we consider a probe mission and shift the performance parameter for the outer planet flybys from transit time to payload increase, there is sufficient advantage to consider this as an electric propulsion mission (based on a typical probe weight of 300 to 350 pounds). Table 1-4 illustrates this point.

Table 1-3. Comparison of Ballistic and SEP Performance for a Pioneer Spacecraft (8 kw Three 30-cm thrusters except Asteroid Belt and Solar Approach which are 5 kw Five 15-cm thrusters and 3 kw Five 15-cm Thrusters Respectively)

	ATLAS LAUNCHED MISSIONS						TITAN LAUNCHED MISSIONS							
	JUPITER OUT OF ECLIPTIC		TEMPEL-II		ASTEROID BELT		SATURN FLYBY		URANUS FLYBY		NEPTUNE FLYBY		SOLAR APPROACH	
	BALLISTIC	SEP	BALLISTIC	SEP	BALLISTIC	SEP	BALLISTIC	SEP	BALLISTIC	SEP	BALLISTIC	SEP	BALLISTIC	SEP
INJECTION C_3 (KM^2/SEC^2)	88	62	**	56	88	69	190	152	190	152	190	152	190	179
INJECTED WEIGHT (LBS)	560	924	**	1032	560	720	560	1029	560	1029	560	1029	560	675
BURNOUT WEIGHT (LBS)	560	759	**	803	560	660	560	899	560	899	560	899	560	604
BURN TIME (DAYS)	0	150*	**	314	0	65	0	145*	0	145*	0	145*	0	80
EQUIVALENT C_3 (KM^2/SEC^2)	88	140	--	--	88	100	190	239	190	239	190	239	190	218
PERFORMANCE PARAMETER	(1)	(1)	**	V_{∞_T}	4	(4)	(3)	(3)	(3)	(3)	(3)	(3)	(2)	(2)
COMPARISON VALUE	32°	92°	**	0	905 DAYS	1145 DAYS	760 DAYS	670 DAYS	1760 DAYS	1480 DAYS	3160 DAYS	2560 DAYS	0.17 AU	0.14 AU

*OUTBOUND THRUSTING STOPPED WHEN MINIMUM THROTTLE (35 PERCENT POWER)
** INSUFFICIENT CHEMICAL ΔV TO ALLOW PIONEER TO ACHIEVE RENDEZVOUS
(1) INCLINATION TO JOVIAN ORBIT PLANE
(2) PERIHELION
(3) FLIGHT TIME
(4) TIME IN BELT

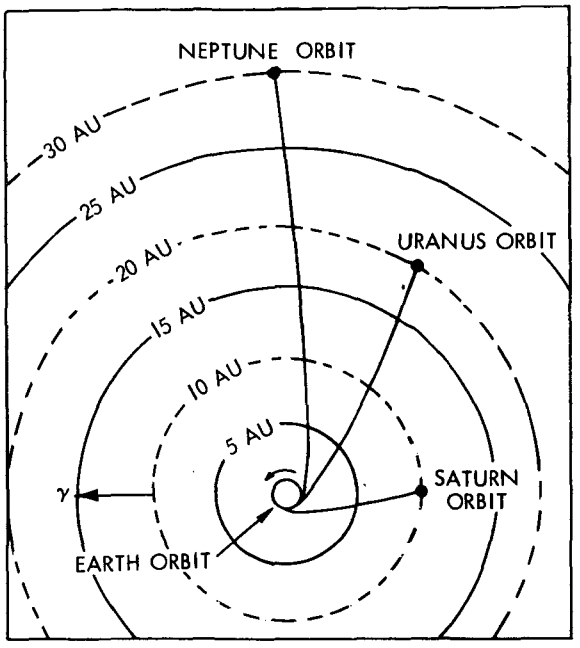

Figure 1-10. Category II Mission Profiles

There are several comets which come within the capabilities of the 8 kw three 30-cm Pioneer spacecraft during the 1975 through 1980 launch dates. These include Kopff (launch date 1980), Tempel II (launch date 1975 and 1980), Tuttle (launch date 1976), and Forbes (launch date 1978). Encke is attractive because its short orbital period has allowed it to be observed on many perihelion passes; thereby better establishing its orbital parameters and perturbative influences. However, as shown in Table 1-3, to achieve the ephemeris of Encke for rendezvous the spacecraft must be in an orbit that reaches 0.34 AU. This is a more energetic mission than can be accomplished with 8 kw of electric propulsion and the low periapsis makes this a mission outside the existing thermal design characteristics of Pioneer. In addition, for the existing configuration, fairing geometric constraints limit the width of the solar array to 6 feet. To reduce the length of each panel below 100 feet for a 20-kw mission (comet Encke) means that the panels would have to be wider and stowed with the width parallel to the spin axis. Following separation these panels would be rotated to a position perpendicular to the spin axis. Accommodation of the necessary five 30-cm thrusters would also be a major problem as would the

Table 1-4. Payload Advantage Resulting from Electric Propulsion

	TITAN LAUNCHED		
	SATURN FLYBY	URANUS FLYBY	NEPTUNE FLYBY
FLIGHT TIME, (YR) (SAME AS BALLISTIC)	2.14	4.83	8.65
ADDITIONAL PAYLOAD, (LB) (DUE TO ELECTRIC PROPULSION)	310	310	310
PAYLOAD INCREASE, (%) (DUE TO ELECTRIC PROPULSION)	55	55	55

accommodation of the power processors. These modifications suggest more major revisions to the Pioneer F and G configuration than was allowable under this study. Table 1-5 summarizes the characteristics and reasons that certain other comets, including D'Arrest, Grigg-Skjellerup and Pons-Winnecke are not good candidates for the Pioneer electric propulsion rendezvous.

Table 1-5. Comet Survey for Solar Electric Pioneer

Comet	Characteristics	Time at Perihelion	Trip Time	Launch Opportunities
Tempel II	p = 5.3 q = 1.37 Q = 4.68 i = 12.5	1972.9 1978.2 1983.5 1988.8 (G)*	1000 days (2.7 yr)	1970.2 1975.5 1980.8 1986.1
Encke	p = 3.3 q = 0.34 Q = 4.09 i = 12.4	1974.3 1977.6 1980.9 (G)*	1000 days	1971.6 1974.9 1978.2
Kopff	p = 6.3 q = 1.52 Q = 5.32 i = 4.7	1977.0 1983.3 (G)*	1000 days	1974.3 1980.6
D'Arrest (large inclination)	p = 6.7 q = 1.38 Q = 5.73 i = 19.6	1976.0 1976.0 1982.7 (G)*	1000 days 650 days 1000 days	1973.3 1974.3 1980.0
Grigg-Skjellerup (large inclination)	p = 4.9 q = 0.855 Q = 4.88 i = 17.6	1982 (G)* 1987 (F)*		
Tuttle-Giacobini-Kresák (small comet)	p = 5.5 q = 1.11 Q = 5.1 i = 13.8	1973.4 1978.9 1984.4	1000 days	1970.7 1976.2
Pons-Winnecke (large inclination)	p = 6.12 q = 1.16 Q = 5.53 i = 21.7	1976.1 1982.2 1988.3 (F)*		
Forbes (small comet)	p = 6.4 q = 1.55 Q = 5.36 i = 4.6	1974.3 1980.7 (F)*	1000 days	1971.6 1978.0

Legend:
p = period (yrs)
q = periapsis (AU)
Q = apoapsis (AU)
i = inclination (degrees)

*A. Friedlander, J. Niehoff, "Comet Sighting Analysis", G = good; F = fair.

The comet rendezvous mission selected for evaluation is a 1975 launch (a 1980 launch window is also available) for a rendezvous with the comet Tempel II. Both the 5-kw and 8-kw electric propulsion systems were evaluated using the Atlas/Centaur/TE-364-4 launch vehicle. The 8-kw system had the advantage of a substantially shorter burn time — 175 days as compared to 550. It would be impossible to perform this mission using only a ballistically launched spacecraft since the spacecraft's propellant fraction (assuming hydrazine I_{sp}) would be in excess of 80 percent for rendezvous.

The solar approach for the electric propulsion spacecraft was evaluated for the Titan and Atlas launch vehicles but only for the 5 kw five 15-cm thruster case. Inbound missions differ in that the spacecraft is retrothrusting to lower the perihelion and the solar array output power is increasing. The Atlas/Centaur/TE-364-4 can achieve a ballistic perihelion of 0.31 AU with a 560-pound spacecraft. A five 15-cm thruster system can reduce this perihelion to 0.27 AU with an 80-day burn time. By comparison, a Titan IIID/Centaur/TE-364-4 vehicle achieves a perihelion of 0.17 AU on a ballistic flight of a Pioneer spacecraft and solar electric augmentation can reduce this perihelion to 0.14 AU. Figure 1-11 shows the trajectories of these two inbound missions with electric propulsion augmentation. In terms of decreasing perihelion on an inbound mission, the SEP thrust over the relatively short period of one-half the orbit combined with the low thrust to mass ratio yields a marginal performance advantage over a ballistic flight.

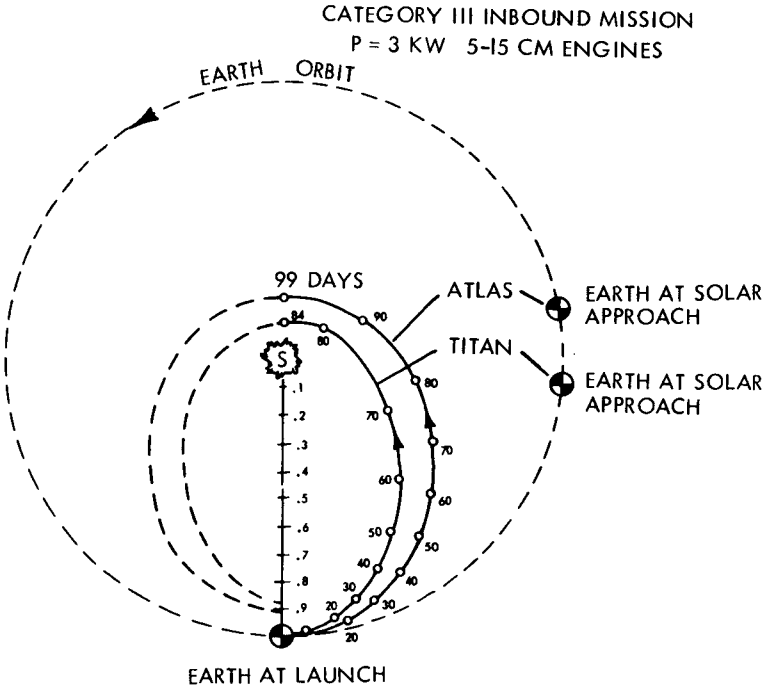

Figure 1-11. Inbound Mission Profiles

An asteroid belt mapper mission could be

performed with a 5-kw spacecraft. The spacecraft would thrust for 150 days and reach an aphelion of about 3.5 AU in about 600 days. It would be within the asteroid belt, between 2 and 4 AU, for about 1000 days. The same spacecraft without electric propulsion augmentation could map the belt for only 600 days. This mission was not emphasized during the study since scientific interest of a mapper per se was small. It is doubtful that if this type mission will be emphasized unless both the Pioneer F and G spacecraft encounter trouble due to a higher than expected flux of asteroid belt particles.

1.6 CONCLUSIONS

Electric propulsion is particularly performance-effective in missions where a major spacecraft maneuver must be performed without the assistance of a large local "gravity well." Such missions include rendezvous with asteroids, comets, satellites of major planets, and even Mercury. This performance-effectiveness results from the high specific impulse of the propulsion system, regardless of the type of spacecraft stabilization used.

Significant performance advantages also exist for missions without major maneuver requirements at destination, thus permitting increased payload mass, reduced flight time or increased inclination angle out of the ecliptic compared to purely ballistic missions; however, these could also be accomplished simply by using a larger boost vehicle. Considering the initial cost and development risks inherent in implementing electric propulsion spacecraft this development is unlikely to occur with missions that are within the launch energy and payload envelope of the available stable of launch vehicles, i.e., the Titan family. It is anticipated that electric propulsion will find its first application in those missions that could not be performed satisfactorily as ballistic missions, notably in small body rendezvous missions.

Additional advantages inherent in the continuous low thrust mission profile is the ability to make major midcourse and terminal guidance maneuvers with small additional propellant expenditure. For example,

the scientific yield of a rendezvous mission to a comet can be enhanced by including flyby of one or several asteroids on the way to the comet, by shaping the trajectory appropriately with excursions of millions of kilometers from the nominal mission profile at small extra propellant cost. In addition, extensive exploration maneuvers at destination can also be performed in a weight-effective manner.

The cost of the program to develop and launch a three-axis stabilized spacecraft would be in excess of three times the cost for the electric propulsion Pioneer and there are a number of good comet missions that can be performed with this considerably less expensive spacecraft. However, the high-energy comet rendezvous missions such as Encke are not practical using the Pioneer F and G configuration, primarily because of the constraints of thrust orientation and solar array pointing imposed by spin stabilization. This mission would require a major retropropulsion effort around the aphelion of the transfer trajectory at 2.5 to 3.5 AU, which cannot be effectively performed by the electric-propulsion Pioneer. For example, at 15 kw of nominal propulsion power only 330 pounds of net spacecraft mass would be delivered by the spinner, and even at 24 kw only 550 pounds. (These data apply to a 950-day mission in 1980). Since the largest practical solar array width for the Pioneer configuration is 6 feet, this means that a 20-kw array would require two panels 200 feet long. Also, the Encke mission would be severely constrained by thermal problems at the small solar distance of 0.34 AU at perihelion, an environment for which Pioneer was not originally designed.

The only other mission evaluated that had obvious merit was the Jupiter swingby to out of ecliptic. For this mission the performance improvement went from 32 to 92 degrees using the Atlas/Centaur/TE-364-4. However, an offloaded Titan/Centaur/TE-364-4 would allow out-of-ecliptic inclinations to 92 degrees without electric propulsion augmentation, thereby reducing considerably the probability that this, as an electric propulsion mission, will ever be flown.

Advantages of the three-axis vehicle are again the higher data rate during the thrust phase, better picture taking capability, and more efficient pointing; disadvantages are higher cost and lower reliability.

The necessary hardware to augment the Pioneer spacecraft with electric propulsion was evaluated and satisfactory solutions were found. These evaluations included the medium-gain off-axis antenna, centrifugally deployed solar array, thrust vector pointing sensor, terminal guidance sensor and accommodation of all electric propulsion components for either a 5-kw solar array with five 15-cm thrusters or an 8-kw solar array with three 30-cm thrusters. Both the medium-gain off-axis antenna and the centrifugally deployed array are new and, while optimization was not possible within the scope of this contract, sufficient evaluation and development were accomplished to prove feasibility. The medium-gain antenna produces larger back lobes than expected which probably will have to be reduced to eliminate interaction with the main lobes when this antenna is mounted in the Pioneer high-gain dish. The centrifugally deployed solar array design was 40 pounds lighter than the GE stem-deployed array. However, a good solution to problems of testing this large nonrigid spinning body in the earth's environment was not found. Unless an acceptable method is found, the GE stem-deployed array will have to be used in spite of the weight penalty.

Solutions were also found to the accommodation of electric propulsion components and to the thrust vector pointing problem for all missions and to the terminal guidance problem for asteroid flyby and comet rendezvous missions. The preferred solution to thrust vector pointing is achieved by addition of an off-the-shelf solar aspect sensor (for precise definition of the attitude in the ecliptic plane), together with the Pioneer F and G stellar reference assembly, to give the out-of-ecliptic plane component. Asteroid flyby and comet rendezvous missions require the addition of a star mapper for terminal guidance. This star mapper also serves to eliminate the stellar reference assembly and solar aspect sensor, and there is considerable merit to using it for all missions. However, the existing stellar reference assembly with the addition of an off-the-shelf solar aspect sensor would provide the minimum modification to the existing Pioneer F and G spacecraft.

2. MISSION DEFINITION AND PERFORMANCE CHARACTERISTICS

The mission analysis performed was in support of a Pioneer derived electric propulsion spacecraft that could accomplish missions in the 1 to 5 AU, 1 to 30 AU, and 1 to ≤0.7 AU regions of space. The missions of particular interest included asteroid belt mapping, Jupiter swingby to out-of-the-ecliptic, asteroid flyby and comet rendezvous, Saturn, Uranus, and Neptune direct flybys, and a direct solar approach. During the initial phase of the study a 5-kw electric propulsion spacecraft, using five 15-cm thrusters and either the Atlas or Titan launch vehicles, was evaluated. However, it became clear that development of the 15-cm thruster had small probability of being funded, therefore the study was redirected toward use of the 30-cm thruster, which is currently under development at NASA/Lewis. Accordingly an 8-kw, rather than a 5-kw solar array was chosen to support the larger thrusters (the 8-kw system is the largest that is acceptable without major redesign to the Pioneer spacecraft). The problem involves a large enough surface area to support the 8-kw-sized power processing units.

During the second half of the study the mission analysis was repeated for five of the seven missions (comet rendezvous, Jupiter swingby to out-of-the-ecliptic, and Saturn, Uranus, and Neptune direct flybys) using the larger 8-kw electric propulsion system. The asteroid belt mapper and solar approach missions do not benefit from an increase in electric propulsion thrust, and therefore the 8-kw configuration was not considered for these missions.

2.1 MISSION AND SCIENCE OBJECTIVES

The basic study objectives were directed toward developing a Pioneer electric propulsion spacecraft that could accomplish the missions described above. Emphasis throughout the study was on the spacecraft hardware and on the required amount of modification to the existing Pioneer spacecraft. Mission analysis was performed only to the extent necessary to establish requirements for hardware. The design criteria for the spacecraft were based on low weight and minimum modification with no requirement for multi-mission operation. The reference science payload for all missions was called out in the statement

of work as the Pioneer 10 payload and is shown, along with the instrument viewing requirements and characteristics, in Table 2-1.

An important problem of electric propulsion is that the by-products interact with on-board scientific measuring devices since the electric propulsion system generates a substantial number of ions and neutrons, and, in addition, these ions sometimes impact portions of the spacecraft and sputter off into the spacecraft environment. Also, the electric propulsion system, operating as it does with a large amount of electrical power, creates RF noise problems for not only the science but for the uplink and downlink communication capability. Fields and particles created by electric propulsion can cause permanent damage to experiments or spacecraft functional parts. However, with proper design of the spacecraft, interaction with the experiments during the thrust phase is the major remaining problem.

The electric propulsion phase for all but the comet rendezvous mission is terminated early and hence RF and experiment interference for the majority of the interplanetary flight is uncomplicated by electric propulsion. The principal area of interaction is, of course, on the rendezvous mission where the electric propulsion is used during most of the flight. However, even in this case the TRW concept would use chemical propulsion for the final terminal maneuver, thereby minimizing interactions during the rendezvous itself. Effects of thruster waste products on the spacecraft communication and solar array and on experiments are currently being evaluated at TRW under a separate contract with NASA/ARC.

Two different computer programs were available to TRW for analyzing the performance of the low-thrust electric propulsion systems. These programs included QUICKTOP and SNOST. QUICKTOP provides capability for evaluating three-dimensional trajectories for a fixed-thruster efficiency and I_{sp}. SNOST provides capability for evaluating two-dimensional trajectories where thruster and I_{sp} can be varied with throttling level.

Table 2-1. Pioneer 10 Science Payload

CODE	INSTRUMENT	BORESIGHT DIRECTION	TOTAL FOV (DEGREES)	REMARKS
A	HELIUM VECTOR MAGNETOMETER (JPL, SMITH) • SENSOR • ELECTRONICS	AXIS PARALLEL TO SPIN AXIS	NONE	KNOW ORIENTATION OF SENSOR AXES TO ±0.5 DEGREE WITH RESPECT TO SPACECRAFT AXES. SENSOR SIZE INCLUDES INSULATION.
B	PLASMA INSTRUMENT (ARC, WOLFE)	0° ELEVATION	20 X 140 FAN	TWO APERTURES. UNOBSTRUCTED FOV THROUGH ANTENNA.
C	CHARGED PARTICLE INSTRUMENT (CHICAGO, SIMPSON)	70° ELEVATION	65 CONE	MAIN TELESCOPE. UNOBSTRUCTED FOV.
		90° ELEVATION	70 CONE	LOW-ENERGY TELESCOPE. UNOBSTRUCTED FOV.
D	GEIGER TUBE TELESCOPE (IOWA, VAN ALLEN)	90° ELEVATION	30 X 60 FAN	GEIGER TUBE TELESCOPE. FOV MAY CONTAIN MAGNETOMETER BOOM.
			45 CONE	LOW-ENERGY DETECTOR. FOV MAY CONTAIN MAGNETOMETER BOOM
E	COSMIC RAY TELESCOPE (GSFC, McDONALD)	90° ELEVATION	33 CONE	DOUBLE ENDED HIGH-ENERGY TELESCOPE. UNOBSTRUCTED FOV.
			50 CONE	LOW-ENERGY TELESCOPE I. UNOBSTRUCTED FOV.
			30 CONE	LOW-ENERGY TELESCOPE II. UNOBSTRUCTED FOV.
F	TRAPPED RADIATION DETECTOR (UCSD, FILLIUS)	90° ELEVATION	120 CONE	DETECTOR C. MINIMUM FOV OBSTRUCTION.
		90° ELEVATION	60 CONE	DETECTOR E. UNOBSTRUCTED FOV.
		90° ELEVATION	60 CONE	DETECTOR S. UNOBSTRUCTED FOV.
		NONE	NONE	DETECTOR M.
G	UV PHOTOMETER (USC, JUDGE)	160° ELEVATION	2.5 X 28.1 FAN	TELESCOPE AXIS TO PASS THROUGH SPACECRAFT SPIN AXIS ±6 MINUTES. UNOBSTRUCTED FOV.
H	IMAGING PHOTOPOLARIMETER (ARIZONA, GEHRELS)	90° ELEVATION, NOMINAL	2 X 2 FAN	UNOBSTRUCTED FOV. TELESCOPE ROTATES ±80° IN ELEVATION. 60° FOV FREE OF SCATTERED LIGHT. REQUIRES DIFFUSER FOR CALIBRATION.
I	INFRARED RADIOMETER (CIT, (MUNCH)	105° ELEVATION	20 CONE	UNOBSTRUCTED FOV. 90° CONE FOV TO BE FREE OF RTG'S
J	ASTEROID-METEOROID DETECTOR (G.E., SOBERMAN) • SENSOR • ELECTRONICS	135° ELEVATION	10 CONE	UNOBSTRUCTED FOV. 2π STERIDAN FOV FREE OF SCATTERED LIGHT.
K	METEOROID DETECTOR (LaRC, KINARD) • SENSOR (12 PANELS) • ELECTRONICS	PLANE OF PANEL: 60° MINIMUM IN ELEVATION.	SENSOR AREAS TO BE UNOBSTRUCTED FOR PARTICLES TRAVELLING PARALLEL TO THE SPACECRAFT SPIN AXIS FROM THE -Z DIRECTION.	

Targeted missions, such as the Jupiter swingby, out-of-ecliptic, and comet rendezvous/asteroid flyby in the 1 to 5 AU category, and Saturn, Uranus, and Neptune flybys in the 1 to 30 AU category were investigated for optimum launch dates within the 1975 through 1980 span. To this end, the optimization program QUICKTOP was modified to analyze a spinning spacecraft thrusting along the spin axis which is oriented at constant solar aspect angle. The basic QUICKTOP program is a Boeing/NASA ARC second generation spacecraft optimization algorithm whose predecessor is the better known and more fully documented CHEBYTOP trajectory program. Untargeted missions and real throttling performance comparisons were investigated with the TRW on-line SNOST program, a rapid integrating planar trajectory model utilizing fixed-steering angles. Comparison test cases between the two programs shows good agreement for near ecliptic plane thrusting.

Basic assumptions for the trajectory analysis were:

a) Array nominal performance, 0.7 to 5.2 AU — JPL profile

b) Nominal array 5 kw, 3 kw and 8 kw

c) Array: 10 w/ft^2 at 1 AU; 0.52 w/ft^2 at 5.2 AU

d) Power conditioning: 91 percent efficiency and 10 pounds/kw

e) Thrusters: 3:1 throttle ratio limit

f) Solar flare array degradation 10 percent of available power

g) Thrust $\approx$7 millipounds per 15-cm thruster and 30 millipounds per 30-cm thruster

h) Total thrust $\approx 35 \times 10^{-3}$ pounds (15 cm) at 1 AU or 60×10^{-3} pounds (30 cm)

i) I_{sp} and efficiency per performance curves

The weight statement used in the mission analyses is shown in Table 2-2 while the weight of mercury propellant by mission is in Table 2-3.

Table 2-2. Weight Summary

	F and G (lb)	5 kw 5 thrusters 15 cm (lb)	8 kw 3 thrusters* 30 cm (lb)
Pioneer F and G gross weight	560		
Remove for baseline			
Hydrazine	-60		
RTG assemblies	-140		
Pioneer F and G baseline weight	360	360	360
Add for electric propulsion			
Thrusters		(5) 35	(3) 45
**Power processors		(5) 30	(3) 90
Solar array assembly (TRW)		146	206
Thruster mounting assembly		4	4
Converter		12	12
Sun aspect sensor		1	1
24-watt TWT's (2)		8	8
Mercury tank and lines		3	3
Hydrazine (nominal quantity)		30	30
Gross weight for 1 to 5 AU missions		649	759
Add for 1 to 30 AU missions			
RTG assembly		140	140
Gross weight for 1 to 30 AU missions		789	899

*Includes one spare thruster and processor

**GE solar array assembly increases weight by 38 pounds for 5-kw and 43 pounds for 8-kw array

Table 2-3. Mission Summary

Mission	Atlas		Titan	
	5 kw 5 15-cm	8 kw 3 30-cm	5 kw 5 15-cm	8 kw 3 30-cm
Out-of-ecliptic	103	165	--	--
Comet rendezvous	227	229	--	--
Asteroid belt mapper	60	--	--	--
Saturn direct	--	--	90	130
Uranus direct	--	--	90	130
Neptune direct	--	--	90	130
Inbound*	56	--	60	--

*3-kw rather than 5-kw solar array

The multitude of missions, boosters, power levels, and thruster sizes investigated in the study are also shown in Table 2-3. The numbers shown indicate the weight of mercury propellant required for the mission specified. When only a dashed line is shown, no analyses was performed.

2.2 LAUNCH VEHICLE PERFORMANCE CHARACTERISTICS

For this study the two launch vehicles, Atlas and Titan IIID were used and the basic vehicle performance of each of these is shown in Figures 2-1 and 2-2. For the Atlas the 370,000 pound thrust engine curve was used and for the Titan the IIID (five segment). The data given in these curves was supplied by the launch vehicle contractors, but in all cases it was checked against data from the basic user. The load factor fairings, and other constraints were similarly determined and the launch vehicle performance shown is compatible with the best available data.

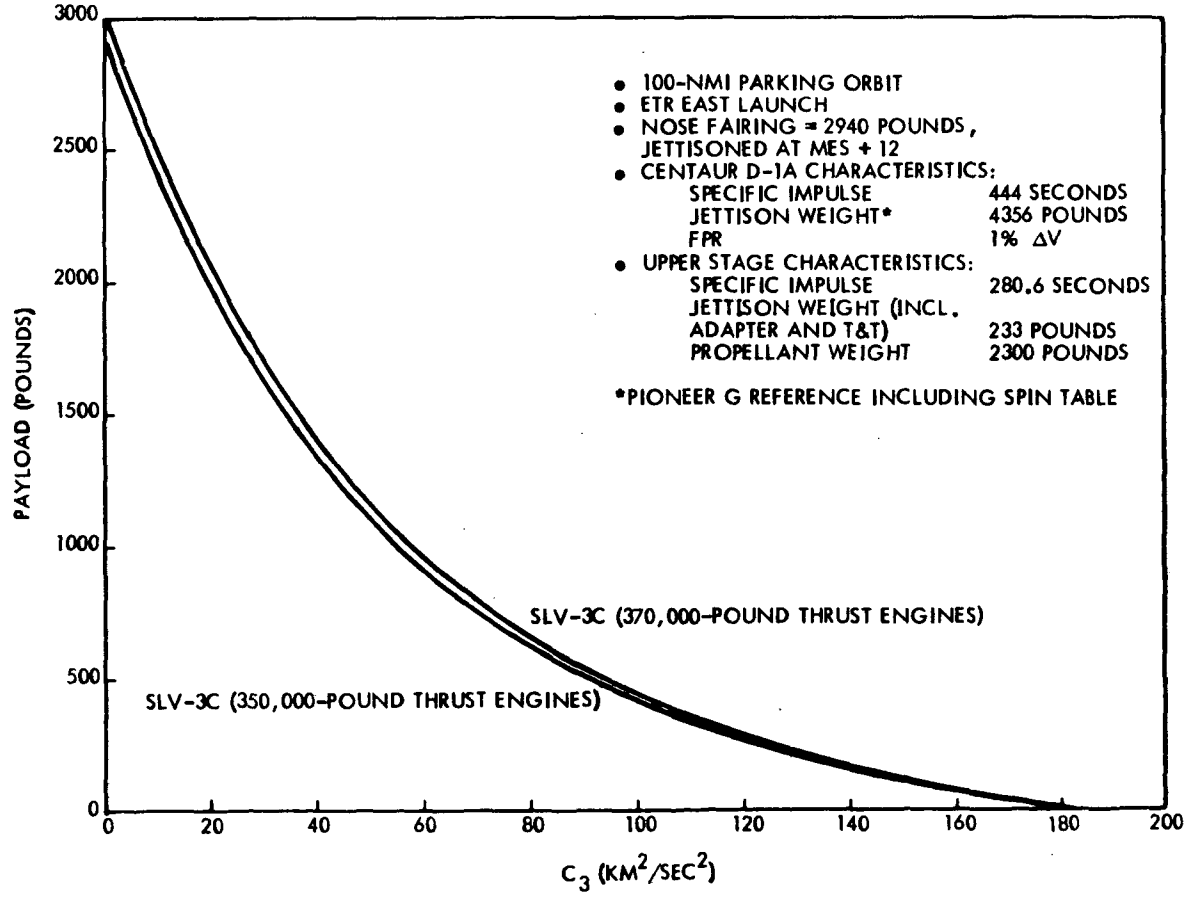

Figure 2-1. Atlas SLV-3C/Centaur-DIA/TE-364-4 Characteristics

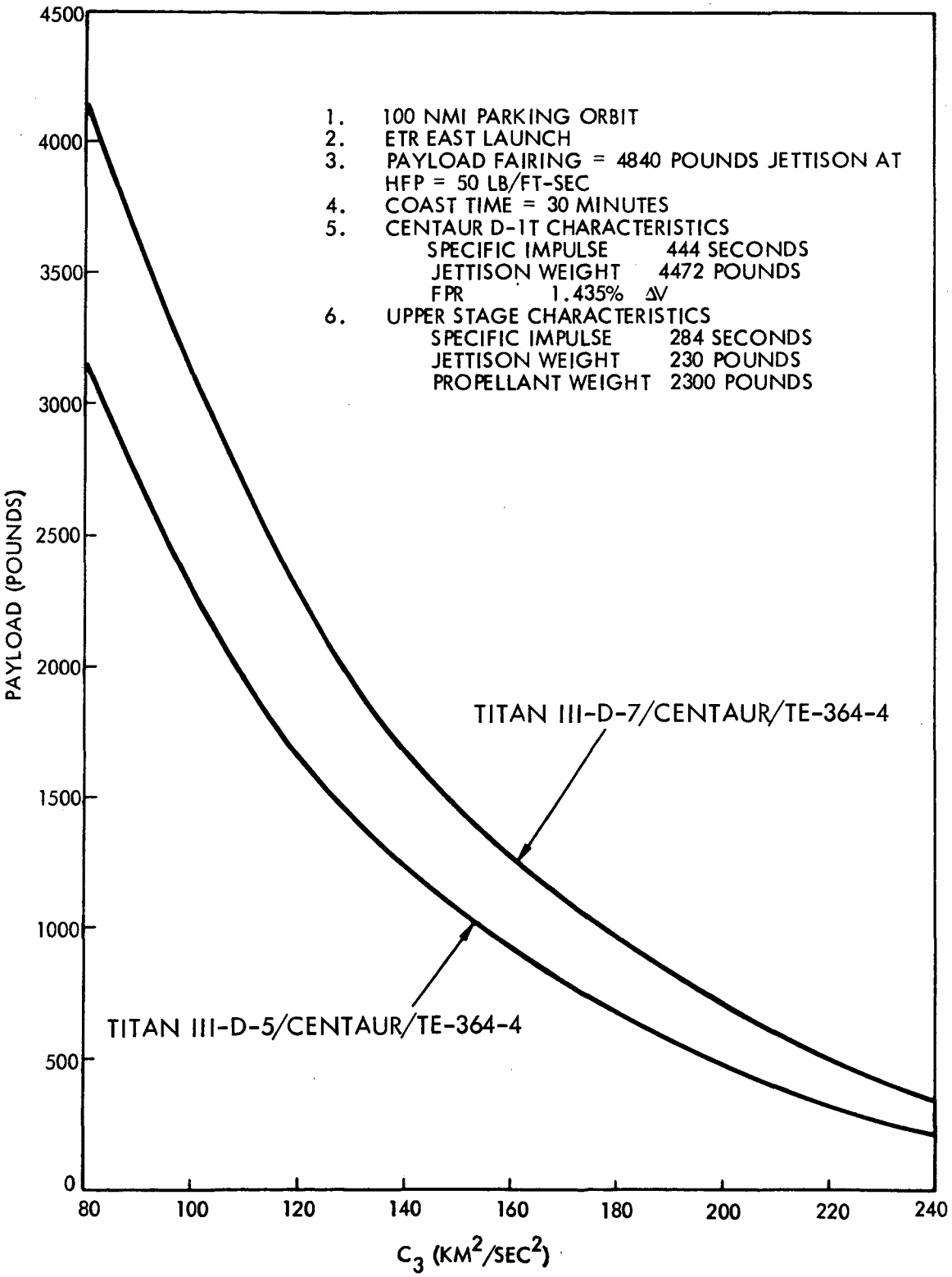

Figure 2-2. Titan/Centaur DIT/TE-364-4 Booster Performance

2.3 ELECTRIC PROPULSION PERFORMANCE CHARACTERISTICS

The principal function of the electric propulsion system is to impart the necessary energy and resultant momentum increment to the spacecraft to achieve the desired orbit dimensions and velocity. An electric propulsion system produces thrust by the electrostatic acceleration of ions. In the case of the subject study, the working fluid is mercury ions. Unregulated electric energy for this acceleration process is supplied by a solar array. This energy is processed into regulated power at the desired voltage levels for efficient thruster operation by a power processing unit. The output of the power processing unit is directly connected to the thruster as shown in Figure 2-3 for the 15-cm thrusters. This is the most reliable and direct method of interconnecting thrusters and power processing units (PPU's).

It was somewhat more difficult to mount the power conditioners for three 30-cm thrusters on the Pioneer spacecraft due to the large mounting area required (6 sq ft per unit). There was no room available to mount three full power processing units. Instead, it was necessary to break up each thruster power processing unit into two basic elements: a beam and arc plus multiple output converters. Each arc and multiple output converter was directly wired to each of the three thrusters. Since there was only room for two beam supplies, a switching network was utilized to interconnect active beam supplies with active thrusters. The utilization of such a switching device adds complexity and cost to the spacecraft. A sketch of the thruster and power processor layout for three 30-cm thrusters is also presented in Figure 2-3.

In the thruster, neutral propellant atoms are ionized and accelerated electrostatically into a highly directed exhaust beam. The resultant reaction force of this high-velocity exhaust beam on the accelerating electrodes produces the desired thrust force on the spacecraft. A schematic drawing of an electric propulsion thruster is shown in Figure 2-4, and Table 2-4 gives the characteristics of both the 15- and 30-cm thrusters. A simplified explanation of the operation of this device is presented below.

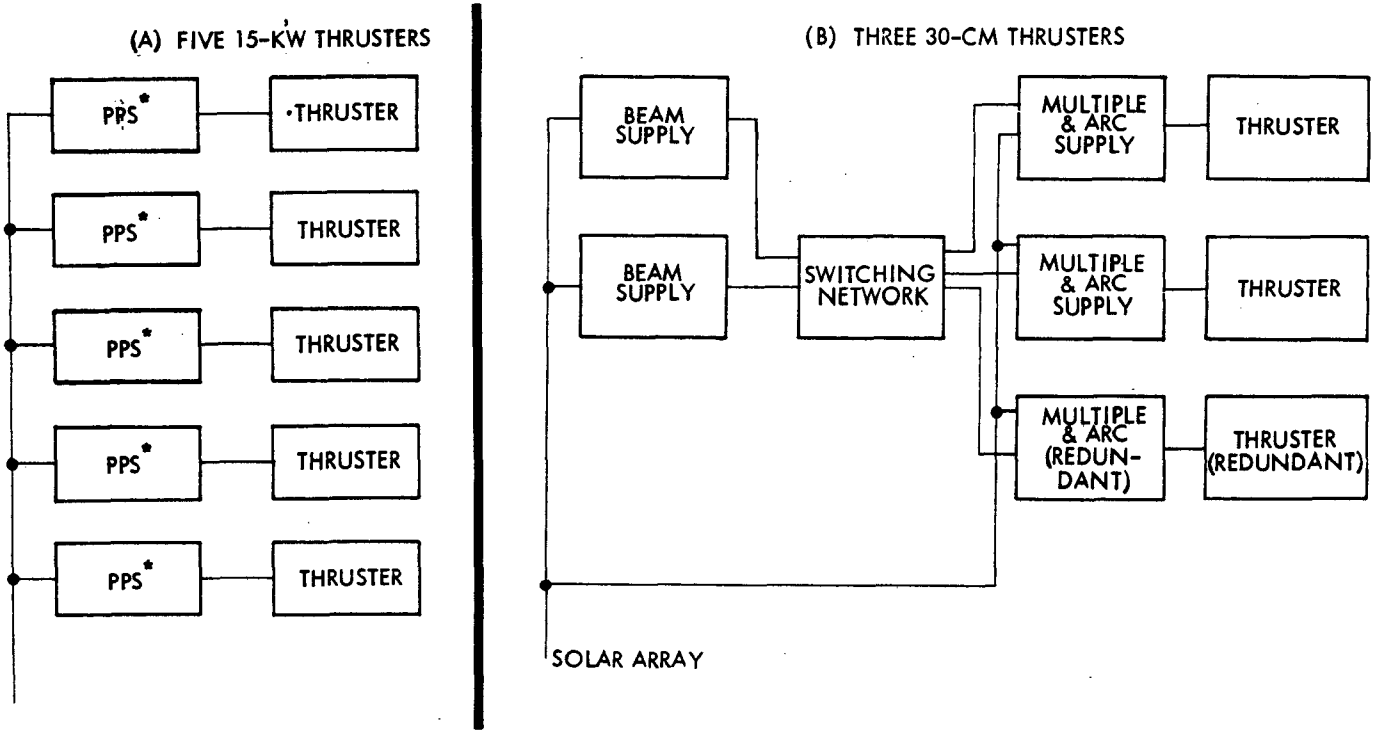

*INCLUDES BEAM, ARC AND MULTIPLE OUTPUT UNITS

Figure 2-3. SEP Electrical Block Diagram

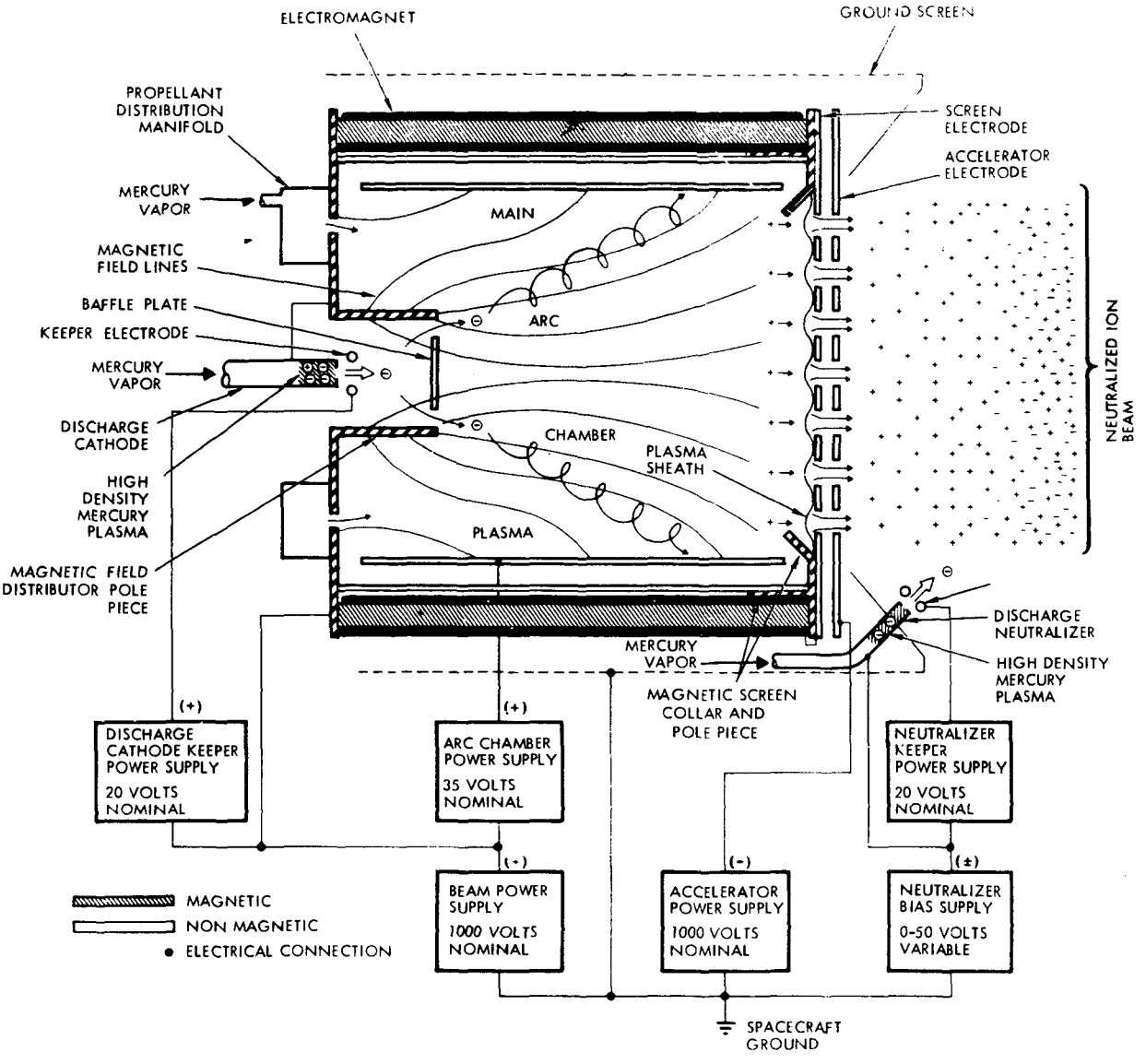

Figure 2-4. Simplified Thruster Block Diagram

Table 2-4. Thruster Characteristics

CHARACTERISTICS	15-CM THRUSTER	30-CM THRUSTER
THRUSTER MASS (POUNDS, MAXIMUM)	7	16
THRUSTER ENVELOPE (INCHES, MAXIMUM)	9 DIAMETER BY 9 LENGTH	16 DIAMETER BY 9 LENGTH
NOMINAL SPECIFIC IMPULSE (SEC)	2620	2940
PEAK THRUST (MLB)	7.4	28
PEAK INPUT POWER (WATTS)	686	2600
MAXIMUM BEAM CURRENT (AMP)	0.5	2.0
MINIMUM INPUT POWER (WATTS)	230	940
NET ACCELERATING POTENTIAL (VOLTS)	1040	1040

Liquid mercury propellant is vaporized in separate feed systems for the propellant distribution manifold, discharge cathode, and discharge neutralizer. At present, thrusters operate with about 78 percent of the flow supplied to the propellant distribution manifold, 10 percent to the discharge cathode, and two percent to the discharge neutralizer. Electrons are drawn out of the high density mercury plasma formed in the discharge cathode by the keeper electrode. These electrons are then dispered by the baffle plate and accelerated into the main arc chamber by a positive anode voltage. When in the main arc chamber, these energetic electrons ionize the neutral mercury propellant and form a mercury plasma. The divergent magnetic field in the main arc chamber, created by the electromagnets and soft iron pole pieces, traps the ionizing electrons and enhances the ionization process. Ions formed in the discharge chamber drift toward the screen electrode. Upon passing through the plasma sheath, the ions are accelerated through the concentric holes in the screen and accelerator electrodes by the applied electric field. The ion beam is then decelerated by the space charge forces in the ion beam to a potential slightly higher than the ambient space plasma potential and neutralized by the electrons emitted by the discharge neutralizer. Over a relatively wide range of thruster performance, the ion beam current and thrust is directly proportional to the mass flow of varporized propellant into the thruster. To throttle the ion engine, the flow rate of propellant into the thruster is varied while the screen and accelerator voltages are maintained constant. The discharge neutralizer is identical to the discharge cathode used to supply electrons to the main arc chamber, except it requires much lower flow of mercury vapor to operate. The thruster is surrounded by a fine screen at spacecraft ground potential to prevent the space plasma or neutralizing electrons from being drawn to the high positive potential of the thruster body and creating severe power losses.

This type of ion engine was invented by Harold Kaufman of the NASA/Lewis Research Center and has been space tested twice. A short-term thruster test was performed on the SERT I spacecraft in 1966 and a long-term test was performed for about 125 days during an orbital test

on the SERT II spacecraft. Various forms of electric thrust subsystem design, based on the original concept, are currently under investigation at NASA/Lewis, JPL, EOS, Hughes Research Laboratories, and TRW Systems.

The Pioneer spacecraft spin axis must be pointed in the direction of the thrust vector, thereby reducing the solar array power and requiring offset antenna pointing. Upon examining antenna pointing, solar array output power and thrust vector pointing requirements it is found that if the spin axis is approximately aligned 45 degrees to the sunline, optimum mission performance is obtained. In establishing solar array output power at this 45-degree angle, the solar distance and operating temperature are the two dominant factors affecting the solar array performance. Other electric propulsion investigators typically compute performance of a solar array at normal incidence. With the solar array at 45 degrees, adjustments must be made for the off-normal incidence and resulting lower array temperatures. The solar array output power P_{SA} at solar distance R is given by:

$$P_{SA}(R) = \frac{\eta_{SA} P_o K_T \sin\theta}{R^2}$$

where

η_{SA} = solar array degradation factor (around 0.90)

P_o = installed power, (i.e., output power at 1 AU for normal incidence)

K_T = thermal power factor

θ = solar incidence angle from plane of the array

The degradation factor, η_{SA}, although a function of time, solar activity and solar distance, asymptotically approaches 0.9 and is conservatively assumed to be constant at that value.

The thermal power factor, K_T, is a function of illumination intensity and is presented in Figure 2-5 at incidence angles of 45 and 90 degrees. The lower operating temperature which results from off

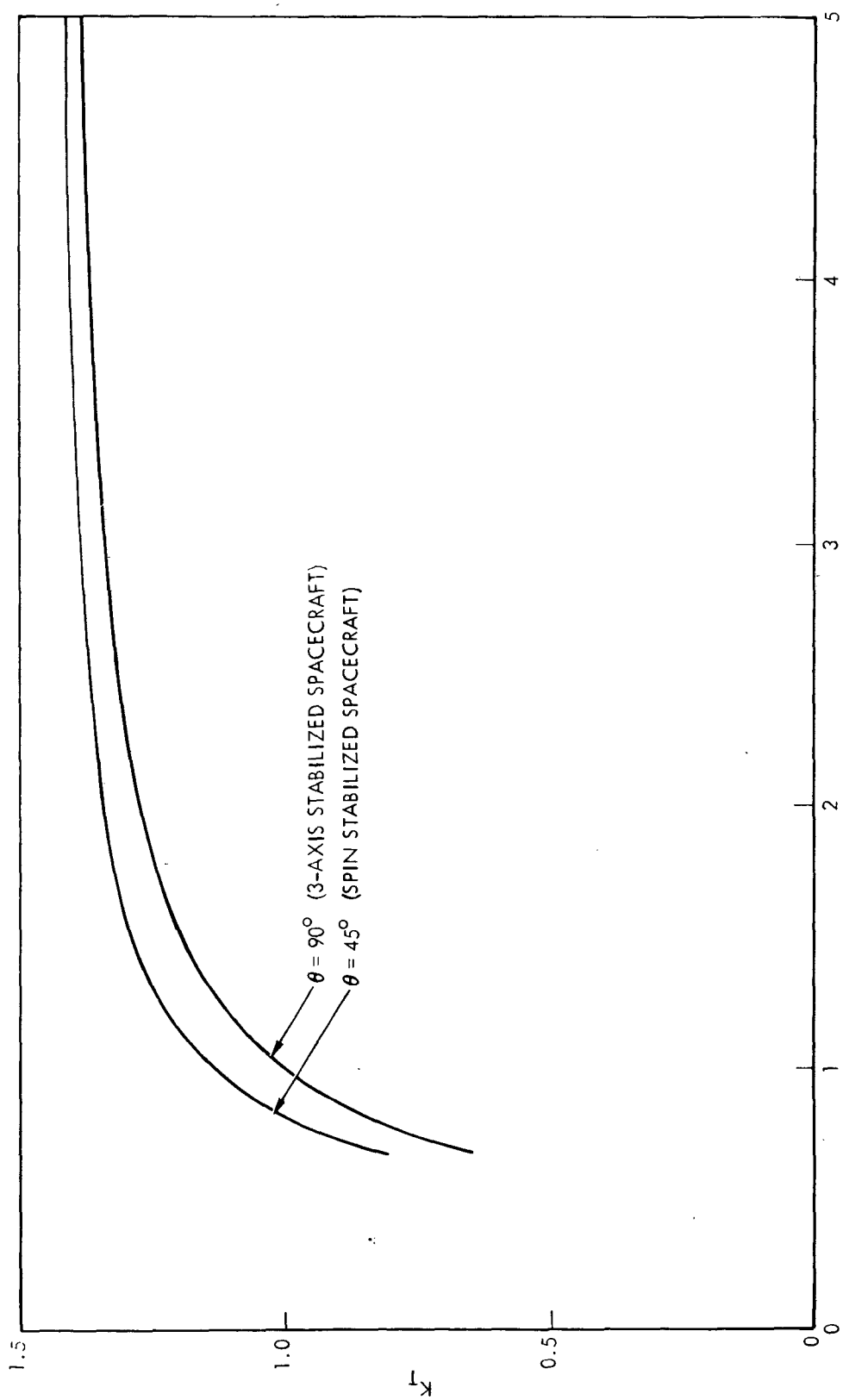

Figure 2-5. Thermal Effects on Array Power Output for Reduced Angle of Incidence

normal solar incidence on the array yields a higher thermal power factor than normal incidence and helps offset the reduction in solar energy flux due to the 45-degree incidence angle.

A composite plot of the relative solar array output power utilized for the mission analysis in this study (θ = 45 degrees) is presented in Figure 2-6. This solar array performance incorporates the thermal power factor of Figure 2-5 and a worst case solar array degradation of 0.9 is assumed to occur at the start of the mission.

Presented in Figure 2-7 are curves of specific impulse and overall thruster efficiency as a function of throttle level. These curves, which are presented for 15- and 30-cm thrusters, bracket the size range of interest for Pioneer and represent the NASA/Lewis projections of the present state of the art.* As per the NASA/Lewis specifications, the thrusters are assumed to reach their throttle limit when the beam current reaches one-third of its maximum value.

As power changes with solar distance the thrusters are throttled to utilize all available power from the PPU's. The specific impulse and thruster efficiencies are quoted for peak design power conditions. Under ideal throttling, I_{sp} and efficiency are assumed constant; however, experimental operation has shown that with actual throttling, the I_{sp} and efficiency decrease with reduced power input. Figure 2-7 (top) shows the decrease in efficiency with reduced power setting and Figure 2-7 (bottom) shows the decrease in I_{sp} with lower throttle settings.

For all missions selected except the direct solar approach, the solar array produces its maximum power at 1 AU and power decreases inversely as the solar distance is squared. For the direct solar approach the available power is continually increasing and therefore the solar array can be a smaller size. In the design approach adopted, the maximum available solar array power is utilized by the propulsion system to impart the highest possible velocity increment to the spacecraft. This power is equal to the solar array output power minus spacecraft housekeeping power.

*W. R. Kerslake, "Discussion of 1973 PTM Thruster Performance Estimate," NASA Lewis Research Center memorandum, April 1971.

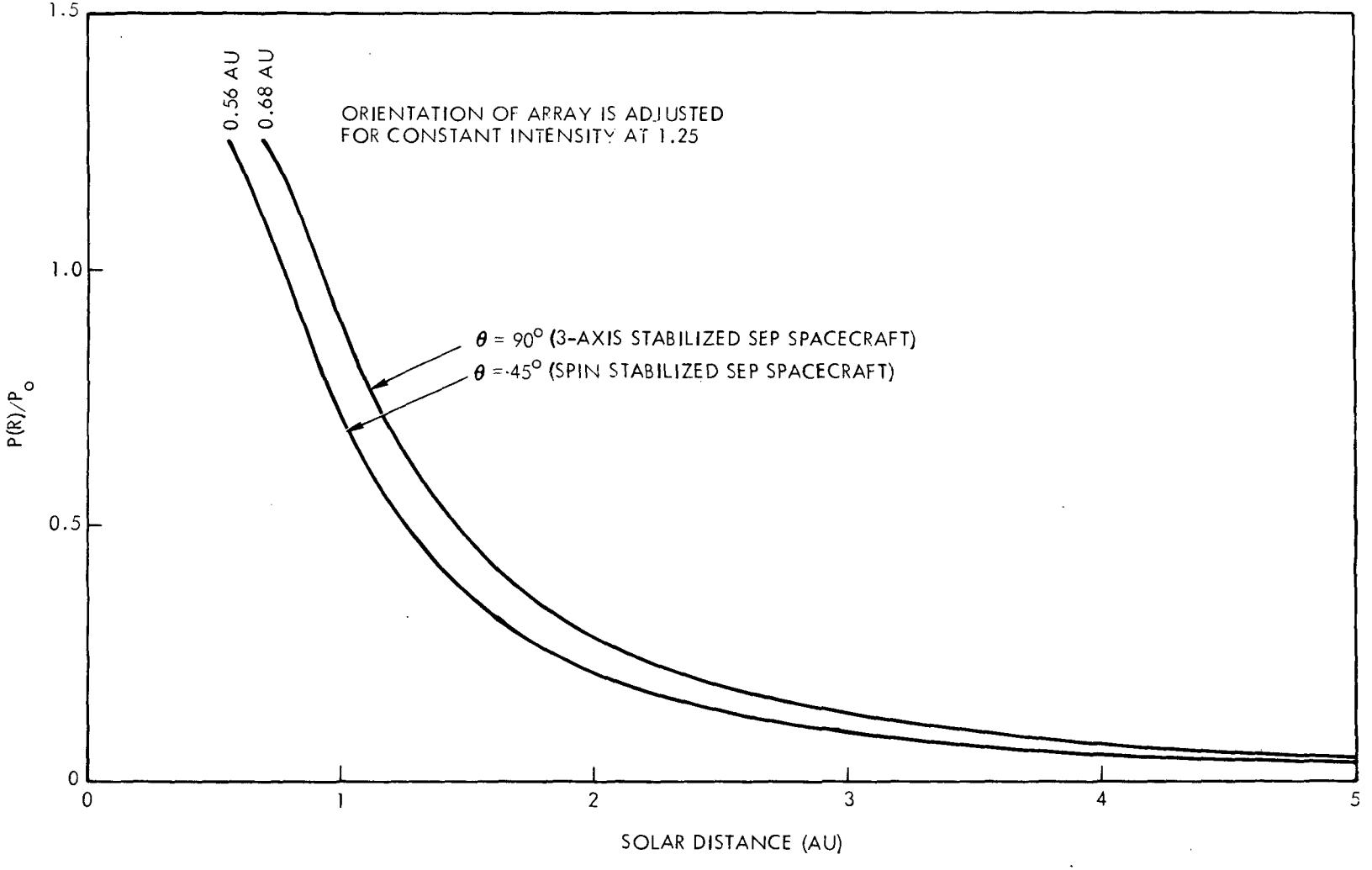

Figure 2-6. Relative Solar Array Power Available vs Solar Distance

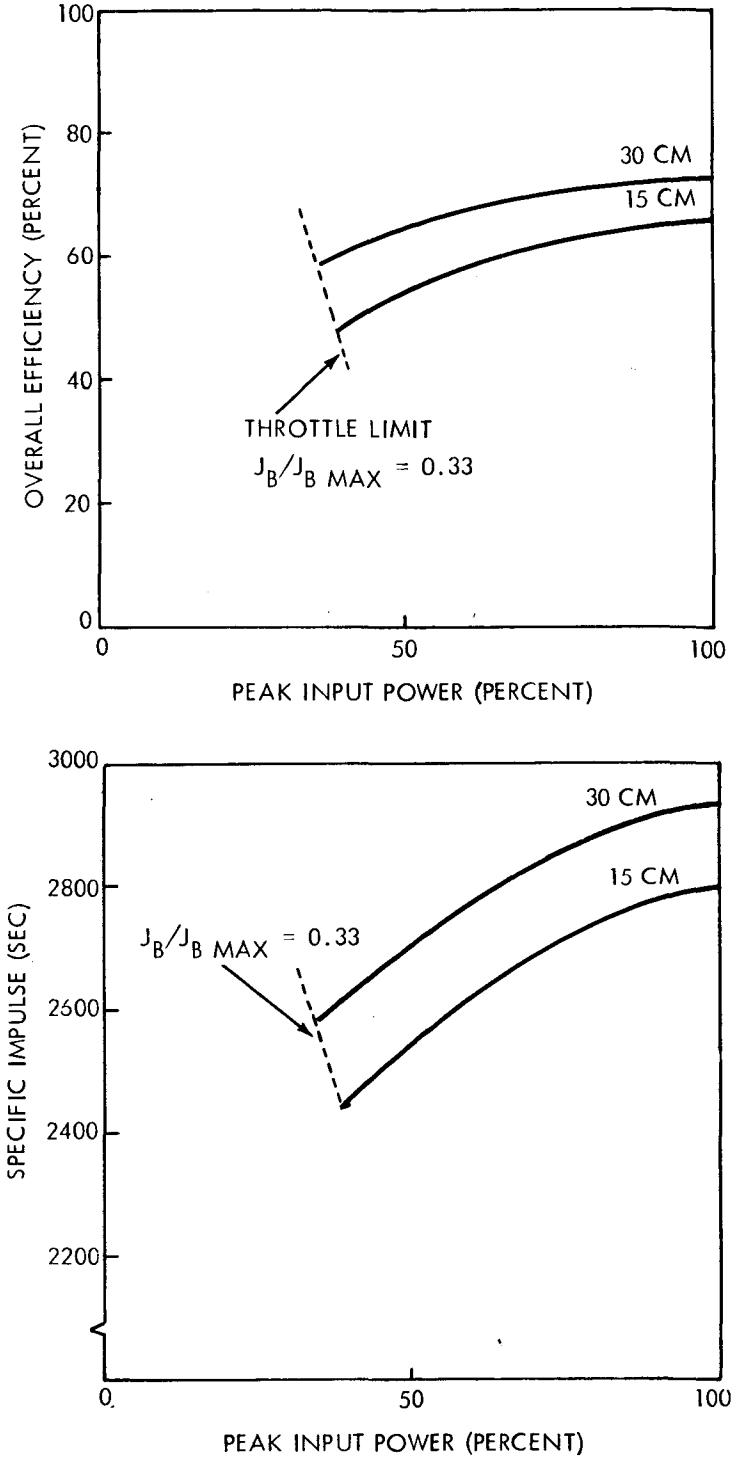

Figure 2-7. Performance Characteristics of Candidate Thrusters

The number of thrusters required for all but the inbound mission, is therefore a function of the maximum available power at 1 AU and the maximum power rating for the thruster power processor. Table 2-5 presents required power per number of thrusters for both the 15- and 30-cm size thrusters, along with the weight for each solar array power processor and thruster. The minimum and maximum power levels shown for the power processor and thruster represent the throttling spread available. It is obvious from this chart that power for the 30-cm thrusters must be available at the solar array in 4-kw increments and in 1-kw increments for the 15-cm thrusters.

As the mission progresses, the thrusters are throttled down to meet the available power. Active thrusters are shut off as soon as a fewer number of thruster units can supply the desired thrust. The maximum possible propulsion system burn time, excluding

reliability considerations, is governed by the time it takes the spacecraft to reach a point where the available solar array output power is equal to the minimum power input to one of the ion engine power processor units. It is therefore evident that for outbound missions with a decreasing power profile, there is an increasing number of spare thrusters with propulsion system burn time. The five 15 cm thruster system, therefore, has greater inherent reliability than the three 30 cm, and, in addition, the 15-cm thrusters can operate with as little as 260 watts available while the 30-cm thrusters take almost a kilowatt.

Table 2-5. 15- and 30-cm Thruster Characteristics and Power Requirements

	THRUSTER			POWER PROCESSOR			SOLAR ARRAY				
NOMINAL THRUSTER DIAMETER (CM)	MAXIMUM INPUT POWER (WATTS)	MINIMUM INPUT POWER (WATTS)	WEIGHT (LBS)	MAXIMUM INPUT POWER (WATTS)	MINIMUM INPUT POWER (WATTS)	WEIGHT (LBS)	ORIENTATION LOSS (WATTS)	DEGRADATION LOSS (WATTS)	DESIGN POWER PER THRUSTER (WATTS)	GE TYPE ARRAY WEIGHT (LB)*
30	2600	940	16	2900	1040	32	796	324	4020	249 (8 KW)
15	680	260	7	750	290	10	207	83	1040	183 (5 KW)

Since the thruster throttling range is limited by efficiency rolloff to a 3:1 beam current ratio, the solar distance of actual thrusting for the mission therefore establishes the number of engines required. For example, if we assume ideal throttling then one engine can throttle to about one-third power, two engines to one-sixth power, three engines to one-ninth power, etc. For 30-cm thruster operation the limit of thrusting capability is reached at approximately 2.4 AU while the 15-cm system can thrust out to 4 AU prior to maximum beam current. However, the larger impulse obtained from the 30-cm thruster more than makes up for this reduction in burn time.

It is noteworthy that the solar array peak design power for a 30-cm thruster is 4 kw compared to 1 kw for the 15-cm thruster. Therefore,

to utilize 30-cm thrusters on outbound missions, the array size must be 8 kw for thrusting beyond 1.67 AU, 12 kw for thrusting beyond 2.37 AU, and 16 kw for thrusting beyond 2.9 AU.

The typical performance of a SEP-augmented Pioneer F and G spacecraft for an Atlas/Centaur/TE-364-4 launch vehicle is presented in Figure 2-8. This figure was prepared for a solar polar passage via Jupiter swingby.

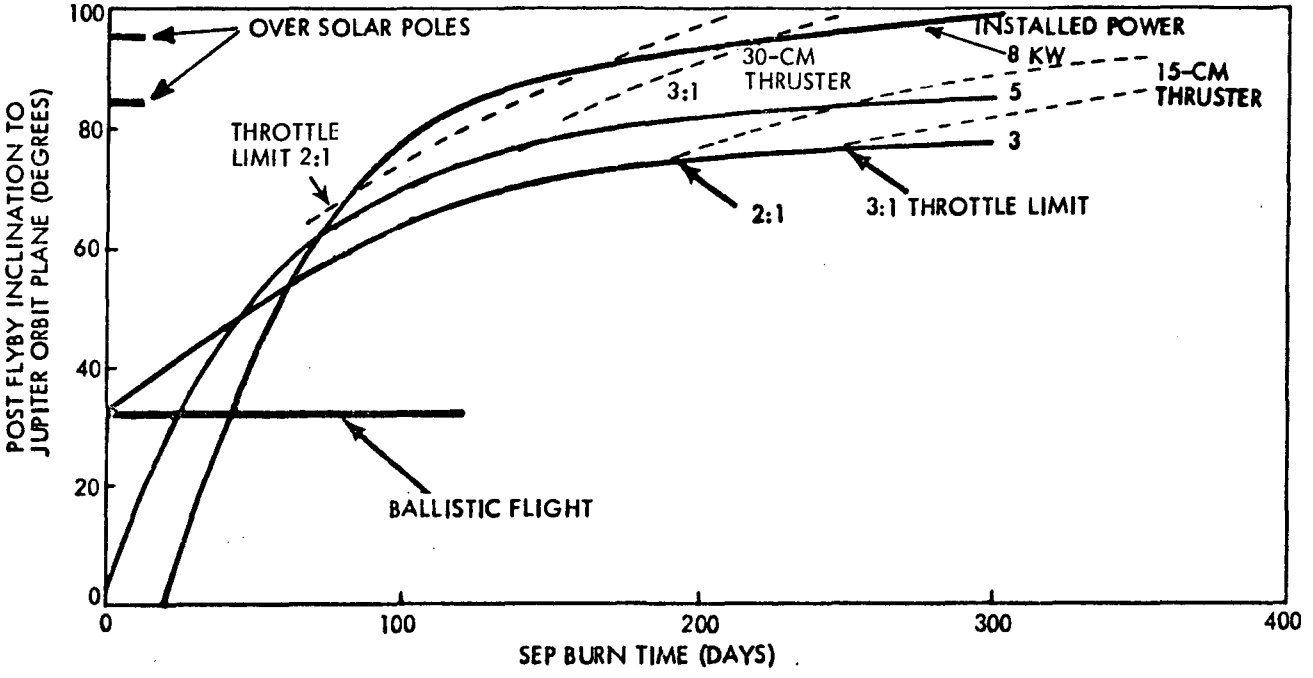

Figure 2-8. Out-of-Ecliptic Mission Performance for 15- and 30-cm Thruster Systems

Examination of Figure 2-8 indicates that the best out-of-ecliptic mission performance is achieved with 8 kw of installed power and 30-cm (three required) thrusters. In addition, the shortest burn time is for the 8 kw three 30-cm system. There appears to be no significant improvement in mission performance for SEP burn times greater than about 200 days.

As expected, the curve further shows the importance of throttling for the three 30-cm thruster 8-kw case and the relative insensitivity for the five 15-cm thruster 5-kw case. Again in Figure 2-9, using the Tempel II rendezvous for illustration, the much shorter operating time

for the 8-kw three 30-cm thruster stands out. Individual thruster unit operating time is 300 days for the 15-cm and only 120 days for the 30-cm thrusters.

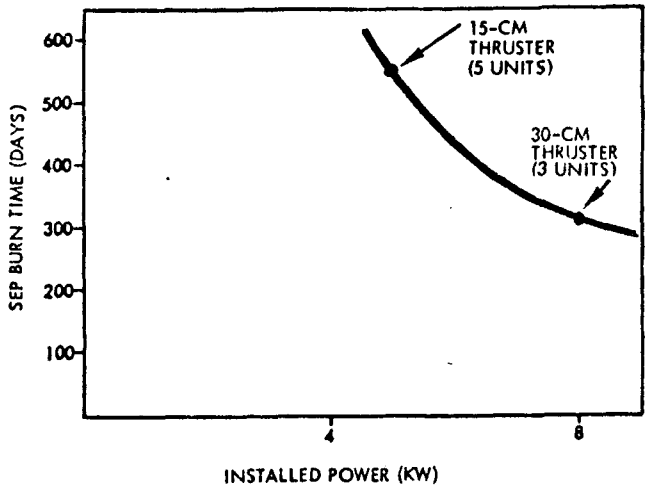

Figure 2-9. Various System Burn Times for Tempel II Rendezvous

The Titan IIID/Centaur/TE-364-4 was utilized for outbound missions with targets between 5 and 30 AU, including direct flybys of Saturn, Uranus, and Neptune. In these missions, the RTG's remain on the Pioneer spacecraft to provide housekeeping power to the spacecraft at solar distances beyond 5 AU where solar power is not adequate. The typical performance characteristics of a SEP-augmented Pioneer for direct outer planet flyby missions are presented in Figure 2-10. Once again, as in the case of Figure 2-8, best performance

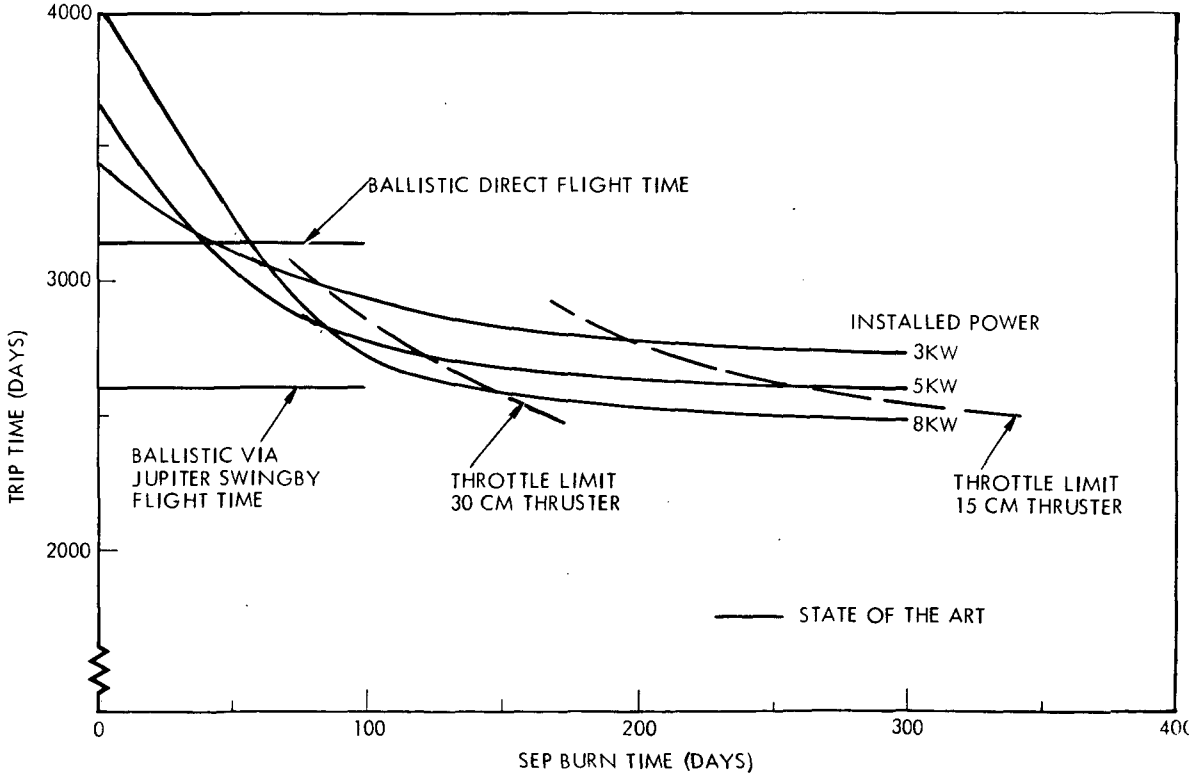

Figure 2-10. Impact of SEP Installed Power and Burn Time on Trip Time for Direct Neptune Flyby Mission Using Titan IIID/Centaur/TE-364-4

is obtained for a SEP configuration consisting of 8-kw installed solar array power and three 30-cm thrusters. In addition, total burn time is reduced from approximately 200 days to 150 days.

It is interesting to note that for the selected propulsion system configuration the nominal thruster unit burn times are about 125 days. There is ample evidence from the SERT II flight test and other supporting ground tests that such a burn time is well within the state of the art. Furthermore, this value of nominal burn time is more than a factor of three less than the design life of the thruster, leading to further confidence that electric thrusters will operate reliably for the mission desired.

For outbound missions more standby thrusters become available as the mission progresses; thus, more failures can be compensated for. Improved reliability can also be achieved through standby redundancy. This approach, although workable, is not as desirable as using smaller thrusters and increasing the number since significant weight penalties can be accrued from standby redundant power processor and thruster units.

Eight thrusters are impractical for the Pioneer solar electric spacecraft from both an accommodation and system complexity standpoint; the three or five thruster case appears most desirable. For the 5-kw installed power level, five 15-cm thrusters would be required.

Use of the 30-cm thrusters, for an 8-kw power level, requires two initially active and one spare unit. System reliability is unacceptable without standby redundancy for this case.

The ability of the electric propulsion system to function properly even after one or more thruster failures is extremely advantageous in selling the SEP concept for scientific missions in the near future. This point can be illustrated by referring to Figure 2-11 where an exaggerated thruster failure situation results in prolonging burn time by only 25 days. The typical sequence of events for a solar polar passage via Jupiter swingby is used for illustration.

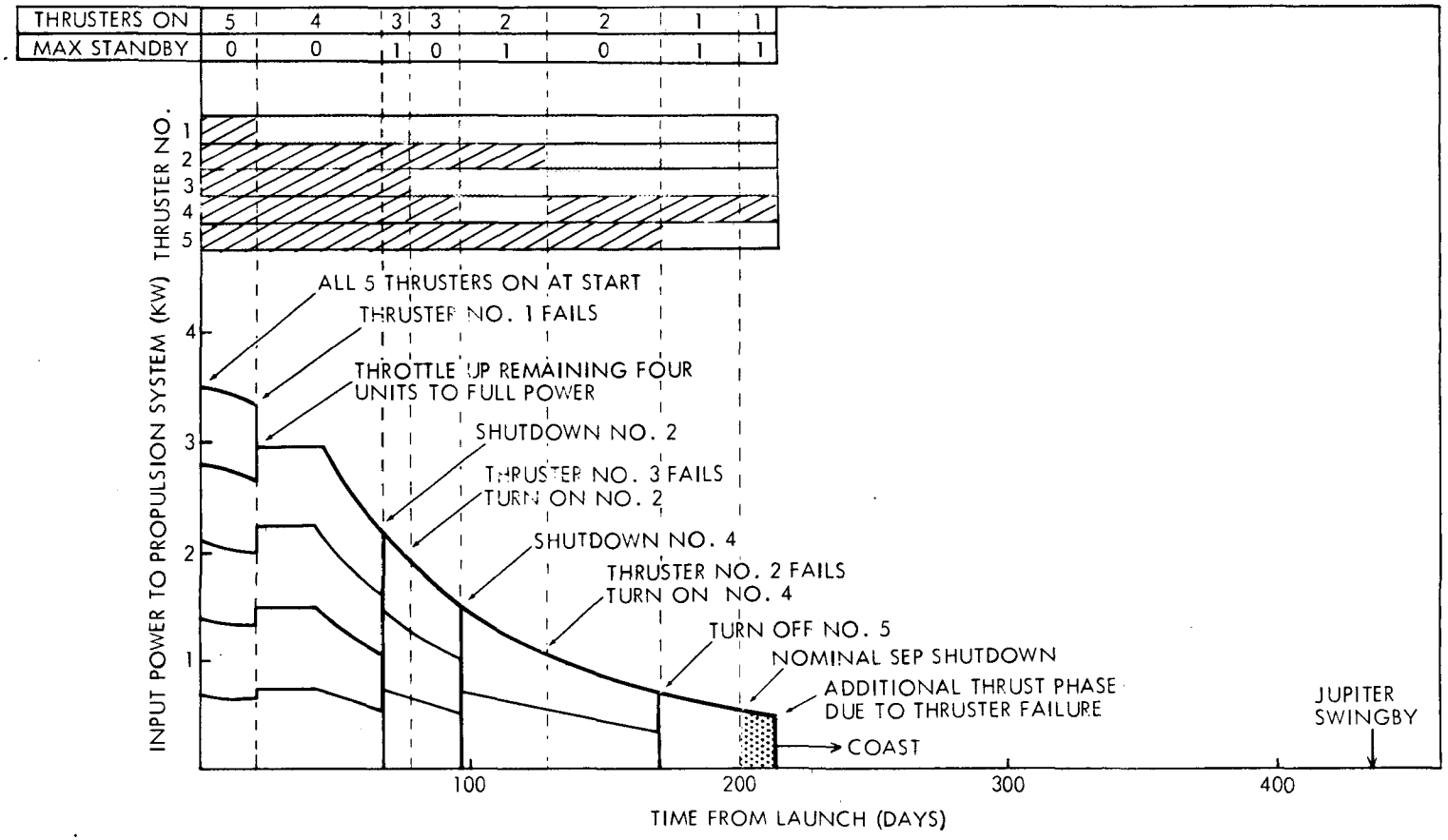

Figure 2-11. Typical Sequence of Events for Out-of-Ecliptic Mission via Jupiter Swingby Mission

About one day after launch, from an Atlas/Centaur/TE-364, the propulsion system is turned on. All five thruster power processors operate at a nominal input power level of 700 watts to meet the 3.5 kw. This is about 12 percent below the peak input power rating of the processors. The thrusters are throttled down to match the available input power as the solar distance increases. About 20 days after launch, thruster No. 1 is assumed to fail. Since there are no spares in this thrust phase, the remaining four units are throttled up to their maximum capacity of 2900 watts which is about 400 watts less than the available input power. These thrusters remain at this maximum level until about 40 days into the mission when the available power for propulsion drops below 2900 watts.

The four thrusters are then gradually throttled down until about 65 days into the mission when available power equals the maximum capacity of three assemblies. Thruster No. 2 is turned off at this point to provide a spare unit at the earliest possible time. Throttling of the three thruster power processor assemblies is continued until about 80 days when thruster unit No. 3 is assumed to fail. Thruster No. 2 is then turned on and the mission continues without any appreciable loss in total impulse; however, once again there are no spare thrusters.

The mission then proceeds in a similar manner, with a shutdown of No. 4 followed by a failure of No. 2 and restart of No. 4 prior to the nominal propulsion system shutdown time at 200 days. At this point the spacecraft has not achieved the necessary velocity for the desired Jupiter swingby maneuver because of the loss in total impulse due to the thruster failure at 20 days. To compensate, the thrust phase is extended 25 days to achieve mission objectives.

Following the thrust phase the spacecraft is reoriented using a sun aspect sensor as reference, to point the high-gain antenna at earth. The remainder of the mission, swinging by Jupiter and over the south pole of the sun, is accomplished with the identical equipment used on Pioneer 10. The advantage derived from solar electric propulsion is a solar polar orbit rather than only about 32-degree inclination to the solar equatorial plane.

Figure 2-12 shows the same type of operational profile for the 8-kw solar array with three 30-cm thrusters using an Atlas/Centaur/TE-364-4 launch vehicle. There is less reliability available since, following a postulated failure at 40 days, there is an approximate 40-day period when no standby unit is available. Also in the fourth phase, assuming the failure of No. 3, there would be no backup thruster available. In addition, it is not possible to extend the thruster time beyond 180 days since this is the limit of the throttling capability. However, the total required thrust time is less and the calculated reliability, while not as high as the five 15-cm configuration, is still conservatively estimated at a 0.9 probability of success.

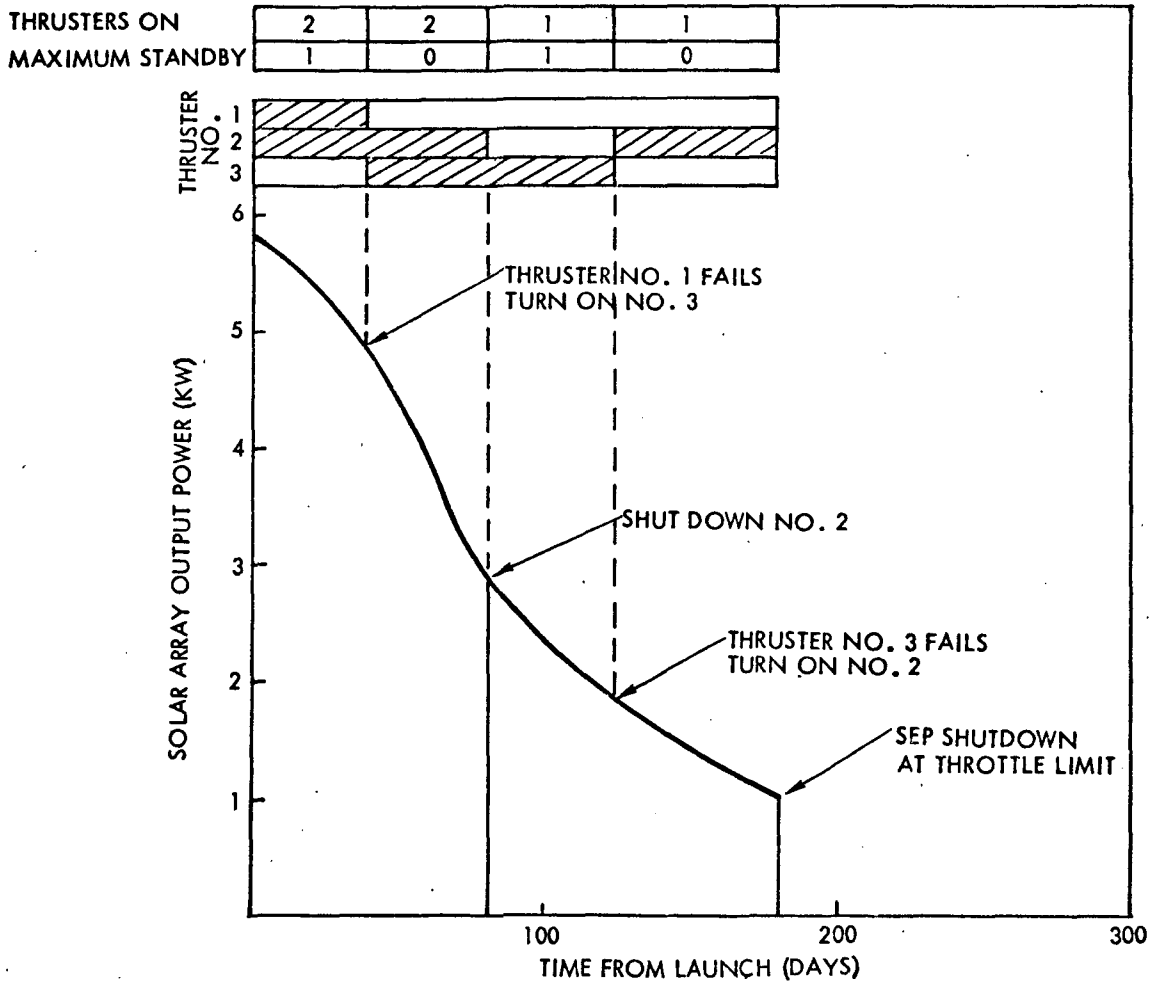

Figure 2-12. Operational Profile for 8-kw Three 30-cm Configuration

3. MISSION ANALYSIS

3.1 1 TO 5 AU MISSIONS

Missions in the 1 to 5 AU range have been analyzed as a category since the solar array can supply adequate spacecraft power throughout the mission with a 5-kw or larger solar array. This allows the radioisotope thermoelectric generators (RTG's) to be removed, thereby reducing the weight by approximately 140 pounds. The following missions are specified for evaluation in the 1 to 5 AU range:

a) Jupiter swingby to out-of-the-ecliptic

b) Asteroid belt mapping

c) Comet rendezvous

The Atlas/Centaur/TE-364-4 launch vehicle was used during the evaluation of the three listed missions since it best meets the energy-weight requirements of the Pioneer electric propulsion spacecraft. For example, use of the five-segment Titan with Centaur and TE-364-4 would allow the spacecraft to pass over both the southern and northern solar poles after Jupiter swingby without solar electric augmentation. The advantage of electric propulsion is in the lower cost of the Atlas and the more readily available launch pad. This mission was evaluated for both the 5-kw and 8-kw systems. The comet rendezvous mission can only be performed using electric propulsion. (Rendezvous refers to attaining the same relative velocity as the comet and therefore the approach velocity attained by the Atlas is more acceptable than the Titan.) Various comets were evaluated and the most likely candidate for either the 5-kw or 8-kw system was Tempel II although there are several other contenders which will also be discussed. As a part of this analysis an evaluation of asteroid flyby enroute to the comet rendezvous was performed. This concept is feasible although the maneuver to the asteroid would require additional quantities of hydrazine. The asteroid belt mapper was evaluated only for the Atlas class launch vehicle and the 5-kw system since this is a relatively low-energy mission, the performance parameter being time and inclination in the belt, in order to determine particle density distribution between 2 and 4 AU and between either ±10 degrees perpendicular to the ecliptic.

3.1.1 Jupiter Swingby to Out-of-the-Ecliptic

A typical Jupiter swingby to solar pole passage mission profile is shown in Figure 3-1. This mission can be performed any year and takes approximately three years to reach the regions of the sun's south pole followed six months later by passage at the sun's north pole. Periapsis is at 1.0 AU with polar passages at 1.4 and 2.2 AU, respectively. The inclination of the axis of rotation to the ecliptic plane would put the south pole at 84.7 degrees and the north pole at 95.3 degrees for Jupiter's orbit plane.

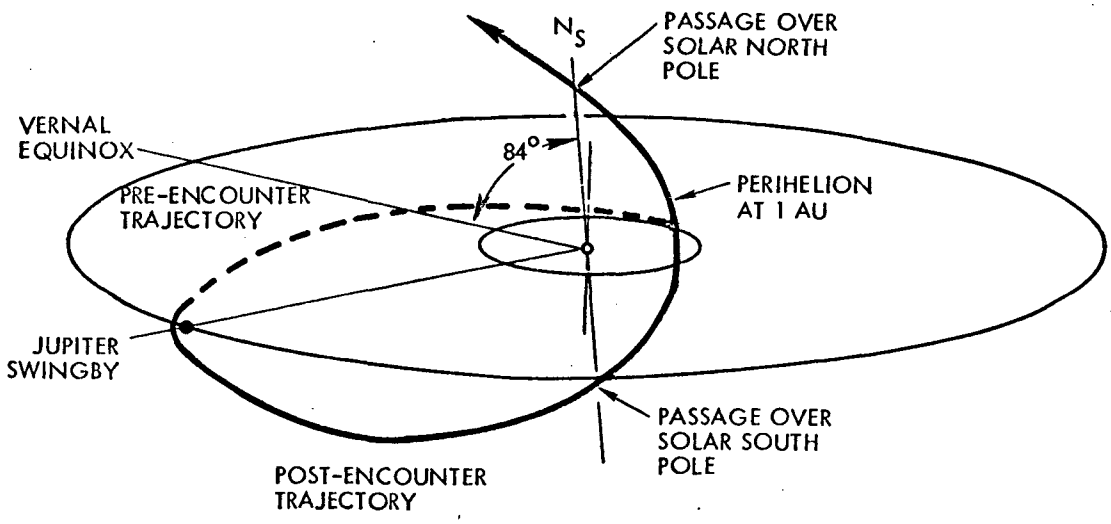

Figure 3-1. Jupiter Swingby Out-of-Ecliptic Mission Profile

Thruster sequencing for the three 30-cm (one thruster in standby) and the five 15-cm systems is shown in Figures 3-2 and 3-3. Note that for the 30-cm configuration one of the two operating thrusters is turned off and the remaining thruster is returned to full throttle at approximately 90 days. Minimum thrust level would allow thrusting out to over 180 days; however the mission is terminated at approximately 150 days since there is no performance improvement after this time due to the low thruster output.

Termination of electric propulsion thrusting nominally occurs at 200 days for the 5 kw five 15-cm thruster configuration. Throttling back

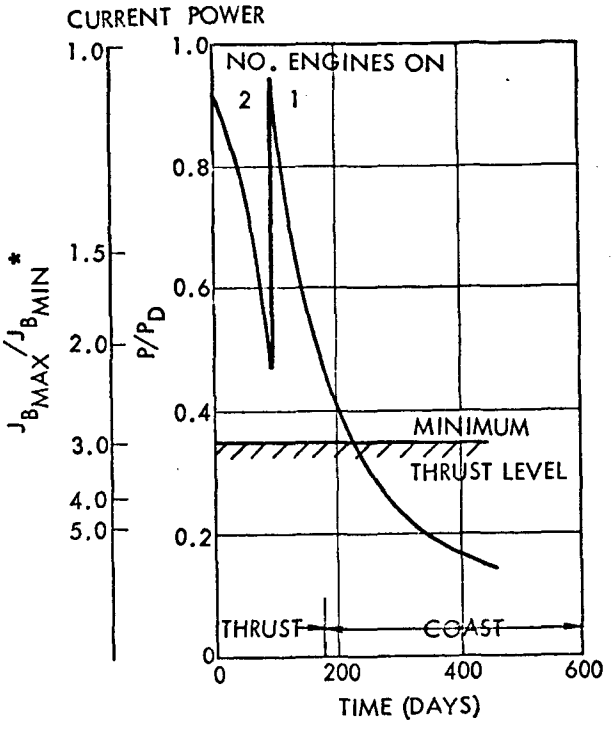

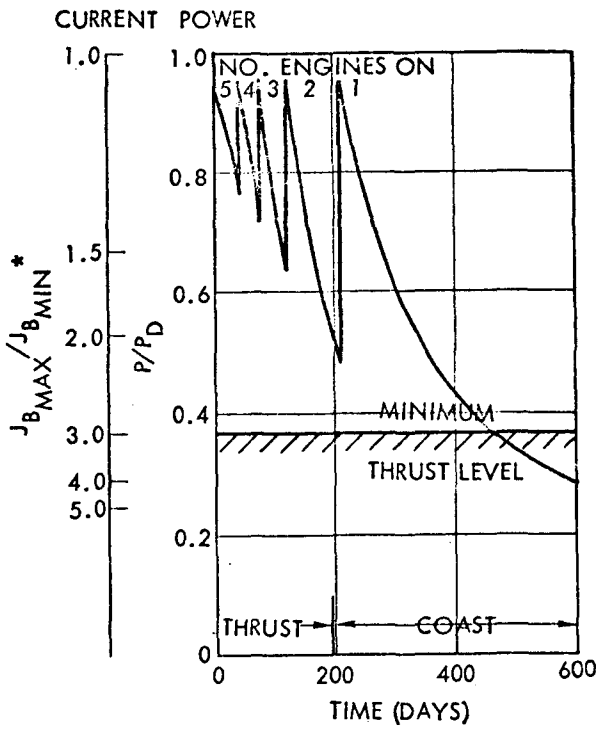

Engine Throttling Profile
(Jupiter Swingby Out-of-Ecliptic Mission, Atlas/Centaur/TE-364-4)

Figure 3-2. 8 kw Three 30-cm Thrusters (One Thruster in Standby)

Figure 3-3. 5 kw Five 15-cm Thrusters

and turnoff of engines as the spacecraft moves away from the sun are obvious from the plot. For either configuration if a failure should occur when no thruster is available in standby, the thrust phase of the mission can be extended to compensate for the loss in available energy and consequently the probability for a successful mission is extremely high.

The reliability of the SEP subsystem was evaluated for the 15- and 30-cm thruster sizes and different numbers of operating thrusters utilizing a Monte Carlo simulation technique. The mission profile for the solar passage via Jupiter swingby was utilized as typical of those for all outbound missions evaluated. The numerical results obtained from the reliability analysis in actuality might differ slightly from mission to mission. However, the general conclusions obtained from the typical profile apply directly to all exclusively outbound missions of interest.

*$J_{B_{MAX}}/J_{B_{MIN}}$, throttling level, a ratio of beam current density (ma/sq cm).

The reliability evaluation was performed with the following assumptions:

a) The thruster failure rate is ten times the nominal estimated value of 5.9×10^{-6} failures per hour.

b) One thruster is assumed to fail at the start of the mission.

c) The nominal thruster unit burn time will be no greater than half the design life of 400 days.

d) Failure of a thruster when there are no standby thrusters can be compensated for by extending the burn time at the end of the thrust phase.

The results of the reliability analysis are presented in Figure 3-4. Notice for the three 30-cm case, one additional unit is required in standby to keep the reliability of the system acceptably high.

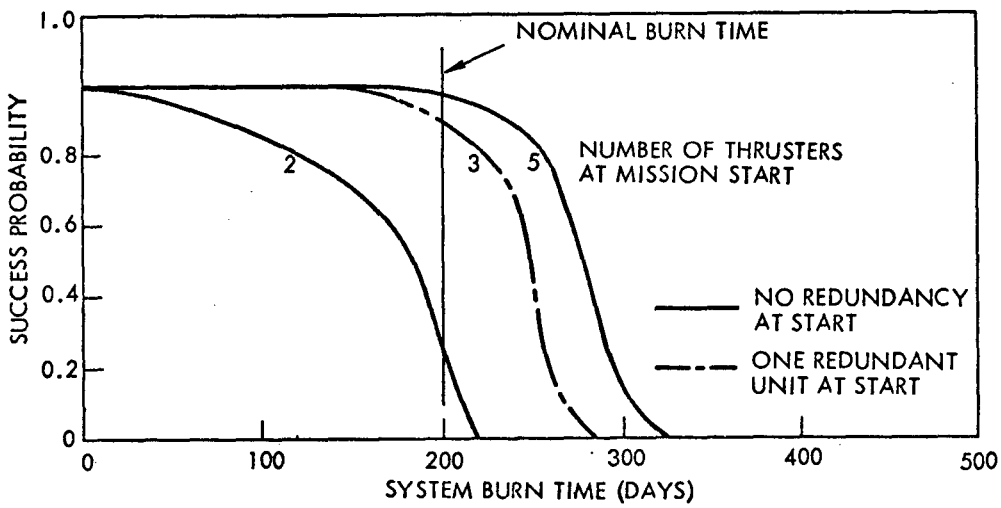

Figure 3-4. Probability of Success as a Function of System Burn Time with Two, Three, and Five Thruster System

It is interesting to note what happens to the three 30-cm thruster configuration when the 5-kw rather than the 8-kw solar array is employed with a 30 percent throttling level. As shown in Figure 3-5, one of the two operating thrusters would have to be shut down earlier as would the single thruster used near the end of burn time. This would result in a

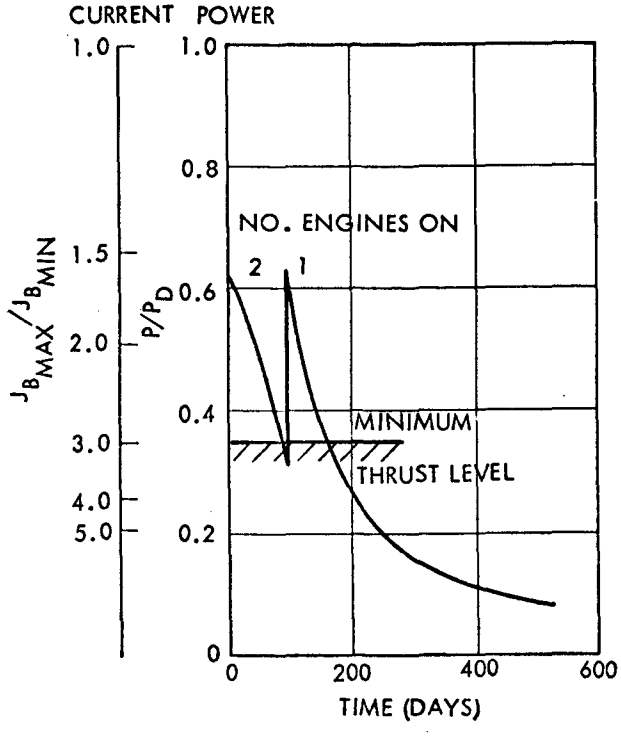

Figure 3-5. Engine Throttling Profile, 5 kw Three 30-cm Thrusters

decrease in burn time of 25 days which is equivalent to reducing the inclination to the Jupiter orbit plane from 92 to 85 degrees.

A summary of weights, burn times, C_3 energy and achievable inclination out-of-the-ecliptic is shown in Table 3-1 for the Pioneer ballistic and the Pioneer solar electric configurations. Inclination to the Jupiter orbit plane is the performance parameter of major interest here, and as can be seen there is a 60-degree improvement from the Atlas/Centaur/TE-364-4 ballistic to this ballistic augmented with an 8 kw three 30-cm thruster solar electric propulsion system.

Table 3-1. Characteristics for Atlas Jupiter Swingby Out-of-Ecliptic

Weight (lb)	Pioneer Ballistic	SEP 8 kw Three 30-cm	SEP 5 kw Five 15-cm
Injected	560	924	752
Mercury	0	165	103
Burnout	560	759	649
Dry SEP	0	199	89
Net Spacecraft	560	560	560
Burn time (days)	0	180	150
C_3 (km^2/sec^2)	88	140	130
Inclination (deg)	32	92	82

While this improvement (32 to 92 degrees) is significant, it is postulated that under normal conditions rather than outfit a Pioneer spacecraft with electric propulsion, a Titan/Centaur/TE-364-4 would be used. This launch vehicle can provide more than sufficient energy to accomplish the mission using the existing Pioneer spacecraft. However, in the event that a Titan launch pad or vehicle is not available a parametric presentation is shown in Figure 3-6 for determining the attainable inclination angle to the Jupiter orbit plane with energy derived from a strictly ballistic launch or a ballistic launch with an 8 kw three 30-cm solar electric propulsion assist. The lower curve on the left is the ballistic curve. Weight of the vehicle under consideration, in this case Pioneer F and G, equates to 88 km^2/sec^2 which, as shown, is equivalent to achieving an inclination to the Jupiter orbit plane of 32 degrees. The locus of points above the lower curve on the left represents the thrust time in days required to make up for the weight of the electric propulsion and associated components. The solar array weight is not included for this example since this is the only source of electric power on-board the spacecraft. For missions that require both RTG's and a solar array the weight of the solar array is included in the delta solar electric propulsion dry weight. The dash dot vertical lines have a slope corresponding to the weight of mercury consumed by the thrusters, and their intersection with the appropriate burn curve gives the burnout weight and the available C_3. This C_3 is equivalent to a given inclination to the Jupiter orbit plane as shown by the curve on the right. For the example shown (8-kw with three 30-cm thrusters) the burn time is 150 days, the burnout weight is 759 pounds, the C_3 = 140 km^2/sec^2 and the inclination to the Jupiter orbit plane is 92 degrees. The 5-kw solar array with five 15-cm thrusters, results, as shown in Figure 3-7, in only a C_3 of 130 and an inclination of 82 degrees following a burn time of 200 days.

3.1.2 Asteroid Belt Mapping

Asteroid belt mapping from a spinning electric propulsion spacecraft was first evaluated in 1971* for a 2- and 3-kw spacecraft having

*TRW Final Report, "Feasibility Study for a Multi-Mission Electric Propulsion Spacecraft," NASA/ARC Contract NAS2-6287, June 1971.

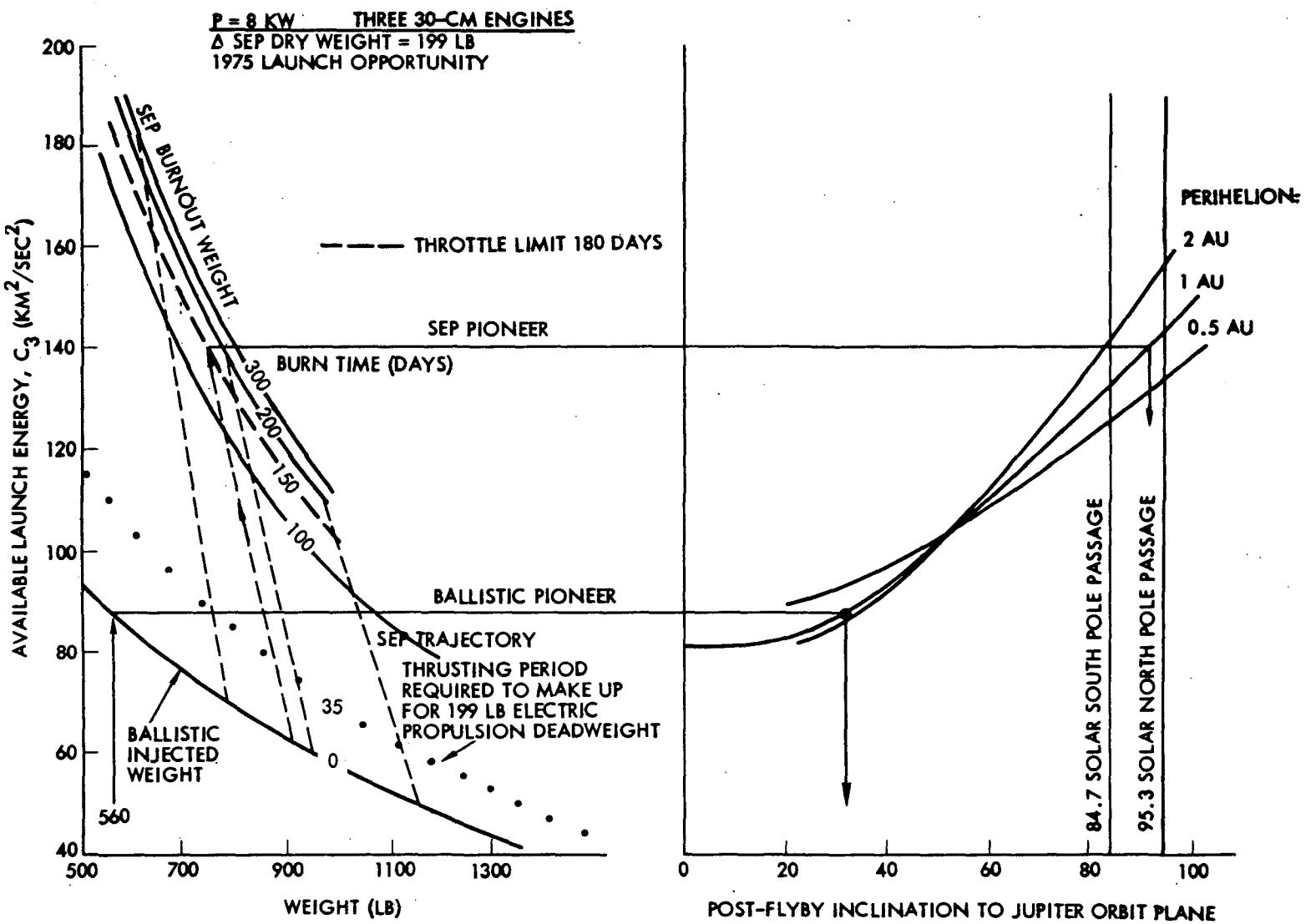

Figure 3-6. Jupiter Flyby Out-of-Ecliptic Mission
Atlas/Centaur/TE-364-4
(8 kw Three 30-cm Engines)

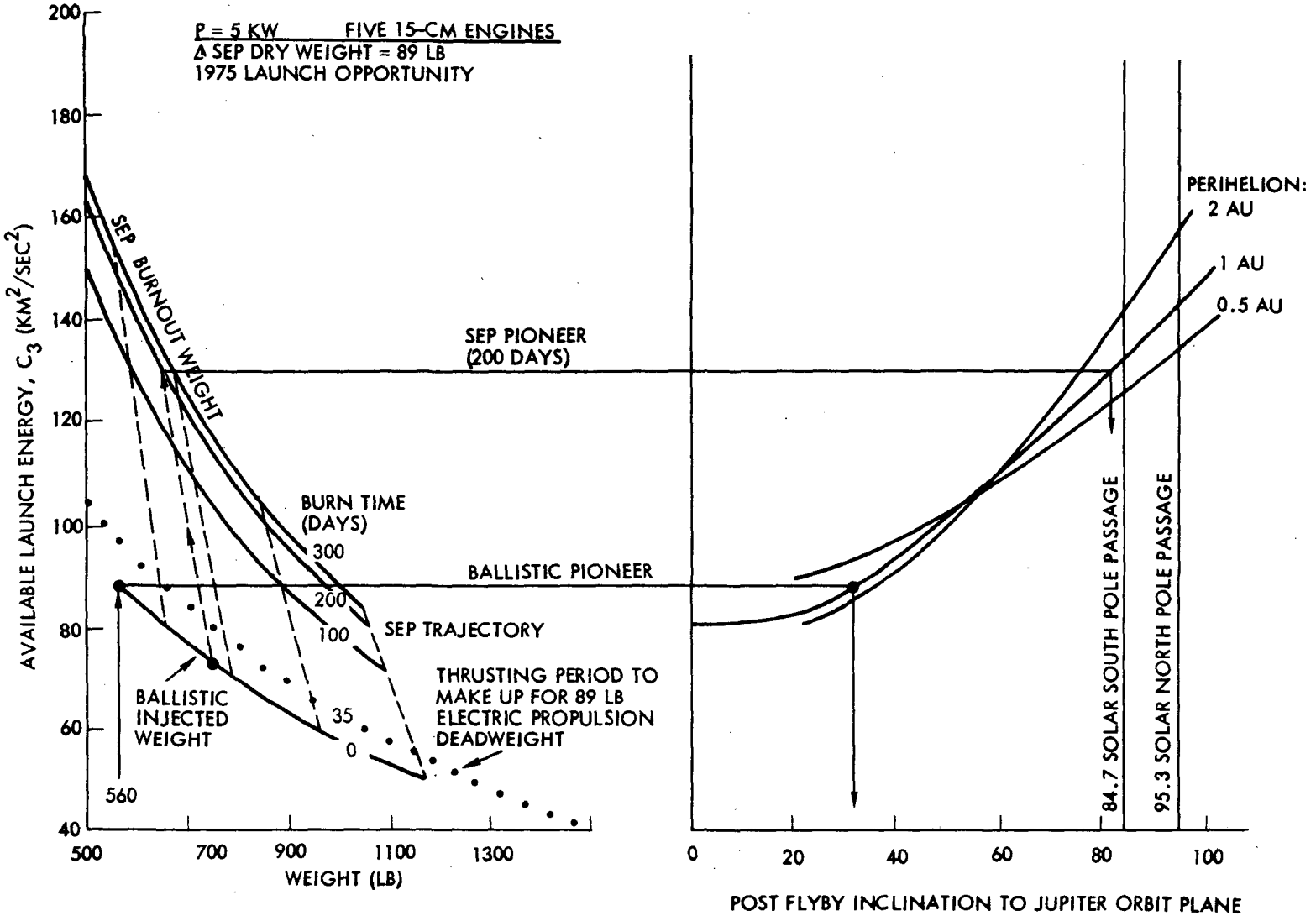

Figure 3-7. Jupiter Flyby Out-of-Ecliptic Mission
Atlas/Centaur/TE-364-4
(5 kw Five 15-cm Engines)

two or three 15-cm thrusters. The spacecraft, smaller than the Pioneer F and G was to be launched from a Thor/Delta/TE-364-4. This was an in-the-ecliptic-plane mission and time in the belt was the comparison value used.

An excellent electric propulsion precursor mission resulted in the trajectory shown in Figure 3-8 for a 3-kw spacecraft with a thrust time of 150 days. At the end of this 150 days one engine would continue to fire for an additional 500 days at 400 watts input power with the thrust axis pointing along the earth line. The effect on the orbit was not significant and the thruster life test was considered an exceptionally good technology

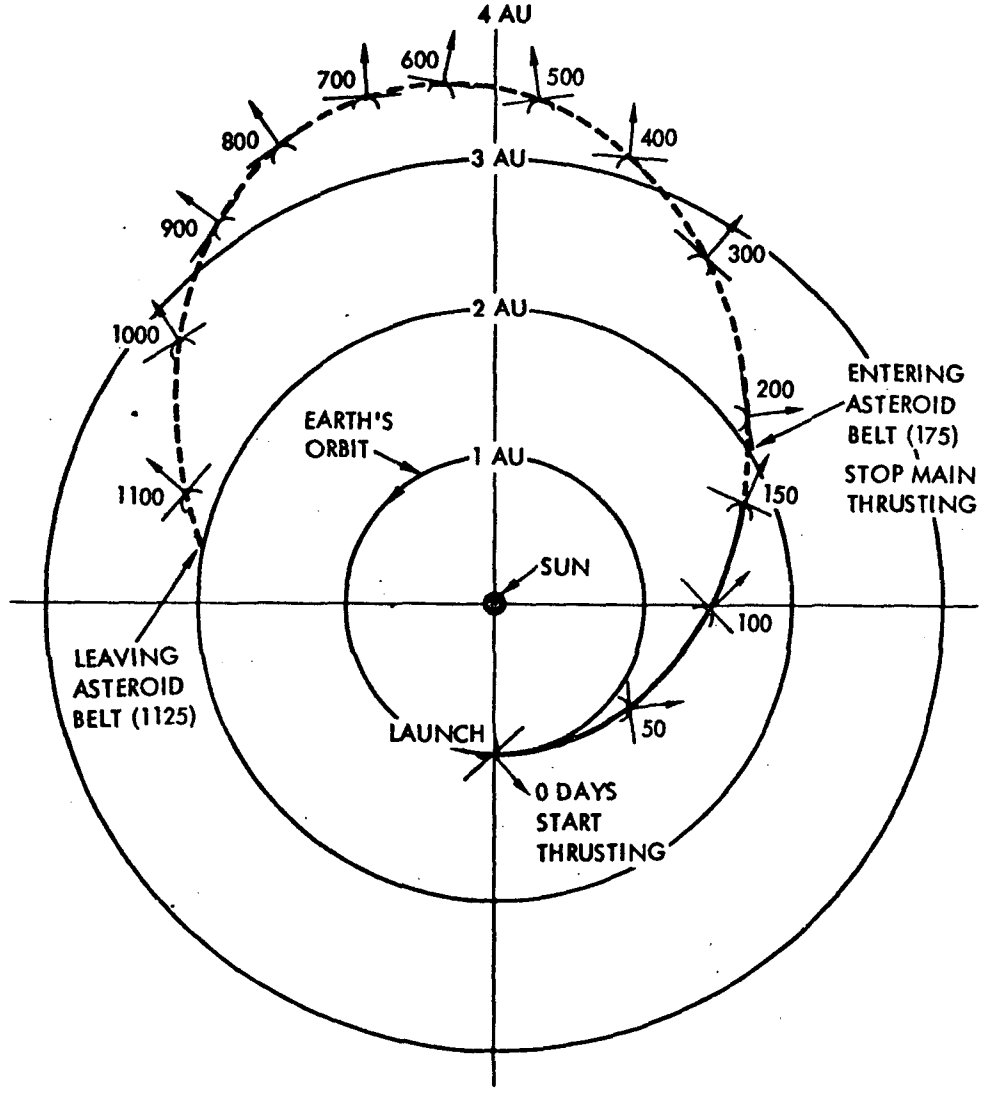

Figure 3-8. Asteroid Belt Mapper with Thor/Delta/TE-364-4 (950 Days in Belt/Mission)

evaluation. The spacecraft proposed for this mission was the 3-kw version; however, the same trajectory could be obtained using the 2-kw spacecraft but with a burn time of 500 days. Also plotted is the trajectory for a straight ballistic spacecraft having a 3-kw solar array but with the weight of the electric propulsion subsystem removed. This mission would reach only into 2.8 AU rather than 3.6 AU and would spend over 50 percent less time in the belt.

The evaluation is noted here to emphasize that asteroid belt mapping is a relatively low-energy mission probably most valuable as an electric propulsion technology development mission. If you look at a Pioneer electric propulsion spacecraft launched from an Atlas/Centaur/TE-364-4 the mapping can be accomplished out-of-plane in the asteroid belt. It is pertinent to consider not only the density of dust particles in the asteroid belt but their distribution normal to the plane of the ecliptic. Figure 3-9 shows the distribution versus heliocentric latitude (with zero degrees taken at the plane of the ecliptic) of 1563 numbered asteroids. It is postulated that dust particles are concentrated more in the plane of the ecliptic than the asteroids; this, by analogy to Saturn's rings, in which

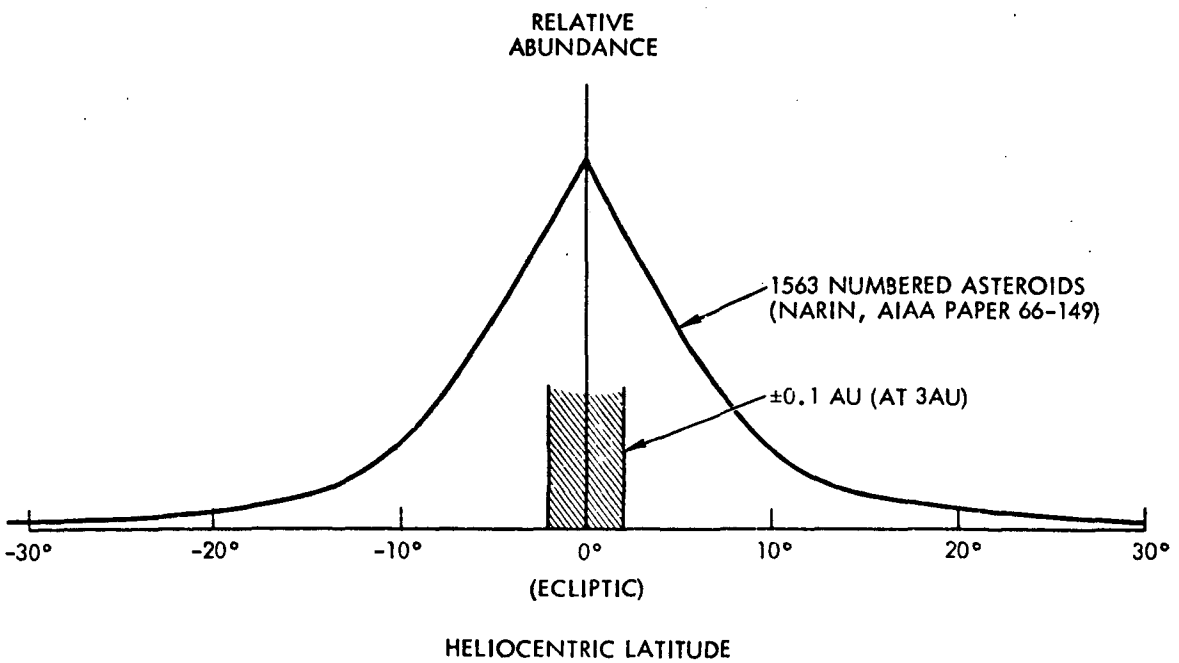

Figure 3-9. Asteroid Distribution Normal to Plane of Ecliptic

the extreme thinness may have resulted from numerous collisions among originally larger bodies. Based on reflected light observations, it has been suggested that the asteroid dust belt is within a band of ±0.1 AU of the ecliptic. This would correspond to ±2 degrees in heliocentric latitude.

The asteroid belt penetration during the mission is inclined to the ecliptic by 10 degrees and energy for this out-of-plane component is taken from the launch vehicle rather than the solar electric propulsion. Even with this use of launch vehicle energy the Atlas is oversized for the mission and would probably be offloaded. Table 3-2 compares the operating characteristics of the electric propulsion mission with the strictly ballistic mission.

Table 3-2. Asteroid Belt Mapper Mission Characteristics

Item	Ballistic	SEP
Injection weight (lb)	560	720
Mercury weight (lb)	0	60
C_3 (km^2/sec^2)	88	68.5
Aphelion (AU)	3.5	4.0
Inclination to belt (deg)	10	10
Time in belt (days)	905	1145
Burn time (days)	0	65
Solar electric configuration	---	5-kw Five 15-cm

A heliocentric trajectory for the solar electric asteroid belt mapper is shown in Figure 3-10. Inclination to the ecliptic can be either ±10 degrees but not both. Five kw with five 15-cm thrusters was selected rather than the 8 kw three 30-cm since this mission has a minimal energy requirement. Advantages of solar electric over ballistic are not significant enough to make this a good Pioneer solar electric propulsion mission.

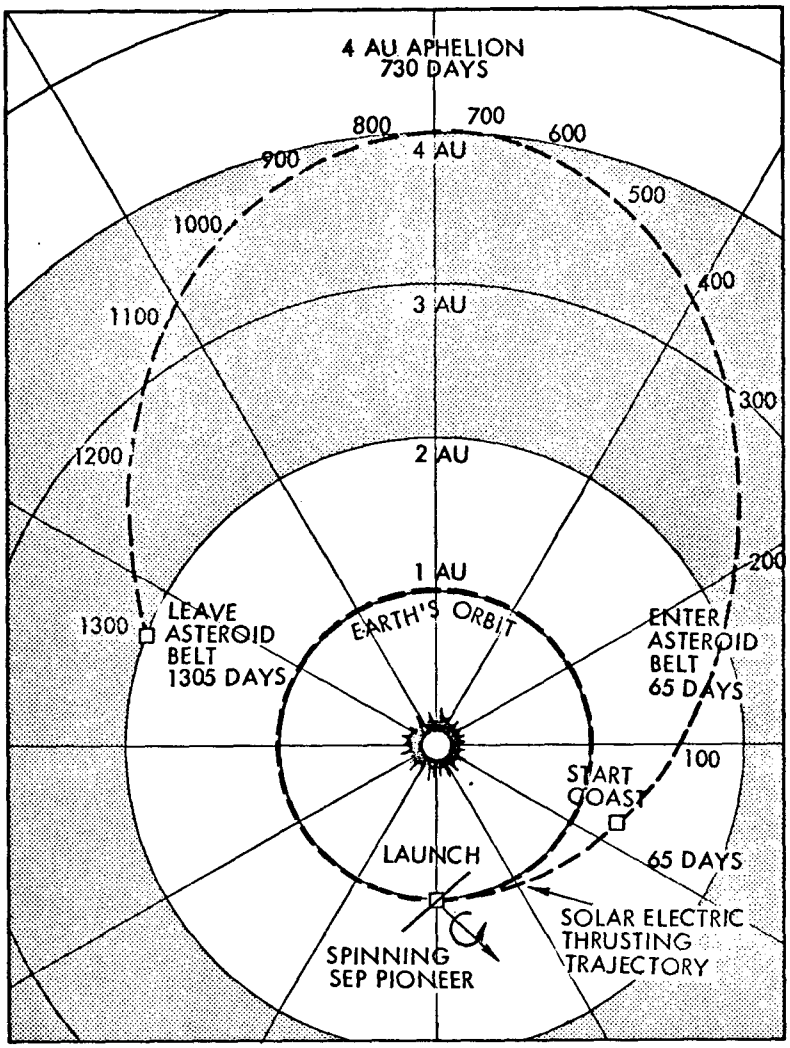

Figure 3-10. Asteroid Belt Mapper Mission Trajectory (Atlas/Centaur/TE-364-4 with 5 kw and Three 30-cm Thrusters)

3.1.3 Comet Rendezvous

A survey was made of comets available for rendezvous during the 1975 through 1980 period and the list of Table 3-3 was compiled.

Tempel II was selected because there were two launch opportunities within the window and because it was a moderately energetic mission which appeared acceptable for either the 5- or 8-kw electric propulsion spacecraft. There was considerable doubt that the D'Arrest rendezvous could be performed with the 5-kw and probably not with the 8-kw because of the almost 20-degree inclination to the ecliptic plane. It was clear that

Table 3-3. Survey of Comets Available for Rendezvous, 1975 through 1980

Comet	Launch (Year)	Periapsis (Year)	Period (yr)	Periapsis (AU)	Apoapsis (AU)	Inclination (deg)
Encke	'78.2	'80.9	3.3	0.34	4.09	12
Tempel II	'75.5	'78.2	5.3	1.37	4.68	12.5
	'80.8	'83.5	5.3	1.37	4.68	12.5
Kopff	'80.6	'83.3	6.3	1.52	5.32	4.7
D'Arrest	'80	'82.7	6.7	1.38	5.73	19.6
Forbes	'78	'80.7	6.4	1.55	5.36	4.6
Tuttle-Giacobini-Kresák	'76.2	'78.9	5.5	1.11	5.1	13.8
Brookes 2	'77.9	'80.6	6.7	1.76	5.36	5.6

the Encke mission could not be performed with these small solar arrays because of the 0.34 AU gravity well. Also the Pioneer spacecraft would require major design modification if it went closer to the sun than 0.7 AU. The other available comet rendezvous missions were considered good candidates for either the 5- or 8-kw Pioneer solar electric spacecraft.

The Tempel II mission was evaluated for both the 5 kw five 15-cm thruster and the 8 kw three 30-cm thruster cases. The 5-kw configuration had a total thruster burn time of 550 days while the 8-kw system reduced the burn time by 43 percent to 314 days. Thruster throttling profiles are shown in Figures 3-11 and 3-12 for the cases mentioned above. The curve in each figure shows the available power divided between the maximum number of thrusters as a duration of days into the mission. The gradual reduction in available power during the outbound leg of the mission requires the thrusters be throttled down to the extent possible, then turnoff of a thruster occurs and return to the maximum thruster output and a commencement of throttling again. During the inbound leg of the mission, as power is gradually increasing, the thrusters are throttled up until sufficient power is available to support another thruster. This thruster is then turned on and the sequence repeated. Following establishment of the trajectory the solar electric

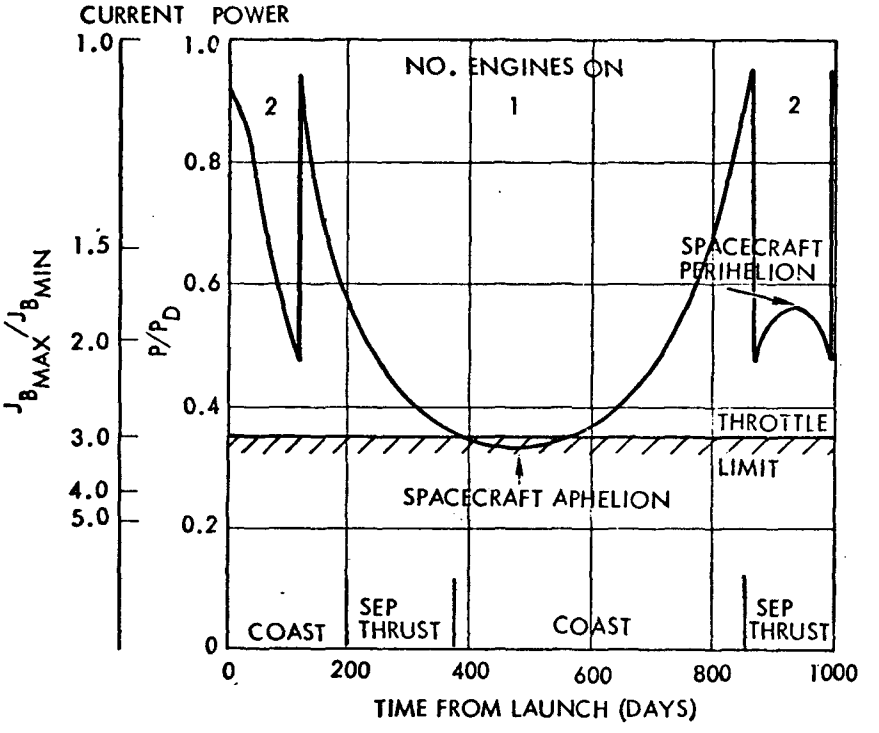

Figure 3-11. Thruster Throttling Profile for 8 kw Three 30-cm Electric Propulsion Configuration (Atlas/Centaur/TE-364-4)

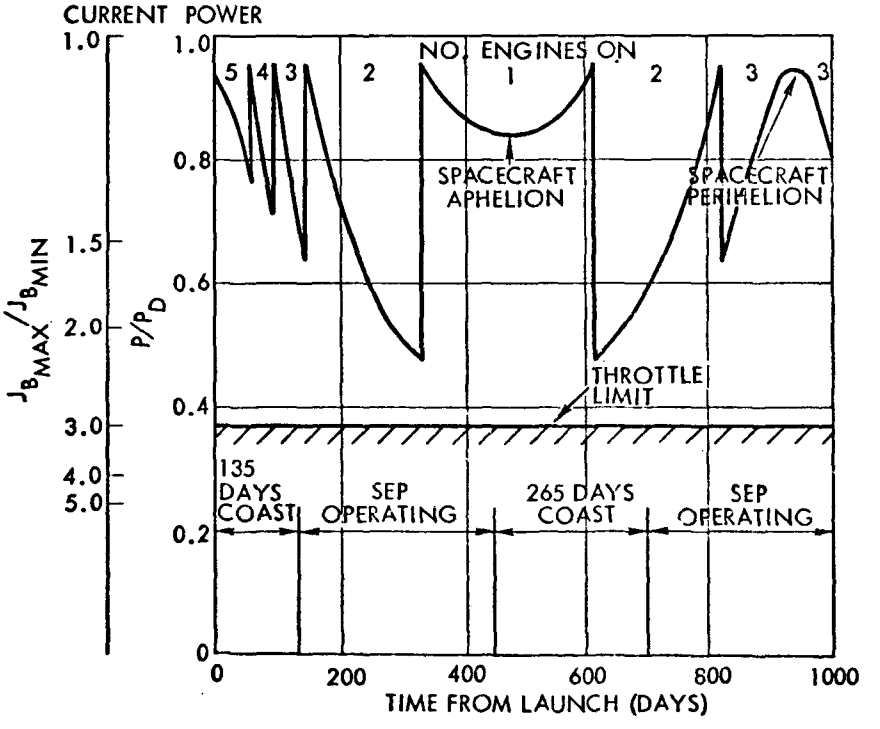

Figure 3-12. Thruster Throttling Profile for 5 kw Five 15-cm Electric Propulsion Configuration (Atlas/Centaur/TE-364-4)

propulsion operating times were included on the abscissa, thereby defining the number of thrusters and their level of throttling as a function of days into the mission. Notice that for the five 15-cm case the fourth and fifth thrusters are in standby and will not be used unless a failure occurs. In the case of the three 30-cm thrusters, one of the three thrusters is in the standby mode. The reliability for both the electric propulsion systems during the Tempel II mission is shown in Figure 3-13.

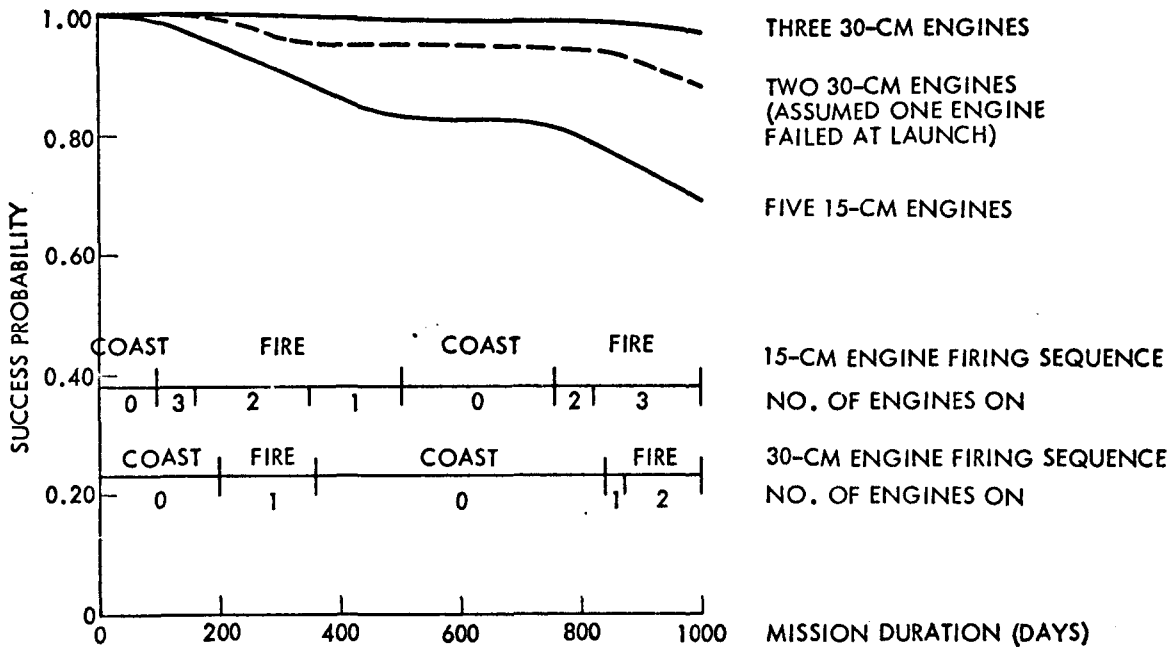

Figure 3-13. Probability of Electric Propulsion Success

Failure rates for the thrusters and associated power processors are discussed in Appendix A. Assumptions for the reliability calculations are given below:

a) Failure rate for the thruster is 5.9×10^{-6} failures per hour operating and 0.59×10^{-6} failures per hour in standby.

b) Failure rate for the power processor is 3.6×10^{-6} failures per hour operating and 0.36×10^{-6} failures per hour in standby.

c) Design life for thruster is 400 days.

d) A standby thruster and power processor is available throughout mission life for the 30-cm configuration and one or more standby thrusters and power processors are available after 40 days for the 15-cm system.

Reliability for the Tempel II mission is not as high as for the strictly outbound missions. This is a result of the rendezvous requirement which means burn times must occur at prescribed intervals for thrust vectoring, while for the strictly outbound missions thrust vectoring is not that critical.

Figure 3-14 shows (for the Tempel II rendezvous mission) the heliocentric trajectory for a Pioneer spacecraft augmented with three 30-cm thrusters and an 8-kw solar array following launch from an Atlas/Centaur/TE-364-4. The burn time for the three 30-cm thruster configuration begins 200 days into the mission and lasts 160 days. Following aphelion passage at 840 days the thrusters are again activated and burn until rendezvous time at 1000 days into the mission.

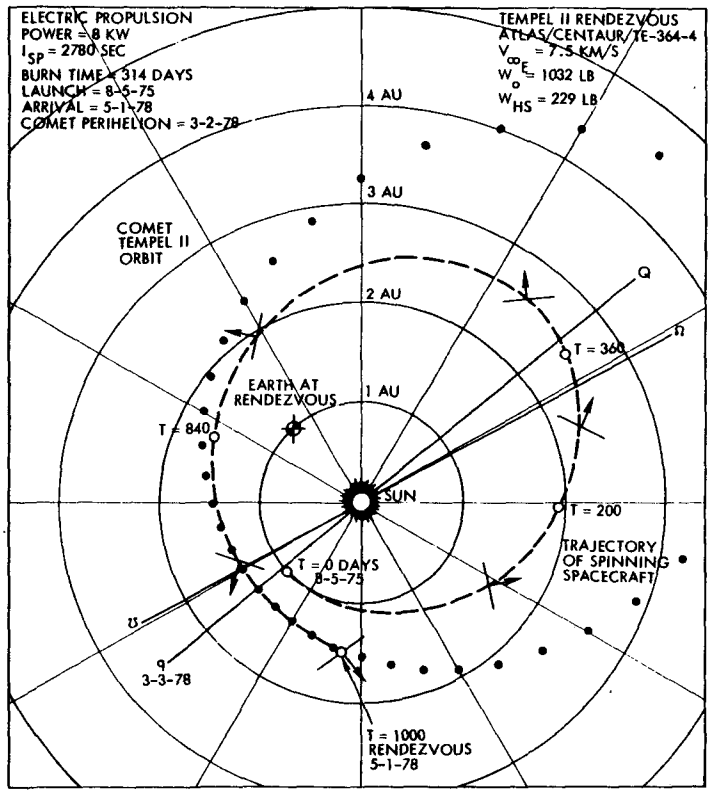

Figure 3-14. Tempel II Heliocentric Trajectory (Atlas/Centaur/TE-364-4)

The heliocentric profile for the 5 kw five 15-cm mission is shown in Figure 3-15. This does not provide as good a performance as the 8-kw system primarily because of the longer burn time and lower overall reliability. Thrusting commences 135 days after launch and continues to day 445 when the direction of thrust no longer contributes to matching the comet's trajectory. Thrusting starts again on the 710th day and continues until just before rendezvous at 1000 days.

Midcourse corrections are continuously in process during the thrust phase as the position of the spacecraft is tracked from the ground and the thrust vector pointing updated as required. Near the end of the mission approximately 70 days prior to rendezvous, following on-board detection of the comet, a hydrazine attitude correction is performed which will remove the errors existing because of the comet ephemeris inaccuracy and the tracking error due to ion engine generated noise.

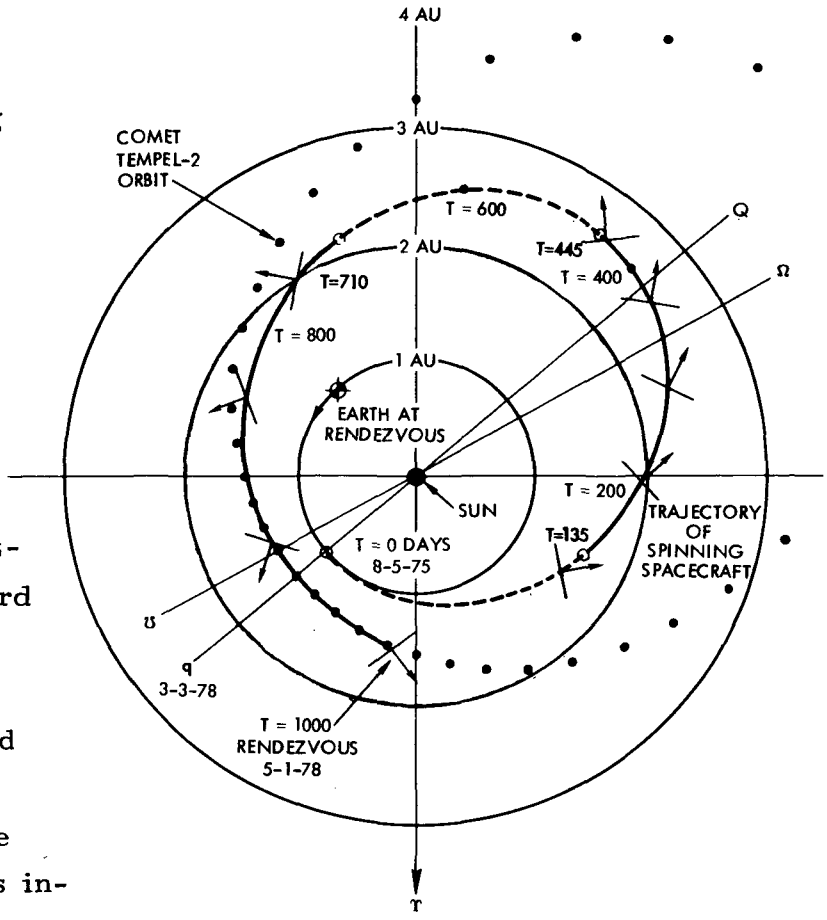

Figure 3-15. Tempel II Rendezvous Mission Profile (5-kw Spacecraft)

Burn time for both the 8- and 5-kw configurations for various injected and burnout weights over an earth injection velocity range of 7 to 9.5 km/sec are plotted in Figure 3-16. These curves point out the difficulty in reducing the burn time below 300 days and the sensitivity of the burn time to spacecraft weight.

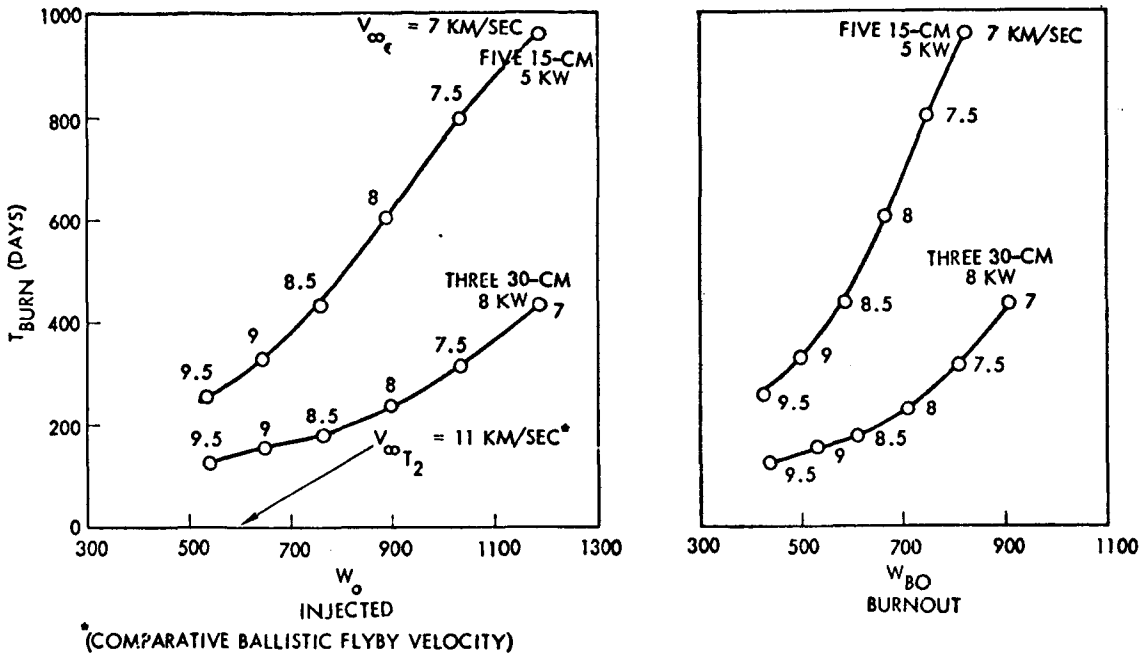

Figure 3-16. Tempel II Rendezvous ($V_{\infty_{T_2}}$ = 0) (Atlas/Centaur/TE-364-4)

3.2 1 TO 30 AU MISSIONS

3.2.1 Saturn, Uranus, and Neptune Flyby

Direct flyby missions to the major planets beyond Jupiter were evaluated to determine the performance advantage derived from the addition of electric propulsion to the Pioneer spacecraft. Both the five 15-cm and the three 30-cm electric propulsion configurations were evaluated for the Saturn, Uranus, and Neptune missions, using the Titan/Centaur/TE-364-4. The performance parameter used for comparison of ballistic with solar electric propulsion augmentation was flight time in transit to the planet and also payload increase if the flight times were held the same as for the ballistic flights.

The performance capability for electric propulsion beyond 5 AU is reduced markedly because of the necessity to supply electric power from a source other than the sun. This necessitates the inclusion of RTG's, similar to those on the present Pioneer, which increases the weight of the spacecraft by 140 pounds. Ejection of the solar arrays following electric propulsion burn time has been evaluated with the conclusion that the small increase in performance does not merit the complexity.

Engine throttling and sequencing profiles for the 8 kw, three 30-cm configuration and the 5 kw, five 15-cm configuration for Saturn, Uranus, and Neptune direct flybys are shown in Figures 3-17 and 3-18. Burn time for one thruster can be extended from 180 to 340 days for the five 15-cm system but with only a small performance improvement. The 30-cm system operates from one thruster after 90 days; however, due to the larger thruster the performance improvement is appreciable out to 145 days

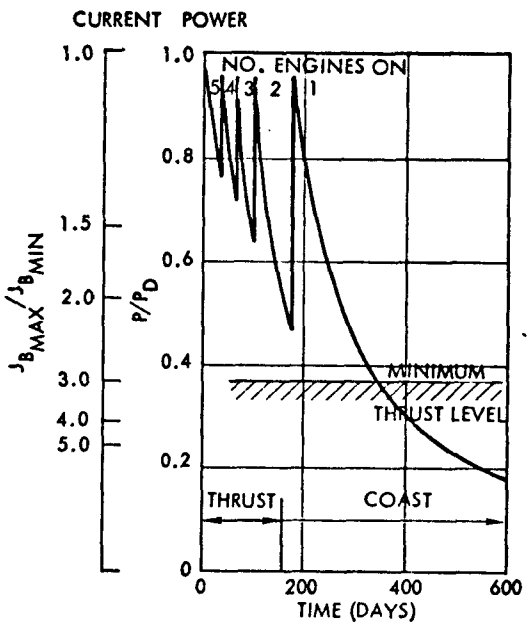

Engine Throttling Profile
(Saturn, Uranus, and Neptune Direct Flyby with Titan/Centaur/TE-364-4)

Figure 3-17. 5 kw Five 15-cm Thrusters

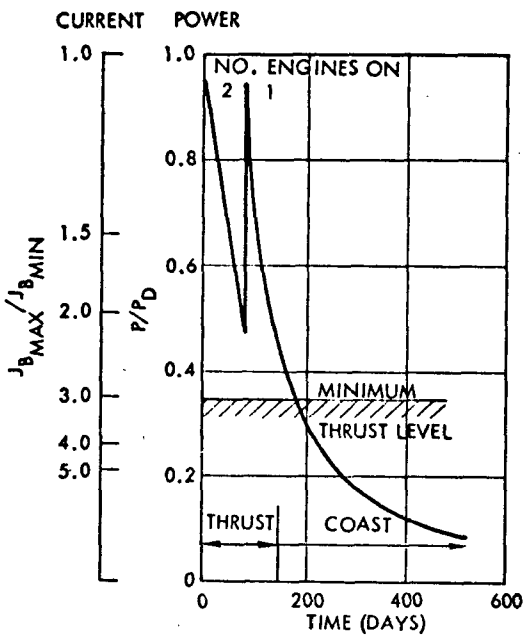

Figure 3-18. 8 kw Three 30-cm Thrusters

which occurs when the throttling ratio is 2.2 to 1. The throttling could be continued out to 3 to 1 at 180 days but with only very slight benefit in performance.

Reliability results for the thruster configurations shown are presented in Figure 3-19. Failure rates for the thrusters and associated power processors are discussed in Appendix A. Assumptions for the reliability calculations are given below.

- Failure rate for the thruster is 59×10^{-6} failures per hour operating and 5.9×10^{-6} failures per hour

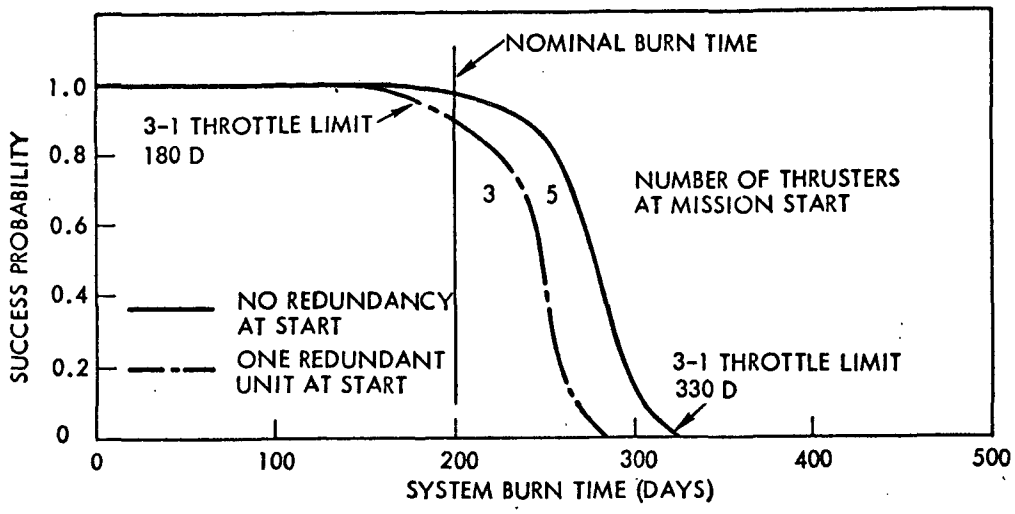

Figure 3-19. Reliability for Electric Propulsion System, Saturn, Uranus, and Neptune with Five 15-cm and Three 30-cm Thrusters (10 Times Anticipated Failure Rate)

in standby. This is 10 times anticipated failure rate for conservatism.

- Failure rate for the power processor is 3.6×10^{-6} failures per hour operating and 0.36×10^{-6} failures per hour in standby.
- Design life for thruster is 400 days.
- A standby thruster and power processor is available throughout mission life for the 30-cm configuration and one or more standby thrusters and power processors are available after 40 days for the 15-cm system.
- Failure of thruster in early part of mission can be compensated for by longer burn time at end of mission.

The improvement in reliability for the five 15-cm thruster system is due to the larger number of standby thrusters available after the first 80 days. This has a stronger influence on reliability than the shorter mission burn time required for the three 30-cm system. Even with 10 times the anticipated failure rate the reliability for either of these configurations is in excess of 0.95. Unlike the comet rendezvous mission, a failure occurring when no redundancy is available is not catastrophic but only extends the burn time or increases the transit time to the planet.

Results of the mission analysis for the 5 kw five 15-cm thruster system using the Titan IIID/Centaur/TE-364-4 launch vehicle are shown in Figure 3-20. This is a parametric presentation which allows variations in spacecraft science or electric propulsion subsystem weight. The method of using the figure is as follows. Enter the curve from the left using the appropriate injection weight; the zero burn time curve is

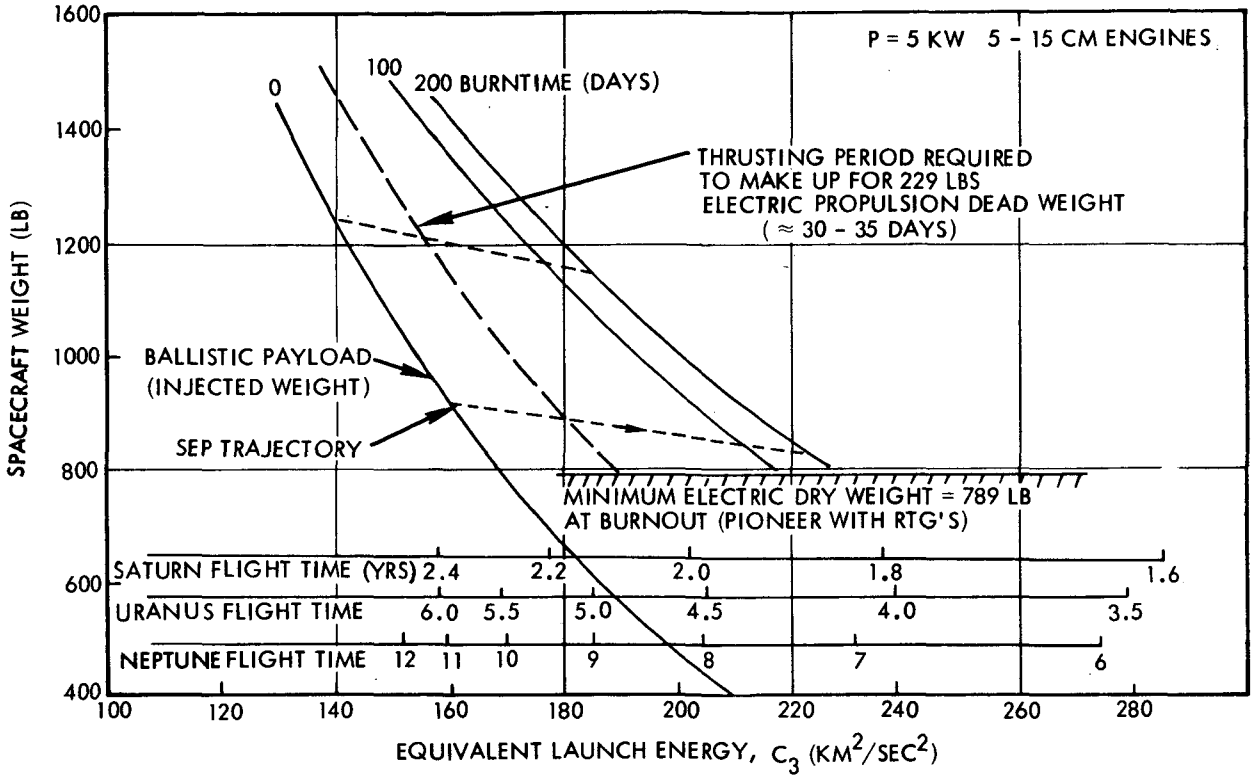

Figure 3-20. C_3 Increase with Solar Electric Augmentation (Titan Launch) (Saturn, Uranus, and Neptune Direct Flyby)

representative of the energy provided by the launch vehicle, in this case the Titan/Centaur/TE-364-4. If the spacecraft does not have electric propulsion augmentation, the transit time to Saturn, Uranus, or Neptune can be found on the abscissa along with the C_3 launch energy (km^2/sec^2). If electric propulsion is provided, follow the SEP trajectory line to the burn time curve. The trajectory line is representative of the weight of mercury consumed during the burn time. In this case, from zero to 200 days consumes 90 pounds of mercury. The required transit time

to Saturn, Uranus, or Neptune can be found on the abscissa at the intersection of the SEP trajectory line with the burn time curve. The dashed burn time line at approximately 35 days is the amount of burn time necessary to compensate for the electric propulsion subsystem gross weight, i.e., solar array, thrusters, power processors, mercury, tankage, plumbing, etc.

As can be seen from Figure 3-20 the C_3 without electric propulsion and a 560-pound Pioneer spacecraft would be 190 km^2/sec^2 which gives a flight time of 2.1, 4.8 and 8.7 years to Saturn, Uranus, or Neptune, respectively. Correspondingly, the electric propulsion Pioneer spacecraft would weigh 789 pounds and have a C_3 of 230 km^2/sec^2 for a 200-day burn, which gives a flight time of 1.9, 4.2, and 7.2 years to Saturn, Uranus, or Neptune; a savings in flight time of 10, 13, and 17 percent, respectively. If the flight time were to remain the same as for the ballistic mission the energy derived from electric propulsion could be used to accommodate a larger payload. The additional payload would be 310 pounds, a 55 percent increase over the 560-pound Pioneer ballistic spacecraft. This 310 pounds might be used for an atmospheric probe drop into the atmosphere of one of the major outer planets or for a deboost engine to achieve orbit.

The electric propulsion results just described were for the 5 kw five 15-cm thruster configuration weighing 789 pounds. Also evaluated was an 8 kw three 30-cm thruster configuration weighing 899 pounds. Figure 3-21 gives the results of these analyses in a parametric form so that changes in weight can be accommodated. The improvement in performance over the five 15-cm configuration, as can be seen, is very slight. The C_3 improvement is only 9 km^2/sec^2, which reduces the flight time to Saturn by 15 days, Uranus 40 days, and Neptune 80 days. There is clearly no significant improvement of one system over the other for this particular set of missions.

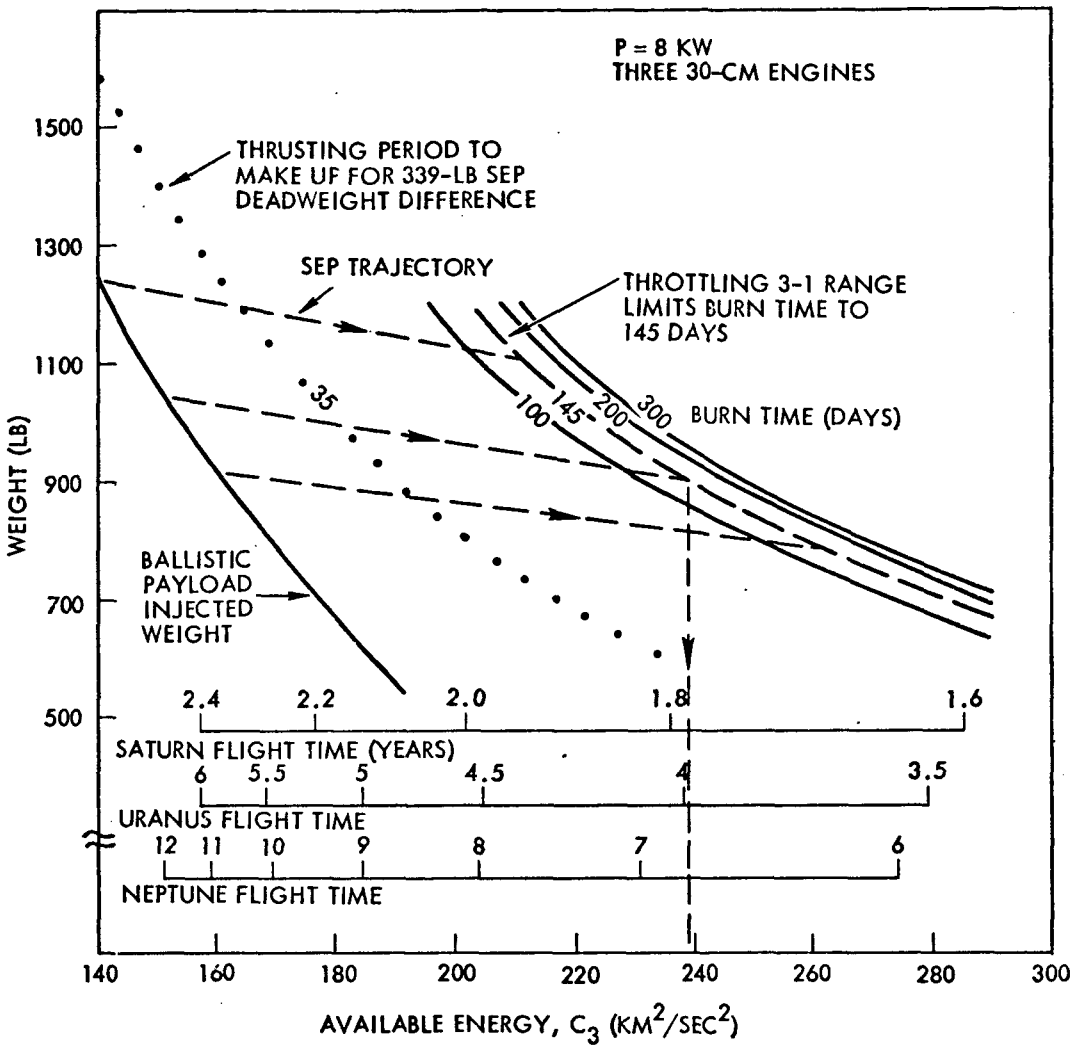

Figure 3-21. C_3 Increase with Solar Electric Augmentation (Titan Launch) (Saturn, Uranus, and Neptune Direct Flyby)

3.3 1 TO ≤0.7 AU MISSIONS

The spin-stabilized electric propulsion spacecraft had not previously been evaluated for inbound missions, nor had the Pioneer spacecraft. Clearly any mission requiring a spacecraft to approach the sun closer than 0.7 AU will require a basic configuration dictated by thermal constraints. A modification of this magnitude to the Pioneer spacecraft was beyond the scope of the study. Nevertheless, the mission analysis was performed in an attempt to learn what other design problems might

exist and what the advantages of electric propulsion might be. Consequently as a part of this study, but with minor emphasis, the electric propulsion and thermal aspects of an inbound mission were evaluated. No specific mission was called out in the Statement of Work and consequently from a mission analysis standpoint, the maximum solar periapsis was used as the performance parameter for comparing augmented electric propulsion capability with strictly ballistic flights. This comparison was made using the Atlas and Titan launch vehicles but only for a 3 kw five 15-cm system.

It was found that the solar array temperatures would remain within fabrication state-of-the-art limits to 0.57 AU. If the arrays were perpendicular to the sun, as with a three-axis spacecraft, only 0.68 AU could have been tolerated. Also, from the standpoint of thermal acceptability without major modifications, the same Pioneer spacecraft proposed for the 1 to 5 AU missions is acceptable into 0.7 AU. Antenna coverage over the necessary thrust vector angles without new development is acceptable into 0.56 AU. A three-axis spacecraft with its gimballed antenna has the advantage of being able to operate in closer than 0.56. However, it has the disadvantage of solar array thermal problems much earlier. This results in the necessity for making the three-axis system's solar arrays rotatable to reduce the sun's angle of incidence when the spacecraft gets closer in than 0.68 AU.

Figure 3-22 shows the throttling sequence for the mission. Notice that the mission requires only a 3-kw solar array because of the increasing solar intensity. The mission starts with five thrusters throttled to a nominal capacity and gradually throttles up to full capacity. The maximum available power cutoff point is a function of temperature. The array will have to be continuously rotated from approximately 0.6 AU on in to periapsis to keep the temperature below 110^{o}C which is a typical solar array design limit.

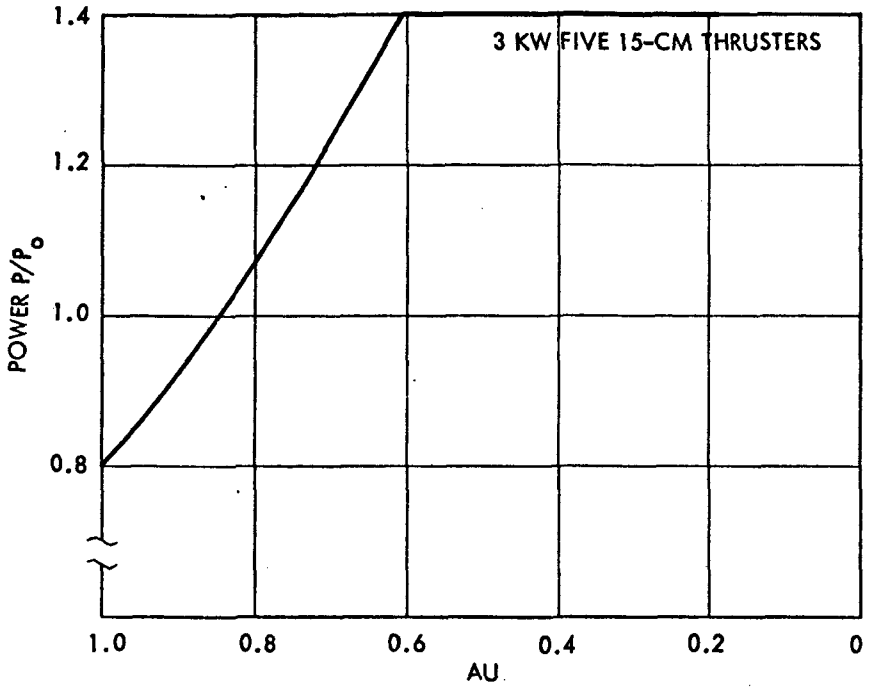

Figure 3-22. Throttling Sequence (Inbound Mission, Titan Launch)

Reliability of the electric propulsion for this mission will be excellent, above 0.98 because the redundancy provided with five thrusters is excellent and since the mission is short — 70 days for the Titan and 80 days for the Atlas. Figure 3-23 shows the heliocentric trajectories for the two missions. Performance for a three 30-cm configuration would have been about the same due to the added weight and the short burn time, and results of the comparison analyses between ballistic and electric propulsion augmentations are shown parametrically in Figures 3-24 and 3-25.

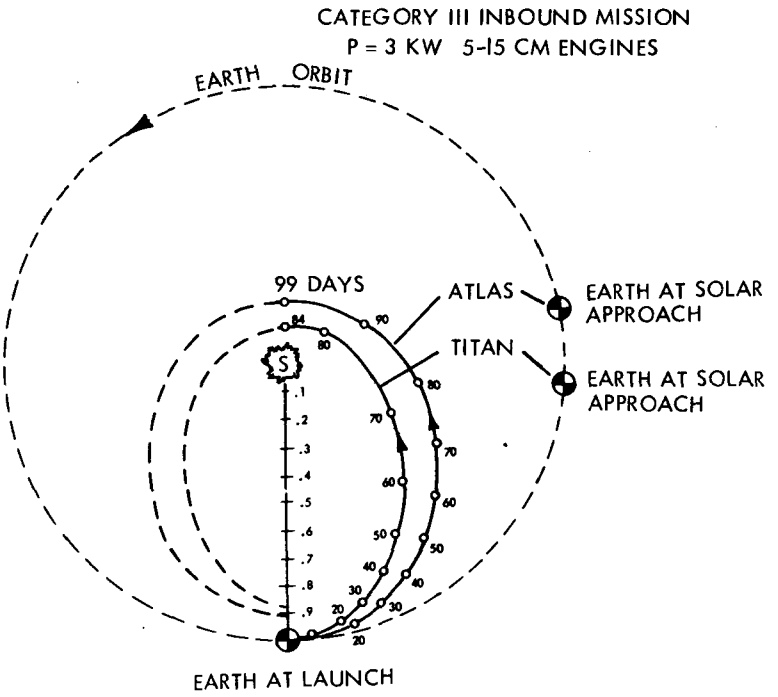

Figure 3-23. Inbound Mission Profiles

Figure 3-24 describes the mission performance using an Atlas/Centaur/TE-364-4 launch vehicle with an injected weight of 660 pounds and Figure 3-25 illustrates use of a Titan/Centaur/TE-364-4 and has a launch weight of 663 pounds. Both spacecraft carry a 3-kw solar array with five 15-cm thrusters. The difference in weight results from three-pound difference in mercury, the Titan carrying the slightly heavier load with 71 pounds of mercury.

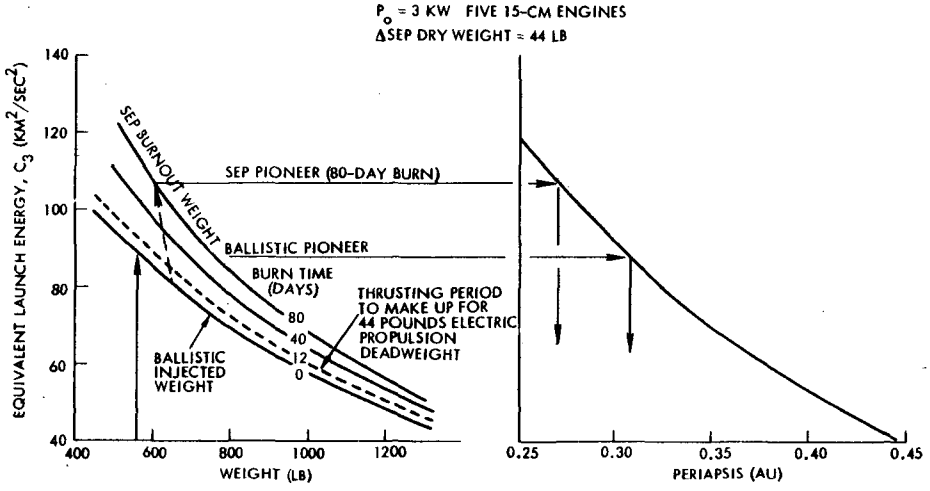

Figure 3-24. Solar Electric Pioneer Inbound Mission, Atlas/Centaur/TE-364-4

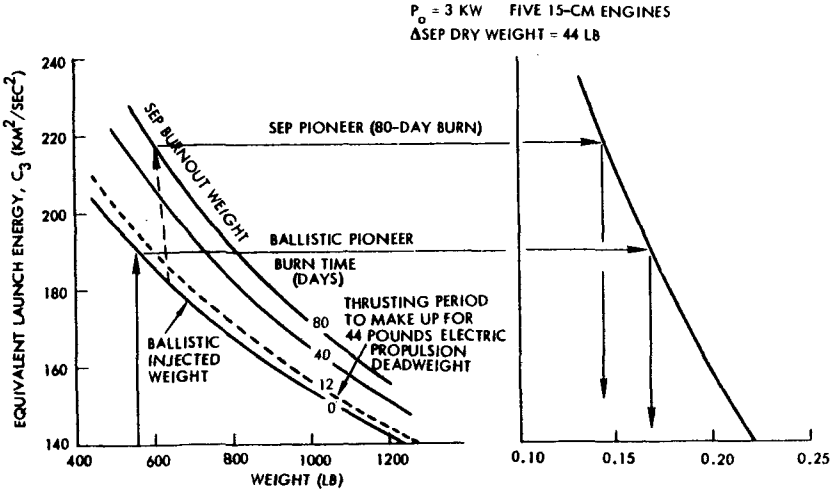

Figure 3-25. Solar Electric Pioneer Inbound Mission, Titan IIID(5)/Centaur/TE-364-4

As can be seen, the electric propulsion thrust over the relatively short period of one-half the orbit combined with the low-thrust to mass ratio yields a marginal performance over a ballistic flight, the Atlas mission increasing perihelion by 10 percent from 0.31 to 0.27 AU and the Titan mission by 18 percent from 0.17 to 0.14 AU.

3.4 GUIDANCE ANALYSIS*

A preliminary guidance analysis was conducted for the Jupiter swingby to out of the ecliptic to determine the special problems arising from a low-thrust spinning spacecraft. This analysis encompassed the low-thrust phase and the terminal guidance phase. The low-thrust phase was done to ensure that injection errors could be corrected and to determine the magnitude of the residual error for midcourse propellant sizing. (Correction of errors made during the low-thrust period were not attempted during the low-thrust but were corrected chemically at the conclusion of thrusting.) The terminal guidance phase was done to ensure that a comet rendezvous mission could be carried out.

3.4.1 Low-Thrust Guidance Phase

A summary of the general guidance analysis made during the low-thrust phase is shown in Figure 3-26. Figure 3-26(b) is for a three-stage launch vehicle with a spin-stabilized third stage. While the magnitude of the injection error shown is not for a specific vehicle, it is typical of three-stage vehicles and is shown projected on the B · T and B · R plane, a plane at the planet perpendicular to the incoming asymptote centered about the target point and in the plane of the ecliptic.

This injection error will be corrected during the low-thrust burn phase, as shown in Figure 3-26(c) while the spacecraft thrust axis is oriented at 45 degrees to the sun line. This fixed orientation requires

*Certain figures and tables in this section were originally published in the "Midterm Briefing for a Multiple Asteroid Flyby Study," TRW for NASA/ARC, Contract NAS2-6866, dated 12 July 1972 and in the final report on the "Feasibility Study for a Multi-Mission Electric Propulsion Spacecraft," TRW for NASA/ARC, Contract NAS2-6287, dated 18 June 1971.

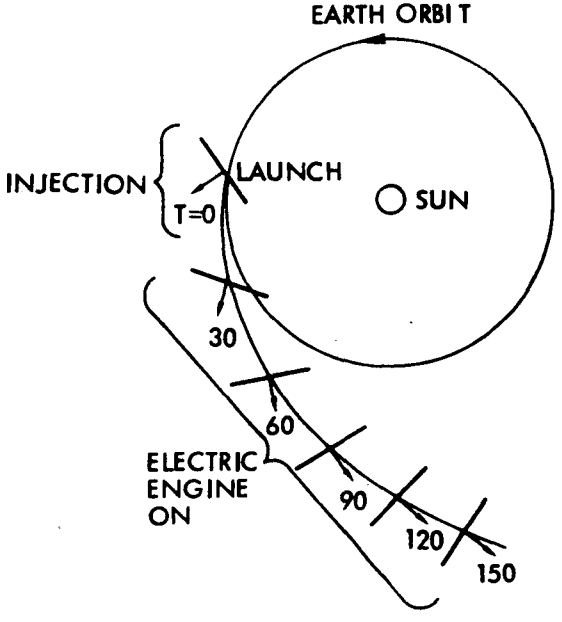

(a)

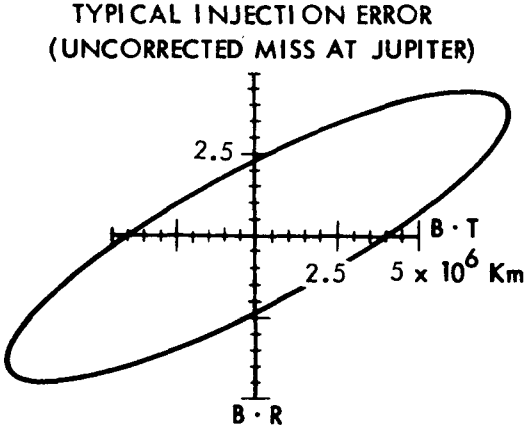

(b)

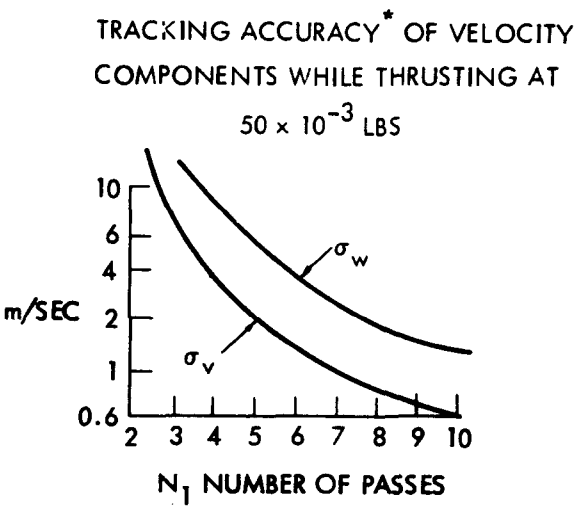

(c)

*JORDAN, REFERENCE

Figure 3-26. Guidance Analysis Summary

that the injection error be corrected when the opportunity is available as shown by the typical correction sensitivities at given flight times in Figure 3-26(c). The semi-major axis of the miss ellipse in Figure 3-26(b) can be corrected and somewhat later the minor axis can be corrected; this can be accomplished with very small changes to the thrust vector axis. Figure 3-26(a) shows the tracking accuracy estimated while the electric propulsion system is thrusting at 50 millipounds.* As can be seen, with a relatively small number of observations, the major error components can be determined during the burn period. From this information the thrust vector is oriented to correct for booster errors.

Correction of the principal execution errors for the spacecraft is affected by the accuracy to which the thrust axis can be oriented. The pointing accuracy developed by the attitude control subsystem (see Section 5) can measure the spin axis orientation to better than 1/4 degree and the attitude control propulsion system can move the spacecraft spin axis to better than 1/4 degree of the desired direction. Since the thrust vector is aligned along the spin axis, the error in the spin axis orientation is acceptably small. The principal error during electric propulsion thrusting is in thrust magnitude and, to the extent that it is random, it is insignificant. To the extent that there is a bias, the spacecraft can be tracked following the low-thrust burn, and these errors eliminated with the chemical midcourse propulsion system. It should also be noted that because of the spin there are no low-thrust alignment problems, and also no torques initiated during a portion of the spin cycle.

A model of the injection error of the Atlas/Centaur/TE-364-4 is shown in Figure 3-27. The 3σ dispersions at injection are indicated both in position and in velocity. It is clear that the velocity components dominate and, in particular, that the 75m/sec along the velocity vector and the 78 m/sec in the "W" direction dominate the entire system. These errors are shown as a simplified nominal Pioneer F and G trajectory error ellipse with a velocity and angle error along the "V" axis. Figure 3-28 shows the Pioneer-corrected error at the center.

*J. F. Jordan, "Orbit Determination for Powered Flight Space Vehicle on Deep Space Missions," Journal of Spacecraft and Rockets, Volume 6, No. 5, May 1969, pp. 545-550.

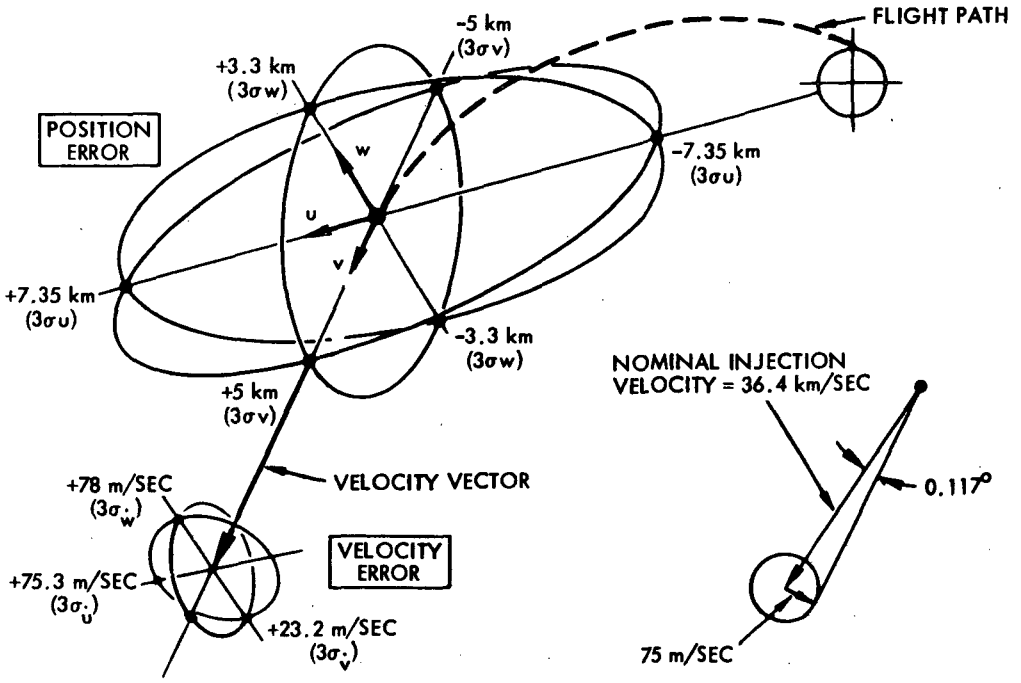

COVARIANCE MATRIX

6.01	-3.02	0.03	12.33	-0.67	0.32
	2.79	-0.02	-1.38	0.78	0.20
		1.22	0.06	0.99	13.74
			629.0	59.4	17.8
					665.0

UNITS
$(KM)^2$
$(10^6\ KM/SEC)^2$

Figure 3-27. Injection Error Model

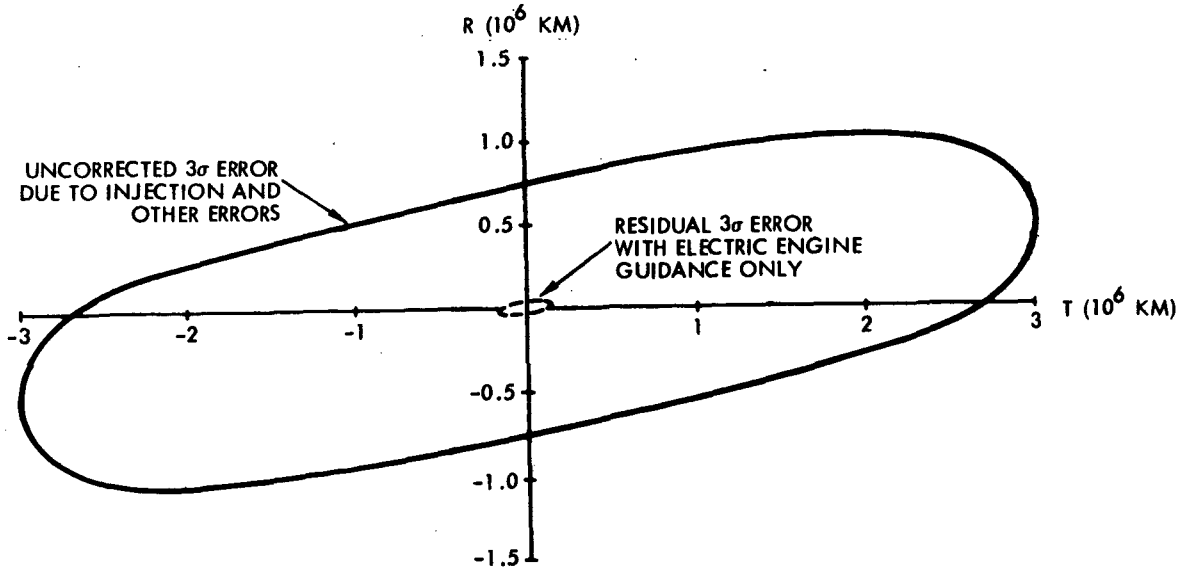

Figure 3-28. Corrected and Uncorrected Miss Distance

The nominal trajectory selected for the study was that of a Jupiter swingby out-of-the-ecliptic mission shown in Figure 3-29.

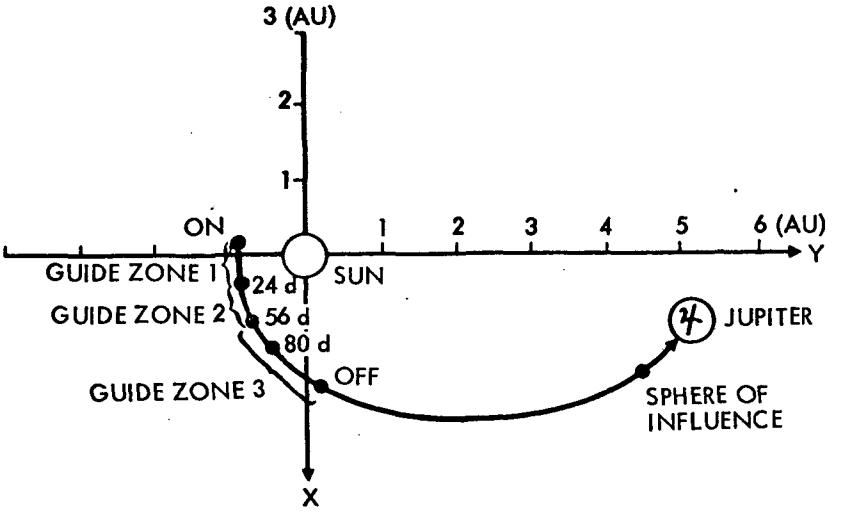

Figure 3-29. Nominal Trajectory

Tables 3-4 and 3-5 give values of time position, velocity, thrust, pointing angles, and spacecraft weight for the duration of the mission. Nominal I_{sp} is 2500 seconds. The coordinates for the yaw and pitch perturbation of the thrust vector are shown in Figure 3-30, while the cone and clock angles of the nominal thrust are indicated in Figure 3-31. The criteria of guidance was to minimize the magnitude of the miss vector shown in Figure 3-32. Such a minimization containing all three components of miss is equivalent to having a restriction on terminal time of encounter.

While a full scale Monte Carlo simulation was not carried out, a simplified study was made with individual 3σ perturbations of position and velocity error components at injection (see also Appendix B). Engine noise and navigation uncertainty were not incorporated in the computer simulation; however, their effects are evaluated in the discussion.

During the period in which the electric engine was on, guide zones were defined as shown in Figure 3-29. During one guide zone the engine thrust guidance parameters (pitch, yaw, and throttling) are fixed, and these parameters are reevaluated only at the beginning of each guide zone.

Table 3-4. Nominal Trajectory Profile

Comments	No.	Time		Position			Velocity		
		Δt	t	x	y	z	$\dot{x}$	$\dot{y}$	$\dot{z}$
		(days)	(days)	(AU)	(AU)	(AU)	$\frac{AU}{yr}$	$\frac{AU}{yr}$	$\frac{AU}{yr}$
	1	--	0	-0.179	-0.999	0.000	7.63	-1.37	0.
Engine On →	2	0.01	0.01	-0.179	-0.999	0.	7.63	-1.27	0.
Guide Zone 1	3	7.99	8	-0.05	-0.998	-0.002	7.62	-0.5	-0.005
	4	8	16	+0.07	-0.995	-0.005	7.568	0.297	-0.01
	5	8	24	0.30	-0.990	-0.007	7.40	0.90	-0.01
Guide Zone 2	6	8	32	0.484	-0.973	-0.001	7.20	1.55	-0.01
	7	8	40	0.65	0.90	-0.001	6.70	2.30	-0.01
	8	8	48	0.75	-0.86	-0.001	6.529	2.888	-0.01
	9	8	56	0.91	-0.80	-0.001	6.18	3.3	0.011
	10	8	64	1.056	-0.720	-0.001	5.71	3.7	-0.011
	11	8	72	1.15	-0.65	-0.0012	5.33	3.95	-0.012
Guide Zone 3	12	8	80	1.30	-0.55	-0.0015	4.90	4.2	-0.012
	13	8	88	1.40	-0.44	-0.0017	4.50	4.34	-0.013
	14	8	96	1.486	-0.352	-0.002	4.18	4.45	-0.013
	15	8	104	1.58	-0.24	-0.0025	3.85	4.52	-0.014
	16	8	112	1.65	-0.15	-0.003	3.527	4.611	-0.015
	17	8	120	1.75	-0.05	-0.0035	3.20	4.62	-0.015
	18	8	128	1.795	0.052	-0.004	2.93	4.65	-0.015
Engine Off →	19	8	136	1.87	0.15	-0.006	2.71	4.65	-0.016
Sphere of Influence →	20	504	640	1.546	4.429	-0.034	-1.35	1.7	-0.016

Table 3-5. Electric Engine Thrust Profile

Comments	No.	Time t (days)	Thrust T (lb)	Thrust Angles Cone (deg)	Thrust Angles Clock (deg)
	1	0	0.03755	135	270.25
Engine On →	2	0.01	0.03755		270.25
Guide Zone 1	3	8	0.03740		270.63
	4	16	0.03683		271.07
	5	24	0.03563		271.52
Guide Zone 2	6	32	0.03433		271.93
	7	40	0.03265		272.32
	8	48	0.03101		272.74
	9	56	0.02907		273.23
	10	64	0.02716		273.78
	11	72	0.02546		274.34
Guide Zone 3	12	80	0.02362		274.83
	13	88	0.02215		275.22
	14	96	0.02053		275.59
	15	104	0.01927		276.03
	16	112	0.01803		276.67
	17	120	0.01680		277.45
	18	128	0.01575		278.04
Engine Off →	19	136	0.01472	135	278.07
Sphere of Influence →	20	640	--	--	--

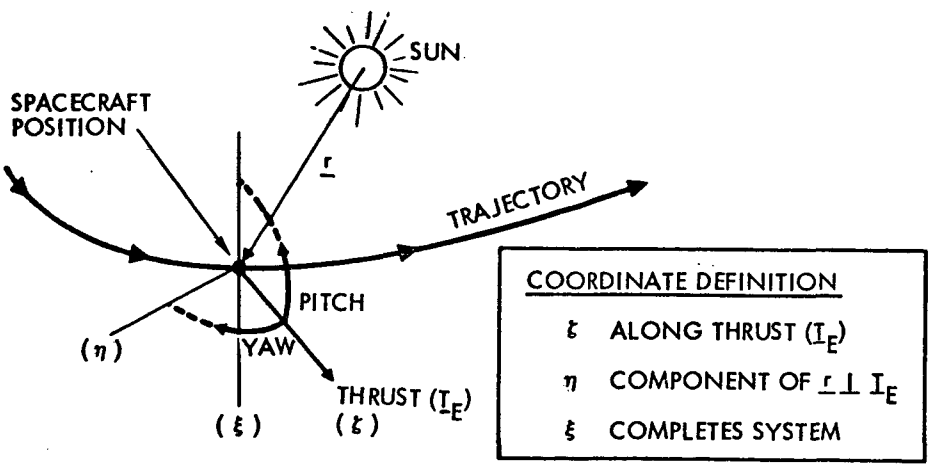

Figure 3-30. Yaw and Pitch Angles

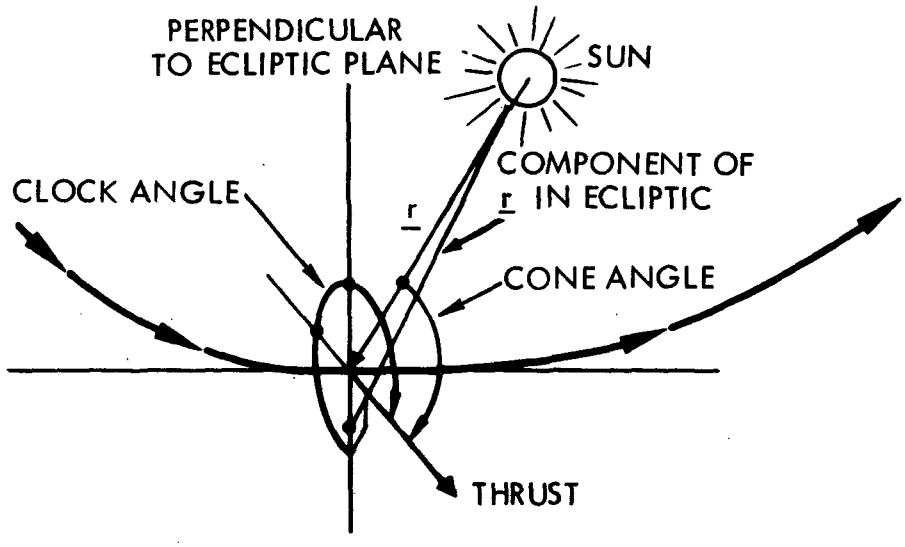

Figure 3-31. Cone and Clock Angles

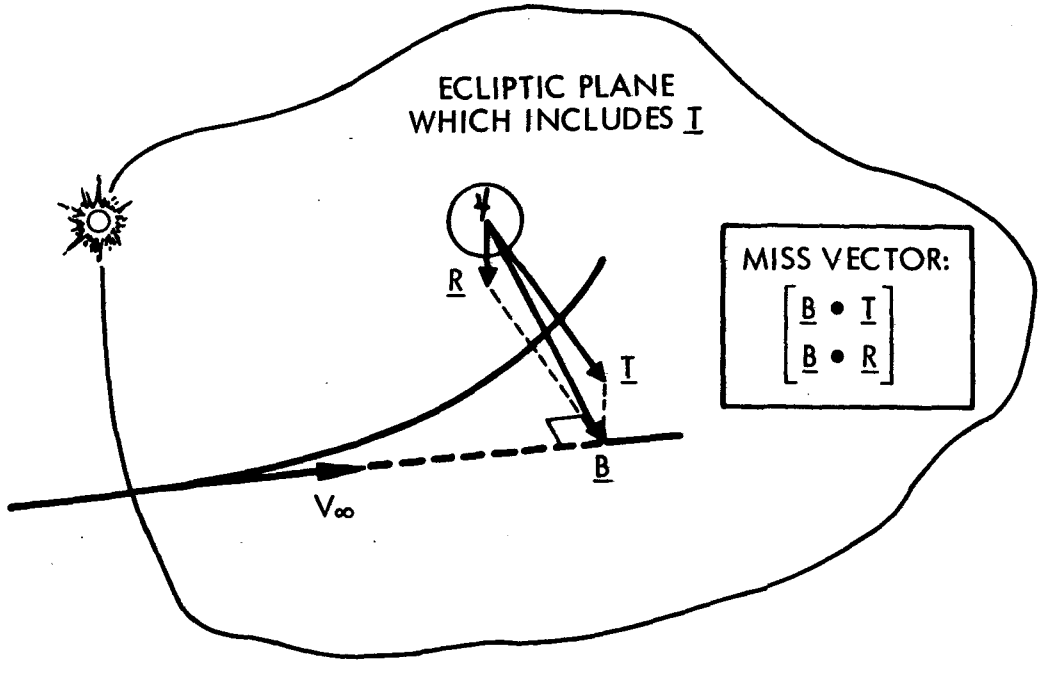

Figure 3-32. Miss Vector Components

State vector errors at injection were propagated forward and perturbed the impact point at Jupiter. In each of the three guide zones, the thrust vector is rotated to an optimum angle to minimize the magnitude of the miss vector and the magnitude of the thrust level is increased when necessary to eliminate the error along the V_∞. When the injection along the velocity vector was too high, the spacecraft electric thruster was cut off early at the time which insured the proper arrival conditions. To minimize propulsion requirements, the time of flight error was not regulated, only the flyby conditions.

The guidance results are shown in Tables 3-6 and 3-7. As can be seen, each component of error and its magnitude is given, and then during each guide zone the magnitude of the unguided component is given, then the reduction of magnitude of those components achieved by rotating the thrust vector at the values shown or by increasing the engine thrust. It is shown that the large (velocity) errors are reduced from a million by 5 million kilometers down to approximately 50,000 kilometers B · T and an order of magnitude less for B · R. An analysis summarized in the table below indicated that these errors can be corrected following low-thrust burn with less than 17 m/sec (3σ) which means basically that the electric propulsion has eliminated approximately 90 percent of the injection error.

Error (3σ)	Source	ΔV Chemical ($\sim 3\sigma$) (m/sec)
Position (8 km)	Residual injection error	~0
Velocity (100 m/sec)	Residual injection error	3.5
Position (15,000 km)	Engine noise	0.5
Velocity (1 m/sec)	Engine noise	3.0
Position (3000 km)	A priori Jupiter position uncertainty	10.0
		17 m/sec

Table 3-6. Velocity Error Guidance Parameters

	$\delta\dot{x}$ 3σ(-22 m/sec)			$\delta\dot{y}$ 3σ(-75 m/sec)			$\delta\dot{z}$ 3σ(78 m/sec)		
Guide Zone	1	2	3	1	2	3	1	2	3
Miss Vector Magnitude δB_o Uncorrected (km)	1.962×10^5	1.876×10^5	1.807×10^5	3.913×10^6	3.161×10^6	2.118×10^6	7.441×10^5	4.883×10^5	2.810×10^5
Miss Vector With Guidance									
Magnitude δB (km)	1.768×10^5	1.767×10^5	1.766×10^5	6.233×10^4	6.330×10^4	6.298×10^4	2.378×10^4	2.376×10^4	2.375×10^4
$\underline{\delta B} \cdot \underline{T}$ (km)	-1.740×10^5	-1.748×10^5	-1.753×10^5	-6.135×10^4	-6.135×10^4	-6.251×10^4	-2.338×10^4	-2.350×10^4	-2.357×10^4
$\underline{\delta B} \cdot \underline{R}$ (km)	-3300.	-326.	3145.	-1109.	-34.8	1266.	-933.	-642.	-296
Asymptotic Velocity Error with Guidance δV_∞ (m/sec)	16.35	16.30	16.23	12.37	12.44	12.32	58.00	58.03	58.13
Ion Engine Thrust Vector Change									
Solid Angle (deg)	0.006	0.034	0.051	1.741	1.757	1.802	2.59	2.59	2.59
Pitch (deg)	0.005	-0.011	-0.044	-0.037	-0.043	-0.057	-2.59	-2.59	-2.59
Yaw (deg)	-0.038	-0.033	-0.026	-1.741	-1.756	-1.801	0.16	0.16	0.16
Increase in Time to Perijove (hr)	-2.54	-2.52	-2.52	5.40	5.42	5.42	-0.14	-0.14	-0.14
Required Chemical Correction ΔV_c Applied 10 Days After Electric Engine Shut Down (m/sec)	--	--	3.1	--	--	1.1	--	--	0.41

Table 3-7. Position Error Guidance Parameters

	δx 3σ(-5 km)			δy 3σ(-7.35 km)			δz 3σ(3.3 km)		
Miss Vector Magnitude δB_o Uncorrected (km)	9.52	7.94	5.72	25.2	20.7	14.3	1.42	0.93	0.56
Miss Vector with Guidance									
Magnitude δB (km)	2.60	2.60	2.60	3.90	3.89	3.89	0.029	0.029	0.029
$\delta \underline{B} \cdot \underline{T}$ (km)	-2.56	-2.57	-2.58	-3.83	-3.85	-3.86	-2.8×10^{-2}	-2.9×10^{-2}	-2.9×10^{-2}
$\delta \underline{B} \cdot \underline{R}$ (km)	-0.049	-0.005	0.047	-7.3×10^{-2}	-6.9×10^{-3}	7.1×10^{-2}	-5.9×10^{-2}	-5.1×10^{-5}	5.3×10^{-4}
Asymptotic Velocity Error with Guidance									
δV_∞ (m/sec)	4.11×10^{-4}	4.12×10^{-4}	4.14×10^{-4}	1.49×10^{-4}	1.47×10^{-4}	1.47×10^{-4}	4.7×10^{-4}	4.7×10^{-4}	4.7×10^{-4}
Ion Engine Thrust Vector Change									
Solid Angle (arc sec)	3.0×10^{-2}	3.0×10^{-2}	3.0×10^{-2}	4.6×10^{-2}	4.6×10^{-2}	4.6×10^{-2}	3.0×10^{-2}	3.0×10^{-2}	3.0×10^{-2}
Pitch (arc sec)	8.7×10^{-4}	1.7×10^{-5}	-1.8×10^{-3}	2.3×10^{-3}	1.1×10^{-3}	-1.6×10^{-3}	-1.7×10^{-2}	-1.8×10^{-2}	-1.8×10^{-2}
Yaw (arc sec)	1.4×10^{-2}	1.5×10^{-2}	1.5×10^{-2}	3.9×10^{-2}	4.0×10^{-2}	4.0×10^{-3}	1.4×10^{-3}	1.4×10^{-3}	1.4×10^{-3}
Increase in Time of Arrival (sec)	4.9×10^{-2}	-4.9×10^{-2}	-4.9×10^{-2}	7.2×10^{-5}	7.2×10^{-5}	7.2×10^{-5}	8.4×10^{-7}	8.4×10^{-7}	8.4×10^{-7}

This guidance study has assumed perfect navigation and error-free engine control. The ability of the deep space network (DSN) to track with ion engine system noise should also be incorporated for guidance evaluation. The Jordan reference previously mentioned is an extensive tracking study which provided the sample position and velocity uncertainties versus time shown in Figure 3-33. At the time of thruster cutoff the position and velocity standard deviations (1σ) are 5000 kilometers and 1 m/sec, respectively. These results are for an ion engine with maximum acceleration of 5×10^{-2} cm/sec and 1 percent acceleration noise. This acceleration value is about one-half as large as the 15-cm engine and one-fourth as large as the 30-cm engine now under consideration, and the 1 percent value may be optimistic. However, during subsequent coast, the DSN should perform more accurately and the required total chemical correction should be no more than 17 m/sec (3σ) to achieve a miss uncertainty of 500 kilometers (3σ) at encounter.

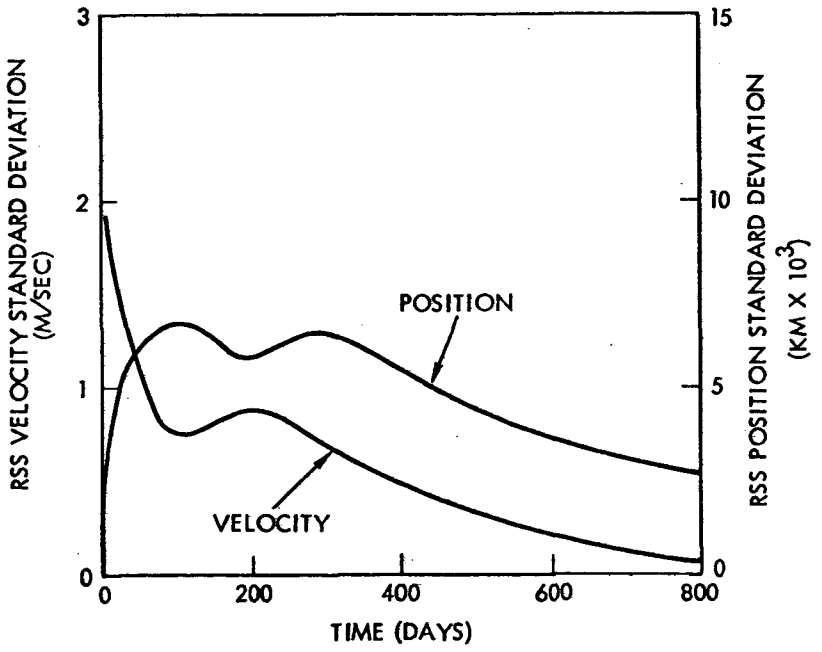

Figure 3-33. Time History of Position and Velocity Uncertainty

3.4.2 Terminal Guidance

The Pioneer comet rendezvous electric propulsion spacecraft has onboard a small telescope system equipped with a V-slit reticle (described in Section 5). This device scans a 3-degree annular strip about the spin axis on each spin cycle and transmits to the ground upon command the timing and cone angle data related to stars and the target as they pass through the V-slit. These star pips and accurate timing data make it possible to measure spin axis orientation to better than 45 arc-seconds. The clock angle and cone angle error sources and their magnitudes are shown in Table 3-8. This sensitivity enables the detection of fifth magnitude objects.

Table 3-8. Star Mapper Error Sources (1σ)

	Error Source Half-Cone Angle	Clock Angle Error (Arc Sec) 90 deg	 22.5 deg	Cone Angle Error (Arc Sec) 90 deg	 22.5 deg
1	Random jitter	11	18	19	31
2	Sky background	7	7	8	8
3	Electronic filter variation	3	3	4	4
4	Threshold circuit variation	5	5	4	4
5	Reticle geometry	3	3	3	3
6	Thermal stability	3	3	3	3
7	Alignment/calibration errors	10	10	10	10
8	Clock stability	1	1	1	1
9	Offset due to finite image size	15	15	15	15
	RSS	23	27	28	37

Figure 3-34 is a parametric plot of the terminal acquisition ΔV required as a function of offset distances and range for various target brightness magnitudes and error detection threshold sensitivities. The reference example shown on the diagram is for a target having twelfth magnitude brightness from earth and fifth magnitude brightness from the spacecraft. The initial offset distance from the target is 3000 kilometers

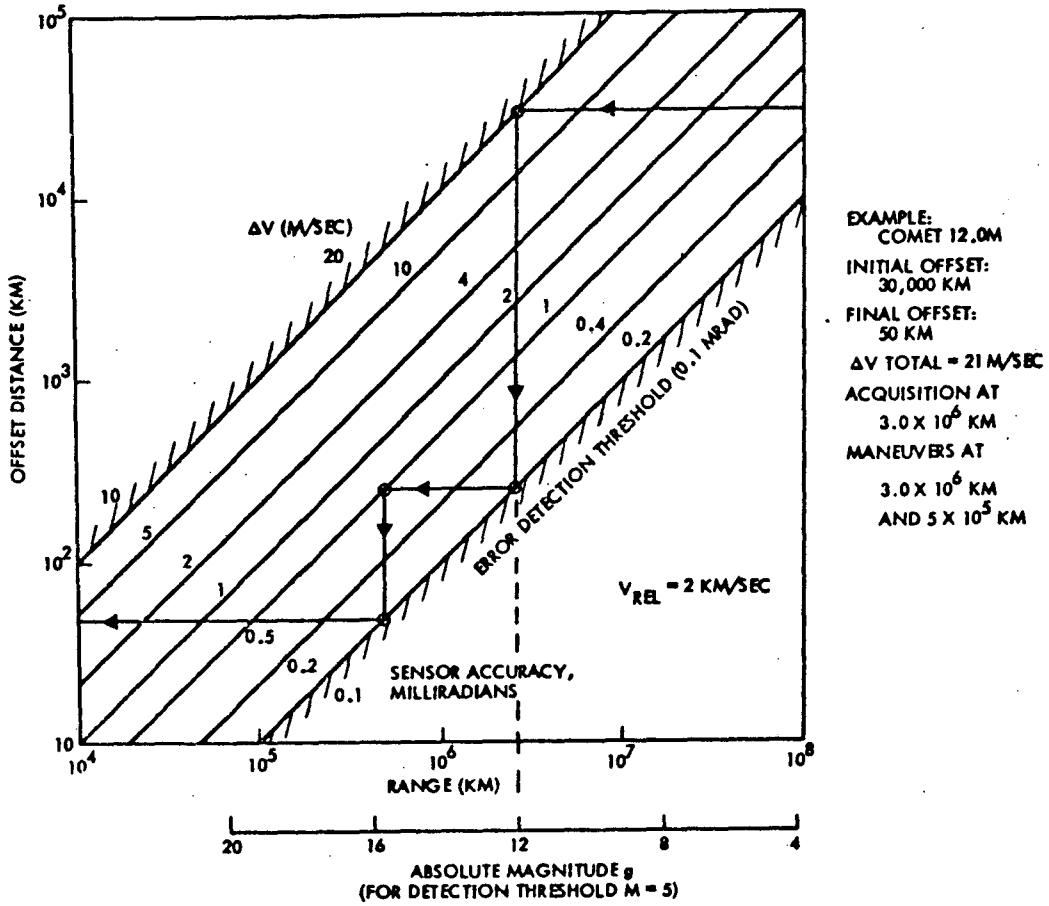

Figure 3-34. Terminal Acquisition and Guidance Maneuver Diagram

with the final offset at 50 kilometers following the expenditure of 21 m/sec of ΔV. Initial acquisition is at 3.0×10^6 kilometers with maneuvers at 3.0×10^6 and 5×10^5 kilometers. The relative velocity for the example is 2 km/sec which is conservative. These maneuvers can be performed using hydrazine propellant or electric propulsion. Electric propulsion thrusting is preferred and seems feasible based on the following evaluation.

Trajectory analysis shows the probe to comet distance to be 3.0×10^6 kilometers at 927 days into the mission which is 73 days prior to rendezvous. This gives us an apparent magnitude of less than 5 as can be seen in Figure 3-35. The insert shows the observed and projected brightness of the comet Tempel II. The projected H_{10} value for a 1978 apparition is 12.5 and the visual magnitude is computed by

$$M = H_{10} + 5 \log R_{pc} + 10 \log R_{cs}$$

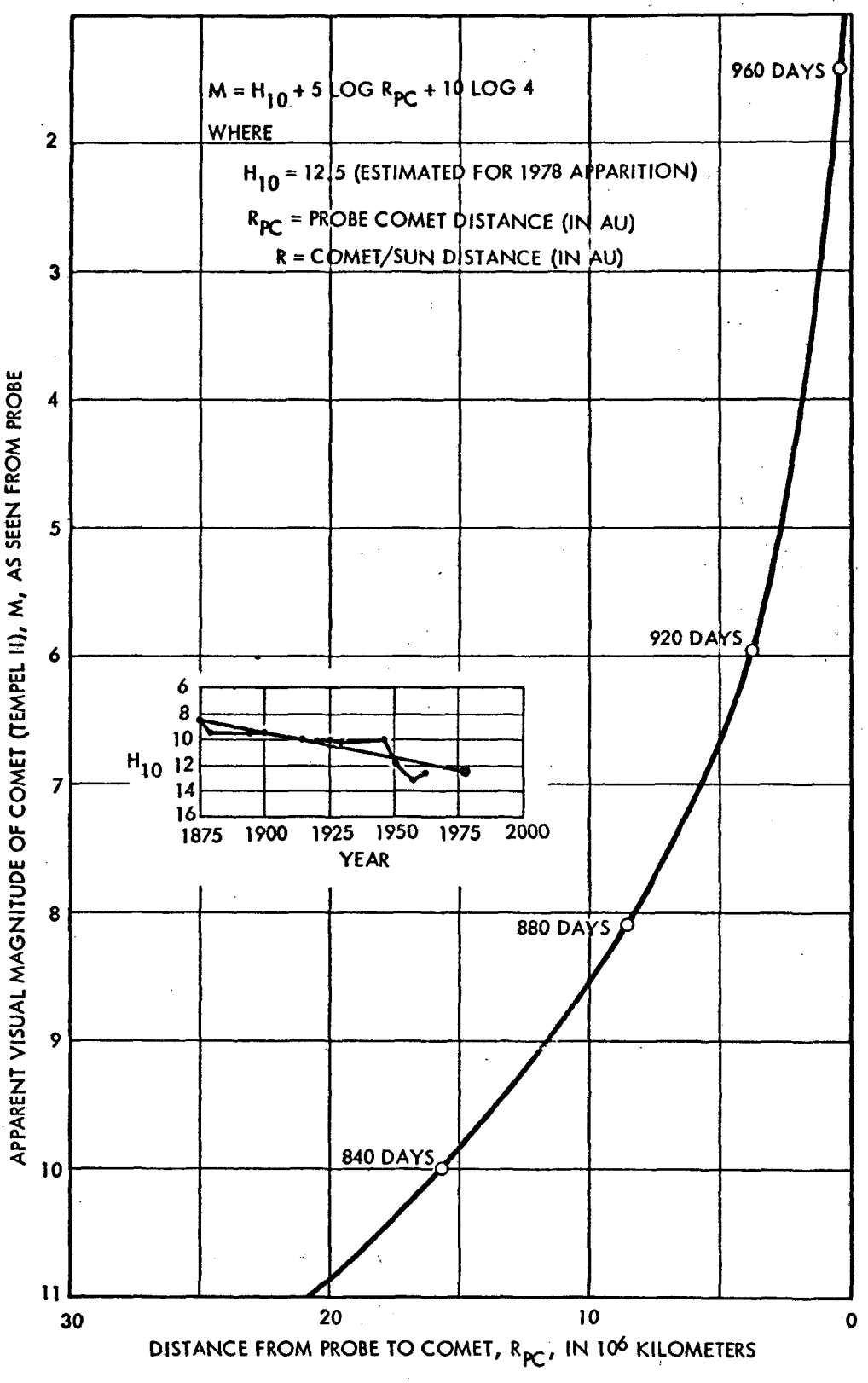

Figure 3-35. Apparent Visual Magnitude of Comet Versus Probe to Comet Distance

where

R_{pc} = probe to comet distance

R_{cs} = comet to sun distance.

The duration of continuous angular offset thrusting required to remove cross-range ephemeris errors of 30,000 kilometers is shown in Figure 3-36. Thirty thousand kilometers was selected based upon preliminary small body ephemeris accuracy studies performed at the University of Cincinnati Observatory. These studies indicated the

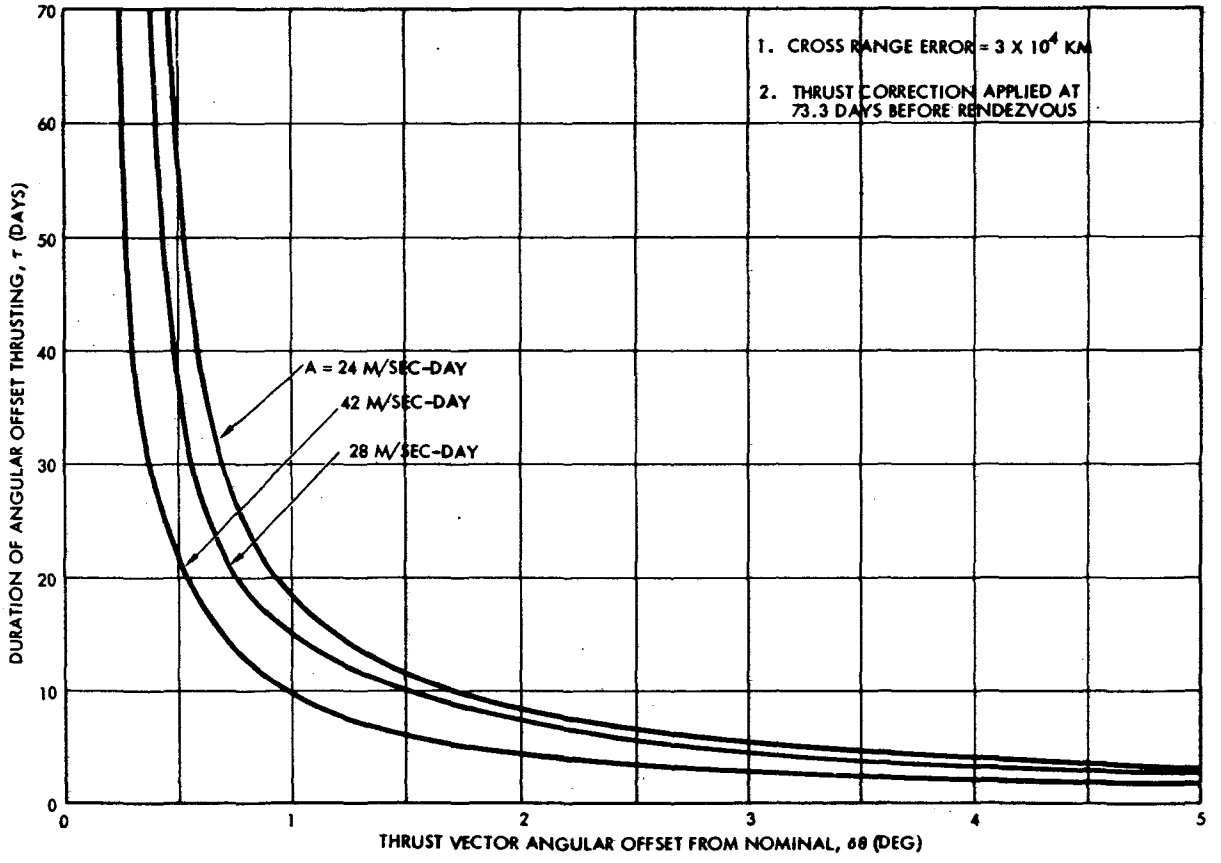

Figure 3-36. Duration of Angular Offset Thrusting Required to Remove Cross Range Error Versus Angular Offset

position uncertainty of small asteroids (for example Asteroid 1473) to be about 10,000 kilometers (1σ). For purposes of this study it has been estimated that the position uncertainty for well-known comets can also be calculated to this accuracy. The parameters of each curve are the acceleration value of the probe, i.e., the magnitude of the acceleration vector which is to be shifted by the amount δθ from its nominal position to achieve a correction in cross-range position by the time of rendezvous, as shown below. The average value of acceleration is about 24 m/sec-day for the 5-kw system with three 15-cm thrusters operating and 28 m/sec-day for the 8-kw system with two 30-cm thrusters operating. The graph indicates that there should be no problem in correcting the 30,000 km error since a thrust vector angular offset of only 1 degree would correct this error in 18-1/2 days with the 5-kw system and 15 days with the 8-kw system. This assumes the angular change is initiated approximately 70 days before rendezvous. If the total 73 days were used and an offset of 4 degrees, as much as 400,000 km of error could be removed.

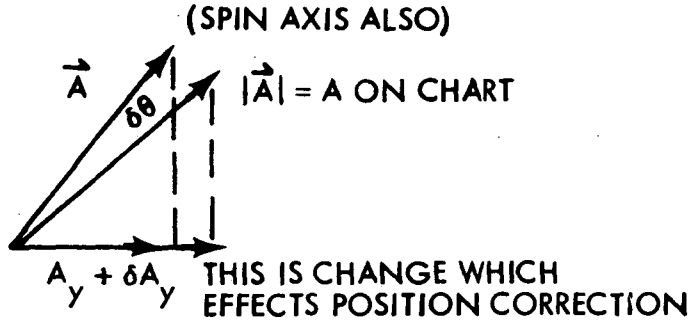

In summary, there appears to be no terminal guidance problems for an intercept of the comet Tempel II that cannot be solved with the inclusion of an on-board star mapping sensor. Design details, history and characteristics of the sensor envisioned are described in Section 5.

The comparative ballistic flyby of a 600-pound Pioneer without electric propulsion would be at approximately 11 km/sec. A three-impulse chemical propulsion trajectory was also made for ballistic comparison. This analysis assumed that hydrazine was used instead of electric propulsion. ΔV requirements are 3.0 km/sec at aphelion for the 12.4-degree plane change and perihelion increase, and 1.5 km/sec at perihelion. With an I_{sp} of approximately 215 seconds, hydrazine thus requires an 88 percent propellant fraction to achieve comet rendezvous at perihelion. These results indicate the comet rendezvous mission without electric propulsion is far from practical.

The comet observation and mapping strategy proposed is illustrated in Figure 3-37.* Shown are regions of special interest in and around the comet, such as the area of the postulated shock front, transition zone, outer and inner coma and contact discontinuity, the region where tail phenomena begin to form, and the nucleus and its halo.

Figure 3-38 shows two types of comet exploration maneuvers previously obtained. The first type has been analyzed by IITRI.** It provides excursions of ±20,000 km from the nucleus for about 60 days, including a stationkeeping period of ten days. The ΔV requirement is about 160 m/sec.

The second type (analyzed at TRW) starts at 50,000 km offset on the sunward side rather than at the nucleus and includes an excursion toward or into the tail to 50,000 km. The time requirement is 30 days, and the total ΔV is about 240 m/sec. The depth of tail exploration can be adapted in accordance with observations from earth, as determined by the presence or absence of a prominent tail. This exploration mode has the advantage that it permits systematic mapping of the coma and tail during the most active phase of the comet while avoiding the more hazardous nucleus environment during that time. It has the disadvantage that it would require a larger hydrazine tank than the 16-inch diameter (200 m/sec, ΔV) spherical tank currently used on Pioneer F and G.

After mapping the coma/tail regions (30 days) and performing closeup observations of the nucleus (20 days) the 80-day primary exploration time still permits 30 days of further exploration. Most of this time may be spent in exploring the coma/tail region, possibly leaving and reentering the comet envelope to explore the contact surface. Three-dimensional coma exploration may also be performed during this time.

By comparison a ballistic flythrough mission can cover only a few of the points of interest and in too little time for systematic mapping.

---

*"Study of a Comet Rendezvous Mission," May 12, 1972, Contract No. 953247, prepared for JPL by TRW.

**"Comet Rendezvous Mission Study," Preliminary Report, IIT Research Institute (final report in preparation), June 1971.

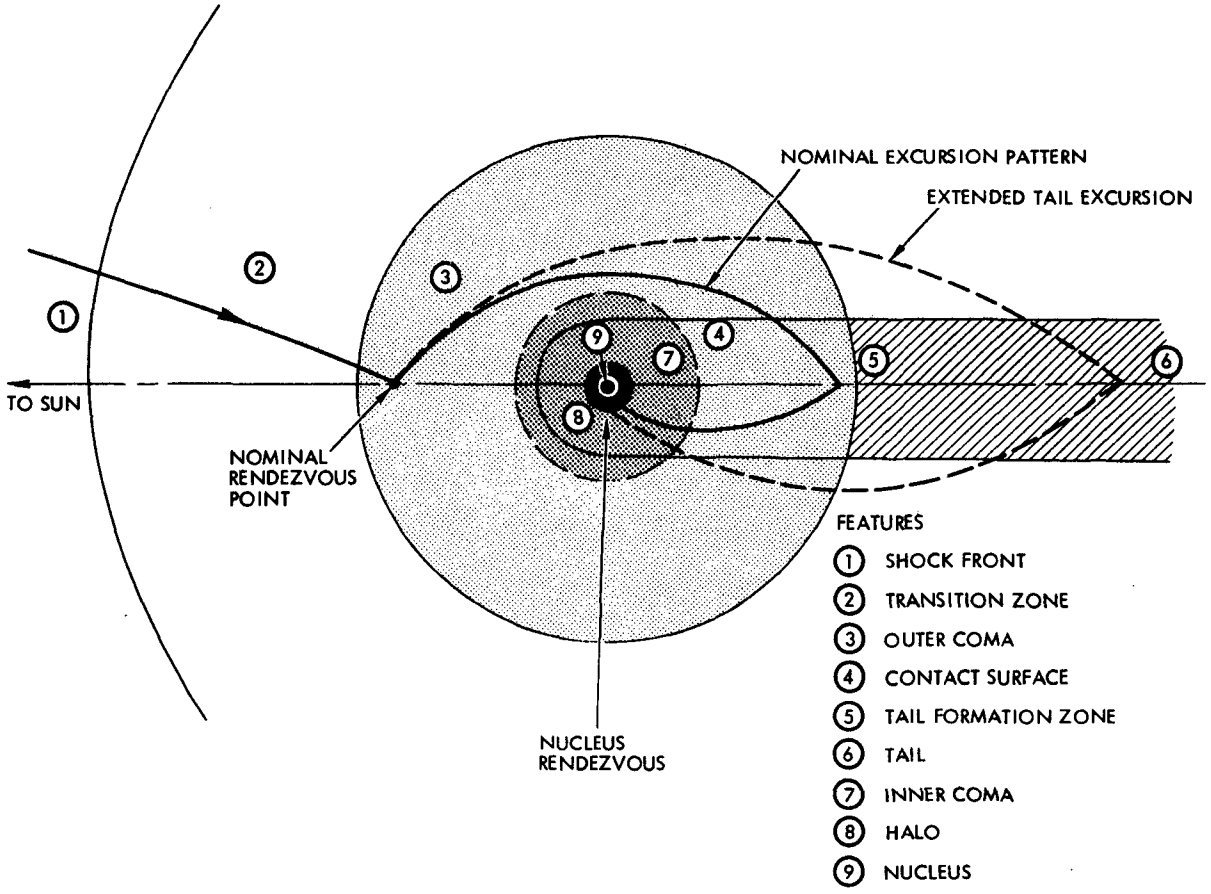

Figure 3-37. Excursions through Principal Comet Features (not to scale)

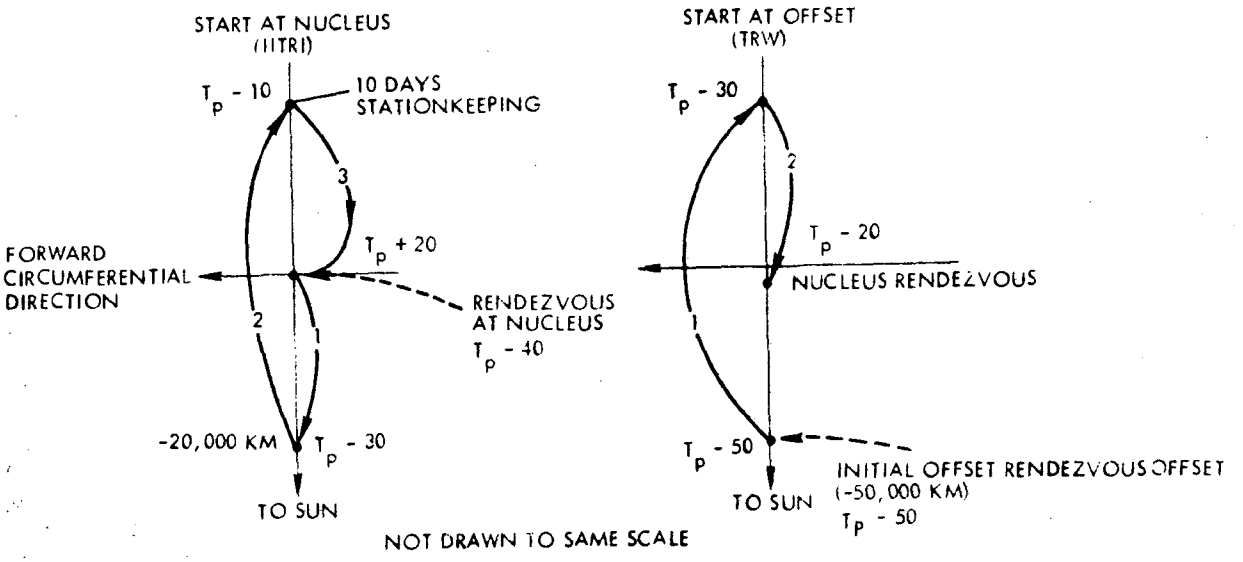

NOT DRAWN TO SAME SCALE

LEG	TIME	ΔV (M/S)	ΔR (KM)
1	T_p - 40	22	0
	T_p - 30	24	-20×10^3
2	T_p - 30	22	-20×10^3
	T_p - 10	26	$+20 \times 10^3$
	T_p - 10 TO T_p	39*	$+20 \times 10^3$
3	T_p	23	$+20 \times 10^3$
	T_p + 20	11	0

*10-DAY STATIONKEEPING

LEG	TIME	ΔV (M/S)	ΔR (KM)
1	T_p - 50	60	-50×10^3
	T_p - 30	61	$+50 \times 10^3$
2	T_p - 30	60	-50×10^3
	T_p - 20	56	-1×10^3

(NO STATIONKEEPING)

Figure 3-38. Comet Exploration Maneuvers

The relative trajectory is nearly a straight line parallel to the $\overline{V}_\infty$ vector and is dictated by mission dates and launch energy. (For selected encounter dates this path can at least be chosen to run roughly parallel to the comet's axis, moving in a radially outward direction.)

An interesting option available to the low-thrust vehicle is variation of the depth of penetration of the coma and tail region, e.g., if ground observation should find that the Tempel II is developing a pronounced tail as the spacecraft approaches rendezvous, a simple change of the exploration path further into the tail region can be made at an acceptable extra propellant and time expenditure.

The "bipolar" plot of the comet trajectory relative to earth, shown in Figure 3-39 has useful properties in the analysis of mission characteristics. It exhibits the earth-comet and sun-comet distances throughout the pre- and post-perihelion phase of the comet's orbit (with earth in fixed reference position) as well as the observability of the comet in terms of sun-comet-earth angles. The two mission opportunities illustrated (with perihelion in March 1978 or June 1983) differ greatly in terms of viewing conditions from earth that are favorable in 1983 and unfavorable in 1978. Similarly, the communication distances between earth and spacecraft at the time of rendezvous and afterwards are much more favorable for the 1983 opportunity. We also note that the comet's tail which extends radially away from the sun can be viewed favorably in 1983 during the period from 100 days before to 100 days after perihelion passage, thus permitting concurrent evaluation of comet phenomena by visual observation from earth and in situ observation by the spacecraft.

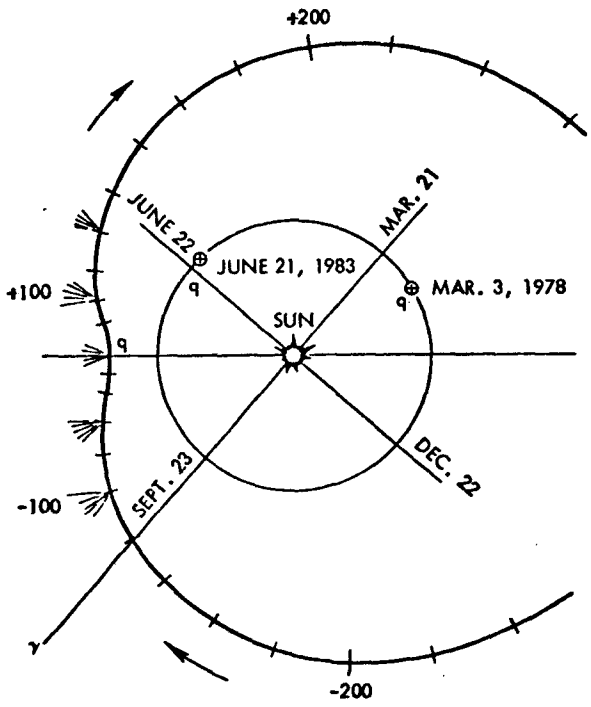

Figure 3-39. Viewing Conditions of Tempel II's Tail from Earth

As a part of the cometary mission analysis, the feasibility of flying by a known asteroid enroute to the Temple II rendezvous was evaluated. The technique utilized was to establish the spacecraft trajectory and then to determine the closest point of approach, without adjustment, to any of the charted asteroids. As shown in Figure 3-40 there were three asteroids that came within 20 million kilometers, which is a reasonable range and quantity of asteroids to show feasibility. A next step in this analysis,

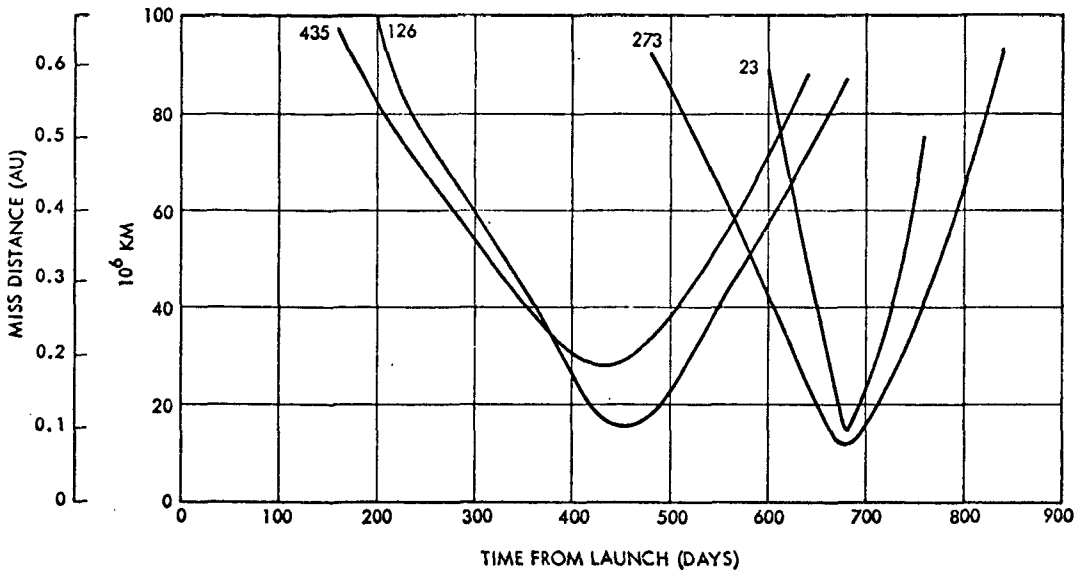

Figure 3-40. Asteroid Closest Approach from Nominal Tempel II Rendezvous Trajectory

not performed here, would be to target on one of these asteroids and optimize the trajectory for comet rendezvous following asteroid flyby. This will increase thruster burn time moderately and probably the required amount of ΔV hydrazine propellant but will also increase the scientific yield of the mission to make it considerably more attractive.

3.5 FLIGHT OPERATIONS

The following description outlines the various steps which occur during the comet Tempel II mission with rendezvous, using an 8 kw three 30-cm electric propulsion system. The major functions are essentially the same from mission to mission, although flight operation sequences will vary somewhat, particularly during the terminal phase.

1) T_o - Liftoff

- Receivers, digital decoder, command distribution and power conditioning units are on the battery and present a total load of 15 watts to the power bus during ascent.

2) T_1 - Spacecraft/launch vehicle separation

- Coarse orientation is established by launch vehicle and the spacecraft is spun up to 52 rpm nominal prior to separation.

- Subsequent to separation, the spacecraft sequencer switches power to the 10-watt S-band transmitter to establish a downlink, deploys the solar arrays and the experiment booms, and provides power to the attitude control subsystem.

- Deployment of the solar arrays and experiment booms despin the spacecraft to 5.0 rpm nominal.

- The ground station interface is through the omni-antenna with the 85-foot dish.

3) T_2 - Acquisition

- The spacecraft is oriented by means of sun sensor position information to point the spin axis approximately to the earth.

- Experiments are individually turned on and calibrated.

4) T_3 - Conscan

- T_o + ~3 days

  Precession maneuver performed to bring spin axis within medium-gain antenna, conical scan beam and then within high-gain antenna conical scan beam.

  Tracking of spacecraft indicates injection error and allows calculation of low-thrust trajectory deviation from nominal to correct for these errors. (Depending on size of injection error short duration electric propulsion maneuver may be required.)

5) T_4 - Start electric propulsion thrust phase 1

- T_o + ~135 days

  Star mapper scans background stars and determines accurately the position of the spin axis.

  Spacecraft reoriented to proper thrust position, approximately 45 degrees off sunline, star mapper scan repeated and second reorientation performed if required.

  Experiments affected by electric propulsion turned off.

  Power applied to each electric propulsion thruster, checking operation individually. Full thrust on two thrusters is then initiated.

Engine throttling varies in accordance with solar array power output determined from telemetry on the ground. The decrease in solar array power as a function of sun distance is then predicted for each subsequent 7-day period. Control logic in the electric propulsion subsystem is then programmed through the command link to throttle engines in predetermined increments as the solar array output decreases during the 7-day period.

- T_o + ~142 days

  The existing Pioneer F and G system incorporates a stored command memory device that will allow the repetition of a command every 8 hours and the attitude control system provides a program storage and execute command capability that will receive this command and automatically process the spacecraft through a prescribed angle. By this means the thrust direction of the spacecraft can be continuously updated. A second approach is to program the ground software to automatically send the necessary commands at frequent intervals.

  At the end of approximately 7 days another star map fix is taken and the spacecraft orientation is updated by ground command to optimize thrust vector pointing. Also if the 210-foot dish has only temporary assignment, a housekeeping data dump would be performed. This weekly check continues throughout the thrust phase of the mission. The precise thrust orientation is determined by the guidance requirements.

  Assuming no prior failures, thrusters two and three will be shut down at approximately 150 and 325 days, respectively, due to the reduction in solar power.

- T_o + ~200 days

  The medium-gain off-axis antenna will intercept the earth and, following a star map check, this antenna should be commanded on in place of the omni.

6) T_5 - First thrust phase complete

- T_o + 445 days

  Shut down electric propulsion system.

  By means of star map check to ascertain the reorientation required to intercept the S-band conical scan high-gain antenna.

Reorient the spacecraft by ground command so that this high-gain antenna beam is earth pointing. The solar array will now be approximately perpendicular to the sunline.

By ground command switch to the high-gain S-band antenna (1024 bits/sec telemetry rate).

7) T_6 - Cruise phase

- T_o + 445 to 710 days

  Turn on all interplanetary experiments and check out cometary experiments.

- Spacecraft pointing is now controlled by conical scan of the uplink RF signal. The star mapper will continue to supply spin reference inputs and can be used as a conical scan backup.

- Tracking of spacecraft indicates initial low-thrust errors and allows calculation of new low-thrust trajectory profile to correct for these errors.

8) T_7 - Start electric propulsion thrust phase 2

- T_o + ~710 days

  Repeat Item 5. Two thrusters are turned on and thruster throttle setting increases to accommodate increasing available solar power.

- T_o + ~820 days

  Third thruster turned on.

9) T_8 - Target acquisition and terminal guidance

- T_o + ~ 930 to 935 days

  Turn off all engines. Set star mapper cone angle for acquisition and identify reference stars. Determining precise spin axis orientation. Acquire target in assigned cone/clock angle region. Perform repeated navigation fixes and compute terminal guidance maneuver.

- T_o + ~935 to 995 days
  (Acquisition at day 1000)

  Turn on two engines and resume thrust phase.

  Repeat above sequence after precessing spacecraft and acquiring on medium-gain conscan. Execute final trim maneuver.

10) T_9 - Encounter sequence

- T_o + ~995 to 1001 days

  Precess spacecraft to acquire ground station on high-gain conscan antenna.

  Command payload pointing sequence and start observations. Acquire data and transmit in real time. Store imaging data and playback.

  Prepare for next stationkeeping maneuver sequence.

4. SYSTEM DESIGN

4.1 DESIGN CONSIDERATIONS

In addition to the major study ground rules enumerated in Section 1.1, many other considerations exist in the conversion of the Pioneer F and G to one employing solar electric propulsion. Some of these design considerations are listed below:

a) Physical limitations of the launch vehicle envelope and physical limits on weight, center of gravity, and moments of inertia.

b) Profile of the mission in terms of aspect angles and distances to the earth, the sun and the target.

c) Requirement that the attitude of the spacecraft be known and controlled to implement the communication link and thrust vector control.

d) State of the art of ion thruster technology in terms of thruster physical size, performance characteristics, and power conditioning technology.

e) Interaction of the various subsystems, particularly the solar electric propulsion subsystems with the science and other subsystems.

f) Requirement for and availability of electrical power during the pre-thrust, thrust, cruise, and encounter phases of the mission.

g) Requirements for and limitations on the communications link between spacecraft and earth, particularly during the thrust phase of the mission.

h) Requirements of the science instruments for unobstructed viewing, electrical and magnetic cleanliness, and contamination-free environment.

These general considerations, combined with the ground rules stated in Section 1.1, constitute the basis for arriving at the spacecraft configuration described in this section. The specifics of each of these considerations are discussed more thoroughly in the following paragraphs.

4.1.1 Physical Limitations

This study has assumed utilization of either of two launch vehicles, the Atlas/Centaur/TE-364-4 or the Titan IIIE/Centaur/TE-364-4. Both vehicles have the 10-foot Centaur fairing with the TE-364-4 third stage and adapter. The envelope of the Centaur fairing with the TE-364-4 is shown below.

Spin stabilization imposes special requirements on the mass properties of the electric propulsion spacecraft. With deployable solar

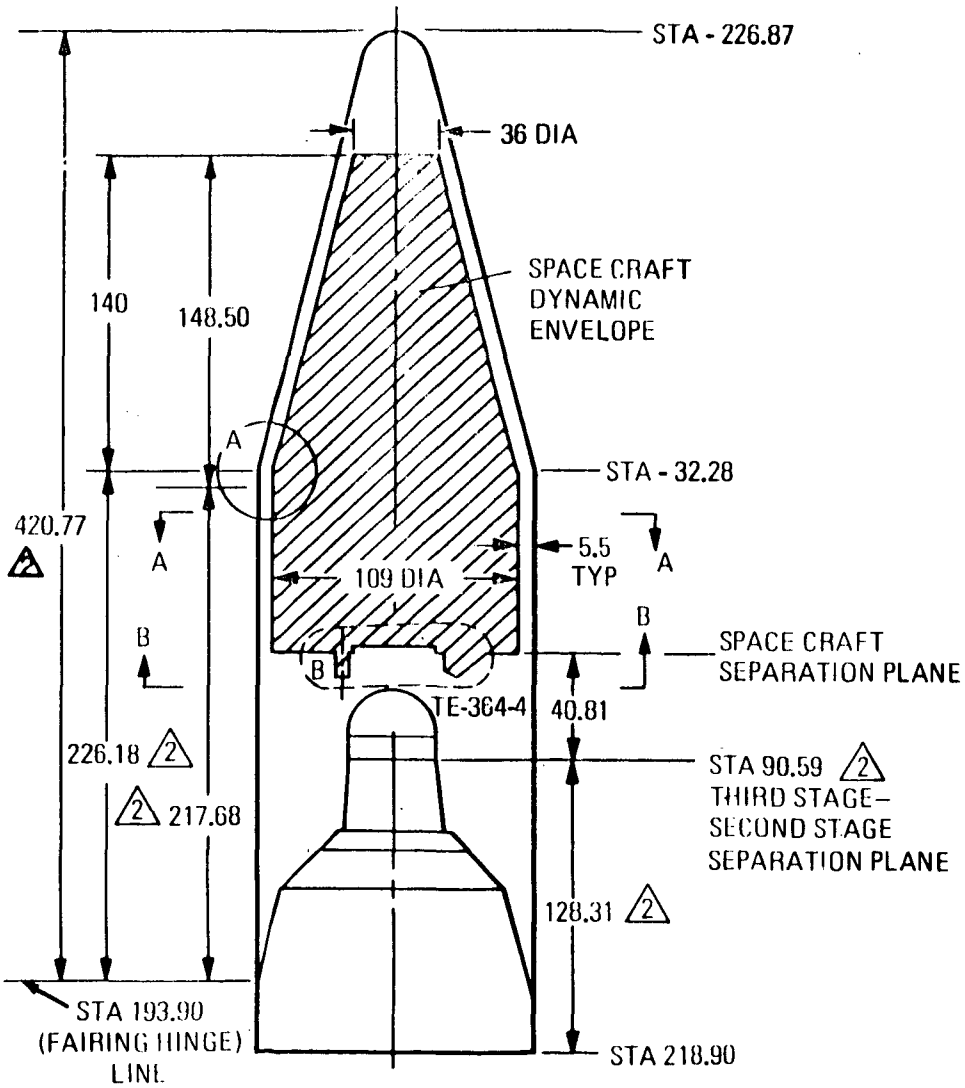

NOTE: ALL STATIONS ARE CENTAUR STATIONS

arrays and a magnetometer boom, maintenance of these mass properties through deployment poses some definite limitations on the overall configuration as shown:

a) The center of mass must be aligned along the geometric centerline of the third stage adapter ring during the third stage boost phase and separation.

b) The principal moment of inertia must be aligned with the longitudinal axis of the spacecraft throughout the pre-deployment and post-deployment phases of the mission.

More specific physical requirements and mass properties characteristics are presented in Sections 4. 2 and 4. 4.

4. 1. 2 Mission Profiles

As was evident in the description of the basic spinner concept in Section 2, the profile of this particular mission imposes specific requirements on the spacecraft configuration. In particular, the aspect angles for earth communication and solar array performance during the pre-thrust and thrust phases suggest special designs for the antenna, aspect sensing, and solar array. During the pre-deployment phase between injection and solar array deployment the spacecraft will be maneuvered from its injection orientation to a 45-degree sun orientation. During this maneuver, the attitude of the spacecraft must be known and monitored to successfully accomplish the maneuver. The Pioneer F and G spacecraft was an earth-oriented spacecraft, utilizing the conical sweep of the medium-gain or high-gain antenna with the attendant signal variations to acquire and maintain the spin axis pointed at earth. With the addition of solar electric propulsion, the spacecraft becomes both earth and sun oriented and the earth's aspect angle varies through a range of values depending on the particular mission. These profiles establish specific design requirements on the antenna and attitude sensing devices.

4. 1. 3 Electric Propulsion Technology

The current state of electric propulsion technology has the most significant influence on the overall spacecraft design. The immediate tradeoff that must be made is selection of the thruster size. Ion thrusters

have been and are being developed in 5-, 15-, 20- and 30-cm diameter sizes with the current emphasis in terms of funding and commitment on the 5- and 30-cm sizes. For optimum thruster operation, the solar array is sized to the thruster peak power requirement (the thruster peak power is approximately proportional to its area). Allowing for the various power losses, the solar array size requirements are shown in Table 4-1.

Table 4-1. Thruster Size and Power Requirements

Thruster Diameter (cm)	Peak Power (watts)	Power Losses (watts)	Solar Array (watts)	Solar Array Area (ft^2)
5	100	60	160	16
15	680	360	1040	104
20	1200	640	1840	184
30	2600	1420	4020	402

Other factors of the electric propulsion technology include size of the power processors, thruster thrust-to-weight ratio, and throttling capability.

4.1.4 Science Requirements

The science payload imposes requirements and limitations which can be summarized as follows:

a) Unobstructed fields of view for most experiment units

b) Specific view direction relative to the spin axis and the sun line

c) Minimum magnetic and electromagnetic interacting fields

d) Minimum contamination by particles and plasmas originating from spacecraft materials or equipment

e) Specific electrical requirements in the form of telemetry, command control, and power.

In accordance with the ground rules of the study, the Pioneer F and G science payload is assumed and its requirements are known in detail.

4.1.5 Electrical System Configuration

In terms of the electrical system configuration, the changes from the Pioneer F and G configuration are much less than might be expected. The major changes are limited to three subsystem areas:

1) The antenna subsystem where a fan beam antenna replaces the medium-gain horn and a forward omni-antenna is added to the subsystem.

2) The electrical power subsystem where the large solar arrays are substituted (for 1 to 5 AU missions) for the RTG assemblies.

3) The attitude control subsystem where a sun aspect sensor is added for all missions except Tempel II and a star mapper replaces the stellar reference assembly and sun aspect sensor for the Tempel II rendezvous mission.

The electric propulsion subsystem is an added subsystem which operates independent of the other subsystems, having only interface with the command and telemetry equipment.

A block diagram of the system configuration is shown in Figure 4-1. In the antenna and communications equipment area, the following features are noted:

a) The 8-watt TWTA's of the Pioneer F and G are replaced by dual mode 10/25 watt TWTA's to provide a nominal 24 to 25 watt radiated power during the thrust phase.

b) A pair of SPDT RF coaxial switches are added to provide the capability for switching between the omni-antennas and the biconical array.

c) A forward omni-antenna is added with a coupler to the present aft omni-antenna of Pioneer F and G.

d) The biconical array with a four-way power divider replaces the medium-gain horn of the Pioneer F and G.

In the attitude control subsystem the following features are noted:

a) A digital sun aspect sensor replaces the solar sensor of the Pioneer F and G.

FOLDOUT FRAME 1

FOLDOUT FRAME 2

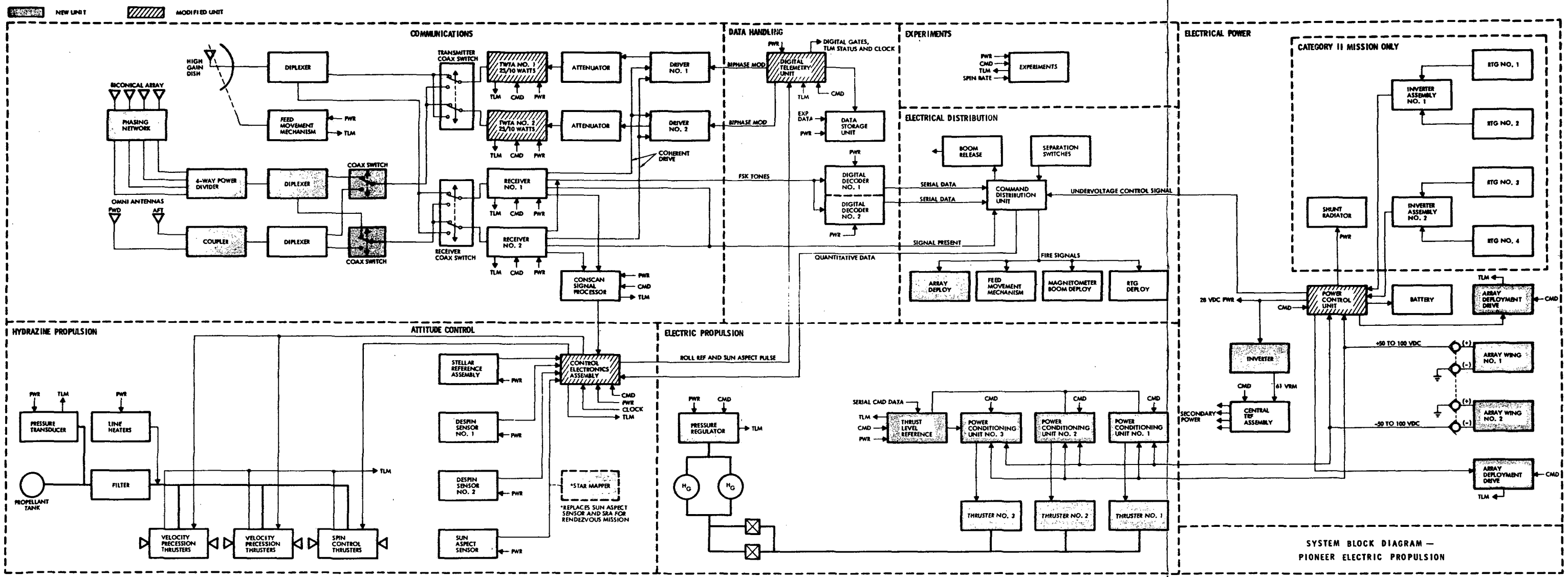

Figure 4-1. Pioneer Electric Propulsion Overall System Block Diagram

4-6/7

b) A star mapper replaces the stellar reference assembly (SRA) and solar aspect sensor for the rendezvous mission. If desired this star mapper would be an acceptable replacement for the SRA and the solar aspect sensor for all missions. However, minimum modification dictates the addition of the solar aspect sensor rather than the star mapper for the majority of missions.

The other major change is in the electrical power subsystem which has the following features.

a) The solar arrays supply dc voltage directly to the PCU and the PCU is redesigned to accept this dc voltage.

b) The inverter is added to operate off the 28 Vdc bus and provides 61 Vrms alternating voltage to the central transformer rectifier filter assembly which therefore does not need to be modified.

c) For the missions beyond 5 AU the RTG's and inverters are added to the power subsystem.

4.2 SPACECRAFT CONFIGURATIONS

The configurations of Pioneer spacecraft with electric propulsion capability were developed for each specific mission using the Pioneer F and G as the baseline design in each case. The configurations were hardware-oriented and emphasized minimum modifications to the Pioneer F and G baseline design.

Information received from McDonnell Douglas indicates that the Pioneer F and G standard third stage/spacecraft adapter (25-inch diameter by 12-inch length) can be modified to accommodate 1100/1200-pound payloads having their cg's 24 inches forward of the separation plane. The TE-364-4 third stage is common to all launch vehicles considered in this study. Use of the 25- by 12-inch standard adapter permits the use of the Pioneer F and G spacecraft interstage envelope for all configurations developed in this study.

Major emphasis has been placed on the minimization of electric propulsion contamination by-products on critical spacecraft components and scientific experiments.

An external view of the Pioneer F and G spacecraft is presented in Figure 4-2. The Pioneer spacecraft is stabilized by spinning about an

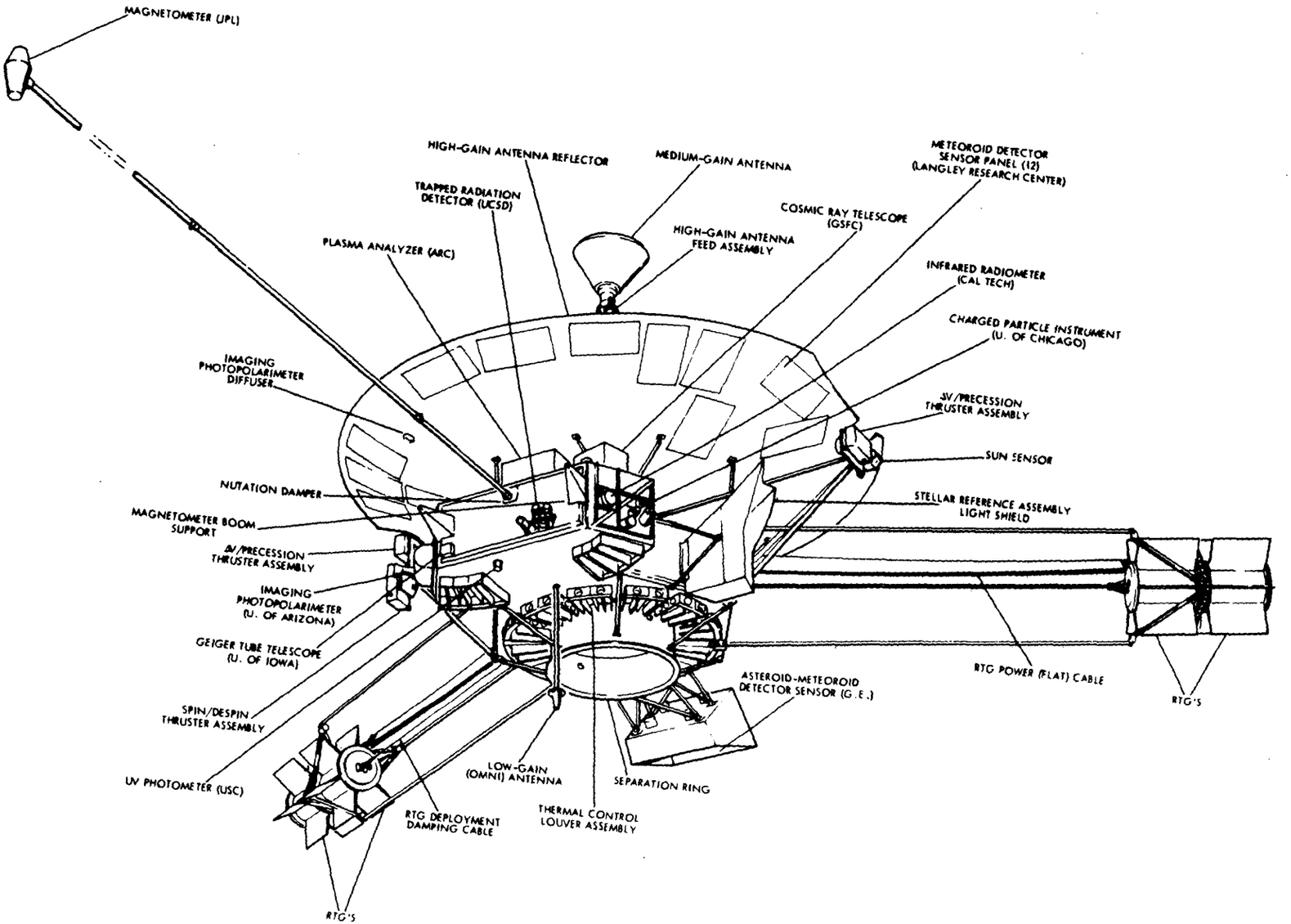

Figure 4-2. Pioneer F and G Spacecraft

axis parallel to the high-gain antenna axis. Four RTG's and the magnetometer science instrument are deployed as three equally spaced masses in a plane perpendicular to the spin axis. Other external features of the spacecraft include several other scientific instrument sensors, a medium-gain horn antenna forward of the high-gain antenna feed directed forward, and a low-gain antenna aft of the equipment compartment directed aft. One-pound hydrazine thruster assemblies are located 180 degrees apart at the rim of the dish and are used for velocity correction maneuvers, precession maneuvers, and spin control. External attitude control subsystem sensors include a sun sensor mounted near one of the thruster assemblies, and the stellar reference assembly with its external light shield.

Figure 4-3 shows the arrangement of the spacecraft equipment compartment. Most of the spacecraft electronic assemblies are located in the central hexagonal portion of the compartment, surrounding a 16.5-inch diameter hydrazine tank. Most of the internal scientific instrument electronic units and sensors are mounted in an instrument bay located on one side of the central hexagon. The equipment compartment is mainly fabricated from aluminum honeycomb sandwich panels which provide structural support and meteoroid protection, and is covered by insulation blankets which, together with active louvers under the mounting platform, provide thermal control.

Including the instruments and RTG's, the Pioneer F and G spacecraft weighs 560 pounds and has a power budget based on 150 watts of initial power from the RTG's and 120 watts at Jupiter encounter — 2.5 years after launch. The normal attitude of the spacecraft during the mission has the spin axis lying in the plane of the ecliptic and directed toward the earth. Therefore, instruments whose fields of view are directed generally perpendicular to the spin axis scan in a plane perpendicular to the ecliptic at a rate of 4.8 rpm.

This, again, was the baseline design to which minimum modifications were independently applied to accommodate each of the missions considered in this study.

The requirements imposed by the study missions on the spacecraft design had certain major features which differed in comparison with the F and G mission, these are:

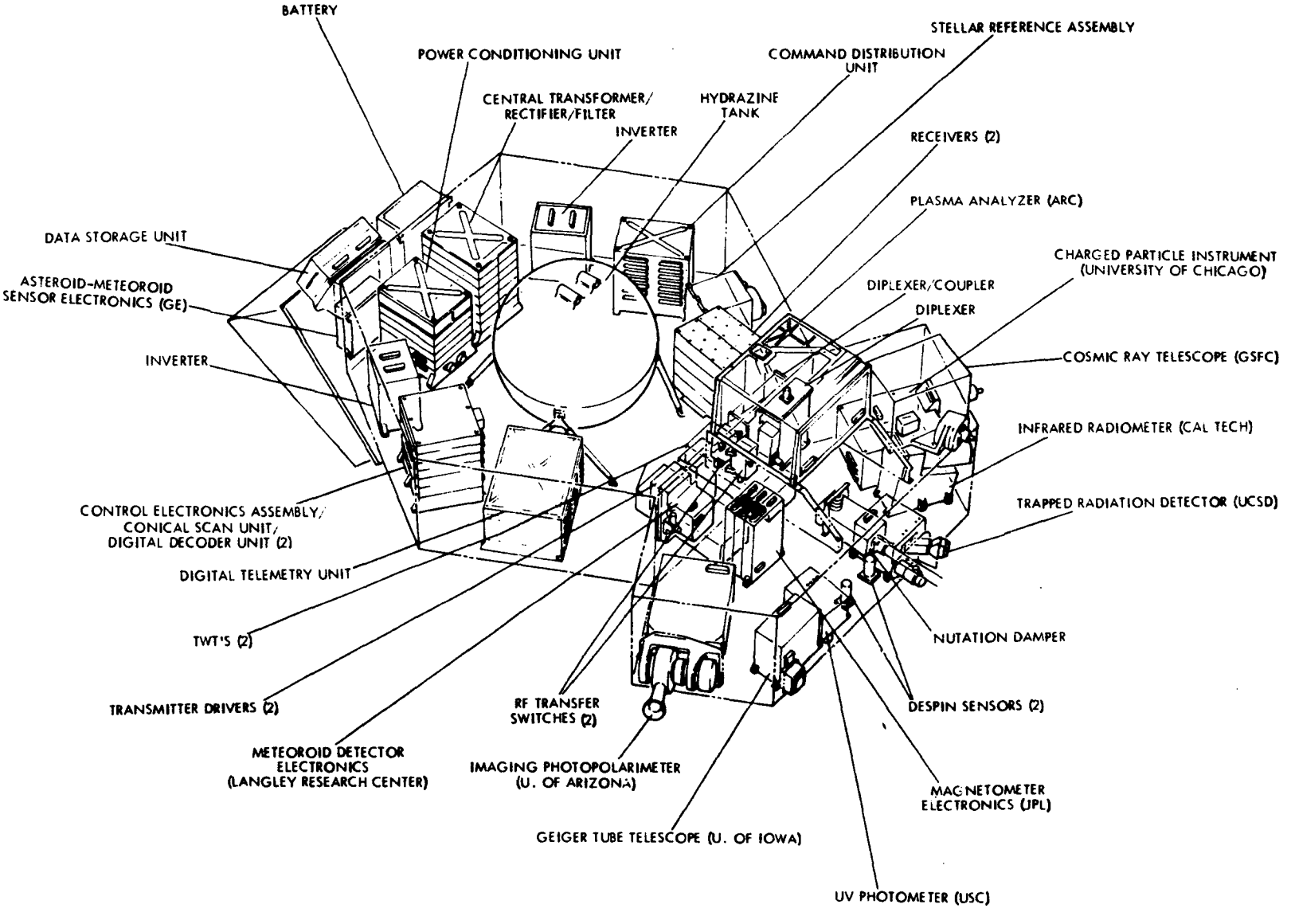

Figure 4-3. Pioneer F and G Equipment Compartment

a) Electric Propulsion. For every mission, the spacecraft must incorporate an electric propulsion system containing from three to five ion thrusters which provide thrust to augment that provided by the launch vehicle. As noted above, the electric propulsion subsystem must be noncontaminating to the maximum extent possible. Associated with the thrusters are electric power processing units of significant size, weight and thermal dissipation requirements which must be incorporated into the spacecraft system.

b) Electric Power. To provide the electric power required by the electric propulsion subsystem, a solar array with up to 8-kw capacity must be added to the spacecraft. Array deployment techniques must be evaluated and a design evolved which utilizes centrifugal force, generated by the spacecraft spin, to deploy the solar array. For most missions the solar array panels are the sole primary power source and replace the Pioneer F and G RTG's. However, for missions beyond 5 AU the solar arrays require augmentation by the RTG's and both systems are carried.

c) Propellant Tanks. The electric propulsion engines use mercury as the propellant, and the missions studied require from 100 to 300 pounds of mercury. The mercury tankage must be added to the existing hydrazine propellant tankage of the Pioneer F and G. Various loading combinations must be accommodated without causing excessive impact to the equipment mounting capability of the compartment. Excessive use of mounting platform by the tankage would make it necessary to enlarge the equipment compartment which would be costly in weight and dollars.

d) Scientific Instruments. As specific scientific payloads were not defined for the missions, the accommodation of the Pioneer F and G science complement was used as the design goal. Flexibility was maintained to accommodate different science payloads.

e) Communications. During the periods of ion engine thrusting the spacecraft axis is tilted so that the solar array plane makes an angle of 45 degrees to the sun-spacecraft line. With the trajectories involved, during these thrusting periods the spacecraft high-gain antenna is not earth-oriented. The Pioneer F and G low-gain (omni) antenna cannot provide communications during these periods.

Therefore, it is necessary to add an antenna system which provides communications while the earth is off the spacecraft axis and the spacecraft is spinning.

In addition to the above requirements, it was necessary for spacecraft configurations generated for the study missions to conform to the interfaces with other project elements. The launch vehicle interface has, among its major significant parts, the following:

a) The launch vehicle performance, given by payload weight versus injection energy at earth

b) The physical space available within the dynamic envelope of the nose fairing, and the dimensions of the interface with the final stages of the launch vehicle

c) The capability of carrying weight and moments loads of the spacecraft by the upper stage and by the spacecraft attach fitting of the launch vehicle.

4.2.1 Configuration Design Approaches

The statement of work required that the configuration for each mission be independently generated from the basic Pioneer F and G spacecraft. The minimum modifications necessary for each design was to be established.

The requirements discussed earlier in this section were common to all the missions and the solutions found were optimum for all.

4.2.1.1 Electric Propulsion/Antenna Interface

The most significant problem — that of incorporating the electric propulsion subsystem thrusters and a new medium-gain antenna into the Pioneer F and G design — was addressed initially.

In the Multi-Mission Electric Propulsion Spacecraft Study* it was determined that communications during ion engine thrusting could be

*"Feasibility Study for a Multi-Mission Electric Propulsion Spacecraft (Pioneer Concept)," Final Report, June 18, 1971, TRW 18305-6001-R000.

accomplished by a biconical horn array acting as a medium-gain antenna. This antenna emits a conical fan beam pattern with the boresight of the beam cross section making an angle of 71 degrees to the forward spin axis. The half-power beamwidth is 17 degrees.

It is extremely desirable to have no spacecraft components forward of the electric engine thruster apertures. Components located forward of the engine apertures become coated with the metallic exhaust components. Additionally, objects located forward of the engine apertures emit secondary metallic particles, when struck by the engine exhaust, and these emissions can metallically coat spacecraft components within their line of sight. In this manner components located aft of the engine apertures can be metallically coated. Antennas and the ion engine themselves can be short-circuited, sensor apertures can be obscured and solar array cells can be coated. Optimum conditions can most readily be achieved with all spacecraft components located aft of the engine apertures, therefore this has become the basic ground rule for configuration design.

Various location geometries of the electric engines and the medium-gain antenna were considered before coming to the conclusion noted above. These are shown in Figure 4-4. The arrangement shown in (A) has the engine located near the periphery of the dish which must have an engine clearance cutout and results in a loss of 4 square feet of reflector. The engine exhaust impinges on the high-gain antenna feed assembly and the medium-gain antenna may be degraded by primary and secondary engine emissions. Spacecraft and science sensor apertures and the solar array would be subject to coating by secondary emissions. In (B) and (C) the engines and medium-gain antenna have been located forward. In (B) only a portion of the medium-gain antenna is directly bombarded by engine exhaust. The antenna is again subject to contamination and the secondary back-scatter, while reduced, is still a significant problem. In (C) high-gain antenna blockage and mass properties problems are maximized. (D), (E) and (F) locate the engine apertures so that no spacecraft component is subjected to direct impact by engine exhaust thereby providing the most benign environment relative to exhaust contamination. The (D) and (F)

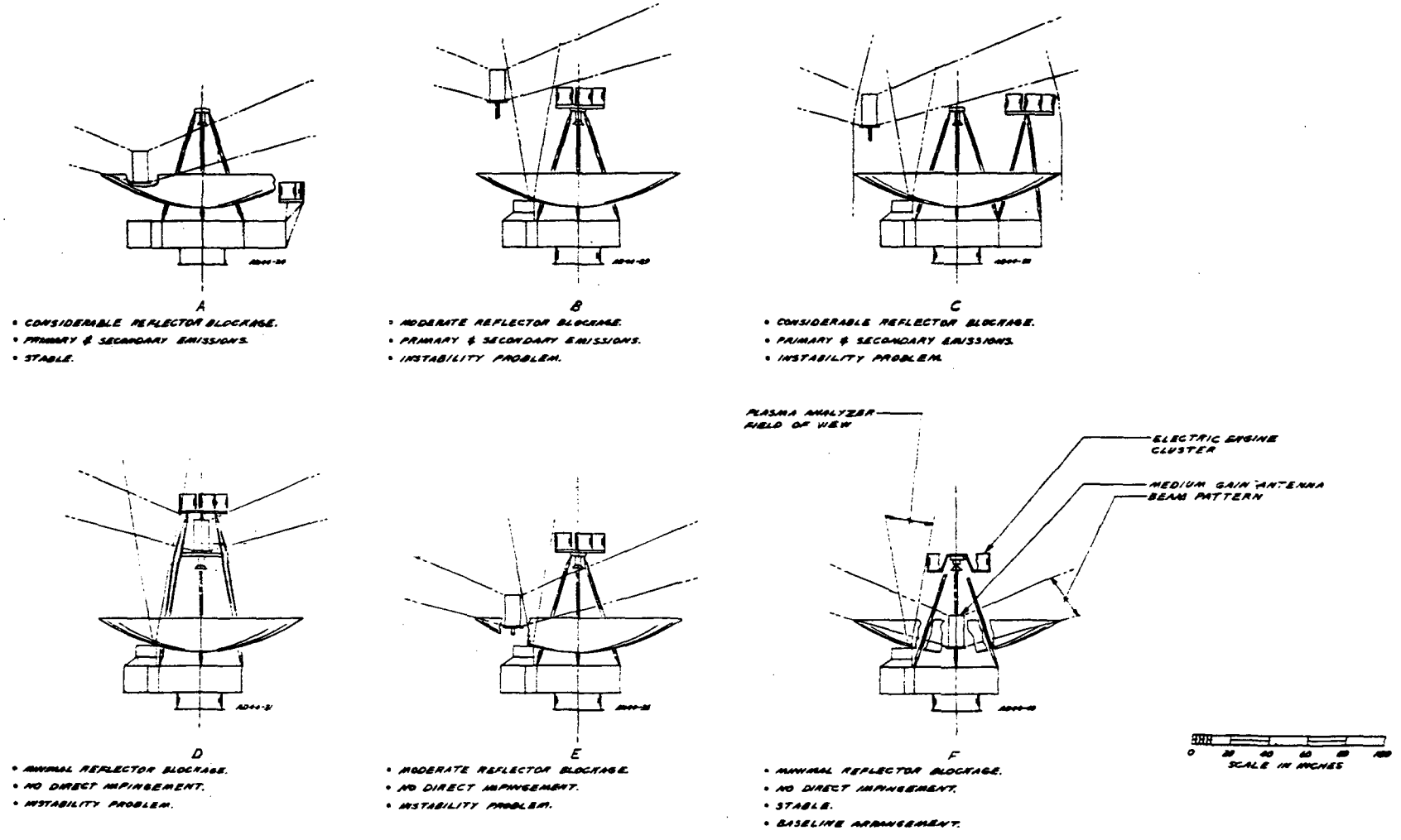

Figure 4-4. Electric Engine/Antenna Arrangement Candidates

configurations provide the least dish blockage but (D) is the heaviest due to the large moment arm and structural requirements of the engine masses. (D) also presents the most severe mass property problem. The (E) arrangement provides slightly more dish blockage, is not as heavy as (D) and reduces (but does not eliminate) mass property problems.

The (F) arrangment clusters the engine around the high-gain antenna feed with the engine apertures slightly forward of all other spacecraft components. This geometry avoids the mass property problem inherent in the other arrangements and is noncontaminating. The fan beam medium-gain antenna is located on the spacecraft centerline where it does not contribute to the blockage of the high-gain antenna reflector. (F) is considered to be the superior arrangement and has been adopted as the basic configuration.

4.2.1.2 Electric Propulsion/Mass Property Interface

The same mass property/dynamic stability problem exists for all of the configurations noted above except (A) and (F). The electric engines and their support structure represent masses approaching 40 pounds. When these are located significant distances from the spacecraft cg they present problems of static balance, unbalanced products of inertia and adverse moment of inertia ratios. The following discussion concerning (E) is generally applicable to all arrangements of Figure 4-4 except (F).

During launch it is necessary to have the spacecraft cg on the launch vehicle thrust axis. Clustering the electric engines symmetrically about the spacecraft centerline, which is coincident with the thrust axis, simplifies this task.

The Pioneer F and G spacecraft is spin stabilized prior to RTG deployment. The spacecraft of configuration (E) is not spin stable prior to appendage deployment due to electric engine placement at significant distances from the cg plane. At that time the moment of inertia about the spin axis is not maximum. Special consideration must be given to the task of appendage deployment, which achieves spin stability (maximum moment of inertia about the spin axis), before catastrophic loss of control occurs. The (F) arrangement permits spin stability to be achieved before appendage deployment.

4.2.1.3 Electric Propulsion/Chemical Propulsion Interface

Another significant problem is concerned with accommodating the electric engine mercury tankage as well as the attitude control subsystem with 30 to 60 pounds of hydrazine. To minimize structural weight it is desirable to locate the masses on or symmetrically about the spin axis and as close as possible to the spacecraft cg and interstage structure as possible. To minimize micrometeoroid protection and thermal control problems, and changes to the Pioneer F and G spacecraft, it is desirable to locate the propellant within the confines of the equipment compartment. If the addition of the mercury tankage displaces electronic units from the currently used areas on the equipment mounting platform, the equipment compartment will require enlargement to accommodate the displaced equipment. This results in additional weight and cost. Also, the mercury tankage must be added in a manner which does not violate the static and dynamic balance of the spacecraft. The Pioneer F and G spacecraft have asymmetrical appendage deployment. Therefore, all expendables and consumables are located on the cg plane to keep the spacecraft spin axis parallel to the high-gain antenna boresight axis before and after deployment.

A great many tankage arrangments were investigated. Four representative arrangements are shown in Figure 4-5. Configuration (A) locates the tankage symmetrically about the spacecraft centerline for balanced booster loads and on the spacecraft cg plane to accommodate asymmetrical deployments. An equipment bay is added at the -X axis to house equipment displaced by the tankage. The tankage of (B) is similar to that of (A) except that four symmetrically located tanks are used to provide a tight cluster around the spacecraft centerline, to use less of the compartment peripheral area and to eliminate the requirement for the extra bay at the -X axis.

The (C) arrangement retains the Pioneer F and G tank installation which is capable of holding 60 pounds of hydrazine. The tank is offloaded as required. The tank as show is on the Pioneer F and G cg station plane but is below the cg plane of the study spacecraft. The mercury is in two tanks which are located forward of the study spacecraft

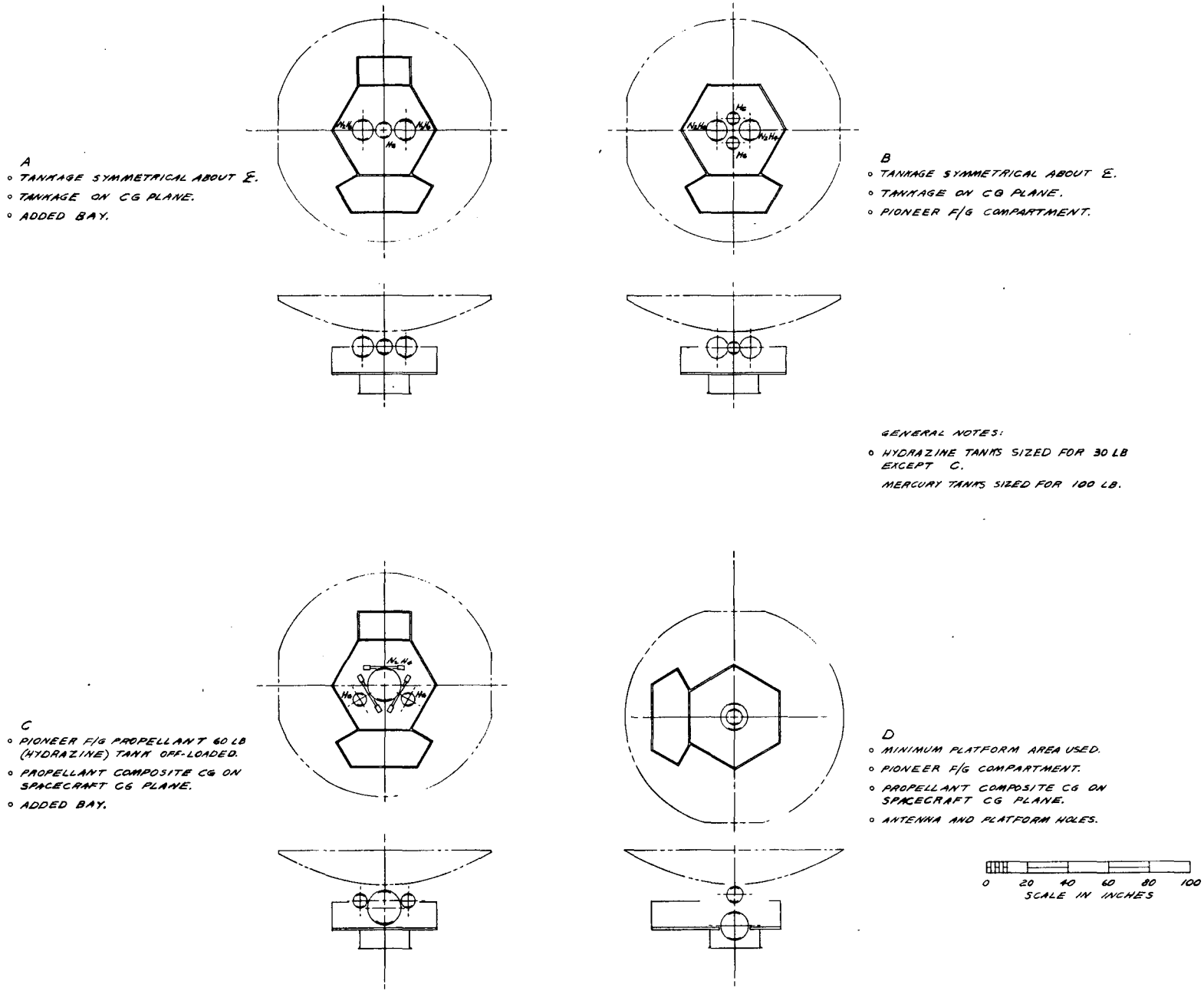

Figure 4-5. Candidate Tankage Arrangements

cg plane so that the composite propellant cg is on the spacecraft cg plane. The dynamic effects of the arrangement are discussed later. In (D) the tanks have been stacked vertically to minimize the number of tanks and the equipment platform mounting space used by the tankage. This arrangement precludes the need for an additional equipment bay. The tank structural support is simple and direct. A flange on the hydrazine tank equator mounts directly (through thermal isolators) to the equipment platform. The vertical loads of the mercury tank are taken by struts to the platform at the intersection with the interstage cylinder. Lateral loads are taken out by struts attached to the forward cover. The composite cg of the tankage is located on the spacecraft cg plane. Holes are required in the platform and dish to accommodate the tankage.

Except for (C) where the hydrazine tank is sized for 60 pounds and is off-loaded, the tankage for Figure 4-5 is sized for 30 pounds of hydrazine and 100 pounds of mercury. Case (C) is therefore recommended for the comet rendezvous mission while all other missions can be accommodated using the case (D) configuration.

In cases (C) and (D), tanks are located forward and aft of the cg plane with the composite tankage cg on the spacecraft cg plane. With this geometry, asymmetrical appendage deployments do not tilt the spacecraft spin axis; the spin axis will remain parallel to the high-gain antenna axis. This condition is also achieved during propellant usage as long as the same percentage by weight is used from each propellant system.

With the study spacecraft, however, the mercury propellant is exhausted during the early portion of the mission while only a portion (25 percent assumed) of the hydrazine is consumed. Preliminary calculations have shown that due to the very large moment-of-inertia ratios achieved with the study spacecraft that, under the conditions noted, the principal axis tils less than 0.1 degree. The principal axis is not tilted when the tanks are full, but begins to tilt as the mercury is consumed at a faster rate than the hydrazine. The tilt reaches a maximum of approximately 0.07 degree when the mercury is fully consumed, reduces as hydrazine consumption continues and returns to a 0.0 degree tilt when the hydrazine is also completely consumed. It is believed that with the

antenna bandwidths involved, the approximately 0.1 degree principal axis tilt is a very acceptable price to pay for the structural and space usage benefits derived from the vertical tankage arrangement of (D).

4.2.2 1 to 5 AU Mission Preferred Configuration

The design shown in Figure 4-6 is the basic configuration developed for the 1 to 5 AU missions with the exception of tankage, as previously mentioned, the comet rendezvous mission requires a larger hydrazine tank. Either a 5 kw five 15-cm system (as shown) or an 8 kw three 30-cm system can be accommodated. The spacecraft shown uses asymmetrical deployment of its solar array panels and magnetometer boom similarly to the RTG and boom deployments of Pioneer F and G.

The design uses the vertical propellant tankage arrangement discussed earlier in order to obtain the advantages of:

a) Simplified structure with minimum change from Pioneer F and G than that obtained with all tankage located on the spacecraft cg plane.

b) Less loss in equipment platform area than would result with all tankage located on the spacecraft cg plane.

Vertically stacked tanks result in the most desirable tankage arrangement as it centralizes their considerable mass (almost 20 percent of the spacecraft total mass) on the booster thrust axis and symmetrically locates them with respect to the Pioneer F and G structure. The tankage can be provided structural support with minimum loss of usable area on the equipment mounting platform. Tanks mounted exclusively in the cg plane make less of the equipment mounting panel area available to the electronic boxes. This tankage arrangement results in a loss of less than 0.1 degree in antenna pointing accuracy which is considered acceptable.

The 120-degree separation between the solar array panels results in these benefits:

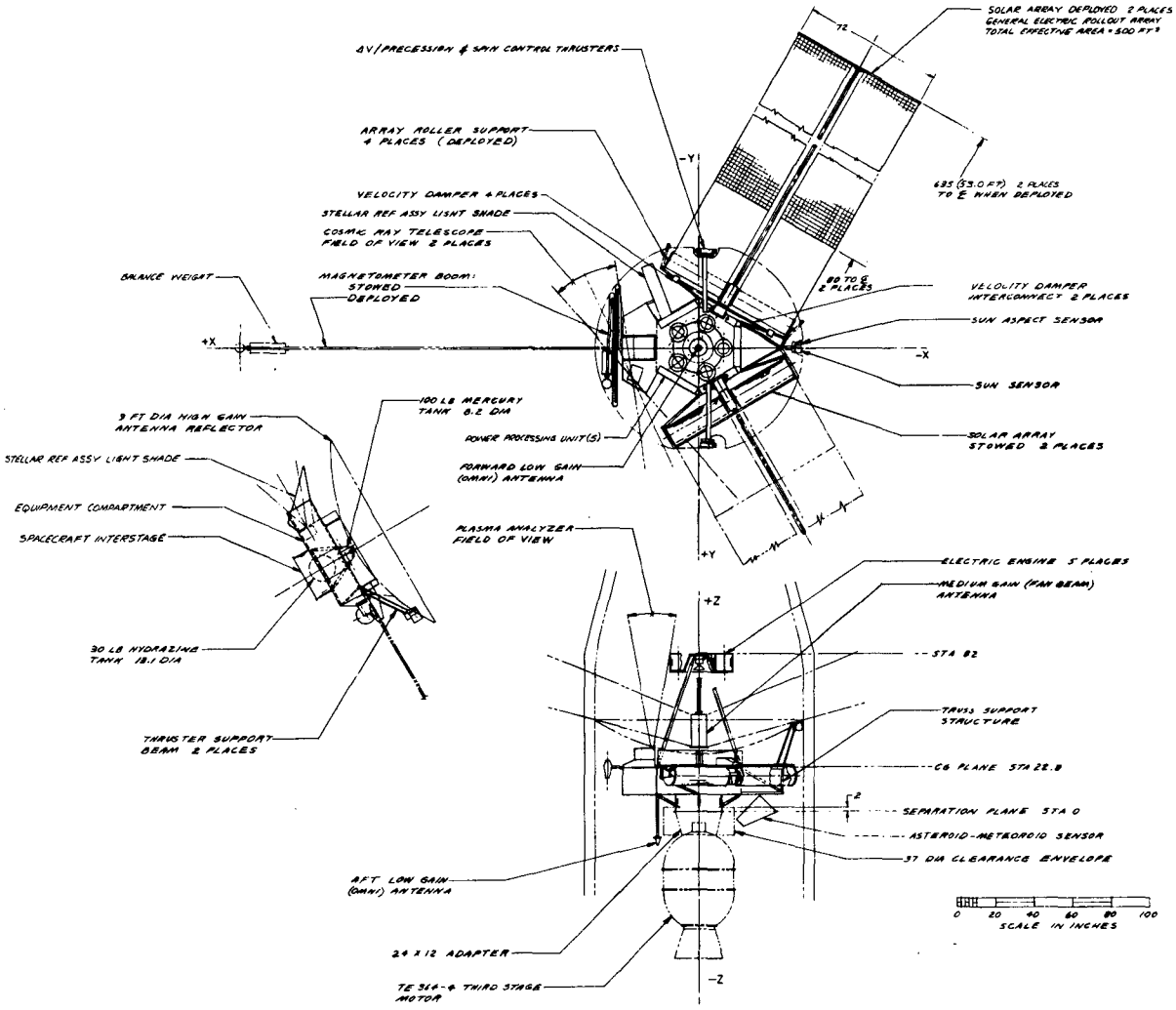

Figure 4-6. 1 to 5 AU Mission Configuration

a) It maximizes the distance between the deployed panels and the majority of the scientific equipment which is located in the bay at the spacecraft +X axis. The array magnetic effects are minimized.

b) The allowable fields of view of the experiments are maximized as the array panels are swept away from the +X axis.

The Pioneer F and G magnetometer boom is used and is mounted in the same general area as on Pioneer F and G. The boom has been moved forward to locate it on the study spacecraft plane. This minimizes spacecraft principal axis rotation and antenna pointing accuracy loss when the boom deploys.

4. 2. 2. 1 Structure and Equipment Compartment

The overall spacecraft is heavier than Pioneer F and G so that the basic structure of the spacecraft will require reinforcement if the "g" levels are not reduced from those of the Pioneer F and G program. Strengthening can be accomplished by increasing skin gages and fitting wall thicknesses and by the addition of reinforcing doublers at strategic locations.

The spacecraft mounts to the TE-364-4 third stage motor with the standard 25-inch diameter by 12-inch long conical interstage envelope used on Pioneer F and G.

The spacecraft's central cylinder and equipment compartment have the Pioneer F and G geometry. The equipment mounting platform is holed to accommodate and support the hydrazine tank. The mercury tank is supported by struts which attach to the platform, similar to the F and G installation, and take out the vertical loads. The torsional and lateral loads are dumped into the forward cover. This tankage installation appears to detract nothing from the equipment mounting area available on Pioneer F and G.

A triangular-shaped truss has been added to the -X axis to provide a support base for the solar array panels and the sun and sun-aspect sensors. The truss is matched to the hexagonal compartment structure to make use of existing hard points and load paths and to minimize weight.

The truss can also be used to support electronic equipment by adding mounting panels to the truss facets.

The solar arrays, sun sensor, sun-aspect sensor, attitude control thrusters, and medium-gain antenna are supported by truss or beam systems anchored to hard-points on the Pioneer F and G structure. Naturally, added fittings will be required.

The stowed solar array panels preempt the space occupied by the thruster Y-Y axis support strut of the Pioneer F and G design. Therefore, the tripod thruster supports have been replaced by cantilevered beams mounted to the compartment forward surface. The thruster clusters have been maintained in their original positions to match the existing cutouts in the reflector. The sun sensor has been relocated on the thruster support bracket at the +Y axis.

The electric propulsion subsystem engines are clustered around the high-gain antenna feed and are supported by the feed support tripod. The tripod members will require strengthening to accommodate the increased loading and will be fabricated from fiberglass to minimize RF blockage of the medium-gain antenna. The F and G struts were fabricated from boron.

Figure 4-7 (A) shows an equipment arrangement for the 5 kw five 15-cm and 4-7 (B) for the 8 kw three 30-cm thruster configuration. Both arrangements are the same except for the electric propulsion PPU's.

The arrangment of the scientific equipment is very similar to that of F and G. The TWT locations and the placement of all of the equipment mounted to the +X axis partial bulkhead are identical to those of F and G. Several of the electronic units mounted in the hexagonal compartment also have F and G positions, but due to the relocation of the stellar reference assembly from the +X+Y quadrant to the +X-Y quadrant, a number of units are located differently. A new sun-aspect sensor electronic unit has been located in the truss area of the -X axis.

Due to unique thermal requirements, the battery and the five power processing units associated with the electric propulsion subsystem have been located externally on the forward cover of the equipment compartment.

EQUIPMENT LIST

1. CONVERTER
2. POWER CONDITIONING UNIT (PCU)
3. ASTEROID-METEOROID SENSOR ELECTRONICS
4. TRANSFORMER RECTIFIER FILTER (TRF)
5. SUN ASPECT SENSOR ELECTRONICS
6. INVERTER
7. COMMAND DATA UNIT (CDU)
8. CONSCAN SIGNAL PROCESSOR, COMMAND ELECTRONIC ASSEMBLY (CEA) & 2-DIGITAL DECODER UNIT (DDU) STACKED VERTICALLY
9. 2-RECEIVER STACKED HORIZONTALLY
10. DIPLEXER/COUPLER
11. 2-TRAVELLING WAVE TUBE (TWT)
12. 2-RF TRANSFER SWITCH
13. 2-TRANSMITTER DRIVER
14. STELLAR REFERENCE ASSEMBLY (SRA)
15. DIGITAL TELEMETRY UNIT (DTU)
16. DIGITAL STORAGE UNIT (DSU) STACKED VERTICALLY WITH DTU
17. CHARGED PARTICLE INSTRUMENT
18. INFRARED RADIOMETER
19. TRAPPED RADIATION DETECTOR
20. 2-DESPIN SENSOR
21. UV PHOTOMETER
22. GEIGER TUBE TELESCOPE
23. MAGNETOMETER ELECTRONICS
24. IMAGING PHOTOPOLARIMETER
25. METEOROID DETECTOR ELECTRONICS
26. DIPLEXER
27. 5-POWER PROCESSING UNIT (PPU)
28. BATTERY
29. COSMIC RAY TELESCOPE
30. PLASMA ANALYZER
31. MAGNETOMETER
32. SRA LIGHT SHADE

MOUNTED TO SIDE PANEL

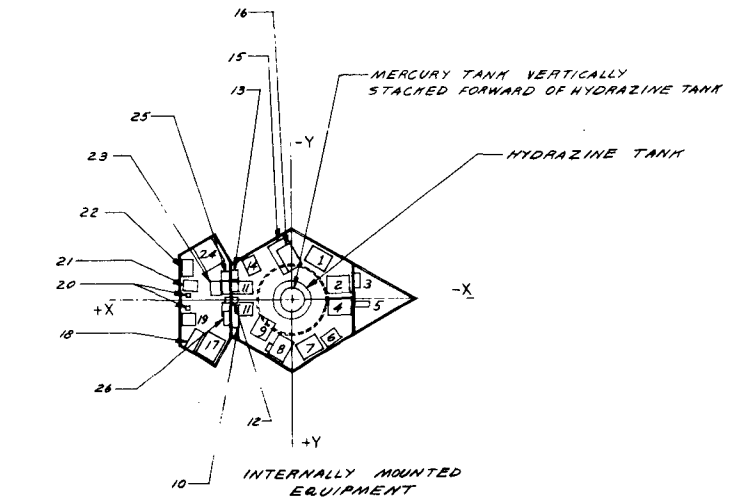

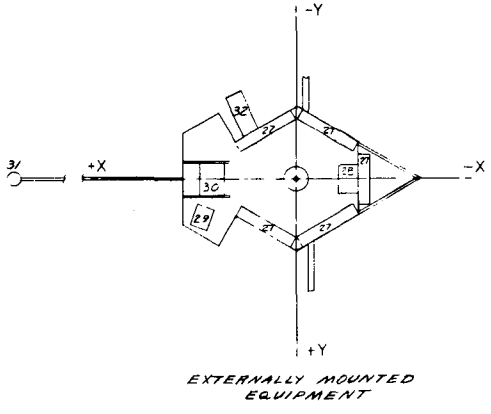

Figure 4-7 (A). Equipment Arrangement – 1 to 5 AU Mission Spacecraft (5 kw Five 15-cm Thruster Configuration)

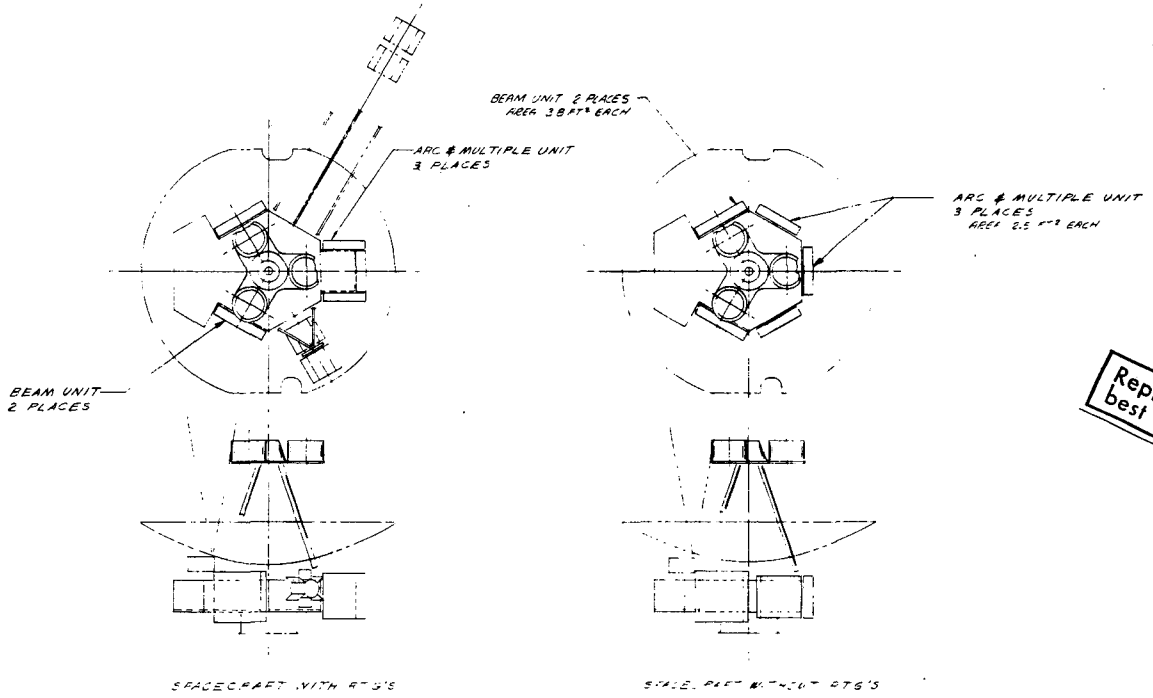

Figure 4-7 (B). Equipment Arrangement – 1 to 30 and 1 to 5 AU Mission Spacecraft (8 kw Three 30-cm Thruster Configuration)

Table 4-2 lists the spacecraft equipment, the number of each unit required, and their physical dimensions and weight.

Table 4-2. Equipment List — 1 to 5 AU Mission Spacecraft

SUBSYSTEM AND UNIT	NUMBER REQUIRED	BASIC SIZE (INCHES) FOOTPRINT WIDTH	FOOTPRINT LENGTH	HEIGHT	TOTAL WEIGHT (POUNDS)	TOTAL POWER DISSIPATED (WATTS)	COMMENTS
ELECTRIC PROPULSION							
ENGINE	5	9.0 DIAMETER x 9.0			35.0		
MERCURY TANK AND N_2 PRESSURANT	1	8.2 SPHERICAL DIA.					100 POUNDS OF MERCURY
POWER PROCESSING UNIT (PPU)	5	10.0	10.0	5.0	50.0		
ELECTRIC POWER							
SOLAR ARRAY PANELS	2	6 FT	46 FT	-			ACTIVE ARRAY BEGINS 80 INCHES FROM SPACECRAFT CENTERLINE
SHUNT RADIATOR	*	*	*	*			PIONEER F AND G WAS 12.5 x 15.0 x 0.4, WEIGHT 0.8 POUND
POWER CONDITIONING UNIT (PCU)	1	6.0	8.0	9.3	10.8		
CENTRAL TRANSFORMER RECTIFIER FILTER (TRF)	1	6.0	8.0	11.3	11.3		
CONVERTER	1	6.0	8.0	10.0	12.0		
INVERTER	1	4.5	6.0	7.0	5.5		
BATTERY	1	7.2	10.0	2.7	5.2		
COMMUNICATIONS							
CONSCAN SIGNAL PROCESSOR	1	6.0	8.0	1.0	1.0		STACKED VERTICALLY WITH CEA AND DDU
RECEIVER	2	3.1	7.3	9.3	10.2		STACKED HORIZONTALLY
TWTA, S-BAND	2	4.5	11.0	3.0	8.0		
DIPLEXER	1	5.5	7.4	2.5	2.0		
DIPLEXER/COUPLER	1	5.5	9.2	2.5	2.3		
TRANSMITTER DRIVER	2	3.6	5.2	2.5	2.8		
RF TRANSFER SWITCH	2	1.8	3.0	1.9	1.3		
ATTENUATOR	2	0.4 DIAMETER x 1.4			0.1		
ANTENNAS							
HIGH-GAIN	1	9 FEET DIAMETER					PIONEER F AND G PARABOLIC, F/D = 0.4, MOVEABLE FEED
MEDIUM-GAIN	1	8.2 DIAMETER x 16.5			4.0		
LOW-GAIN (OMNI)							
CONICAL LOG SPIRAL	1	3.0 DIAMETER x 4.4					
CUPPED DIPOLE	1	3.0 DIAMETER x 3.0					
DATA HANDLING							
DITITAL TELEMETRY UNIT (DTU)	1	7.5	11.3	5.7	7.0		MAY BE VERTICALLY STACKED WITH DSU
DIGITAL STORAGE UNIT (DSU)	1	5.6	8.4	3.9	4.0		MAY BE VERTICALLY STACKED WITH DTU
DIGITAL DECODER UNIT (DDU)	2	6.0	8.0	1.0			VERTICALLY STACKED WITH CEA AND CONSCAN
COMMAND AND ELECTRICAL DISTRIBUTION							
COMMAND DATA UNIT (CDU)	1	6.0	8.0	8.9	9.5		
TEST PANEL ASSEMBLY	1	*	*	*			
WIRING HARNESS	1	*	*	*	28.0		
ATTITUDE CONTROL							
STELLAR REFERENCE ASSEMBLY (SRA)	1	4.5	6.0	6.3	2.6		
SRA LIGHT SHADE	1	*	*	*			
SUN SENSOR ASSEMBLY (SSA)	1	3.4	3.6	2.1	1.1		
SUN ASPECT SENSOR (SAS)	1	2.6	2.2	1.0	0.8		
COMMAND ELECTRONIC ASSEMBLY (CEA)	1	6.0	8.0	6.8	5.0		STACKED VERTICALLY WITH CONSCAN AND DDU
DESPIN SENSOR	2	1.5	1.5	2.0	0.5		
NUTATION DAMPER	1	5.5	4.3	6.0	1.2		ACTIVATED BY MAGNETOMETER BOOM
SAS ELECTRONICS	1	2.0	4.0	5.0	1.5	0.5	
CHEMICAL PROPULSION							
HYDRAZINE TANK AND N_2 PRESSURANT	1	13.1 SPHERICAL DIA.					30 POUNDS OF HYDRAZINE
THRUSTER CLUSTER ASSEMBLY	3	4.8	9.4	2.3	9.0		

*TO BE DETERMINED

4.2.2.2 Science

As noted earlier, the configuration retains the Pioneer F and G science compartment geometry, provides similar equipment compartment internal and external mounting surfaces, and a similar magnetometer boom installation. Table 4-3 lists the Pioneer F and G scientific

Table 4-3. Pioneer F and G Scientific Instrument List

CODE	INSTRUMENT	BASIC SIZE (INCHES) FOOTPRINT WIDTH	BASIC SIZE (INCHES) FOOTPRINT LENGTH	HEIGHT	WEIGHT (POUNDS)	POWER (WATTS)	BORESIGHT DIRECTION	TOTAL FOV (DEGREES)	REMARKS
A	HELIUM VECTOR MAGNETOMETER (JPL, SMITH)					5.2			KNOW ORIENTATION OF SENSOR AXES TO ±0.5 DEGREE WITH RESPECT TO SPACECRAFT AXES.
	• SENSOR	5.0 DIAMETER X 9.0			1.5		AXIS PARALLEL TO SPIN AXIS	NONE	SENSOR SIZE INCLUDES INSULATION.
	• ELECTRONICS	3.8	5.0	9.8	4.5				
B	PLASMA INSTRUMENT (ARC, WOLFE)	11.5	11.0	6.0	12.3	5.0	0° ELEVATION	20 X 140 FAN	TWO APERTURES. UNOBSTRUCTED FOV THROUGH ANTENNA.
C	CHARGED PARTICLE INSTRUMENT (CHICAGO, SIMPSON)	7.0	9.0	6.9	7.8	2.2	70° ELEVATION	65 CONE	MAIN TELESCOPE. UNOBSTRUCTED FOV.
							90° ELEVATION	70 CONE	LOW-ENERGY TELESCOPE. UNOBSTRUCTED FOV.
D	GEIGER TUBE TELESCOPE (IOWA, VAN ALLEN)	6.0	3.8	5.7	3.7	0.7	90° ELEVATION	30 X 60 FAN	GEIGER TUBE TELESCOPE. FOV MAY CONTAIN MAGNETOMETER BOOM.
								45 CONE	LOW-ENERGY DETECTOR. FOV MAY CONTAIN MAGNETOMETER BOOM
E	COSMIC RAY TELESCOPE (GSFC, McDONALD)	6.0	8.0	6.5	7.8	2.4	90° ELEVATION	33 CONE	DOUBLE ENDED HIGH-ENERGY TELESCOPE. UNOBSTRUCTED FOV.
								50 CONE	LOW-ENERGY TELESCOPE I. UNOBSTRUCTED FOV.
								30 CONE	LOW-ENERGY TELESCOPE II. UNOBSTRUCTED FOV.
F	TRAPPED RADIATION DETECTOR (UCSD, FILLIUS)	5.0	4.7	3.8	4.0	3.0	90° ELEVATION	120 CONE	DETECTOR C. MINIMUM FOV OBSTRUCTION.
							90° ELEVATION	60 CONE	DETECTOR E. UNOBSTRUCTED FOV.
							90° ELEVATION	60 CONE	DETECTOR S. UNOBSTRUCTED FOV.
							NONE	NONE	DETECTOR M.
G	UV PHOTOMETER (USC, JUDGE)	4.0	5.0	3.0	1.5	0.7	160° ELEVATION	2.5 X 28.1 FAN	TELESCOPE AXIS TO PASS THROUGH SPACECRAFT SPIN AXIS ±6 MINUTES. UNOBSTRUCTED FOV.
H	IMAGING PHOTOPOLARIMETER (ARIZONA, GEHRELS)	7.5	18.0	4.6	9.1	2.8	90° ELEVATION, NOMINAL	2 X 2 FAN	UNOBSTRUCTED FOV. TELESCOPE ROTATES ±80° IN ELEVATION. 60° FOV FREE OF SCATTERED LIGHT. REQUIRES DIFFUSER FOR CALIBRATION.
I	INFRARED RADIOMETER (CIT, (MUNCH)	3.9	6.4	9.0	4.4	1.8	105° ELEVATION	20 CONE	UNOBSTRUCTED FOV. 90° CONE FOV TO BE FREE OF RTG'S
J	ASTEROID-METEOROID DETECTOR (G.E., SOBERMAN)					2.3			
	• SENSOR	18.0	18.0	12.5	5.5		135° ELEVATION	10 CONE	UNOBSTRUCTED FOV. 2π STERIDAN FOV FREE OF SCATTERED LIGHT.
	• ELECTRONICS	8.5	6.0	2.2	1.9				
K	METEOROID DETECTOR (LaRC, KINARD)					0.7			
	• SENSOR (12 PANELS)	7.4	12.5	0.6	3.2		PLANE OF PANEL: 60° MINIMUM IN ELEVATION.	SENSOR AREAS TO BE UNOBSTRUCTED FOR PARTICLES TRAVELLING PARALLEL TO THE SPACECRAFT SPIN AXIS FROM THE -Z DIRECTION.	
	• ELECTRONICS	3.1	3.2	3.0	0.9				

instrumentation, the unit size, weight, power dissipation, boresight direction and field-of-view requirements, and miscellaneous information. Figure 4-8 illustrates the fields of view provided with respect to the geometry of the 1-5 AU mission baseline spacecraft. The Pioneer F and G science payload is shown installed in the 1 to 5 AU mission baseline spacecraft in the same or similar positions they presently occupy. The field of view requirements are also satisfied to a large extent. The changes from the Pioneer F and G installation and violation of the Pioneer F and G field-of-view requirements are:

a) The magnetometer boom (JPL/Smith) has been moved forward to the cg plane. This location minimizes the spacecraft principal axis rotation and antenna pointing errors caused by the magnetometer deployment.

b) The plasma analyzer (ARC/Wolfe) field of view is intruded 0.8 inch by the electric engine installation. However, an unobstructed field of view can be provided readily by any or a combination of the following changes:

- A smaller engine cluster diameter
- Reduction in engine size
- Asymmetrical relocation of the engines.

c) The cosmic ray telescope (GSFC/Mc Donald) has the +Y axis solar array panel in the field of view of the high-energy telescope front aperture.

d) The main 2 x 2 degree field of view of the imaging photopolarimeter (Gehrels/University of Arizona) is unobstructed. The additional F and G requirement for a 60-degree full conical field of view to be free of scattered light also appears to be met. However, the effect of the -Y axis solar array panel should be checked with the experimenter. An extension of the stellar reference light shade may intrude into the field of view to be free of scattered light.

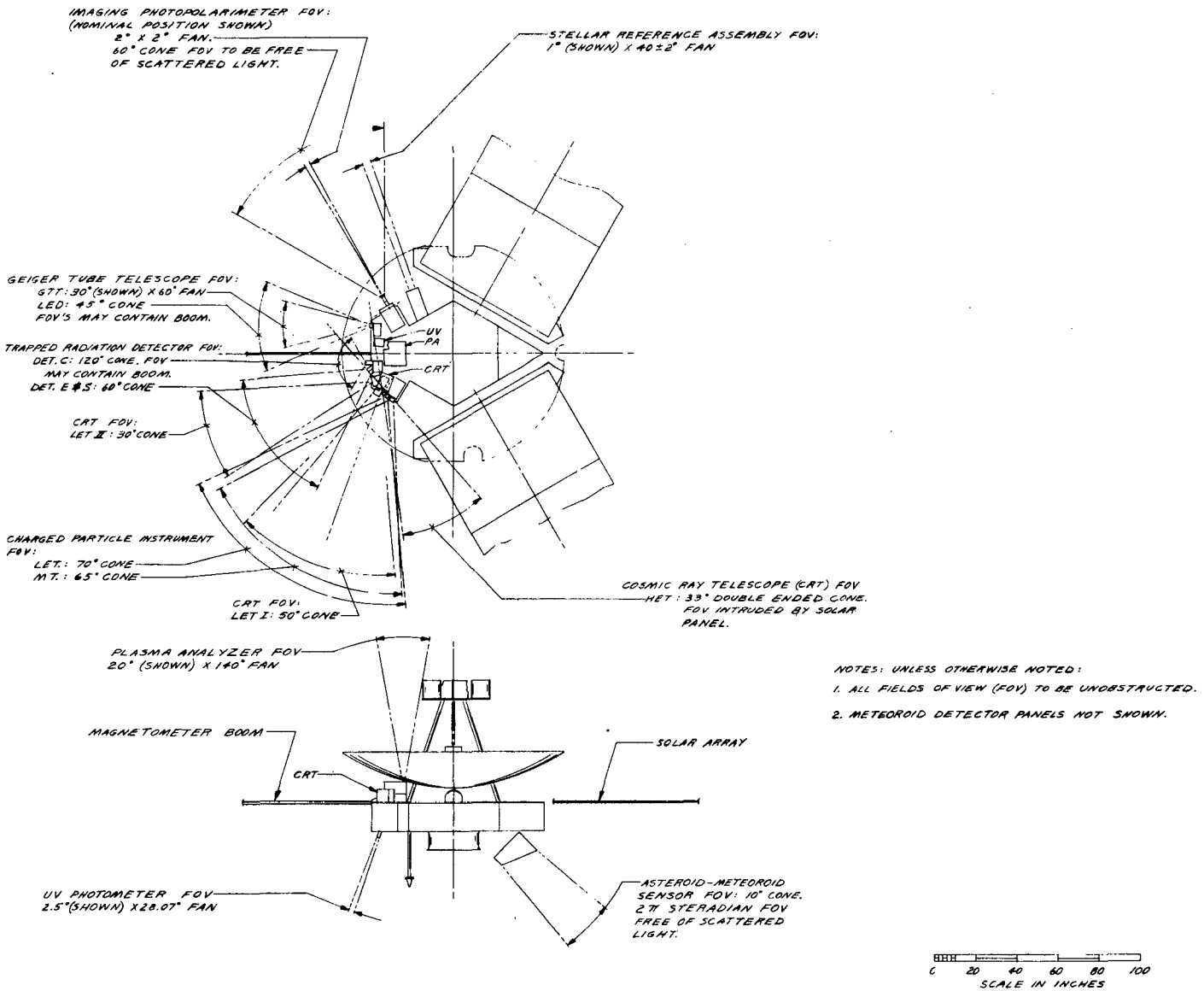

Figure 4-8. Science Fields of View for the 1 to 5 AU Mission Spacecraft

e) The light shade of the asteroid-meteoroid detector (GE/Soberman) may require modification due to the effects of the deployed solar array panels.

f) A number of the elements of the meteoroid detector (LaRC/Kinard) are shadowed by:

- Solar array panel support structure
- Stellar reference assembly light shade.

It is not possible to completely satisfy the requirements of the Pioneer F and G science payload. The inclusion of the large solar array necessary to support the electric propulsion subsystem makes is reasonable to expect that some scientific instrument modification will be made to optimize the overall system. As an example, there is no location on any of the study spacecraft which will satisfy the unobstructed field-of-view requirements of the cosmic ray telescope.

4.2.2.3 Electric Propulsion

The five 15-cm electric thrusters (three 30-cm thrusters could be accommodated equally as well) are shown located forward of the high-gain antenna feed to eliminate any direct impingement on spacecraft components by the engine exhaust. No spacecraft components are forward of the engine apertures. The engines are symmetrically clustered around the spacecraft centerline to minimize high-gain antenna RF blockage and to minimize unbalanced masses of the spacecraft stowed configuration. The engines are mounted to a hat-shaped structure which is in turn supported by the feed support strut assembly.

An 8.2 inch inside diameter spherical propellant tank is located on the thrust axis, as shown in the figure. This tank will accommodate 100 pounds of mercury and the associated gaseous nitrogen pressurant. The power processing units are located on the forward surface of the equipment compartment. In this location they are provided structural support, micrometeoroid protection, and view of deep space for heat rejection capability.

4.2.2.4 Chemical Propulsion

A 13.1-inch inside diameter spherical tank containing 30 pounds of hydrazine and the associated gaseous nitrogen pressurant is located on the thrust axis and, through thermal isolators, is mounted to the equipment platform. The system is the same single step blowdown system used for Pioneer F and G. The tank utilizes an equatorial flange to mount to the forward surface of the platform. As previously noted for the comet rendezvous mission, a return to the currently used 16.5-inch tank and possibly an 18-inch tank will be required. This accommodation technique has been shown in Figure 4-5 (C).

4.2.2.5 Attitude Control

The ΔV/precession and spin/despin thruster clusters and their physical locations are unchanged from Pioneer F and G. As noted earlier, the structural supports have been modified. To provide a field of view clear of the solar array panels, the sun aspect sensor has been located on the -X axis and is supported by a cantilevered beam. A cutout has been added to the high-gain antenna reflector to accommodate the sensor field-of-view.

The stellar reference assembly has been relocated to the +X-Y quadrant of the spacecraft with its boresight axis at an angle of 20 degrees with the -Y axis. Interference by the solar array panel made the existing location (+X+Y quadrant) unacceptable. In order to minimize electronic changes in the assembly electronics it is desirable to rotate the stellar reference assembly sensor boresight axis (in the spacecraft XY plane) in increments of 45 degrees. The stellar reference assembly location on the study spacecraft complies with this goal. The SRA light shade is also relocated and revised.

4.2.2.6 Electric Power

Electric power is provided by either a 5000-watt array or an 8000-watt array, consisting of two deployable panels mounted to the compartment as shown in Figure 4-6. The mechanical and operational details relative to the arrays are contained in Section 5.3. Similarly to the RTG installation on F and G, the solar array panels are located 120 degrees

apart to provide a symmetrical mass distribution with the science compartment, to maximize the science aperture field of view and to minimize magnetic effects on the instrumentation. The arrays are located on the spacecraft cg plane and separated from the thrust axis the distance necessary to provide a spin-stabilized spacecraft before appendage deployment. The panel width is maximized to yield the minimum aspect ratio. The array shown is for the 5-kw version and is 6 feet wide with cells on the outboard 46 feet of its length. The active area is initiated 80 inches from the spacecraft components for sun angles up to 45 degrees with the spacecraft centerline.

Two types of solar arrays, as described in Section 5.3, have been evaluated during the study: the bistem motor driven and the centrifugal force deployment. Following is a description for the centrifugal-type in which the motor acts as a damper for the bistem-type, eliminating the need for a special rotary velocity damper. However, the bistem ends up being considerably heavier, due to the requirement for the boom, motor, slip V-rings, etc.

On signal the panels are released permitting centrifugal forces to extend them to their deployed positions. The deployment velocity is maintained within acceptable limits by cable restraints located at both ends of each panel. One end of each cable is attached to the spacecraft while the other end is wound around the reel of a deployment mechanism. The spools for each panel are interconnected to maintain the amount of deployment of each end of the array equal. After full deployment the cables are released from the reels and are jettisoned from the spacecraft.

The uncelled inboard section of the array is fabricated from mesh to minimize the impingement of exhaust gases from the attitude control thrusters.

4.2.2.7 Communications

Except for the feed strut structural changes noted earlier, the high-gain antenna installation is similar to that of Pioneer F and G. Two cut-outs have been added in the reflector: one to accommodate the redundant sun aspect sensor fields of view, and a second to accommodate the medium-gain antenna support mast.

The medium-gain antenna has been located on the thrust axis forward of the high-gain antenna reflector. It is composed of a stacked biconical array to provide a conical fan beam 17 degrees wide and pointing at an angle of 71 degrees to the forward spin axis.

The low-gain omni-antenna system contains two elements. The existing conical log spiral antenna installation provides coverage aft and direct RF communications with the spacecraft when it is housed within the fairing. Forward coverage is provided by a cupped dipole antenna located on the thrust axis. The antenna aperture lies in the same plane as the electric thruster apertures.

4.2.2.8 Thermal Control

The Pioneer F and G thermal control system is utilized on this configuration. The spacecraft is wrapped in thermal blankets and the equipment compartment is thermally isolated from all external appendages by supporting them with nonmetallic materials of low thermal conductance to minimize uncontrolled heat loss. The compartment aft surface is fitted with the existing active thermal louver control system to reject excess heat to space.

Table 4-4 lists a summary of the spacecraft changes from Pioneer F and G.

4.2.3 1 to 5 AU Mission Alternate Configuration

The configuration shown in Figure 4-9 was developed to determine if the advantages of the vertically stacked tanks could be obtained without paying even the small associated penalty required by the design of Figure 4-6. In Figure 4-6 the spacecraft principal axes rotated approximately 0.07 degree due to vertically stacked tanks and asymmetric propellant usage. In that spacecraft (as on F and G) the operational spin axis does not coincide with the spacecraft centerline.

In order to avoid any rotation of the spacecraft spin axis, which would result in its being nonparallel to the high-gain antenna boresight axis, all spacecraft deployment appendages shown in Figure 4-9 are symmetrically deployed. This retains the spacecraft spin axis coincident with the booster thrust axis through all phases of the mission. The

Table 4-4. 1 to 5 AU Mission Baseline Spacecraft Summary of Changes from Pioneer F and G

Subsystem	Modifications
Electric propulsion - added	• Electric thrusters • Power processing units • Mercury tankage
Electric power	• Deleted RTG's, guide rods, black boxes, and associated fittings • Added two solar array panels and support structure • Added converter, deleted one of two inverters, changes battery, and changed shunt radiator
Science	• Relocated magnetometer boom to new cg location • Cosmic ray telescope high-energy telescope front aperture field of view has solar panel interference
Antennas	• Added cutouts in high-gain reflector for sun and sun aspect sensors, medium-gain antenna support • Added biconical stacked array medium-gain antenna • Deleted Pioneer F and G horn medium-gain antenna • Added forward low-gain (omni) antenna • Modified high-gain feed support strut assembly
Attitude Control	• Added sun aspect sensor and electronics • Relocated sun sensor • Relocated stellar reference assembly and modified light shade
Chemical Propulsion	• Redesigned thruster support structure
Structure	• Added solar array support truss • Miscellaneous changes for sun and sun aspect sensors, antennas, magnetometer boom, etc.

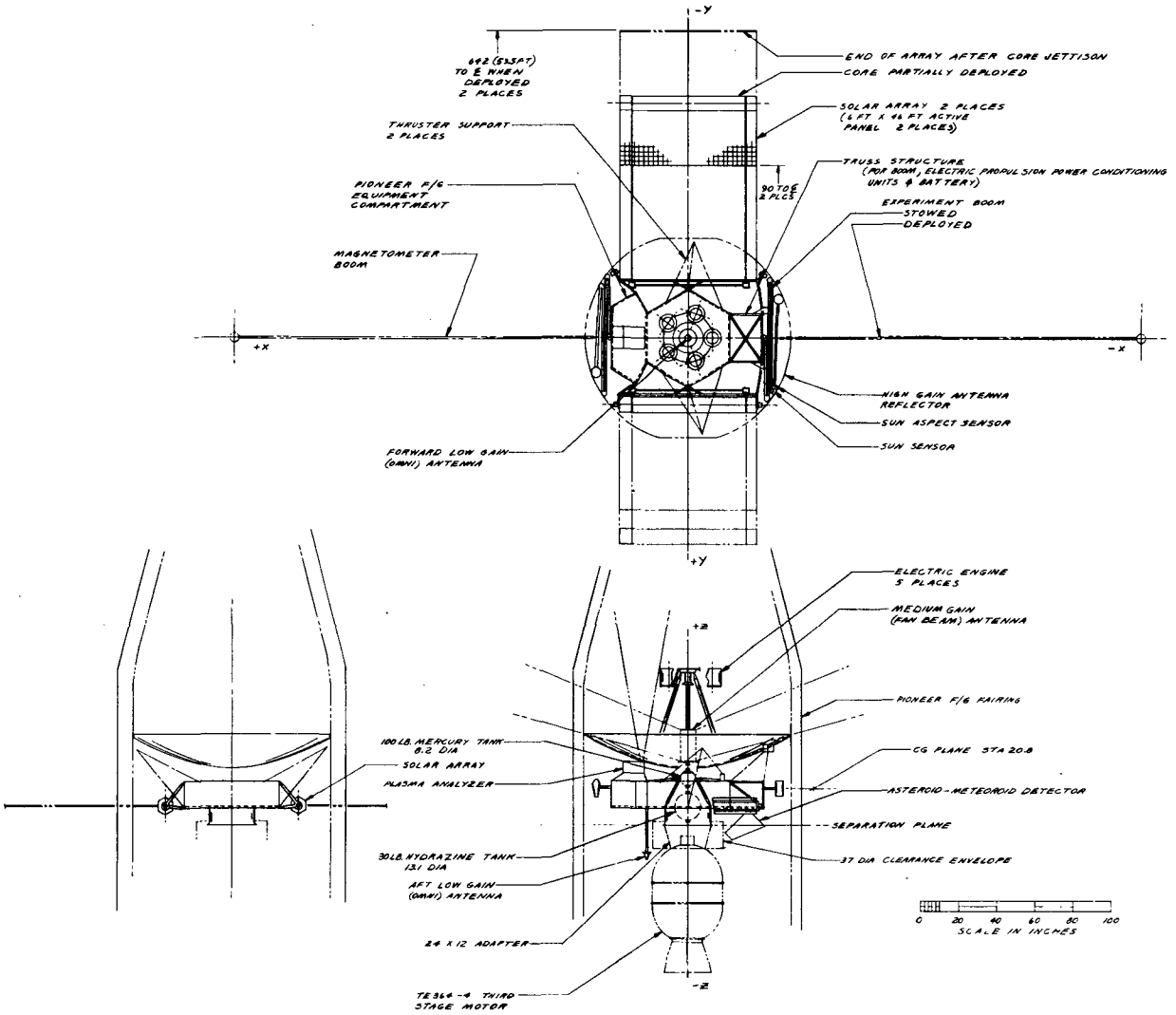

Figure 4-9. 1 to 5 AU Mission Alternate Configuration

spacecraft cg moves aft and forward along the spacecraft centerline as the propellants are consumed but remains on the centerline. In this manner the advantages of the vertically stacked tanks, noted earlier, is obtained and no loss in antenna pointing accuracy occurs due to asymmetrical propellant usage.

A deployable experiment boom similar to the one used for the Pioneer F and G magnetometer is located on the -X axis to dynamically balance the deployable magnetometer boom located on the +X axis. A truss structure supports the boom, the battery and the electric propulsion subsystem power conditioning equipment. These masses located on the -X axis side of the spacecraft compensate for the mass of the +X axis experiment compartment.

Analyses have shown that satisfactory mass properties can be obtained with only one deployable experiment boom if it is located on the spacecraft cg plane. The principal axes rotation and the resulting loss in antenna pointing accuracy that occurs due to asymmetrical propellant usage is inconsequential.

The optional configuration includes the following:

a) Location of the magnetometer boom on the -X axis

b) Deletion of the boom on the +X axis

This provides the science in the +X axis experiment compartment with unobstructed 180-degree fields of view.

Due to the relative location of the solar array panels, the basic attitude control thruster cluster support structure can be retained — which was not possible for the baseline design.

Several disadvantages result from the symmetrical locations of the solar panel of Figure 4-9.

a) The scientific experiment aperture fields of view toward the -X axis are decreased.

b) Any magnetic effects of the panels on the scientific units are increased.

c) The ratio of the moment of inertia about the spin axis to the maximum transverse moment of inertia is minimal.

The following paragraphs indicate only the design differences of the Figure 4-9 alternate configuration from the baseline configuration of Figure 4-6 discussed previously.

4.2.3.1 Structure and Equipment Compartment

The basic structure is the same as that of the baseline configuration. The -X axis truss structure is rectangular (instead of triangular) in plan form in order to support the experiment boom, battery and power processing equipment. Equipment mounting provisions can be supplied for any of the rectangular facets of the truss as the need is established. Any surface provided with sandwich panels for equipment mounting would eliminate the need for truss members on that surface.

The thruster cluster support trusses remain unchanged. The sun sensor has been relocated from its F and G location on the thruster cluster support bracket on the +Y axis. If need for dynamic mass balance of the truss system, a small mass (1.1 pounds) will be mounted on the bracket to replace the sun sensor mass.

Except for the stellar reference assembly and the imaging photopolarimeter, the internal equipment arrangement of Figure 4-7 is suitable for the alternate design. The stellar reference assembly can be located on the forward surface of the experiment compartment in the +X-Y quadrant. The power processing units are mounted to the external surfaces of the spacecraft in the -X area for static balance purposes.

4.2.3.2 Science

The accommodation of the science instrumentation in the alternate configuration is the same as in the baseline with the following exceptions:

a) It is recommended that the magnetometer boom be located on the -X axis to provide clear fields of view for the major portion of the science equipment.

b) The charged particle instrument (Simpson/University of Chicago) has the +Y axis solar array panel in a portion of its field of view.

c) The imaging photopolarimeter (Gehrels/ University of Arizona) requires relocation due to solar panel interference.

d) The principal 20-degree conical field of view of the infrared radiometer (Münch/ California Institute of Technology) is unobstructed. The instrument also required a 90-degree conical field of view to clear hot objects such as the RTG's. The RTG's are not carried but the intrusion of the +Y axis solar array panel in the latter field of view will be evaluated.

e) The light shade of the asteroid/meteoroid detector (Soberman/General Electric) may require some modification due to the effects of the -X axis experiment boom.

4.2.3.3 Attitude Control

The ΔV precession and spin/despin thruster cluster installation of F and G has been retained. As noted earlier, the sun sensor has been removed from the F and G mounting bracket and relocated to the position shown in Figure 4-9. The relocation was required to provide a field of view clear of the solar array. A sun aspect sensor is mounted adjacent to the sun sensor and was not required on Pioneer F and G. A field of view cutout has been added to the dish. The stellar reference assembly and its light shade are not shown but would be mounted to the experiment compartment.

4.2.3.4 Electric Power

The solar array geometry differences from the baseline spacecraft have already been discussed in detail. In the alternate configuration, the inactive area of the array extends 90 inches from the spacecraft centerline as compared to 80 inches on the baseline. The array is located further aft than on the baseline design, therefore the shadows extend further outboard.

Table 4-5 summarizes the changes of the 1 to 5 AU mission alternate spacecraft from Pioneer F and G. This configuration (solar array with 80-degree separation) has the advantage of improved stability with no loss in antenna pointing accuracy due to asymmetrical propellant usage. The disadvantages are a reduction in acceptable fields of view for the

experiments and more extensive changes to the Pioneer F and G spacecraft. Since the antenna pointing inaccuracies are small (on the order of 0.1 degree) the previous configuration having 120-degree separation of the solar arrays was chosen as the preferred configuration.

Table 4-5. 1 to 5 AU Mission Alternate Spacecraft Summary of Changes from Pioneer F and G*

Subsystem	Modifications
Electric power	• Relocated solar array panels (symmetrical deployment, located aft of cg plane)
Science	• The charged particle instrument field of view is obstructed by solar panel • The imaging photopolarimeter requires relocation due to solar panel interference
Mass properties	• Lateral cg shift eliminated • Spin to maximum transverse moment of inertia ratio is minimal
Structure	• -X axis truss network geometry is modified
Attitude control	• Stellar reference assembly relocation

*All changes same as for preferred configuration except as noted.

4.2.4 Comet Rendezvous Mission Configuration

The spacecraft configuration shown in Figure 4-10 is the design selected for the comet rendezvous mission. The design is very much like that developed for the 1 to 5 AU mission which is depicted in Figure 4-6.

The weight of mercury propellant required increased from 100 pounds to 256 pounds. The weight of the attitude control hydrazine returns to 60 pounds, the same as Pioneer F and G. The vertical stack tankage arrangement has been retained with the tanks relocated to maintain their composite cg on the spacecraft cg plane.

4.2.5 1 to 30 AU Mission Configuration

The spacecraft design shown in Figure 4-11 is the configuration developed to satisfy the requirements of missions beyond 5 AU from the sun. For distances in excess of 5 AU the sun becomes ineffective as an

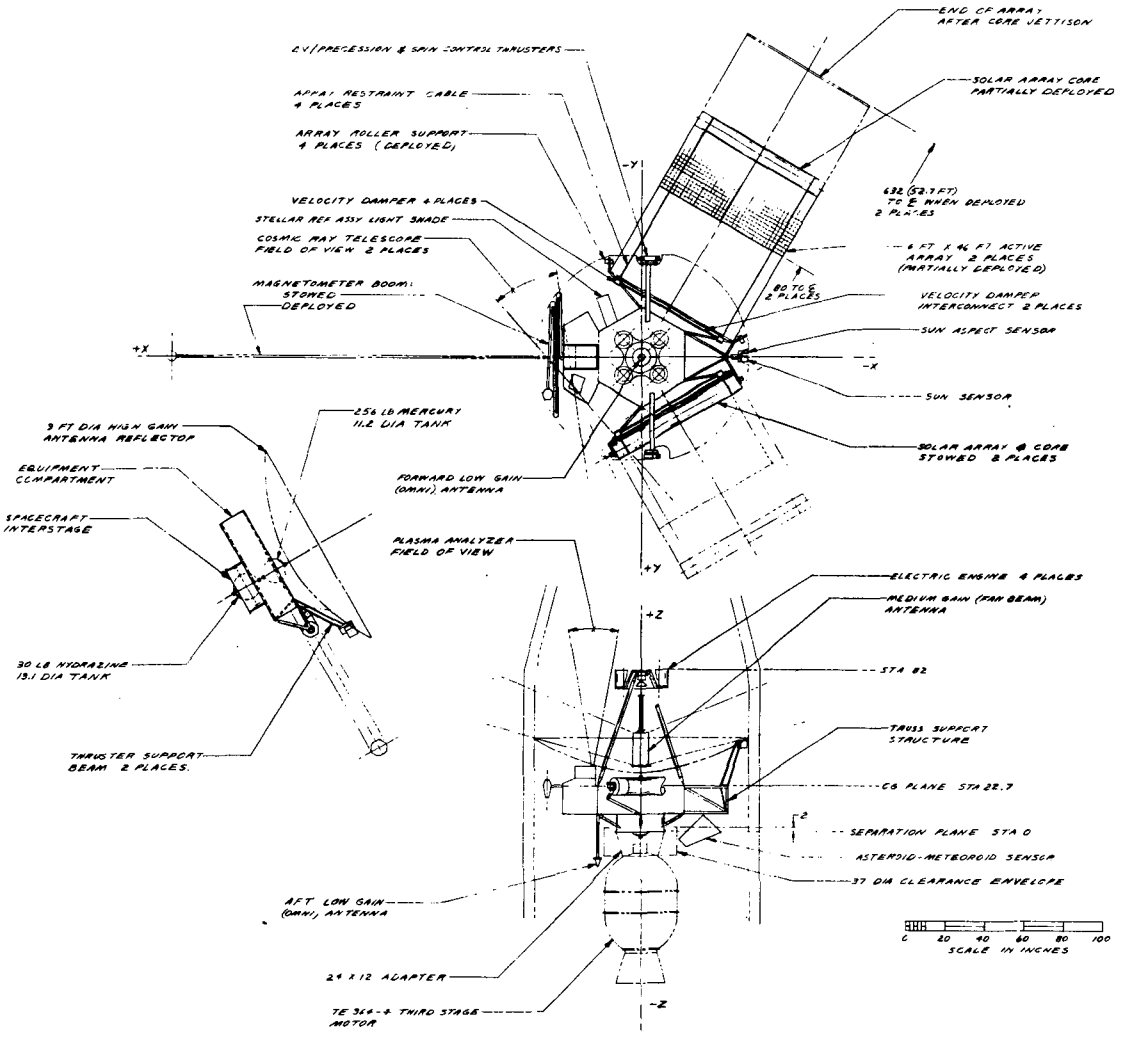

Figure 4-10. Comet Rendezvous Mission Configuration

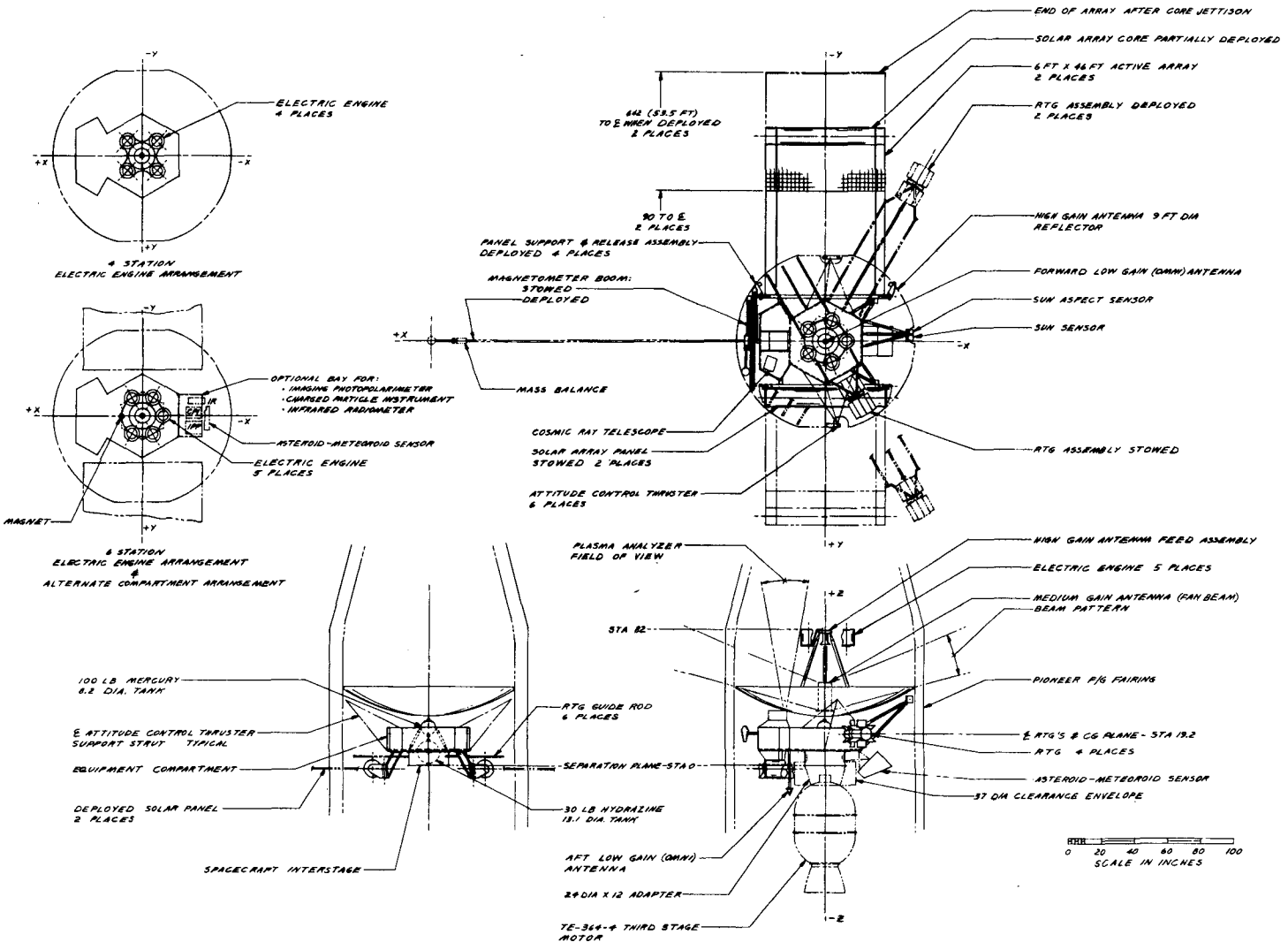

Figure 4-11. 1 to 30 AU Mission Configuration

electric power source and an auxilliary power source must be used. In this design the Pioneer F and G RTG installation is carried intact and becomes the prime electrical power source beyond 5-AU distances from the sun. A 5000- or 8000-watt solar array is also carried to support the electric propulsion subsystem during the periods of electric engine firing which occur during the early part of the mission. After their useful period has expired the solar array can be retained or jettisoned as desired. The configuration has either five 15-cm thrusters or three 30-cm thrusters with associated power control units, and carries 30 pounds of hydrazine and 100 pounds of mercury.

In keeping with the concept of minimum change to the Pioneer F and G spacecraft, the RTG installation of that vehicle is utilized. During launch when the RTG's and other deployable appendages are stowed, the spacecraft cg must be located on the launch vehicle thrust axis. The RTG's deploy asymmetrically (120 degrees apart) and therefore must deploy in the spacecraft cg plane to prevent spacecraft principal axis rotation and loss of antenna pointing accuracy. It is also desirable to locate the magnetometer boom and consumable propellants on the spacecraft cg plane. The solar array panels are symmetrically mounted and deployed and are therefore relieved of the necessity of being mounted on the spacecraft cg plane. The solar panels are located slightly aft of the separation plane and provide a first moment balance to the electric engines which are mounted at the high-gain antenna feed.

In order to provide the instruments with the same science installation and field of views as on Pioneer F and G it is necessary to jettison the solar array panels. In that event, the spacecraft cg moves forward, the asymmetrically deployed RTG's are no longer in the spacecraft cg plane, the spacecraft principal axes rotate and antenna pointing accuracy is lost.

There are several methods by which the principal axes shift can be avoided.

a) At the time the array is jettisoned, the electric engine installation is also jettisoned. This maintains the spacecraft cg plane coincident with the RTG, and magnetometer deployment

plane and principal axes rotation is avoided. Jettison of the electric engine installation involves severance of structural ties, large electrical cable bundles, and the mercury propellant line. This method involves great complexity and low reliability and therefore has been rejected.

b) Reduce the panel width to minimize field of view interference. As this is only a partial fix which results in extremely long solar panels with very large aspect ratios and introduces more severe dynamic and mass property problems, this method is also rejected.

c) Locate a jettisonable mass on the spacecraft such that the product of inertia of the mass equals that of the deployed RTG's relative to the spacecraft cg after array jettison. A mass of approximately 14 pounds is required together with support structure and the ballast weights necessary to balance the deployable mass when the spacecraft is in the stowed configuration. This method was also rejected due to the complications of jettisoning a mass along with the solar arrays.

d) Another approach has been shown in the left-hand lower view of Figure 4-11. A small equipment bay has been added at the -X axis to house the photopolarimeter, charged particle and infrared instruments which are the units whose field of views are intruded on by the solar array. In their new locations the charged particle and infrared instruments are provided with the required unobstructed field of views. The field of view of the polarimeter is improved, but in the aft pointing direction it is affected by the asteroid-meteoroid sensor light shade.

e) Locate a mass (of approximately 20 pounds) on the magnetometer boom so that the first moments of the boom and the deployed RTG's are equal. The spacecraft cg and principal axis remain on the spacecraft centerline and no principal axis rotation results upon solar array jettison. Additionally, the placement of the symmetrical array in the forward and aft direction, to force the spacecraft cg to the RTG cg plane, is no longer critical. However, the location shown in the figure is optimum

and has not been changed. It is believed that this method is the least complex and most reliable of the methods noted and has been selected as the preferred approach. It provides for science installations and viewing capabilities almost identical to those of Pioneer F and G.

In summary, the baseline configuration has the following features:

a) A symmetrical solar array which is jettisoned after electric propulsion engine firing has terminated.

b) A mass balance on the magnetometer boom.

c) A science installation the same as on Pioneer F and G and science field of view characteristics almost identical to that of Pioneer F and G after solar array jettison.

With the exception of the solar array geometry and the RTG installation, the configuration is similar to the 1 to 5 AU mission configuration of Section 5. 2. 1.

Table 4-6 summarizes the principal changes from the Pioneer F and G design and is followed by a subsystem-oriented description of the spacecraft.

Table 4-6. 1 to 30 AU Mission Spacecraft Summary of Changes from Pioneer F and G

Subsystem	Modification
Structure	• Strengthen structure • Added solar array supports • Added sun and sun aspect sensor supports
Science	• Added balance mass to magnetometer boom
Electric propulsion subsystem - added	• Five 15-cm thrusters • Five PPU's • Mercury tank
Chemical propulsion	• Modified and relocated hydrazine tank
Attitude control	• Relocated sun sensor • Added sun aspect sensor and electronics
Electric power	• Added two rollout solar array panels • Added converter
Antennas	• Deleted horn antenna • Added reflector cutouts for sun and sun aspect sensors • Added medium-gain antenna • Modified feed support assembly
Command and electrical distribution	• Rearranged electronic equipment

4.2.5.1 Structure and Equipment Compartment

The launch vehicle adapter and the spacecraft interstage and equipment compartment have the same basic geometry as the Pioneer F and G spacecraft but require strengthening to support the greater weight of the study spacecraft (approximately 900 pounds). A hole is required in the equipment mounting platform to accommodate the hydrazine tank, and secondary structures are added to support the solar array, the solar aspect sensors, tankage, and medium-gain antenna. The feed support struts are modified to support the electric engine installation.

Each solar panel is supported by two fittings equipped with the separation hardware required to jettison the panels on command. The fittings at the +X axis ends are incorporated into machined bracked attached to the aft surface of the compartment. The brackets are stiffened to take loads parallel to any spacecraft axis.

The internal electronic equipment is located similarly to the arrangement shown in Figure 4-7. Due to the RTG installation and the associated guide rods and electric cable slack boxes, the use of the compartment forward surface for mounting the electric subsystem PPU's is limited. The PPU's are mounted to the outboard surfaces of the compartment access doors.

4.2.5.2 Science

The Pioneer F and G science instruments are accommodated in the same positions used on Pioneer F and G. The list of the scientific instruments, their characteristics and requirements are shown in Table 4-3. As previously noted, it is not possible to satisfy all of the instrument requirements with the solar panels permanently attached to the spacecraft. The changes from Pioneer F and G installation and violations of the Pioneer F and G field of view requirements (with solar array attached) are noted below.

a) The electric engine installation, as shown, intrudes 0.8 inch into the plasma analyzer field of view but the engine installation can be modified to provide field of view clearance.

b) The charged particle instrument field of views are intruded by the +Y axis solar panel.

c) The cosmic ray high-energy telescope front aperture field of view is intruded by the +Y axis solar panel.

d) The polarimeter field of view is intruded by the -Y axis solar panel.

e) The asteroid-meteoroid sensor principal field of view is unobstructed but the solar array panels protude beyond the light shade aperture and may violate the 2π steradian field of view to be clear of reflected light.

f) Several of the meteoroid detector panels are partly shadowed by the solar array structure.

Most of the field of view deficiencies are eliminated when the solar array is jettisoned; however, the asteroid-meteoroid sensor will still probably require slight relocation and/or light shade extension.

4.2.5.3 Electric Propulsion

The electric thrusters are symmetrically clustered around the high-gain antenna feed in the same configuration used for the 1 to 5 AU mission spacecraft as described earlier. No spacecraft components are located forward of the engine apertures to minimize engine exhaust contamination. The 8.2-inch diameter mercury tank installation containing 100 pounds of mercury and nitrogen pressurant is the same as that used for the outbound 1 to 5 AU mission spacecraft. The power processing units are mounted to the external surfaces of the equipment compartment access doors.

4.2.5.4 Chemical Propulsion

The 13.1-inch diameter tank containing 30 pounds of hydrazine and nitrogen pressurant is installed in the same manner as on the outbound 1 to 5 AU mission spacecraft. The tank is mounted by a cylindrical ring to the equipment mounting platform aft surface bracket.

4.2.5.5 Attitude Control

The Pioneer A and G ΔV/precession and spin/despin control thruster clusters and support structure are utilized. A 1.1-pound mass

balance is required on the +Y thruster mounting bracket to compensate for the removal of the sun sensor from the bracket. Alternatively, the support bracket could be redesigned and the thruster relocated to place its cg at the apex of the tripod support structure. Further analysis is required to determine the optimum solution. The inboard ends of the solar array panels are fabricated from mesh to minimize the exhaust impingement of the ΔV precession thrusters on the array.

Due to the effects of the solar array, the sun aspect sensor which replaces the sun sensor used on Pioneer F and G has been located at the -X axis where it is supported by a tripod structure. The antenna reflector is cut out to accommodate the sensor field of view.

The magnetometer boom actuated nutation damper requires revision due to the incorporation of the mass balance on the boom.

4.2.5.6 Electric Power

The solar array composed of two deployable rollout arrays are symmetrically located on the spacecraft Y-Y axis. Details of the packaging containment, release, deployment and jettisoning provisions are given in Section 5.3. The inboard ends of the flexible array panels are of mesh construction to minimize attitude control gas jet impingement on the panels. The array is retained through electric engine thrusting and is jettisoned to provide the scientific experiments unobstructed field of views.

The Pioneer F and G RTG installation is retained without change to provide power after array jettison.

4.2.5.7 Communications

The high-gain antenna feed support struts are strengthened to accommodate the electric engine installation and are fabricated from fiberglass (in lieu of boron on Pioneer F and G) to minimize medium-gain antenna loss. The stacked biconical horn array medium-gain antenna is located on the spin axis forward of the high-gain antenna reflector. The Pioneer F and G conical log spiral low-gain antenna installation has been retained. To provide forward coverage, a cupped dipole antenna is located on centerline at the top of the high-gain antenna feed.

4.2.5.8 Thermal Control

The Pioneer F and G thermal control louver system is utilized to reject excess heat to space as is the Pioneer F and G thermal control concept. The equipment compartment is insulated from the space environment and thermally isolated from the spacecraft external appendages as on Pioneer F and G.

4.3 MASS PROPERTIES

A weight summary for the 5-kw configuration with five 15-cm thrusters and the 8-kw configuration with three 30-cm thrusters is given in Table 4-7. The method utilized in the table was to start with the Pioneer F and G weight, remove those items not used on the solar electric configuration and then add the solar electric components. The gross weight for the 1 to 30 AU missions is obtained by adding the weight for the RTG assemblies. Chemical propellant has been assumed at 30 pounds and mercury propellant, since it varies from 60 to 250 pounds depending on the mission, is not included.

The TRW solar array weight is included in Table 4-7. A breakdown of this weight is shown in Table 4-8 where it is compared to the General Electric prototype design which has a motor driven bistem boom for deployment. The TRW design utilizing centrifugal force to deploy the array offers a weight saving of nearly 40 pounds over the powered deployment design.

The inertia properties of the 1 to 5 AU mission configuration with five 15-cm ion thrusters is given in Table 4-9. The minimum inertia ratio is the I_z/I_y in the fully stowed condition. To be certain that the spacecraft is stable, the inertia ratio should be greater than 1.05. The I_z/I_y value of 1.08, is therefore an acceptable value for spin stability. The table shows a shift in the center of gravity of nearly 24 inches, which must be considered in the dynamic stability of the solar arrays. The centrifugal force in the solar array changes direction in the process of deployment, therefore the arrays must be properly positioned to prevent distortions of the array caused by forces transverse to the array axis.

Table 4-7. Weight Summary — Baseline Configuration

	F/G	5 KW 5 THRUSTERS 15 CM	8 KW *3 THRUSTERS 30 CM
PIONEER F/G GROSS WEIGHT	560 LBS		
REMOVE FOR BASELINE			
HYDRAZINE	-60		
RTG ASSEMBLIES	-140		
PIONEER F/G BASELINE WEIGHT	360	360 LBS	360 LBS
ADD FOR ELECTRIC PROPULSION			
THRUSTERS		(5) 35	(3) 48
POWER PROCESSORS		(5) 50	(3) 96
SOLAR ARRAY ASSEMBLY (TRW)		146	206
THRUSTER MOUNTING ASSEMBLY		4	4
CONVERTER		12	12
SUN ASPECT SENSOR		1	1
24 WATT TWT'S (2)		8	8
MERCURY TANK AND LINES		3	3
HYDRAZINE (NOMINAL AMOUNT)		30	30
GROSS WEIGHT FOR 1-5 AU MISSIONS		649 LBS	759 LBS
ADD FOR 1-30 AU MISSIONS			
RTG ASSEMBLY		140	140
GROSS WEIGHT FOR 1-30 AU MISSIONS		789 LBS	899 LBS

Table 4-8. Solar Array Comparative Weight Summary

GE PROTOTYPE DESIGN	5 KW (WEIGHT, LB)	8 KW (WEIGHT, LB)	TRW CONCEPTUAL DESIGN	5 KW (WEIGHT, LB)	8 KW (WEIGHT, LB)
SOLAR ARRAY BLANKET ASSEMBLY	46.58	74.50	SOLAR ARRAY BLANKET ASSEMBLY	49.0	78.4
INBOARD MESH	1.20	1.20	ROLLER ASSEMBLY	7.2	7.2
DRUM ASSEMBLY	17.60	17.60	INBOARD STIFFENERS	1.7	1.7
BOOM ACTUATOR	11.73	16.58	RESTRAINT CABLES	1.8	2.7
CENTER SUPPORT	1.33	1.33	STRUCTURAL SUPPORT	6.8	6.8
STRUCTURAL SUPPORT	8.00	8.00	DEPLOYMENT CONTROL DEVICE	1.5	1.5
LEADING EDGE MEMBER	1.07	1.07	DAMPER MECHANISM	0.8	0.8
OUTBOARD END SUPPORTS	4.10	4.10	SEPARATION HARDWARE	4.1	4.1
MOUNTING HARDWARE	0.13	0.13			
TOTAL EACH PANEL	91.74	124.51	TOTAL EACH PANEL	72.9	103.2
TOTAL EACH SPACECRAFT	183.48	249.02	TOTAL EACH SPACECRAFT	145.8	206.2
			WEIGHT SAVING	37.7	42.8

Table 4-9. 1 to 5 AU Configuration Mass Properties Estimate (Five 15-cm Thrusters)

Condition	Weight (lb)	Center Gravity (in.)			Moment of Inertia (slug-ft^2)			Inertia Ratio	
		$\overline{X}$	$\overline{Y}$	$\overline{Z}$	I_x	I_y	I_x (Roll)	I_z/I_x	I_z/I_y
Spacecraft with loaded TE-364-4	~3040	0	0	-18.9	588	594	190	0.32	0.32
Spacecraft with burned-out TE-364-4	~ 940	0	0	11.9	211	217	114	0.54	0.53
Spacecraft - fully stowed	750	0	0	22.8	93	99	197	1.15	1.08
Spacecraft - with 25 percent array deployed (magnetometer stowed)	750	-11.0	0	22.8	747	297	959	1.28	3.23
Spacecraft - with 50 percent array deployed (magnetometer stowed)	750	-16.7	0	22.8	1536	534	1984	1.29	3.72
Spacecraft - with 75 percent array deployed (magnetometer stowed)	750	-20.1	0	22.8	2235	747	2896	1.30	3.88
Spacecraft - solar array fully deployed (magnetometer stowed)	750	-21.3	0	22.8	2537	840	3291	1.30	3.92
Spacecraft - fully deployed	750	-19.7	0	22.8	2536	908	3359	1.33	3.70
Spacecraft - end of life (less 100 lb H_g and 30 lb N_2H_4)	620	-23.8	0	22.8	2535	894	3345	1.32	3.74

Figure 4-12 presents the deployed spacecraft spin rate relative to the fully stowed spin rate and the hydrazine propellant required to achieve the 5 rpm spin rate for mission operation.

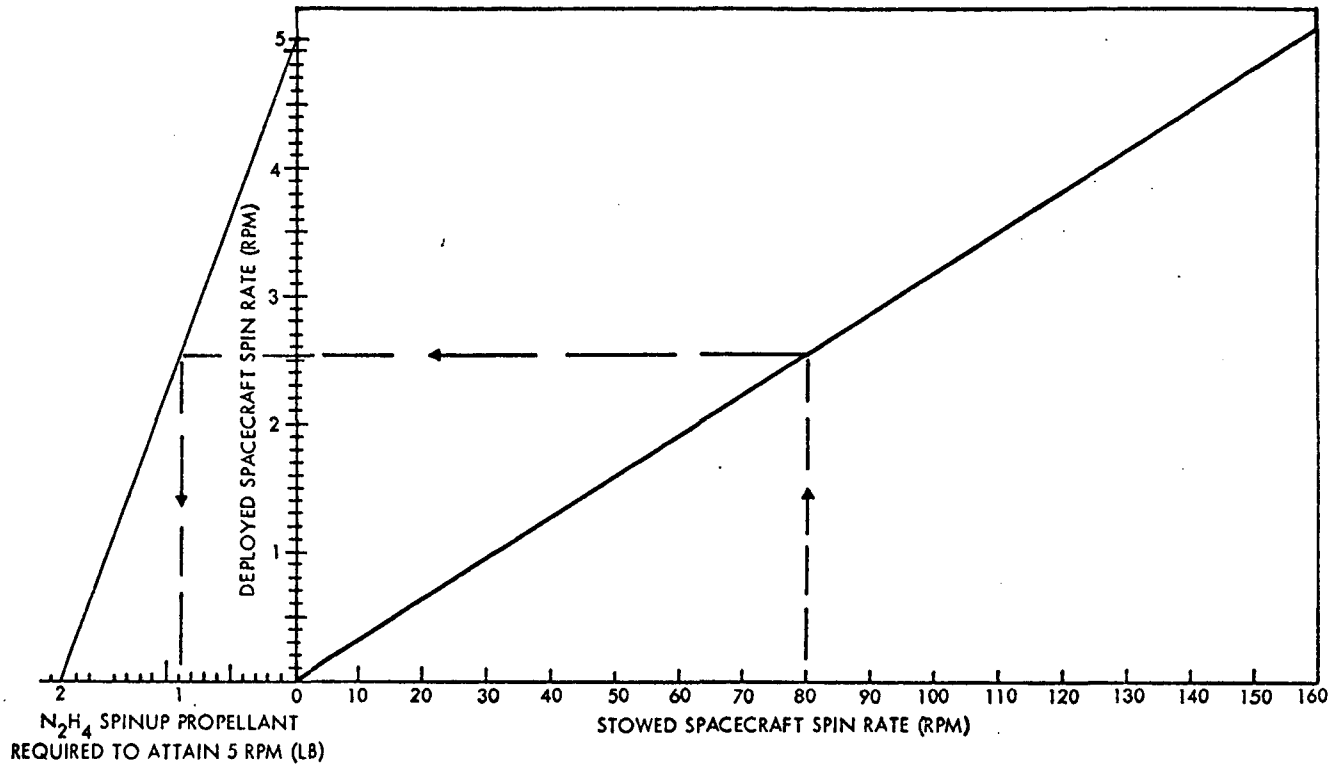

Figure 4-12. Baseline Configuration — Spacecraft Spin Rate and Spinup Propellant Relationship

4.4 DYNAMICS

The bulk of the dynamics analysis was performed on the TRW centrifugally deployed solar array configuration in order to obtain quantitative results on which to evaluate the particular design approach. As an alternate scheme, the GE boom-deployed solar array was also analyzed to determine its dynamic properties. The relevant dynamic characteristics of each design were studied during deployment, spinup, precession and ΔV maneuvers.

Primary results of the dynamics analysis are summarized in Table 4-10.

Table 4-10. Dynamics Analysis Summary

	GE Boom Design	TRW Centrifugal Design
Dynamic balance	Expected boom misalignment indicates that the arrays should be hinged at their spacecraft interface	Design effectively produces a hinge at the spacecraft interface providing satisfactory balance characteristics
Deployment	Controlled constant deployment rate (<1 ft/sec) produces acceptable structural loads	Wide range of available centrifugal deployment force (180 → 0.2 pound) may necessitate deployment aid during final deployment phase
Precession maneuver	Root damper needed to attenuate induced wobble	Root section must be stiffened and root damper needed to attenuate induced wobble
Spinup maneuver	Angular accelerations up to 0.01 rad/sec^2 in magnitude can be tolerated with acceptable structural loads	Requirements will depend on actual array design and a more detailed structural analysis; no problems anticipated
ΔV maneuver	For rigidly fixed boom (no hinge), deboost acceleration must be less than 0.05 g	Requirements will depend on actual array design and a more detailed structural analysis; no problems anticipated
Solar torque disturbance	Spin axis drift is less than 0.01 deg/day for 2 rpm spin at 1 AU	Spin axis drift is less than 0.01 deg/day for 2 rpm spin at 1 AU

4.4.1 Spacecraft Dynamic Balance Requirements

Pointing requirements for the high-gain S-band antenna require that the spin axis shift due to dynamic imbalance be less than 0.6 degree. The solar arrays inherently contribute the largest effect on spacecraft imbalance. The main structure with appendages stowed can be balanced to inertia values in the range of 10 to 100-in^2; these tolerances have negligible effect on principal axis misalignment. A small angular displacement of the developed solar arrays, however, can result in a significant spin axis drift.

Consider the Pioneer configuration with boom-deployed arrays rigidly cantilevered to the main spacecraft body (e.g., the GE array design). For the proposed 5-kw configuration, a 1.0 degree misalignment of each boom in opposite directions will result in a 0.6 degree principal axis shift. The estimated misalignment for fixed booms is 0.5 degree which results in a 0.3 degree principal axis shift (see Figure 4-13). This is caused by mechanical angular misalignment and warpage of the boom stem due to manufacturing anomalies. For the 3-kw asteroid belt mission configuration a 0.5 degree solar array misalignment will result in a 0.45 degree principal axis shift. Since the magnitude of angular misalignment for fixed booms is uncertain due to limited data and since the predicted misalignment produces a marginally acceptable principal axis shift, hinging of the arrays is strongly recommended. Such hinging enhances the effect of centrifugal force in aligning the booms. Hinge friction and bias in the zero point of the wire bundle provide the only torques which then have to be overcome by the centrifugal force. It is estimated that the principal axis shift can be limited to less than 0.1 degree for hinged booms. This considers translational misalignment in addition to the effects of hinge friction and wire bundle bias. The effect of thermal bending is not important because of symmetry and since the most critical pointing requirements occur near Jupiter where thermal bending is small (approximately 1.5-inch total tip deflection).

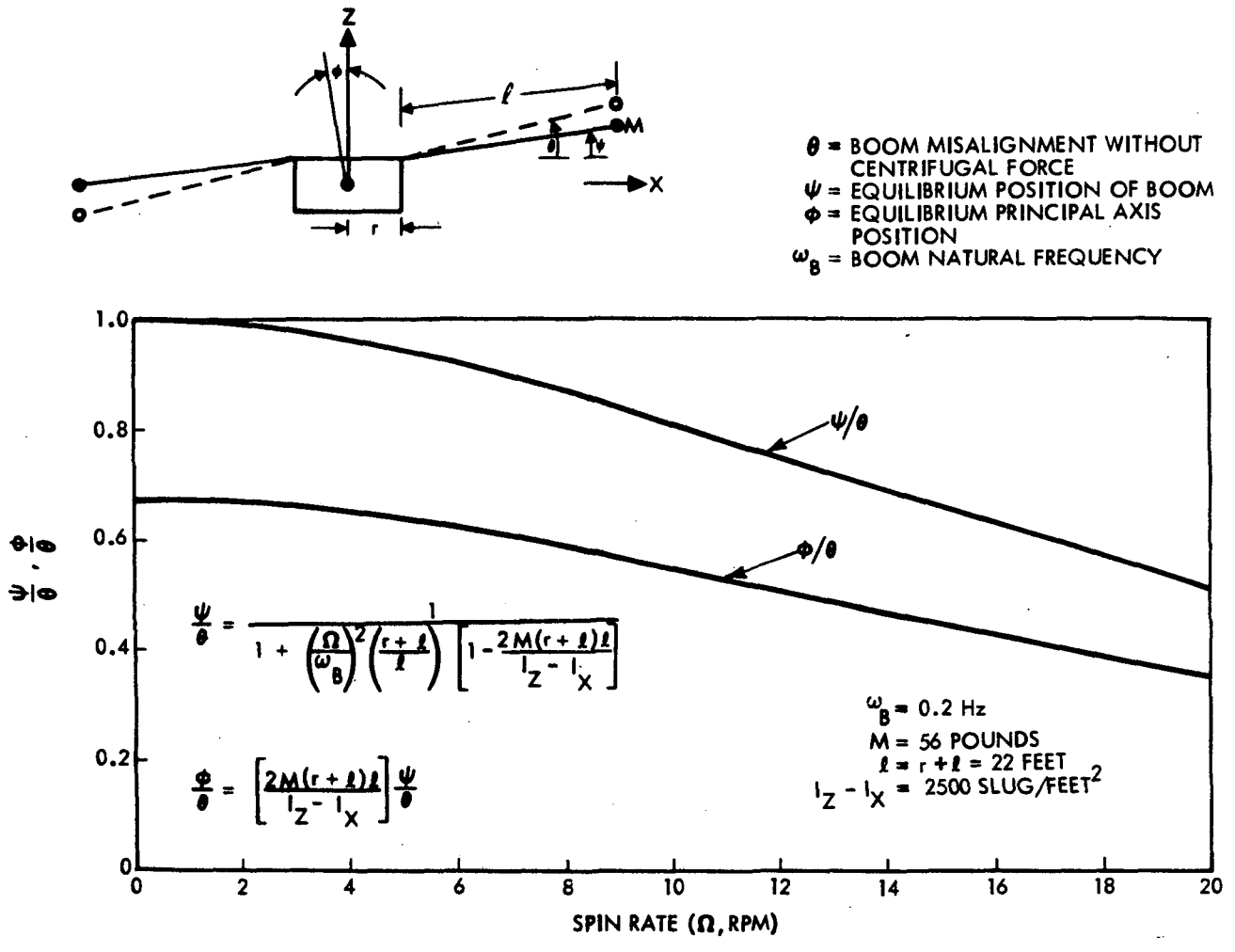

Figure 4-13. Effect of Boom Angular Misalignment on Principal Axis Shift For Rigidly Mounted Booms

The utilization of hinged solar array booms or of flexible array blankets introduces questions related to stability and relative boom motion induced by attitude and ΔV maneuvers. These are addressed in the following discussion.

Stability is achieved if the following relation is satisfied for the configuration shown in Figure 4-13.

$$\frac{I_{zi}}{I_{xi}} > \frac{2mr\ell}{I_{xi}}$$

where

I_{xi} = transverse moment of inertia of spacecraft with booms stowed about axis normal to plane of booms

I_{zi} = spin moment of inertia of spacecraft with booms stowed

m = boom mass

r = hinge point radial distance from spacecraft centerline

ℓ = hinge point to boom cg distance

For the case where the booms have a nonzero stiffness about the hinge point, the stability criteria has the following form:

$$\frac{I_{zi}}{I_{xi}} > 1 - \frac{2mr\ell}{I_{xi}} \left[\frac{m(r + \ell)\ell\Omega^2 + k(1 + \ell)}{m\ell(r + \ell)\Omega^2 + k} \right]$$

where

k = the effective boom hinge stiffness

It is noted that if the spacecraft is stable before deployment, i.e., $I_{zi}/I_{xi} > 1$, it will be stable after deployment. This condition is met for the proposed configuration. The stability criteria can be physically interpreted as follows. If the stability criteria is satisfied, a small perturbation to the boom will result in a smaller magnitude perturbation of the spacecraft principal axis. The misalignment between the resulting centrifugal force vector and the boom axis will result in a restoring moment tending to align the boom to its initial position. If the stability criteria is not met a small perturbation to the boom will result in a larger

perturbation to the spin axis and the resulting centrifugal force vector will produce a diverging moment acting on the boom. Another way to interpret this criteria is from minimum energy considerations. For a given amount of spacecraft momentum, which remains constant in the absence of external torques, the configuration with lowest kinetic energy is stable. For the proposed configuration, the booms oriented radially outward represents the lowest kinetic energy.

4.4.2 Solar Array Deployment Dynamics

As part of the dynamic analysis of the solar array deployment, the spacecraft spin rate profile during deployment was calculated. Figure 4-14 presents the spin rate profile for both the TRW array concept and the General Electric array design. The spin rate decreases much more rapidly with the TRW design since the mass of the complete roller assembly is moving radially outward causing a greater increase in the spin moment of inertia during the initial deployment phase. Note that the fully deployed spin rates are essentially equal.

Since the TRW array concept is based on the use of centrifugal force as the deploying mechanism, it is imperative that the actual centrifugal force on the array roller be known as a function of deployed position. Figure 4-15 presents such a graph of the available deployment force on the array roller. It is significant to note that during deployment the centrifugal force varies through almost three orders of magnitude, from nearly 200 pounds at deployment initiation to 0.2 pound at the fully deployed position. This dramatic decrease is primarily due to the fact that the deployment force is proportional to the square of the instantaneous spin rate — the rapid decrease in the spin rate has already been shown in Figure 4-14. The small final deployment force may need to be augmented (e.g., by strain energy storage devices) to insure complete deployment.

Because there exists a positive deploying force on the roller at all times, an appropriate restraint mechanism must be utilized to control the deployment rate. Dynamic analysis was performed on both (a) velocity-

proportional rate damper restraints (as on the RTG booms of Pioneer F and G) and (b) constant rate restraint devices (e.g., stepper motors). As might be expected, the rate damper produced a significant initial deployment surge due to the high initial deployment force and a very slow final deployment phase due to the small final deployment force. Because of the accompanying high initial array stresses with the rate damper concept and because of the far greater control afforded by a constant rate restraint device over such aspects as array deployment time history and simultaneity in deployment of both array wings, a constant rate restraint device was selected as the preferred deployment restraint mechanism.

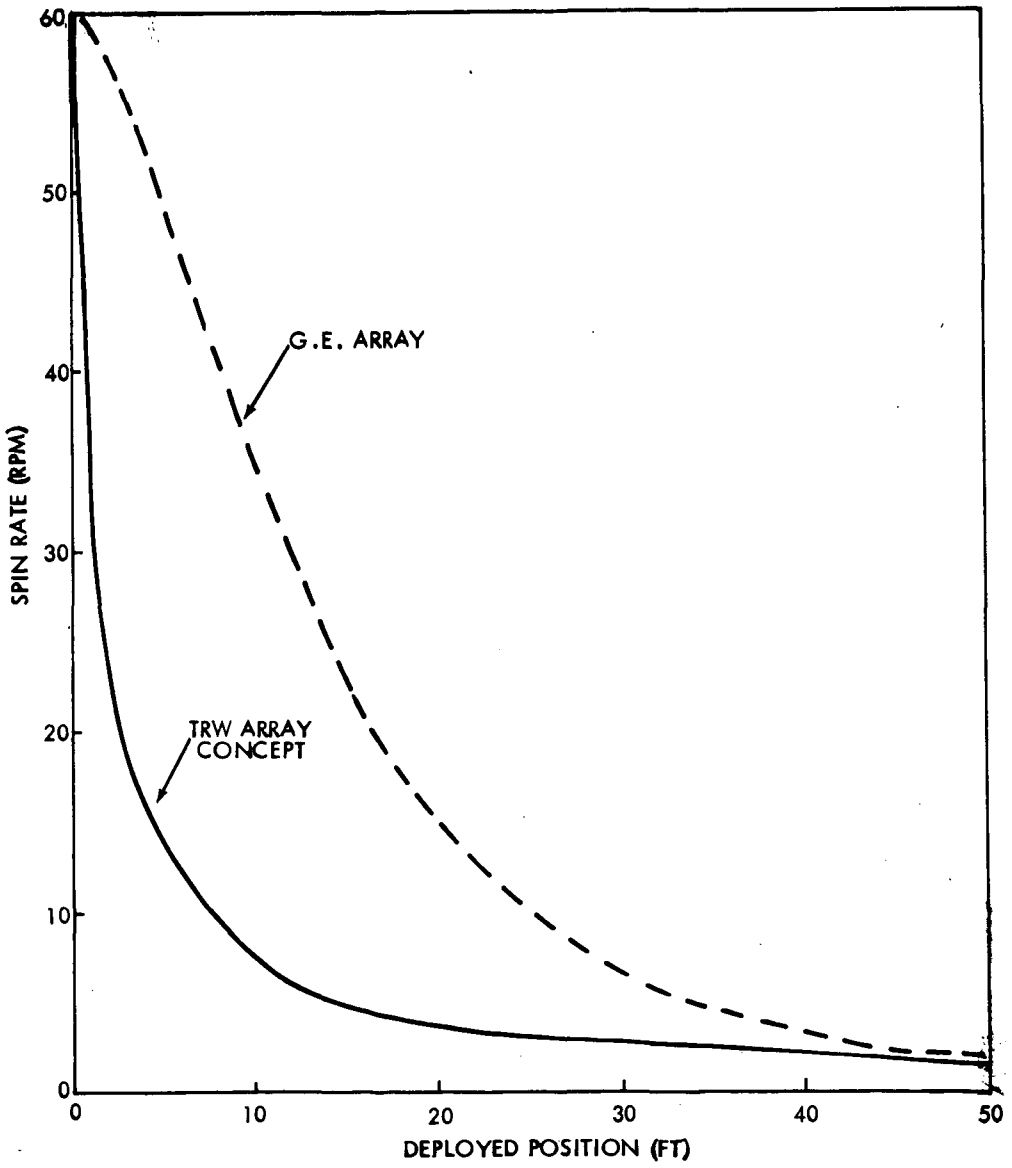

Figure 4-14. Spin Rate During Deployment

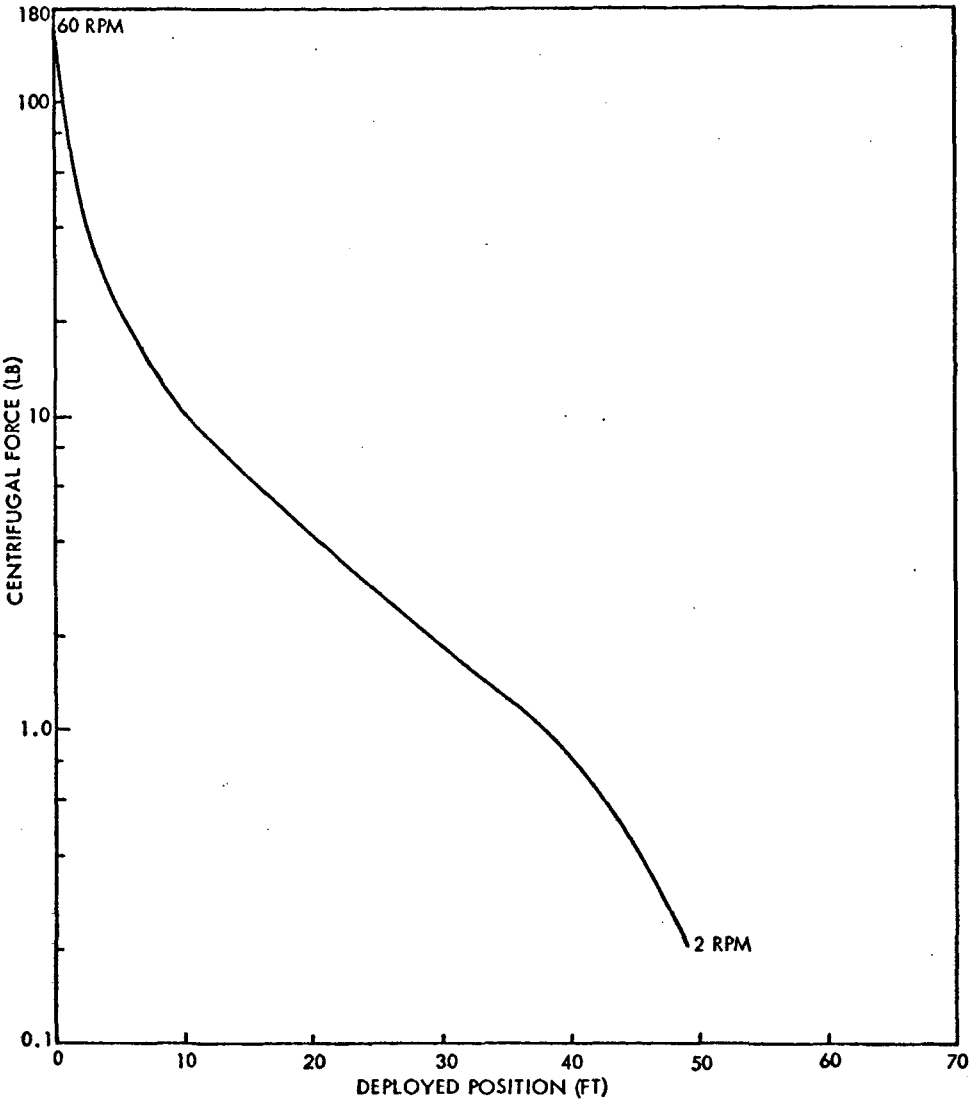

Figure 4-15. Available Centrifugal Deployment Force

The actual longitudinal force which must be carried by the root section of the TRW solar array blanket itself is shown in Figure 4-16. Since the bulk of the centrifugal force is taken up by the restraint cables, only the deployed portion of the array produces tension in the sheet. As a consequence, the sheet tension at the root of the TRW design is nearly constant and of a relatively low magnitude (<2 pounds) throughout array deployment. Also shown in Figure 4-16 is the root longitudinal force on the General Electric array sheet and bistem. The curves assume a smooth deployment history; impulsive effects of sudden starts or stops in the deployment rates must be carefully examined when considering specific rate restraint mechanism designs.

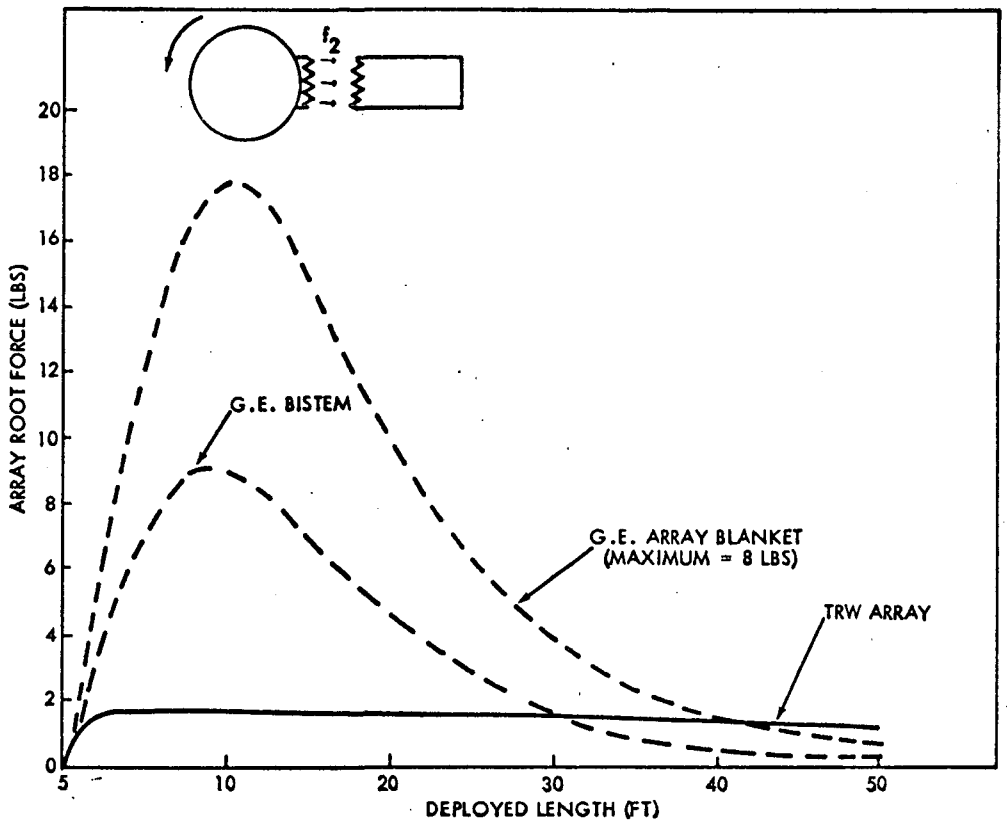

Figure 4-16. Array Root Longitudinal Force

As the solar array is deployed, the despin effect on the spacecraft produces a transverse force on the array. In the case of the TRW array concept, the array merely pivots at the root section to relieve the transverse stresses. Figure 4-17 presents the bistem root shear force (F_t) in pounds and the root bending moment (M_t) in foot pounds for the deployment of the General Electric array. These forces are proportional to the deployment rate and are presented for a rate of 0.1 ft/sec.

As a result of the deployment dynamics analysis performed to date, no serious problems are anticipated in the deployment of either the TRW array concept or the General Electric boom design.

4.4.3 Dynamics of Spacecraft Maneuvers

Because of the great size and the extreme flexibility of the solar arrays in the proposed Pioneer spacecraft design, a thorough analysis of spacecraft response during anticipated maneuvers is critically important. Although spinup and ΔV maneuvers do not present serious difficulties as

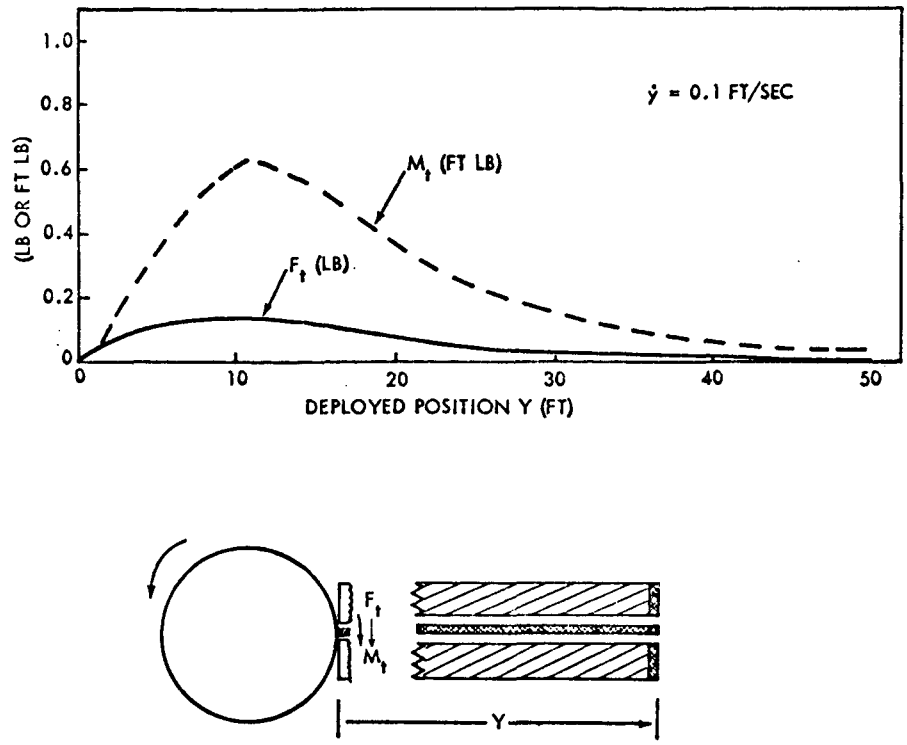

Figure 4-17. GE Boom Root Shear Force and Bending Moment

they can be performed sufficiently slowly to avoid deleterious dynamic response of the spacecraft system, the required precession maneuvers must be examined in detail.

Since precession (reorientation of the spin axis) of any spin-stabilized spacecraft is accomplished by torquing the vehicle about an axis perpendicular to the spin axis, wobble motions are necessarily induced to the vehicle with each torque pulse. In essence, a precession maneuver consists of two phases. In the first phase the torque pulse rotates the spacecraft angular momentum vector (initially coincident with the spin axis) through an angle θ which is called the precession angle; at the same time, the spin axis of the spacecraft is given a wobbling (coning) motion about the new angular momentum vector. In the second phase on-board damping mechanisms dissipate the wobble energy and align the spacecraft spin axis with the new angular momentum vector so that the spacecraft is now spinning steadily with its spin axis rotated through the angle θ from its initial position.

For a single rigid body vehicle, the magnitude of the induced wobble motion is of the same order as the precession angle itself; moreover, if a vehicle consists of a rigid central body with hinged appendages having

inertias small with respect to the central body, the precession behavior is similar to that of the single rigid body and precession analysis is straightforward.

However, in the case of the present configuration, 90 percent of the spin inertia of the vehicle is provided by the hinged arrays. Thus, precession dynamics must be analyzed by considering a multibodied model such as is shown in Figure 4-18.

The initial dynamic analysis of the Pioneer spacecraft with the large solar arrays during precession maneuvers was performed by computer simulation utilizing the TRW Unified Flexible Spacecraft Simulation Program (UFSSP). The General Electric array design was studied using the model of Figure 4-18, while the TRW array concept was studied using a six-body model wherein each array was modelled as two hinged bodies in order to introduce the effects of a stiffened inboard section. (The UFSSP admits an arbitrary model of up to 18 interconnected bodies, and a short run with a 14-body model of the TRW array concept showed good agreement with the basic six-body model.)

Results of the simulation study are presented in Table 4-11. Significantly, the simulation study has shown that the present Pioneer damper concept (a single wobble damper coupled to the hinged magnetometer boom) is not adequate to damp out the wobble motion induced by the precession pulse. However, the results also show that an acceptable precession maneuver can be realized by hinging the arrays to the spacecraft and providing a wobble damper at the hinge interconnection. (Note that for the TRW array concept this involves stiffening a root section of the array in order to provide a moment arm on which the damper can react.) Thus, although much further detailed dynamic analysis must be performed on any specific design because of the inherent complications of the large flexible members, the present simulation study definitely indicates that the basic configurations proposed can be designed to provide acceptable dynamic response during anticipated vehicle maneuvers.

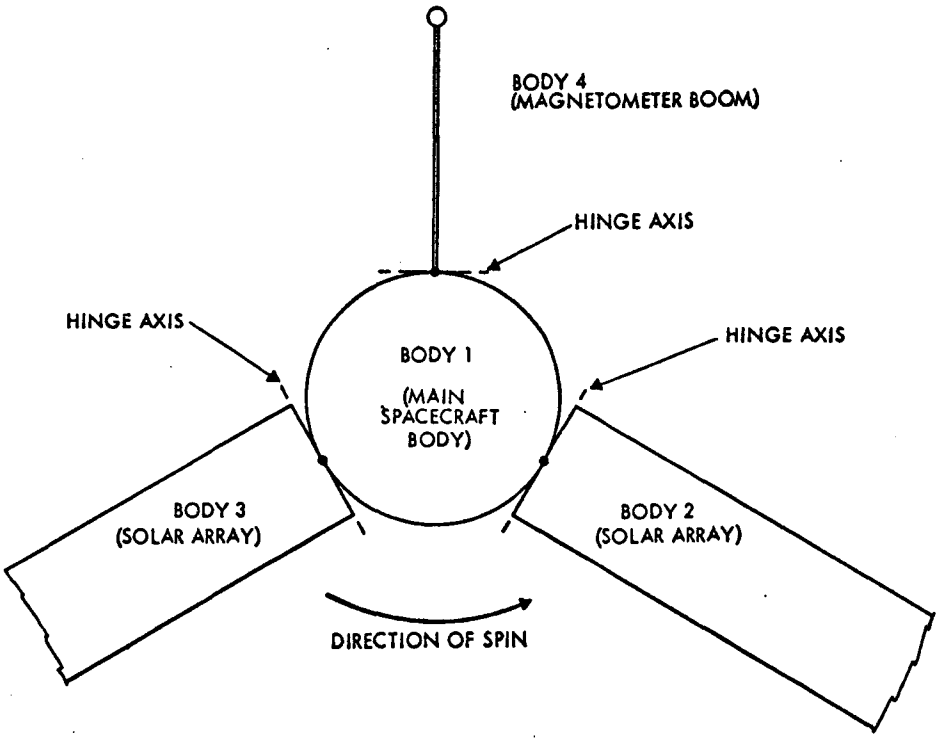

Figure 4-18. Simple Four-Body Model for Precession Analysis

Table 4-11. Precession Simulation Results (Spin rate = 2 rpm; torque pulse = 0.1 ft-lb-sec; precession angle from a single pulse = 0.01 deg)

	*MAGNETOMETER DAMPER ONLY		*MAGNETOMETER PLUS ARRAY ROOT DAMPERS	
	TRW ARRAY	GE ARRAY	*TRW ARRAY	GE ARRAY
INITIAL WOBBLE ANGLE INDUCED BY A SINGLE PRECESSION PULSE, DEG	1.2	0.12	0.17	0.03
WOBBLE DAMPING TIME CONSTANT, MIN	15	INEFFECTIVE	3	0.9

*REPRESENTATIVE VALUES AS DAMPER CONSTANTS NOT OPTIMIZED

4.5 THERMAL CONTROL DESIGN

4.5.1 Power Processing Units (PPU's)

The problem of thermal control design on the solar electric propulsion Pioneer lies principally in the temperature control of the ion thruster power processing units. The problem is more acute with the larger 30-cm thruster PPU's which dissipate 268 watts of power in each unit. The general problem of spacecraft thermal control is somewhat simplified from the Pioneer F and G by deletion of the RTG assemblies. The predeployment phase poses no thermal control problem with the absence of the RTG's.

To alleviate the severe mounting problems of large power processor units for the 30-cm ion thrusters, the PPU's were separated into two separate boxes: a beam power unit and an arc unit. The package size of the separate processor units is more manageable for placement and mounting on the present Pioneer spacecraft.

The radiator area requirements of the power processor units for the 15- and 30-cm size thrusters is shown in Table 4-12.

Table 4-12. Power Processor Radiator Area Requirements

Thruster Size (cm)	Processor Units		Required Radiation Area (ft^2)
	Maximum Power (watts)	Operating Temperature (^oC)	
15	76 each	60 (140^oF)	1.7
30	185 (beam power processing unit) each	60 (140^oF)	3.8
	83 (arc and multiple unit) each	60 (140^oF)	2.5

The following guidelines should be observed in selecting mounting locations:

- 15-cm thrusters: mount processor units vertically along the top edges of the equipment compartment (under the antenna) to provide good radiation to space. Radiator

surfaces not exposed to sunlight can be white paint (Dow Corning 92-007 or S-13G). Second surface mirrors are required on radiator surfaces exposed to sunlight. Non-radiating surfaces can be insulated to minimize heater requirements during power-off periods. Isolate units from the spacecraft by means of low thermal conductance structural attachments.

- 30-cm thrusters: mount the higher powered beam processing units along the sides of the equipment compartment away from the solar arrays. The lowered powered arc and multiple units can be mounted on the remaining sides. Use second surface mirrors on the main radiating surface. Other surfaces can be insulated to minimize heater requirements during cold operations. Isolate units thermally from the spacecraft.

To maintain the minimum allowable turn-on temperature of -40°C during processor unit power-off periods, the following heater requirements are specified:

a) 15-cm thrusters - 28 watts for each PPU

b) 30-cm thrusters - 45 watts for each beam PPU

- 30 watts for each arc and multiple PPU

The heater requirements specified above include an arbitrary 20 percent contingency to account for conduction losses to the supporting structure.

The conclusion to this analysis is that the temperature control of the spacecraft and the components of the solar electric propulsion can be achieved but with some inconvenience in packaging. The size and heater power required for the thruster power processor units are the major impact on the overall system configuration.

4.5.2 Solar Approach Missions

Category II missions evaluate the capability of the Pioneer electric propulsion spacecraft to approach the sun to distances closer than or equal to 0.7 AU. The improvement in mission capabilities for an electric propulsion spacecraft have been discussed in Section 3, "Mission Analysis." An evaluation of thermal considerations has shown that the Pioneer spacecraft would require major redesign for inbound missions approaching the sun closer than 0.7 AU. However up to 0.7 AU minor modifications are all that would be required. Assuming the normal spin-stabilized electric

propulsion thrust vector pointing angle of 45 degrees between the spin axis and the solar vector and a solar distance of 0.7 AU, some of the units would exceed their acceptance temperature limits. Table 4-13 presents the temperature prediction at 0.7 AU compared to the acceptance limit. Units not listed have predicted temperatures within the acceptance limit.

Table 4-13. Predicted Unit Temperature and Limits for 0.7 AU Mission

Unit	Temperature (°F)	Acceptance Limit (°F)	Δ (°F)
Battery	87	70	17
PCU	167	160	7
TRF	144	140	4
Inverter (-Y)	149	145	4
CDU	109	109	4
Receiver (-Y)	104	100	4
Receiver (+Y)	102	100	2
Driver No. 1	111	100	11
Driver No. 2	108	100	8
Diplexer No. 1	106	100	6
Diplexer No. 2	107	100	7
DTU	107	95	12
CEA	110	105	5
Conscan	110	105	5
DDU	111	105	6
Trapped radiation experiment	116	104	12
Cosmic ray	110	104	6
Plasma	112	100	12

All other units are within their acceptance limits. Note that all TRW units are qualified to temperatures 30°F greater than their acceptance limits.

Now by making the following minor design changes it should be possible to reduce the temperatures to within their present acceptance limits:

a) Battery DTU. These units are mounted external to the equipment compartment and have second surface mirrored radiating windows (-X axis). Increasing the area of the radiating windows will drop these unit temperatures to within acceptable limits.

b) Equipment Compartment Mounted Units. The temperature of these units may be decreased to within acceptable limits by the addition of a second surface mirrored radiating area of annular shape external to the louver actuators (radially) on the -Z face of the equipment compartment.

c) Experiments. The addition of a 3-blade louver bank radiating area to the -Z face of the experiment compartment between the two existing louver banks should lower the experiments to an acceptable level.

With the increased solar input it will also be necessary to increase the size of the RTG fins over that of Pioneer F and G. The increase should not be overly significant as the amount of absorbed solar energy to be dissipated should still be small with respect to the nuclear heat to be dissipated. Utilizing the fin notching technique defined for Pioneer F and G the fin diameter can be increased without impact to the spacecraft design with respect to clearance. However, the increased weight may necessitate redesign of the RTG vertical attach fittings.

The high-gain antenna has a nominal temperature of 35°F at 1.0 AU distance from the sun, front sun condition, so that at 0.7 AU from the sun and a 45-degree sun look angle its temperature would be approximately 82°F so no problem should be encountered.

For the sun sensor assembly it will probably be necessary to alter the external coating of the package slightly by increasing its hemispherical infrared emittance. This may readily be accomplished.

5. SUBSYSTEMS DESIGN

5.1 COMMUNICATIONS, TELEMETRY AND COMMAND

5.1.1 Requirements

The communications requirements for the solar electric propulsion Pioneer differ from that of the Pioneer F and G only during the thrust phase of the mission. During this time, with the spin axis fixed at 45 degrees to the sunline, the view angle to the earth does not remain fixed but changes over a wide range. The bit rate requirement during this phase is quite low since the experiments are off and only the electric propulsion system and attitude control system are active. A nominal bit rate of 8 bps is used as a basis for design.

The general requirements for the communications can be seen from Figure 5-1, where the communication distance is plotted against angle from the spin axis to the earth line-of-sight. The mission elapsed time marks are indicated on the curves as a third parameter. Four missions are plotted, the Atlas launch of a Jupiter flyby out of ecliptic, and a Titan launch of direct flybys to Saturn and to Uranus or Neptune. The diagonal scale on the right side of the figure gives the bit rate capacity as a function of the effective radiated power to earth in dBW. As an example a 24-watt (13.8 dBW) transmitter with a 0 dB antenna radiates 13.8 dBW to earth, as shown. The bit rate capability for the 13.8 dBW erp is 256 bps using the 210-foot DSN antenna or 16 bps with the 85-foot ground antenna.

At this point, somewhere near 80 days into the mission, the omni-antenna would be switched out and the thrust phase medium-gain fan beam antenna would be switched in. As an example, if this were a 6.2 dB antenna there would now be 20 dBW erp available which would give at least 8 bps out to approximately 150 days using the 85-foot ground antenna. Although the curves are shown out to 200 days the outbound missions will be terminated within 150 days using the 8 kw three 30 cm-thruster configuration. Therefore, the medium-gain fan beam antenna requirement is to design a biconical antenna that has at least 6.2 dB gain and covers a region of approximately 20 degrees with the beam peak approximately 60 degrees off axis.

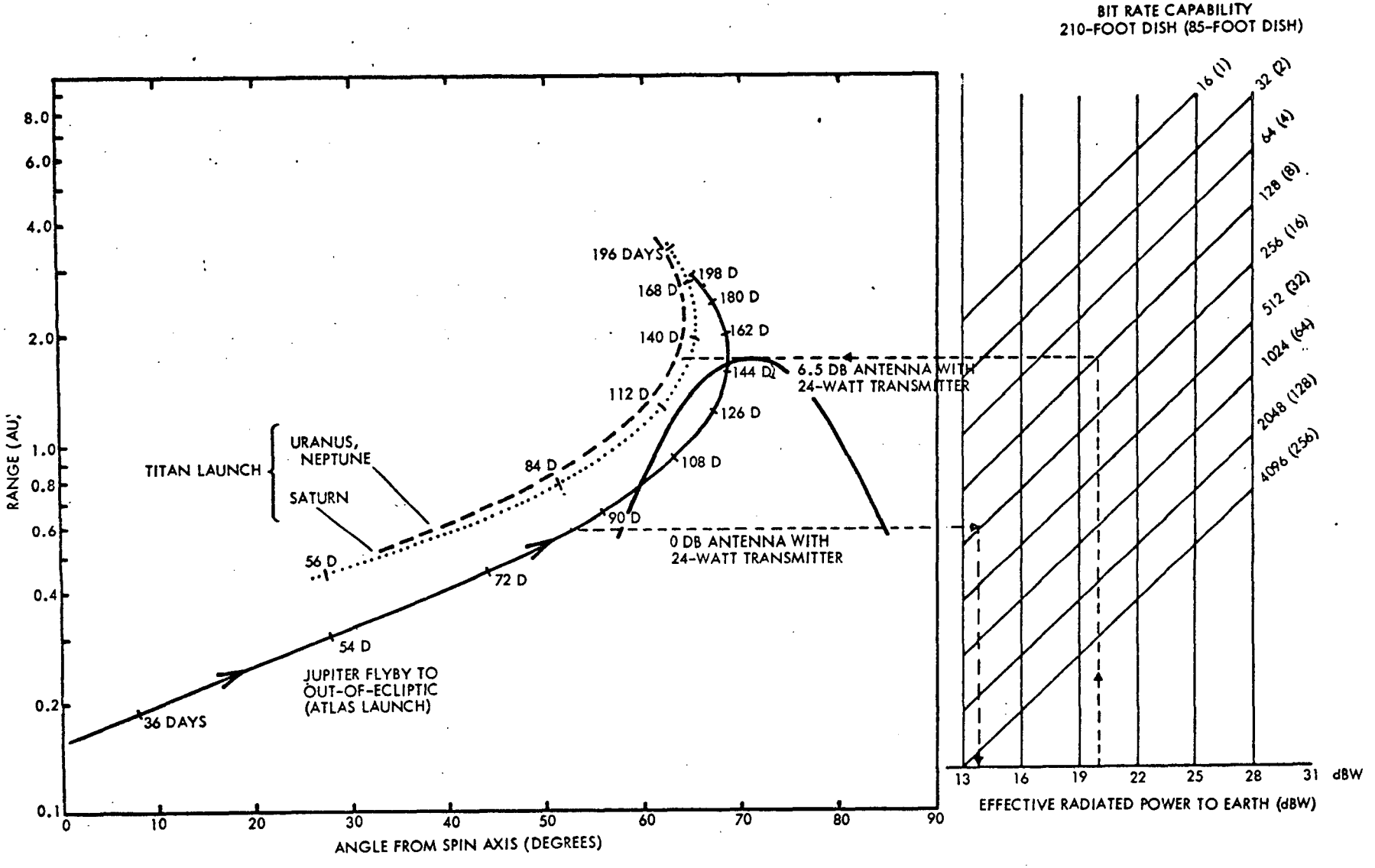

Figure 5-1. Communications Requirements versus Trajectory During Thrust Phase of Outbound Missions

5.1.2 Antenna

The requirement for an antenna having an axially symmetric pattern with the peak gain at 60 to 65 degrees off the axis can be seen from the previous figure. The antenna bandwidth must be sufficiently broad to allow for the excursion of the earth view angle throughout the trajectory. Practical limitations on antenna design prevent use of the medium-gain fan-beam antenna throughout the thrust phase, therefore the omni-antennas are used in the early portion of the thrust phase until the look angle moves into the medium-gain pattern.

The beamwidth requirement is determined by the point in the mission where the omni-antenna begins to approach an inadequate communication margin at the minimum desired bit rate (8 bps). From the figure, this occurs at approximately 0.6 AU at 40 degrees off axis. With a peak gain at 60 degrees off axis at 3.6 AU, the antenna must be at least ±20 degrees wide at -16 dB down. Assuming a trigonometric form for the pattern, the half power (-3 dB) points should then be about 10.5 degrees from the peak gain point. The maximum gain achievable can be computed by the solid angle of a 21-degree spherical sector bounded by half-angle cones of 49.5 and 70.5 degrees.

$$\frac{\Delta\Omega}{4\pi} = \frac{1}{2}(\cos\theta_1 - \cos\theta_2) = 0.15782$$

$$10 \log \left(\frac{4\pi}{\Delta\Omega}\right) = 8 \text{ dB}$$

This is the theoretical limit for a 21-degree spherical sector antenna with the beam peak at 60 degrees off axis.

An axially symmetric fanbeam antenna which fulfills the foregoing requirements was developed in the course of this study. The specific requirements at the onset of the study were for an antenna with the beam at 71 degrees from the spin axis. Subsequent mission analysis revealed the requirements for a 60-degree off-axis beam as shown in Figure 5-1. However, the antenna development had proceeded on the basis of a 71-degree beam angle such that this effort was continued to completion of the prototype hardware. The beam angle can be varied by modification of the

antenna dimensional parameters in order to meet specific requirements for beam angle.

The prototype antenna developed in this program is shown in Figure 5-2 which includes a summary of its characteristics. The polarization is linear and normal to the axis of the antenna to minimize the effects of the tripod support struts in the path of the antenna beam.

A representative test pattern of this antenna is shown in Figure 5-3. The main beam is centered at 71 degrees, meeting the design objective. The test pattern shown was obtained with the antenna free standing whereas, in the spacecraft configuration proposed, this antenna would be mounted

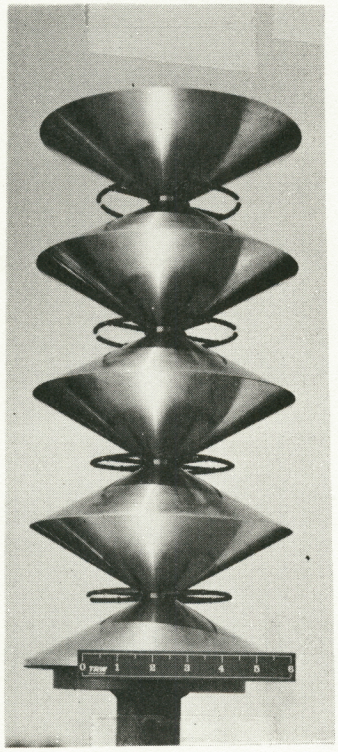

CHARACTERISTICS

SIZE: 8.2" DIA X 16.5"

GAIN: 6.5 DBI

BEAMWIDTH: (3 DB) 17.5°

COVERAGE: 360° WITH <1 DB VARIATION

WEIGHT: FOUR LBS

BEAM ANGLE: 71° TO SPIN AXIS

POLARIZATION: LINEAR

ACTIVE ELEMENTS:
FOUR-WAY DIVIDER PROGRESSIVELY PHASED
FOUR-QUAD DIPOLE FEEDS SPACED AT 0.8λ (4.1")

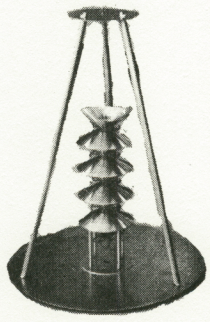

Figure 5-2. Single-Beam Position Biconical Horn Array Antenna

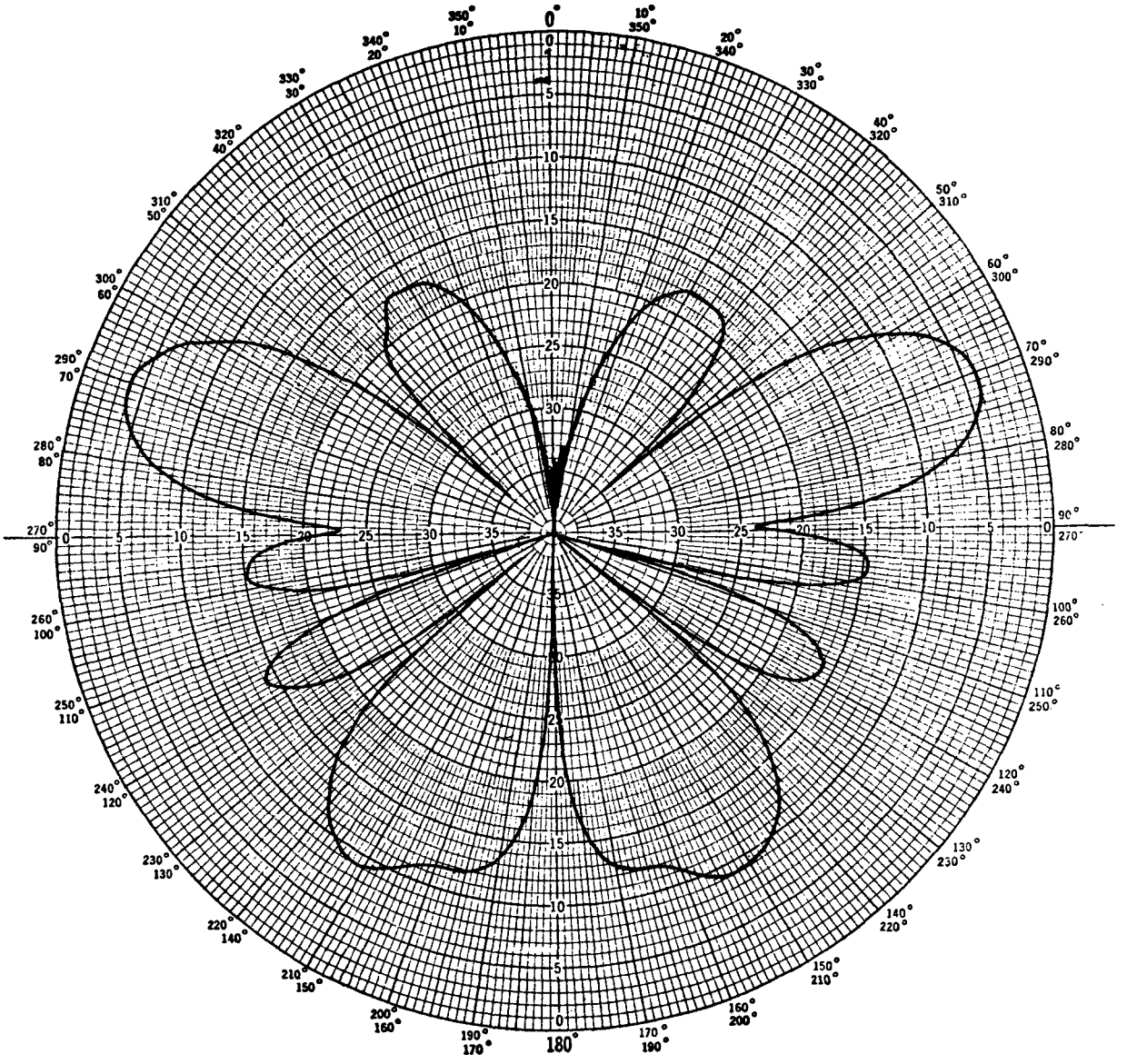

Figure 5-3. Fan Beam Biconical Horn Prototype Test Pattern

near the high-gain dish as shown in Section 3. 2. The effect of this placement of the fan beam biconical antenna on the resulting pattern was not established within the scope of this study. The backlobe at 150 degrees from the forward axis would be affected by the dish displacement.

The side lobes on the pattern are very close to the theoretical predictions as can be seen from Figure 5-4 where the theoretical pattern is plotted with the actual test pattern. The main derivation from the theoretical occurs on the lobe at 150 degrees where the magnitude is about 3 dB higher than expected.

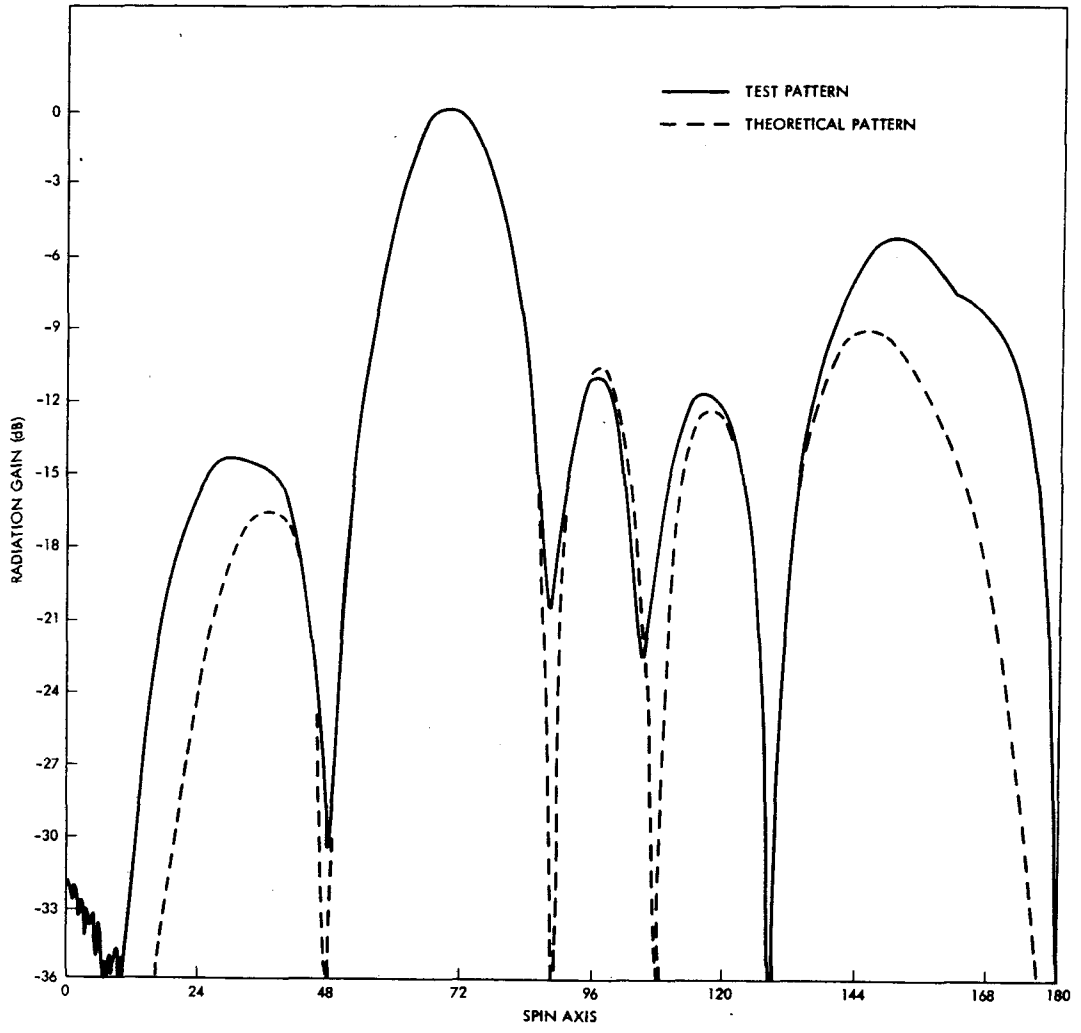

Figure 5-4. Comparison of Test and Theoretical Patterns For Fan-Beam Biconical Antenna

To determine the precise gain figure for the antenna requires an additional test beyond that accomplished in the course of this study. This test entails taking circular cuts through each of the lobes in the patterns, integrating the total power in the pattern and determining the relative power in each lobe.

A good estimate of the relative gain from the primary lobe of the pattern was calculated by summing the solid angles and relative power in each lobe. It can be assumed with reasonable accuracy that the solid angle of each lobe is bounded by the half power points relative to the lobe peak. The fractional solid angle, ρ, of a spherical sector bounded by cone angles θ_1 and θ_2 is given by

$$\rho = \frac{1}{2} \cos \theta_1 - \cos \theta_2$$

Table 5-1 presents the analysis of the test pattern obtaining a nominal gain of 6.5 dB for the prototype antenna. The loss due to the feed elements, power dividers and phasing elements was only estimated since these elements in the prototype were not optimized and therefore caused much greater losses than would occur in a flight unit.

Table 5-1. Analysis of Prototype Antenna (Free Standing Pattern)

Lobe i	Magnitude 10 Log (P_i/P_1) (dB)	-3 dB Angles		ρ_i	P_i/P_1	P_i/P_o
		θ_{i1} (deg)	θ_{i2} (deg)			
1	0	62	79.1	0.1402	0.1402	0.7440
2	-14.0	22	42.7	0.0961	0.00385	0.0204
3	-11.0	92.5	101.5	0.0779	0.00617	0.328
4	-12.3	112	124	0.0923	0.00543	0.0288
5	-5.3	140.5	163.5	0.0936	0.0276	0.1464
6	-8.2	157.7	174.2	0.0347	0.00521	0.0276

$$P_o = \sum_{i=1}^{6} P_i/P_1 = 0.1885, \quad \sum_{i=1}^{6} P_i/P_o = 1$$

Main lobe reference gain (10 log $(1/\rho_1)$	8.5 dB
Losses to side lobes (10 log P_1/P_o)	-1.3 dB
Passive element losses (estimated)	-0.7 dB
Probable gain realized	6.5 dB

The capability of the 24-watt transmitter with the forward omni- and medium-gain biconical array antennas is summarized in Figure 5-5. The 6.5 dB peak gain of the biconical array with the 24-watt transmitter yields a peak effective radiated power of 20.3 dBW. Referring again to Figure 5-1, the omni-antenna can be used on the Jupiter out-of-ecliptic mission for the first 75 days with the 85-foot ground antenna at 16 bps.

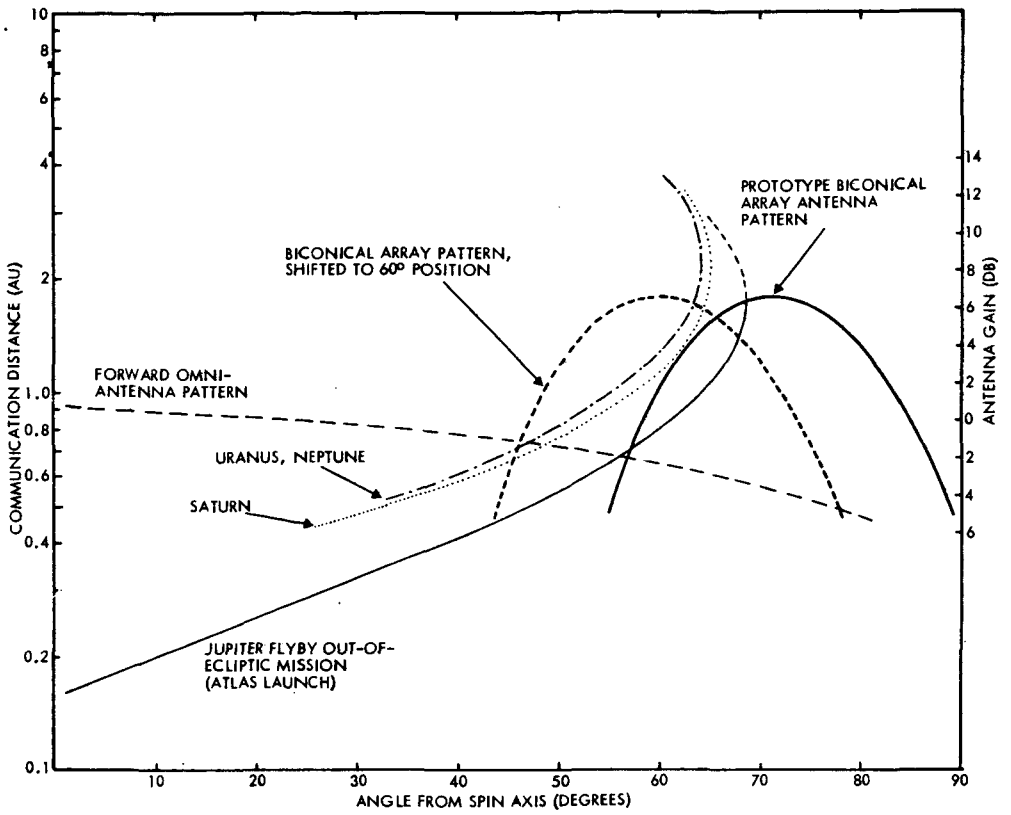

Figure 5-5. Omni- and Medium-Gain Antenna Capability

At this point the bit rate can be switched to 8 bps until 90 days into the mission. At about 90 days the earth view angle has moved into the pattern of the biconical antenna and a command is sent to switch from the omni to the biconical array antenna. This antenna is acceptable until about 150 days into the mission, utilizing the 85-foot ground antenna only. With the 30-cm thrusters on the spacecraft, the thrust period can be terminated at 150 days. At this point the spacecraft is oriented to the earth-pointing position and the transmitter switched to the high-gain dish at 10 watts radiated power for the remainder of the mission.

The Tempel II comet rendezvous mission presents a more complex communications problem from the standpoint of the earth view angle excursion. Figure 5-6 presents the earth view angle plot for the complete mission with the required antenna patterns. A selectable two-beam position antenna is required. Note that with the 30-cm thrusters, the spacecraft coasts for the first 200 days during which time the spacecraft can be oriented at any convenient position for communications.

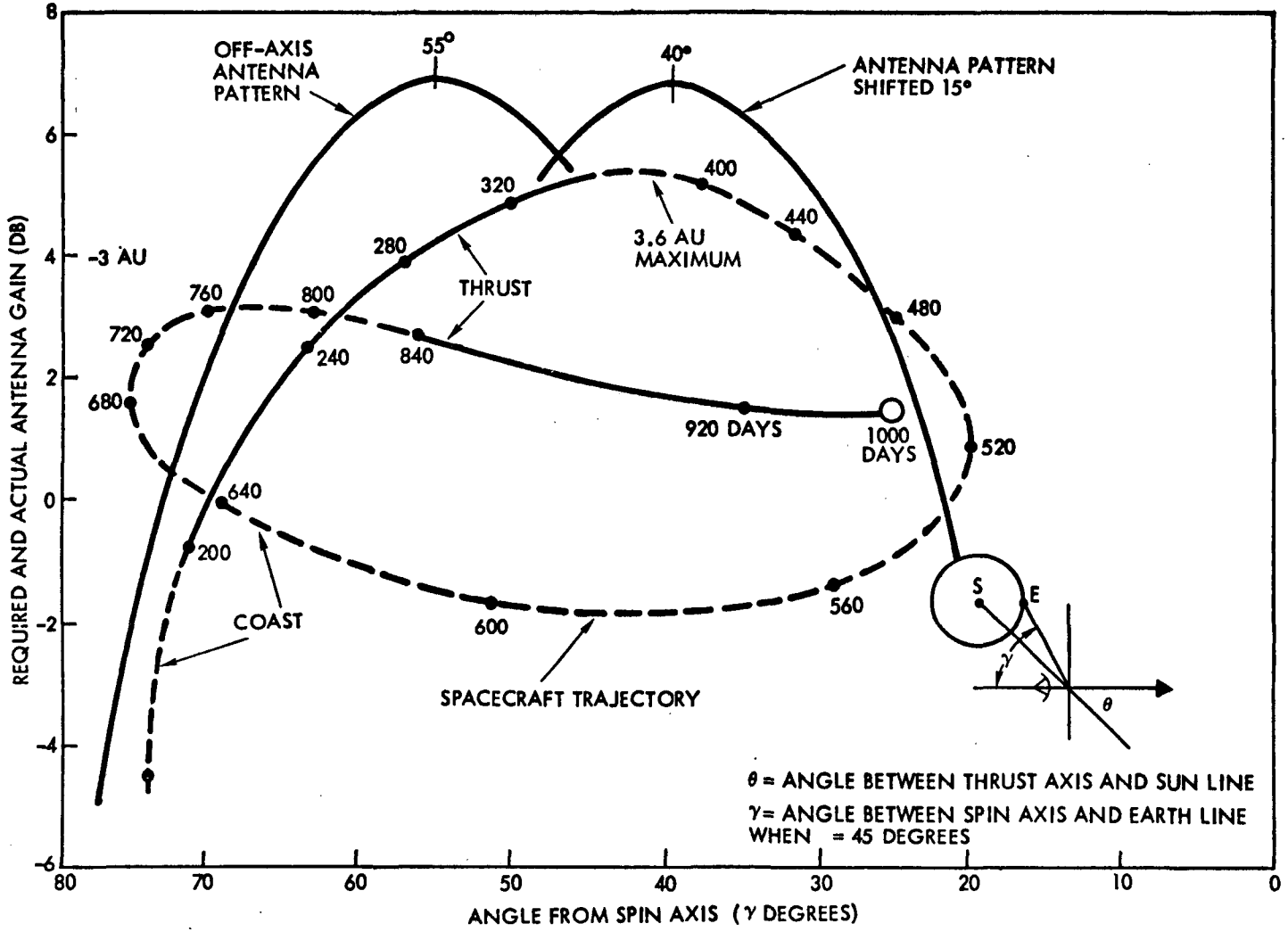

NOTE: GAIN REQUIREMENT BASED ON 8 BITS/SECOND DATA RATE MINIMUM WITH 24-WATT SPACECRAFT TRANSMITTER AND 210-FOOT GROUND ANTENNA. DURING COAST PERIOD (360-840 DAYS) HIGH-GAIN ANTENNA AND 85-FOOT GROUND ANTENNA COULD BE USED.

Figure 5-6. Antenna Gain Required for Tempel II Mission and Estimated Antenna Patterns

During the first thrust period from 200 to 360 days an off-axis antenna with a 28-degree beamwidth at 55 degrees off axis is used for communication with the 210-foot DSN ground antenna. At 360 days, the thrust is terminated and the spacecraft returns to the Pioneer high-gain communications system. At 840 days into the mission, the thrusters are again turned on and the off-axis antenna is used for telemetry. At about 900 days, the earth view angle has moved to the edge of the off-axis pattern. To maintain coverage, the antenna phasing network is switched such that the beam center is at 40 degrees off axis. This two-beam position antenna design is shown in Figure 5-7. A solid state storage unit capable of storing up to 500,000 bits of data is provided for this mission to retain housekeeping information up to approximately one week without 210-foot ground antenna coverage.

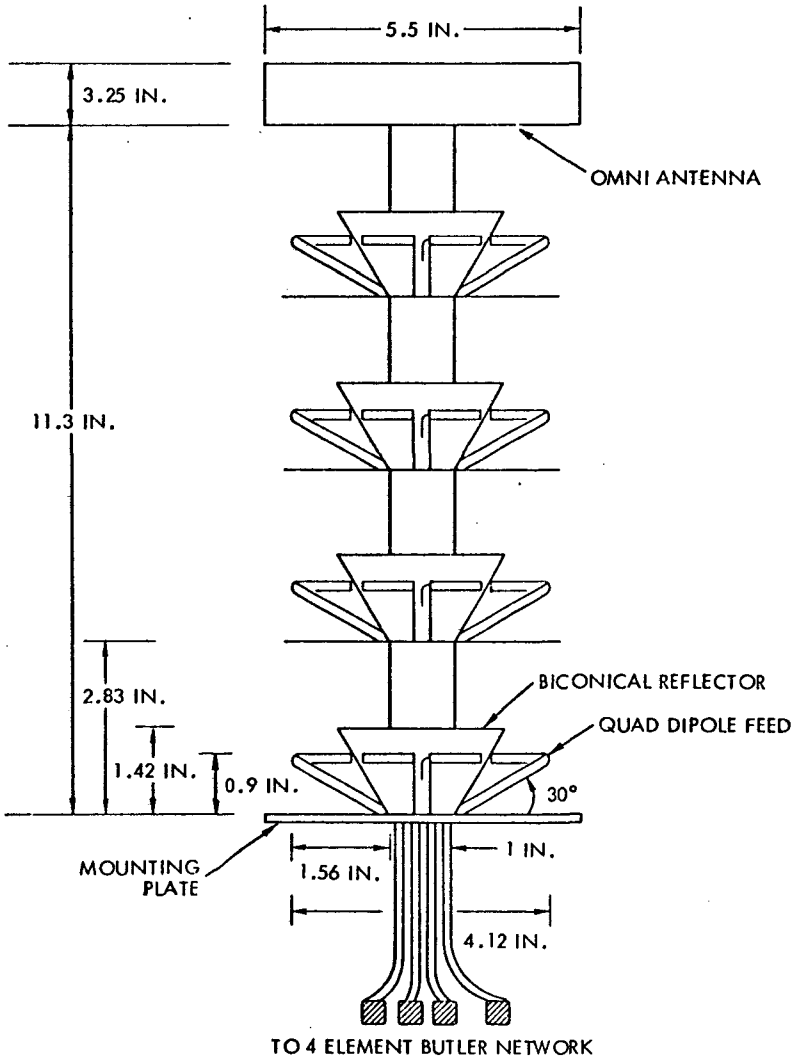

Figure 5-7. Tempel II Biconical Horn Array

The Pioneer F and G 9-foot diameter high-gain antenna must incorporate an X-band feed for the missions beyond Jupiter and X-band as well as S-band transmitter must be provided. This results in approximately 10 dB additional gain which improves the bit rate by approximately a factor of 10. For this configuration the X-band feed at the focal point of the rigid parabolic reflector provides a secondary pattern centered along the spacecraft spin axis. The S-band feed is offset from the antenna axis to provide a conical scan pattern with the spinning spacecraft, as in Pioneer F and G, and a conical scan processor produces firing pulses to the attitude control system. A combination of the Pioneer F and G cavity-backed crossed dipole S-band feed with a separate X-band waveguide was considered first but the S-band feed was too far off center and too susceptible to damage by the ion engine beam. A combination S- and X-band open-ended ridge waveguide was thus chosen to enable the phase centers of the two feeds to be placed closer together as shown in Figure 5-8. The waveguides are fed by orthogonal probes to achieve circular polarization and the antenna has a gain at S-band of about 29.5 dB on boresight with a 5-degree beam at the half power points. The S-band gain on the spin axis is about 28 dB and the X-band gain is about 41 dB since the X-band feed is not offset.

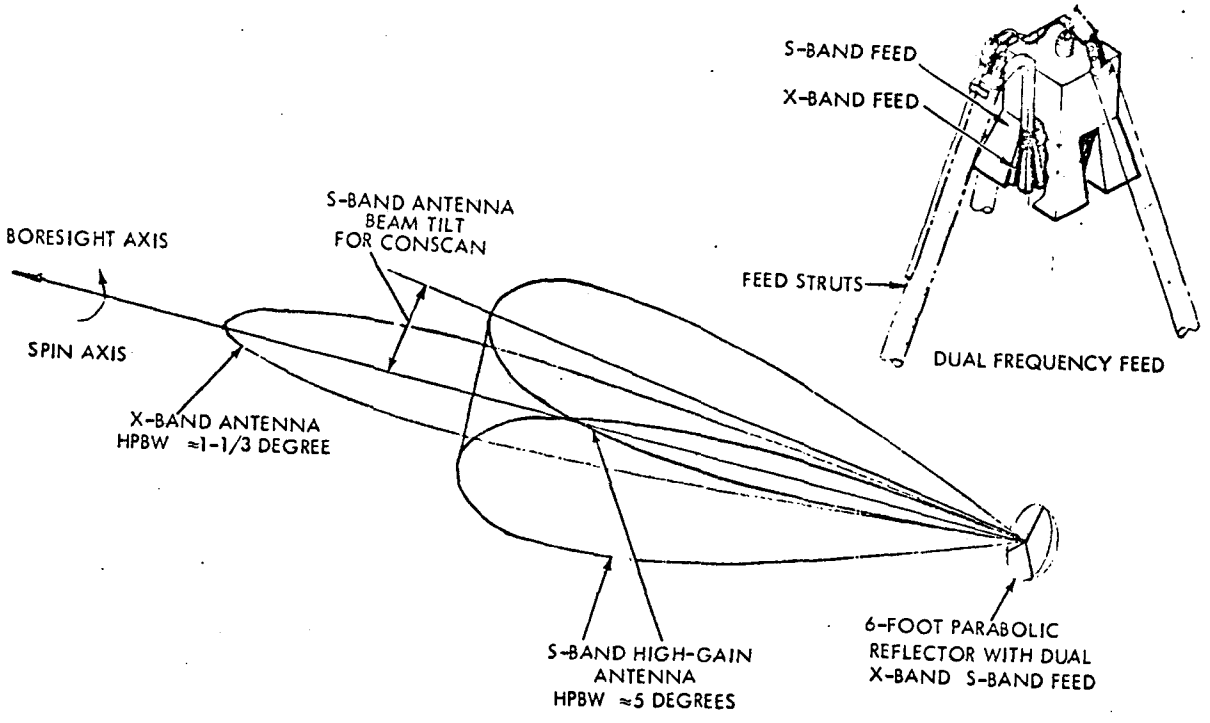

Figure 5-8. S-Band and X-Band Antenna Pattern Characteristics

5.1.3 Transmitter

The performance curves shown in Figure 5-9 indicate that the required performance during the thrust phase can be obtained at S-band with a power output of about 24 watts. This value falls conveniently in the range of travelling wave tube amplifiers already developed and some of which have been space-qualified. The operation on the high-gain antenna after the thrust phase does not require any more than 10 watts of the original Pioneer F and G design. Table 5-2 shows that a dual power mode S-band travelling wave tube amplifier is available, giving either

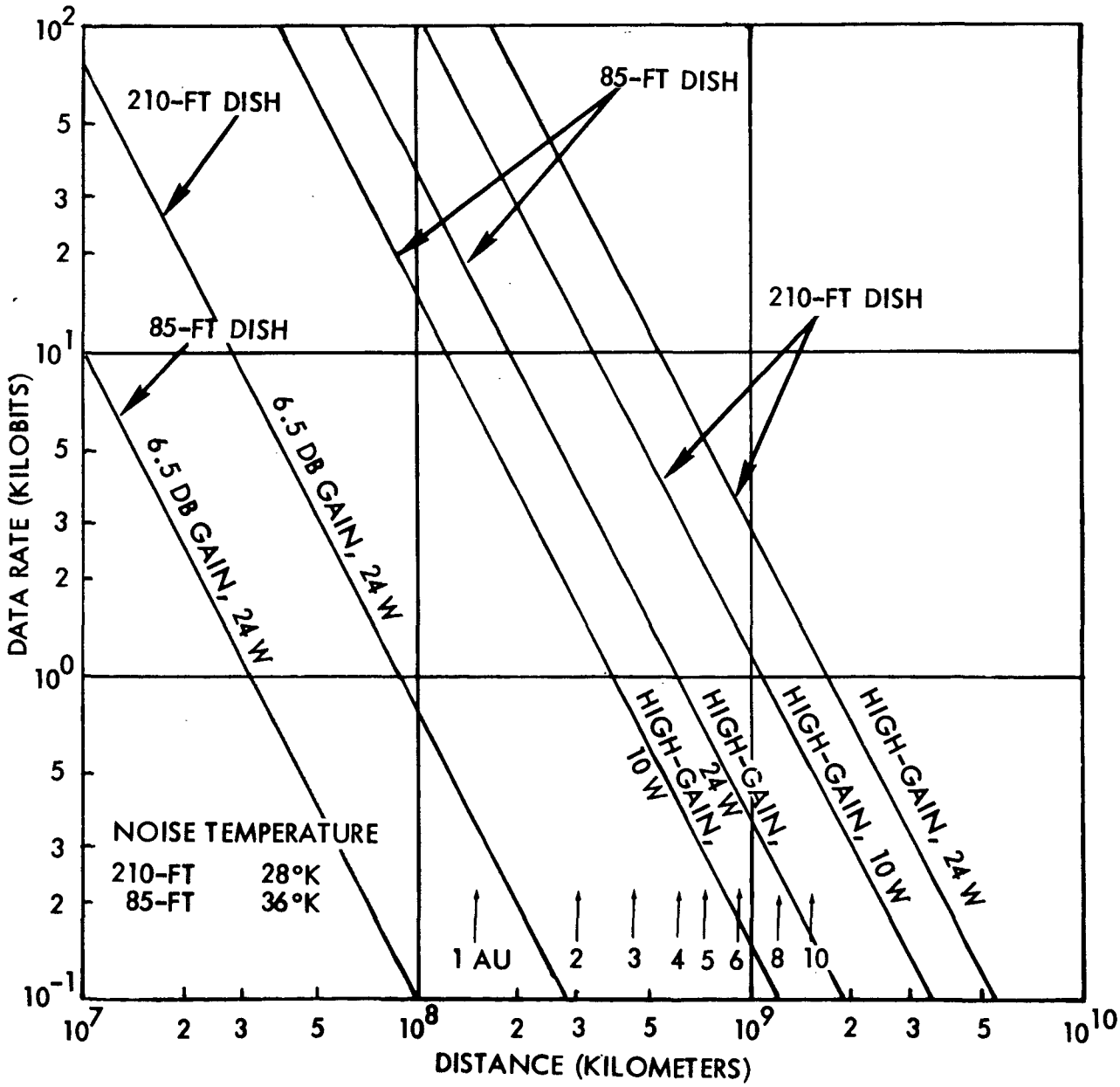

Figure 5-9. Downlink Communication Capability (High-Gain Spacecraft Antenna)

Table 5-2. TWTA Specifications

Characteristics	Watkins-Johnson, Series WJ-1171
Performance Capabilities	
Frequency	2.2 to 2.3 GHz
Saturated power output	12/24 watts
Efficiency overall	30.6 percent/34.9 percent
Saturated gain	28/31 dB
Output VSWR (cold)	1.25:1
Electrical Characteristics	
Primary voltage	+28 vdc +3 percent
Primary power	39.2/68.7 at 28 volts -3 percent 40.4/70.7 at 28 volts 41.6/72.8 at 28 volts + 3 percent
Telemetry outputs:	
Cathode and helix currents, and collector temperature	0 to ±3 vdc
Delay time before 100 percent	
Carrier power	90 to 150 seconds
Mechanical Characteristics	
Baseplate dimensions	4.58 x 12.00 inches (123 x 305 mm)
Height (excluding connectors)	3 inches (76 mm)
Weight	4.55 pounds (2.06 kg)
Connector types	TNC or
RF in and out	3 mm female
Power/telemetry/command	Cannon Golden "D"

*Data extracted from Watkins-Johnson, Series WJ-1171, TWTA Model Number 1171-3, associated TWT 274-9.

24 watts at about 34 percent efficiency or 12 watts at 30 percent efficiency in a package which is not much heavier (2.06 kg) than the corresponding 24-watt single mode package (1.91 kg). This would permit operation at half the data rate with a saving of nearly half the prime power and is a simple method of saving prime power at the cost of a slight decrease in reliability.

An S-band transistor power amplifier is a possible alternative to the travelling wave tube amplifier in solar electric propulsion space vehicles in which efficiency is not of overwhelming importance. Overall

C.3

efficiency is reported at 20 to 25 percent depending on the environment. This is competitive with travelling wave tube amplifiers and the use of several stages in parallel (Figure 5-10) with diode switching enables multiple power mode operation to be readily achieved without the normal travelling wave tube amplifier efficiency degradation. Moreover, the transistors themselves are inherently long lived and reliable and the elimination of the high voltage power supply also improves the reliability considerably. Lastly, the multiple power level transistor output stage should be lighter than that of a travelling wave tube amplifier of the same flexibility of operation.

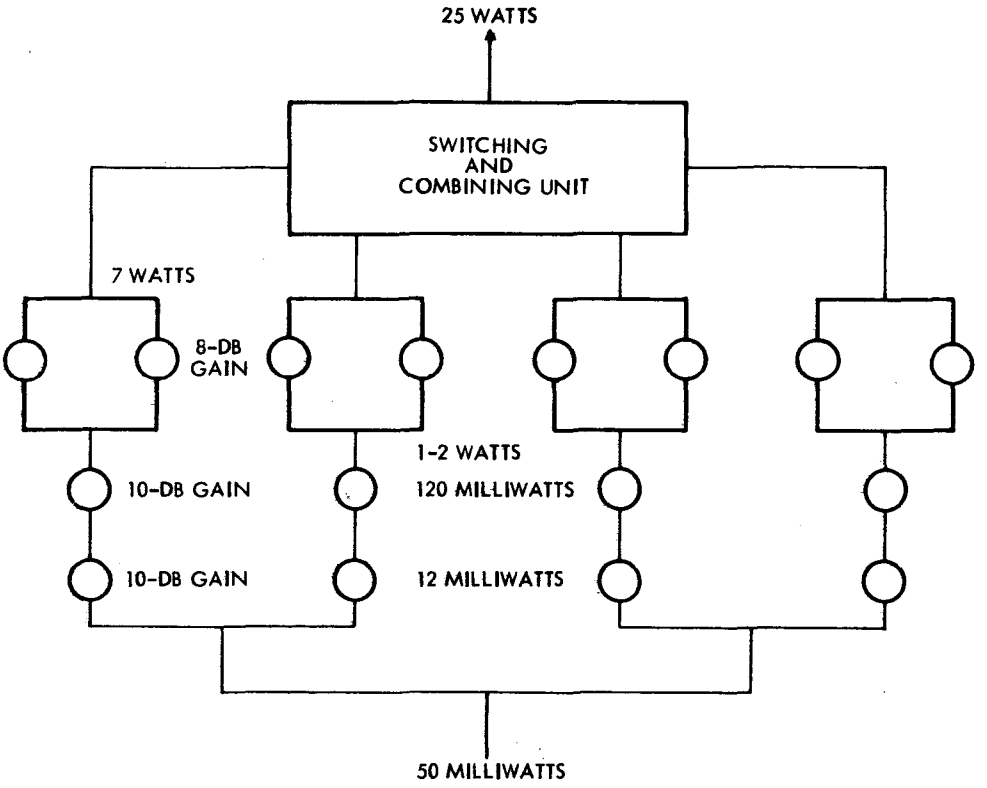

*THEORETICAL EFFICIENCY ≈33 PERCENT. 20-25 PERCENT OVERALL IN PRACTICE DEPENDING ON POWER CONVERTER AND ENVIRONMENTAL REQUIREMENTS.

Figure 5-10. Outline Configuration of a Transistor, 25-watt Amplifier Using Existing Devices

An overall block diagram (Figure 5-11) shows that the other components of the communication subsystem are identical with those of the Pioneer F and G spacecraft or require only small modification. The additional antenna requires a pair of SPDT coaxial switches for switching

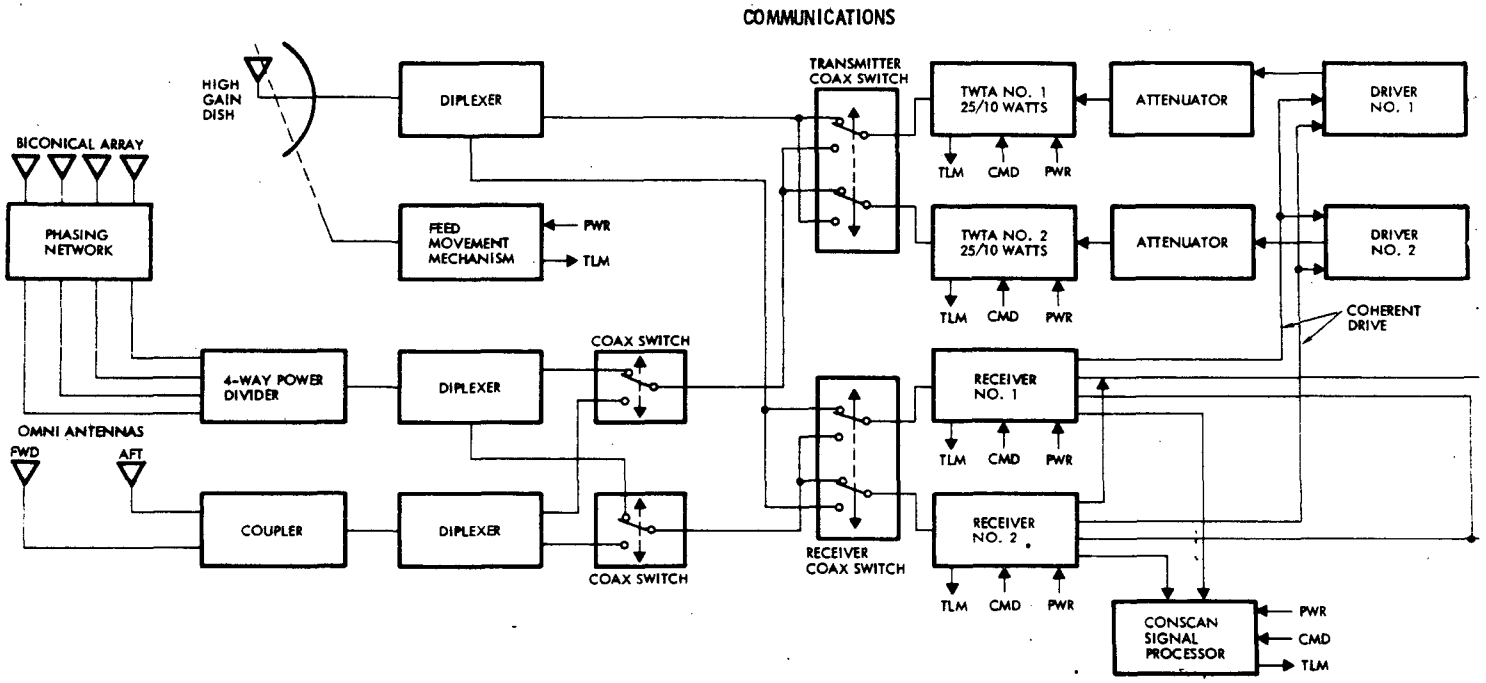

Figure 5-11. Communications Subsystem Block Diagram

from the omni-antenna to the medium-gain horn. The transmitter driver will require an additional transistor output stage to provide a higher drive level for the input to the higher output tubes. The Pioneer F and G receiver may be used in its existing form unless a small improvement in maximum distance for range measurement is found necessary for some missions. The existing diplexer couplers and transfer switches should be adequate but would require qualification for operation at the higher power level and the Conscan signal processor should require no change.

5.1.4 Data Handling Telemetry and Commands

The data handling telemetry and command subsystem shown in Figure 5-12 is almost identical to that of the Pioneer F and G spacecraft and consists of a digital decoder (for commands), digital telemetry unit, and a storage unit. The data storage unit (DSU) for all but the Tempel II mission uses core storage and has a capability of nearly 50 kb consisting of the Pioneer F and G unit weighing 3.5 pounds and consuming less than 1/2 watt in standby and less than 1 watt during readout. The digital decoder output goes to the command distribution unit (CDU) which has a programmable command capability allowing storage of five discrete commands for sequential execution at a later time.

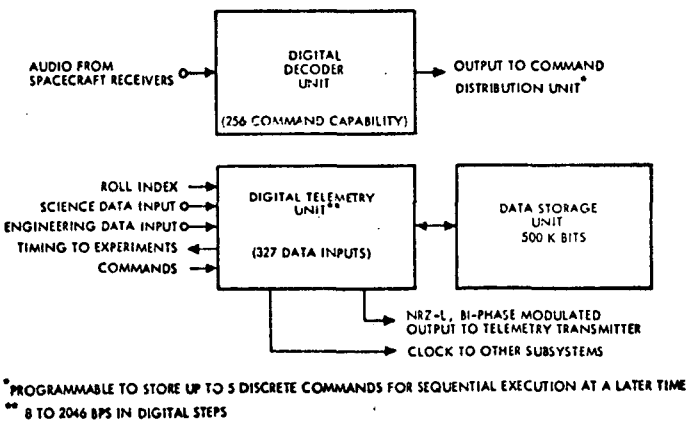

Figure 5-12. Data Handling Subsystem Block Diagram

The existing system is designed to handle variable bit rates from 16 to 2048. The requirement during the thrust phase at the low end, of 8 bits per second results in a minor change of one telemetry bit rate from 64 bps to 8 bps.

The system recommended for the Tempel II mission requires a much larger storage than for the Pioneer F and G missions. The type of storage unit suggested is presently under development at TRW and elsewhere, and uses P-mos techniques to provide a storage capacity of about one-half million bits for a weight of 2 pounds and a power consumption of 4 watts. A read-in rate of 2 bps to this solid-stage storage unit would allow a once a week readout to the 210-foot DSN ground antenna of engineering and housekeeping data during portions of the Tempel II mission. During these intervals there would be no downlink communication. However, tracking would be maintained using the carrier with the 85-foot ground antenna.

5.2 ATTITUDE DETERMINATION, GUIDANCE AND CONTROL

5.2.1 Attitude Determination Requirements

The addition of solar electric propulsion to the Pioneer spacecraft creates four distinct phases of a typical mission:

1) The prethrust phase beginning at separation from the TE-364-4 and ending when the spacecraft is oriented 45 degrees to the sunline with the solar arrays deployed.

2) The thrust phase wherein the spin axis is maintained at 45 degrees to the sunline and the ion thrusters are operating. Communication is on the omni- then medium-gain antenna.

3) The cruise phase wherein the spin axis is pointed at the earth and communication is via the high-gain antenna.

4) The encounter phase during which the experiments are operating and terminal guidance is in effect (if required).

Each of the first three phases of the mission has specific attitude determination requirements which in conjunction establish the attitude sensing requirements for the spacecraft.

General requirements for unambiguous determination of spacecraft attitude are for sensing of two reference bodies, such as the sun and a star, earth and sun, earth and a star, etc. Pioneer 10 used earth as a primary attitude reference by utilizing the offset antenna angle to align the spin axis with the line of sight to the earth. This insured that the spin axis remained in the ecliptic plane. The sun was used as a secondary reference with a sun sensor which provided a pulse at each sun crossing. The sun sensor provided an inertial reference in rotation and the antenna provided a means for alignment of the spin axis to the earth line. Thus the orientation of the spacecraft is completely determined. The Pioneer F and G sun sensor does not provide sun aspect information since this is known by the ephemeris of the spacecraft. The stellar reference assembly (SRA) also provides a clocking pulse each rotation that is somewhat more accurate than the sun pulse and provides an alternate reference, particularly during small sun angles near syzygy of the spacecraft, earth and sun.

As stated earlier, the addition of solar electric propulsion to the Pioneer requires the spacecraft to be sun-oriented during the thrust phase of the mission rather than earth-oriented. Without the offset medium-gain horn used on F and G, neither the position of the earth nor the angular position of the sun relative to the spin axis are explicity known. Thus additional sensing devices must be added to determine the spacecraft orientation. To maintain the spin axis 45 degrees to the sun, a sun aspect sensor is required. This sensor will also provide a sun pulse each rotation for clocking purposes. Details of this sensor are given in the next section.

Knowledge of the sun angle is not sufficient to completely determine attitude as can be seen by Figure 5-13. The coordinates (X_s, Y_s, Z_s) are the axes of a sun-oriented reference frame with Z_s pointed at the sun and Y_s normal to the ecliptic plane. The spacecraft spin axis is Z_b. The aspect sensor yields the angle c between Z_b and Z_s, which is held at 45 degrees during the thrust phase. With sun aspect angle information only, the position of the spin axis Z_b is determined to be on the cone C. To determine the out-of-ecliptic angle, ϵ, an additional sensor must be provided. In this design, the stellar reference assembly is used which produces a pulse when Canopus crosses the field of view. By clocking the time interval, τ, from the SRA pulse to the sun pulse, the angle α is determined by

$$\alpha = \tau \dot{\phi} - \Phi \qquad 5\text{-}1$$

where

$\dot{\phi}$ = spin rate

Φ = angular displacement between SRA axis and SAS axis

The angles and λ are known by the position of the spacecraft and the ephemeris of Canopus and the sun. With a, α, and c known, γ is computed by the law of sines

$$\sin \gamma = (\sin c \sin \alpha)/\sin a \qquad 5\text{-}2$$

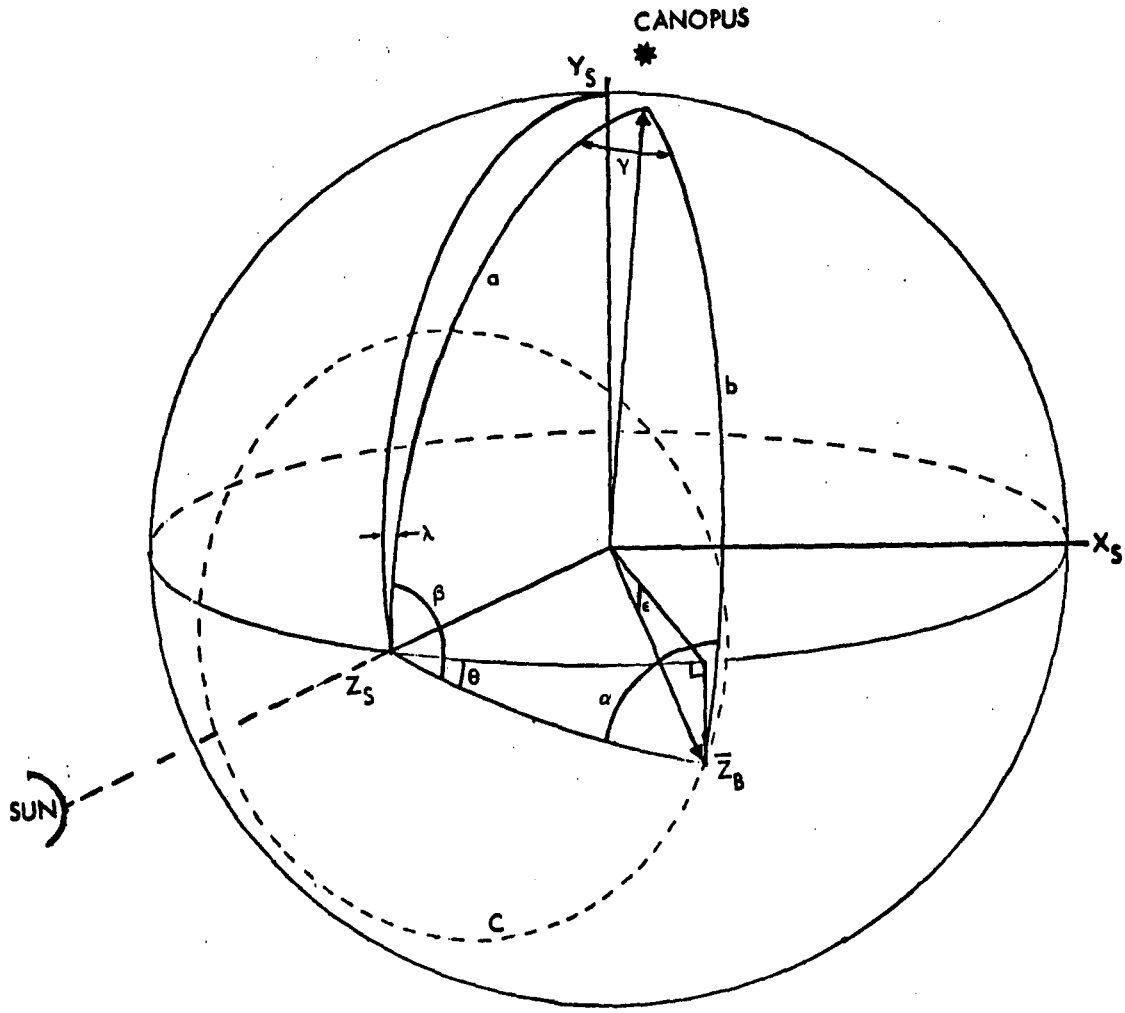

Figure 5-13. Attitude Determination Geometry

Then by Napier's analogies, b and β are computed by

$$\tan 1/2\, b = \frac{\tan 1/2\,(a - c)\, \sin 1/2\,(\alpha - \gamma)}{\sin 1/2\,(\alpha + \tau)} \qquad 5\text{-}3$$

$$\cos \beta/2 = \frac{\tan 1/2\,(\gamma - \alpha)\, \sin 1/2\,(a + c)}{(\sin 1/2\,(c - a)} \qquad 5\text{-}4$$

Note from Figure 5-13 that θ is determined by

$$\theta = \pi/2 - (\lambda + \beta) \qquad 5\text{-}5$$

and the out-of-ecliptic angle ϵ is computed by

$$\sin \epsilon = \sin \theta \sin c \qquad 5\text{-}6$$

The coordinates of Z_b in the sun-oriented ecliptic coordinates are then

$$Z_b = \sin \tan^{-1}\left((\tan c \cos \theta)\right) \bar{e}_x + \sin \epsilon \bar{e}_y + \cos \tan^{-1}\left((\tan c \cos \theta)\right) \bar{e}_z$$

If a Canopus sensor is used as with the SRA on Pioneer F and G, the value of a is within 14 degrees of 90 degrees. With $c = 45 \pm 1/4$ degrees, the error in ϵ can be estimated. The error in α is the clocking error, and if a 12 bit counter is used, the error would be 0.09 degree. The major error is in c (± 0.25 degree). Assuming nominal values for a, c, and α, the error in determining ϵ is less than ± 0.2 degree.

For those missions requiring terminal guidance, such as the comet rendezvous, a star mapper sensor is installed in place of the stellar reference assembly. Although a star mapper can provide complete attitude information, the solar aspect sensor might want to be retained since it can be utilized more readily to maintain the 45-degree sun attitude in a closed loop fashion.

Alternative methods of achieving the secondary reference for attitude determination have been considered in this study, including utilizing the doppler data on the omni antenna in the following manner: with partial deployment of the solar arrays, the center of mass is offset from the geometric axis of the spacecraft. The forward omni then travels in a circular motion as the spacecraft spins about the now-displaced center of mass. The initial orientation maneuver is programmed to bring the spacecraft around to an earth pointing position. This maneuver may be verified by the doppler data on the omni antenna which will be sine wave modulated until an earth pointing position is achieved.

The disadvantage of using this technique is that the doppler data does not indicate the direction of the misalignment (with the earth). Therefore, the final part of the maneuver must be a trial and error procedure. If accurate time correlation between the doppler signal and the on-board sun pulse timing could be achieved, the orientation of the spacecraft could be determined. This however, is an elaborate procedure for the tracking station.

Using this technique, the spacecraft would be initially pointed at earth then programmed to precess the 45-degree sun orientation using the updated calibration of the ACS. The subsequent determination may be accomplished by utilizing the calibration on the doppler technique and resulting measurement on the earth-spacecraft angle which will improve the confidence level of programmed maneuvers.

Another technique briefly considered was aligning the conical beam medium-gain antenna at an angle to the spin axis and using the coning motion of the antenna pattern to determine the earth aspect angle. This method is defeated by the fact that with the spacecraft fixed at 45 degrees, the earth aspect moves from -40 degrees through the spin axis and then to about 65 degrees from the spin axis in the course of the mission. The antenna with maximum gain at about 65 degrees could not be utilized for communications at all until 70 to 90 days into the mission, and attitude information is needed long before that time.

The conclusion to the attitude determination requirements study is that use of the solar aspect sensor and the stellar reference assembly provide the most direct and accurate means of determining attitude. The light shield of the SRA must be modified however, to tolerate the 45 degree sun aspect. A preliminary sketch of the SRA light shade modification is shown in Figure 5-14. This shield is designed such that second reflections from the 45-degree sun line do not occur. If a specific mission is established the light shield detailed design would require additional analysis using nominal mission parameters before a firm design is frozen. In contrast to Pioneer F and G the SRA on the solar electric missions must be operational very early in the mission under the 45-degree sun angle conditions. The use of the SRA near the encounter must be evaluated in terms of interference by the target body and/or its satellites.

5.2.2 Sun Aspect Sensor Characteristics

Orienting and maintaining the spacecraft spin axis at 45 degrees to the sun line during the thrust phase of the mission requires a solar aspect sensor that can be readily integrated with the existing control electronics assembly. A number of candidate solar aspect sensor designs which

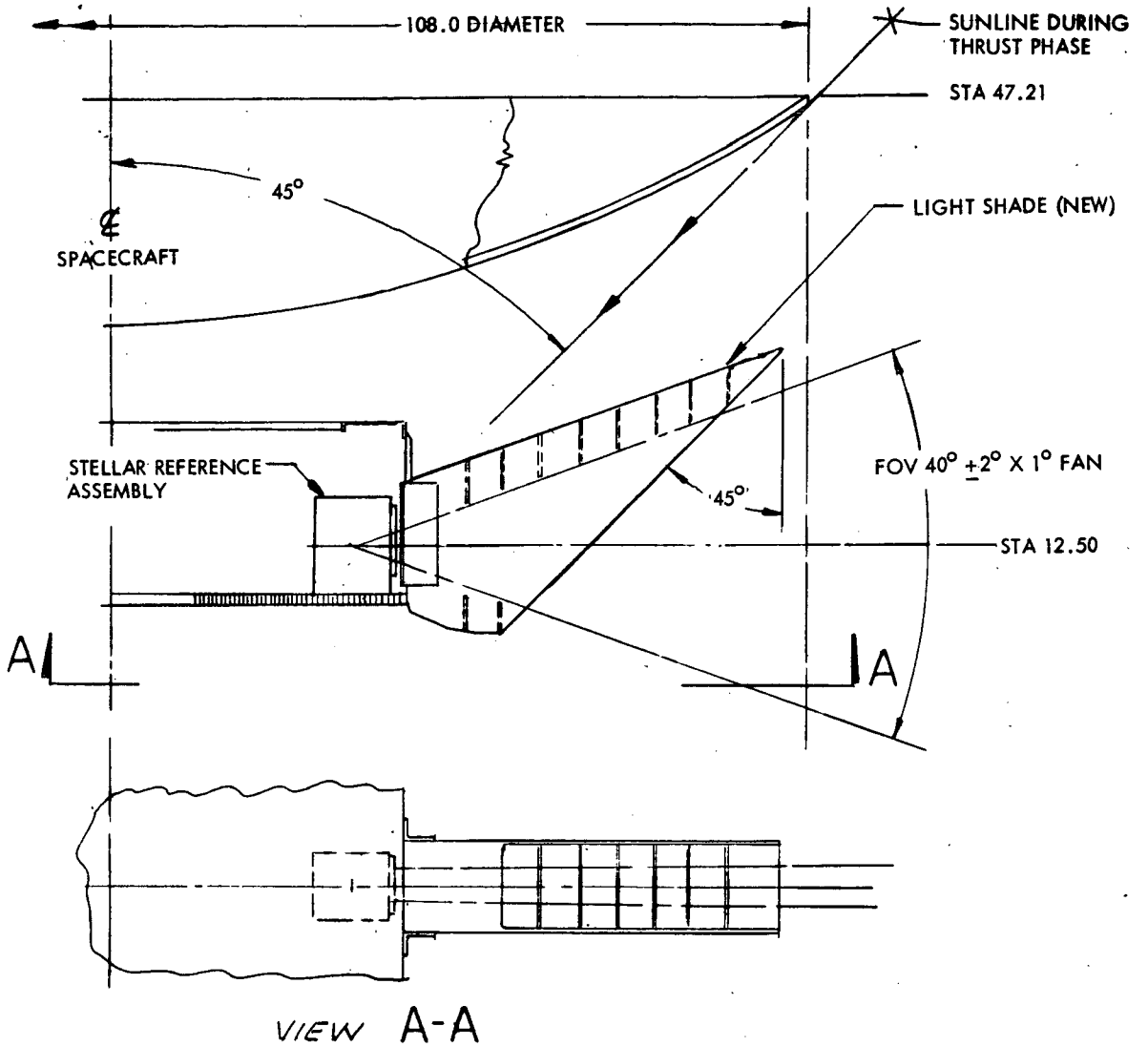

Figure 5-14. Modified Light Shade Stellar Reference Assembly

have flight experience were evaluated in the study. A summary of the characteristics of these candidate sensors is given in Table 5-3. The sensor chosen for the solar electric Pioneer is the Adcole model 10941 digital solar aspect sensor for spinning spacecraft. The choice was based on the following criteria:

- Digital output signal simplifies integration with CEA
- Adequate accuracy (1/4 degree) and resolution (1/2 degree) for this application
- Small size and weight
- Sufficient field-of-view range (64 degrees) for mission

Table 5-3. Candidate Solar Aspect Sensors

1. MANUFACTURER AND MODEL NO.	ADCOLE MODEL 14148	ADCOLE MODEL 10941	TRW E-232794
2. TYPE	DIGITAL, SPINNING	DIGITAL, SPINNING	V-SLIT ANALOG, SPINNING
3. PRIOR APPLICATION	GERMAN RESEARCH SATELLITE (BBRC)	USAF SATELLITE (LOCKHEED)	INTELSAT III
4. ASPECT FIELD-OF-VIEW	128 DEGREES	64 DEGREES	130 DEGREES[1]
5. RESOLUTION	1/2 DEGREE	1/2 DEGREE	BIT-LIMITED BY EXTERNAL CLOCK
6. ACCURACY	±1/4 DEGREE	±1/4 DEGREE	±0.2 DEGREE[2]
7. OUTPUT	8-BIT BINARY, 1-BIT COMMAND EYE	7-BIT BINARY, 1-BIT COMMAND EYE	SINGLE LINE OUTPUT, TWO PULSES WITH Δt PROPORTIONAL TO ASPECT
8. WEIGHT[3]			
SENSOR	0.4 POUND	0.2 POUND	0.4 POUND (TOTAL)
ELECTRONICS	0.75 POUND	0.75 POUND	
9. SIZE[3]			
SENSOR (L X W X H)	2.2 X 1.2 X 1.0 INCHES	1.7 X 1.2 X 0.9 INCHES	1.9 X 1.9 X 1.4 INCHES
ELECTRONICS (L X W X H)	5.0 X 2.0 X 2.0 INCHES	5.0 X 2.0 X 2.0 INCHES	
10. POWER[3]			
SENSOR	-	-	0.05 WATT
ELECTRONICS	0.25 WATT	0.25 WATT	PLUS EXTERNAL CLOCK

[1] REQUIRES MODIFICATION TO EXISTING SLIT MASK. EXISTING MASK COVERS ±85 DEGREES WITH DETERIORATING ACCURACY BEYOND ±65 DEGREES

[2] ELECTRONIC ERRORS ARE NOT INCLUDED

[3] VALUES ARE FOR SINGLE UNIT. FOR SPACECRAFT DESIGN, A REDUNDANT UNIT MUST BE ADDED. VALUES INCLUDING REDUNDANT UNIT FOR ADCOLE MODEL 14148 ARE LISTED IN "PIONEER ELECTRIC PROPULSION – EQUIPMENT LIST"

- Automatic level adjust for varying solar distance
- Extensive flight history
- No development or modification costs
- Low cost per unit
- Provides a sun crossing pulse for clock angle timing.

An engineering sketch of the sensor unit is shown in Figure 5-15, and a drawing of the electronics unit is shown in Figure 5-16. Figure 5-17 presents the principle of operation of the Adcole digital solar aspect sensor. Light passing through a slit on the top of a quartz reticle is screened by a Gray-coded pattern on the bottom of the block to either illuminate or not illuminate each of the silicon photocells directly below the pattern columns. Which cells are illuminated depends upon the angle of incidence. The outputs from each cell are amplified, and the presence ("one") or absence ("zero") of a signal is stored and processed in the electronics to provide the desired output for telemetry.

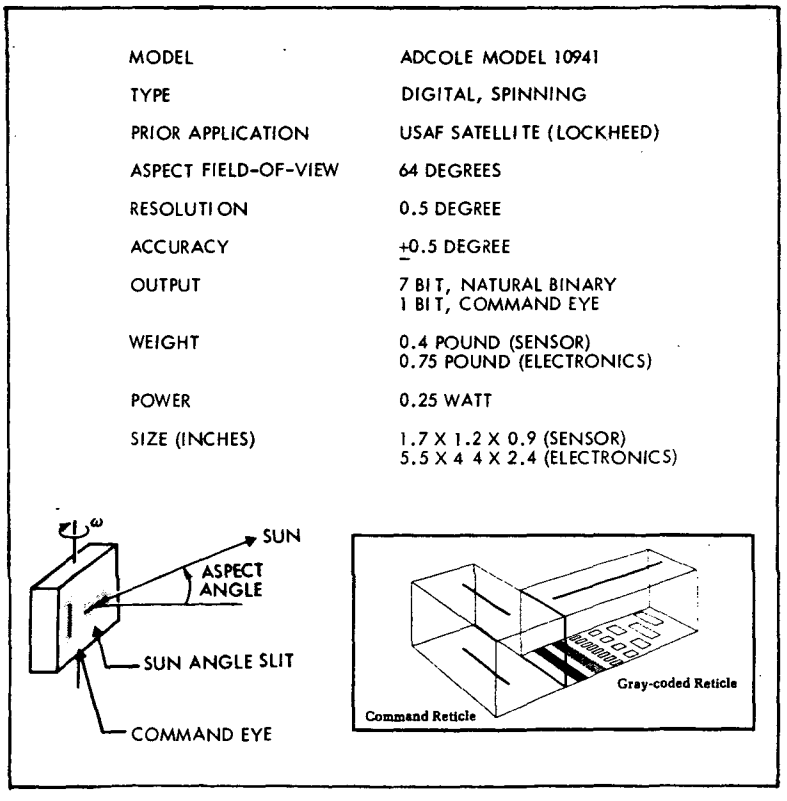

Figure 5-15. Adcole Model 10941, Solar Aspect Sensor Characteristics

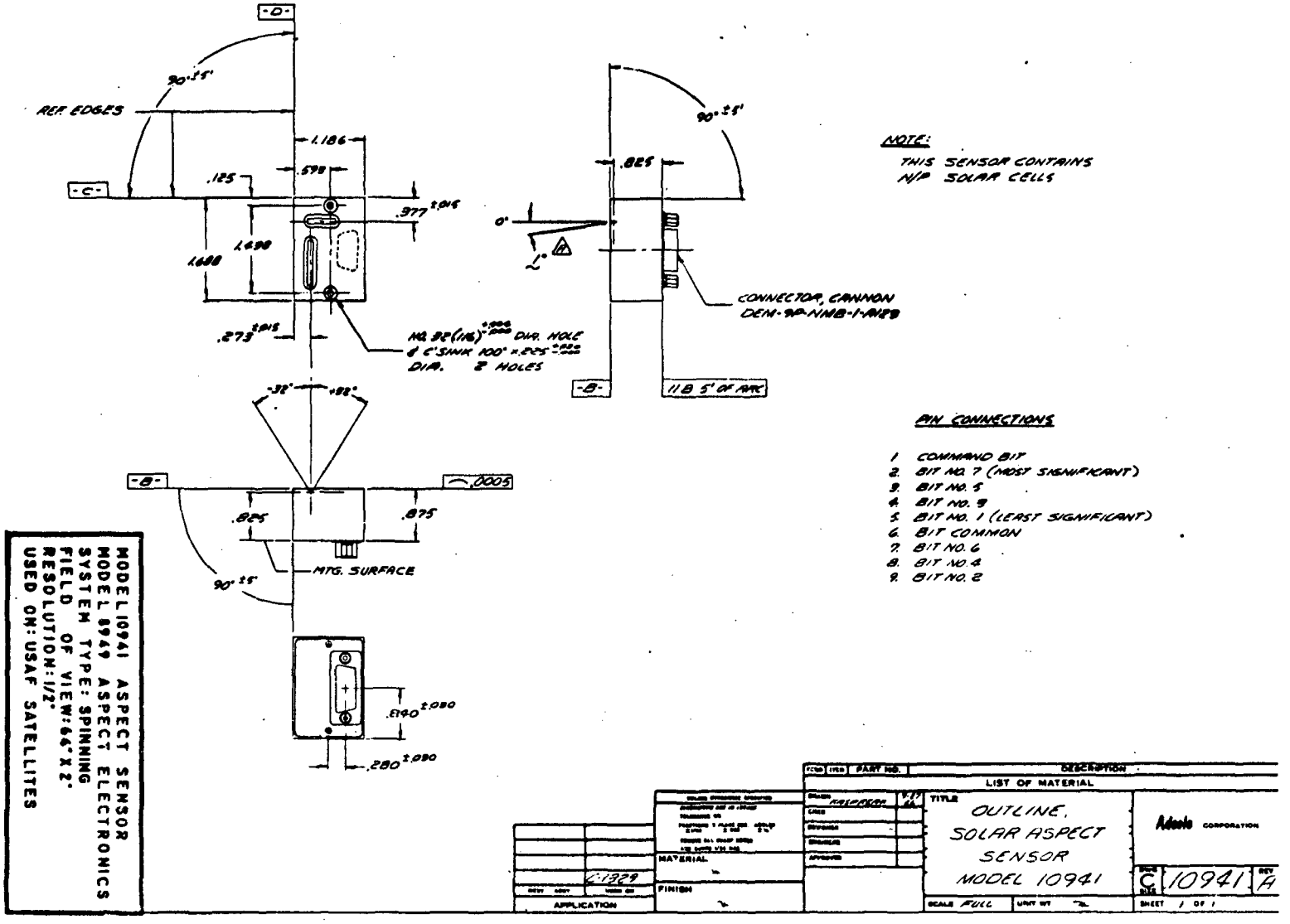

Figure 5-16. Solar Aspect Sensor Configuration

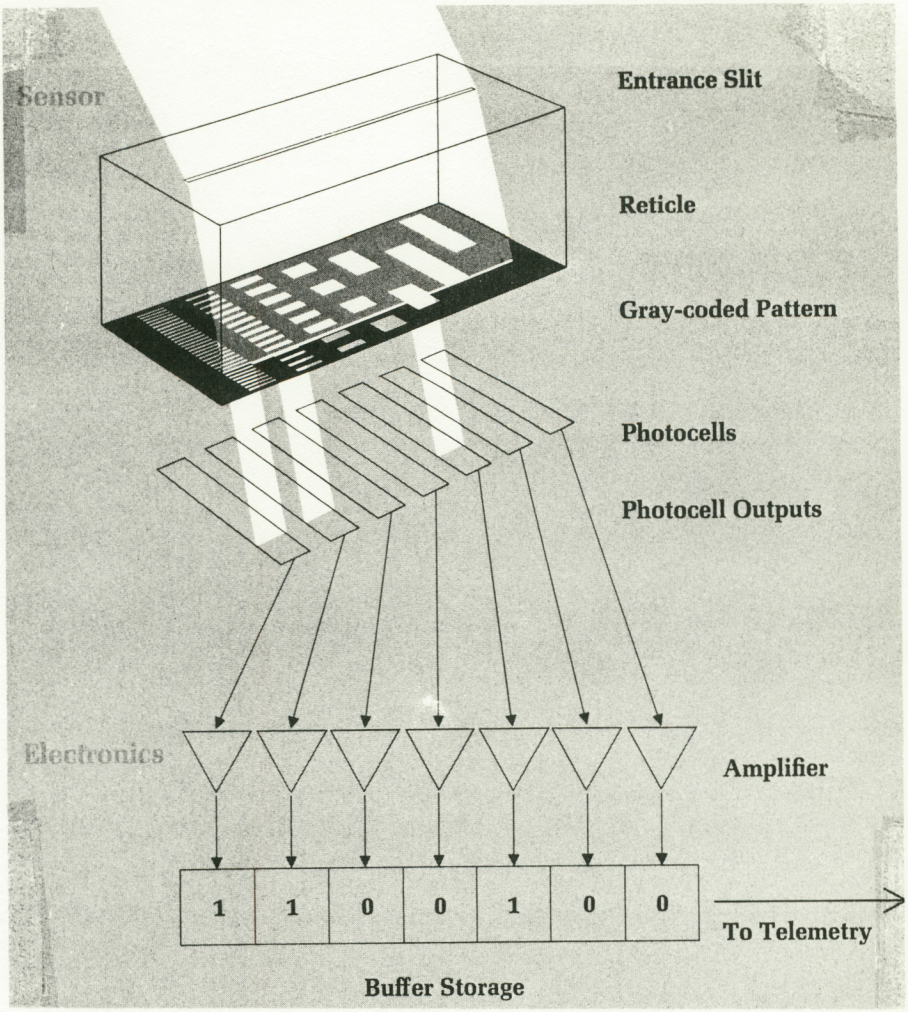

Figure 5-17. Adcole Solar Aspect Sensor Operation

On spinning vehicles, the scanning effect of the spin can be utilized. That is, the aspect systems for these spacecraft can be considered to have a fanned beam which sweeps out a large volume of space as the vehicle rotates. When the fanned beam crosses the solar disc, readout occurs. The angle of incidence measured will be the address of a particular fan segment.

The sun angle is read only when the sun is in a plane normal to the sensor slit (once per revolution). This is accomplished with a "command eye" reticle, oriented 90 degrees to the Gray-coded sensor reticle. The command reticle can be considered to have single slits on its top and bottom surfaces which lie in a plane parallel to the spin axis. These slits are mounted over a photocell, the output of which is "anded" with the signal from the photocells under the Gray-coded reticle to produce fanned beam coverage.

That the 64-degree range in aspect is adequate for solar electric Pioneer missions can be seen from Figure 5-18 which shows the relative angular position of the spin axis, sun, earth, and the optic axis of the sun aspect sensor during a representative mission. In this figure, Z_b represents the spacecraft spin axis, ⊙ identifies the sun pointing vector, ⊕ indicates the earth pointing vector and B is the solar aspect sensor optic axis. During the first 90 to 100 days the spacecraft is maintained at 45 degrees to the sunline and communication is via the omni antenna. Thus, the position of the earth is not critical. At about 90 days into the mission the spacecraft may be maneuvered to a 50-degree sun angle to bring the earth into the medium-gain pattern at an earlier time in the mission. As the position of the earth moves deeper into the conical antenna pattern, the spacecraft can be maneuvered back to the 45 degree orientation with an optimized communication link on the biconical antenna. At completion of the thrust phase (200 days) the spacecraft is maneuvered to the earth-pointing position and to a handover from the medium-gain antenna to the high-gain dish. During this maneuver, the sun aspect moves across the spacecraft spin axis causing a 180-degree shift in the time phasing of the sun pulse. Depending on the particular mission, the sun angle during the cruise portion of the mission remains within 25 degrees or so of the spin axis, well within the 64 degree range of the selected sun sensor.

5.2.3 Star Mapper Detection Capability

The capability of a star mapper sensor was analyzed in terms of its ability to discriminate pulses from the comet in a star background. As a basis for analysis, the following assumptions were made about the sensor:

a) A "V-slit" type sensor with 4-inch diameter optics. Dispersion of the lens results in a 3 arc-minute blur spot diameter. Field of view; 3 degrees.

b) Spectral response characteristics of the photo-multiplier tube are optimally matched to the spectrum of the comet.

c) Pulse threshold is adjustable and set at 80 percent of predicted brightness of the comet.

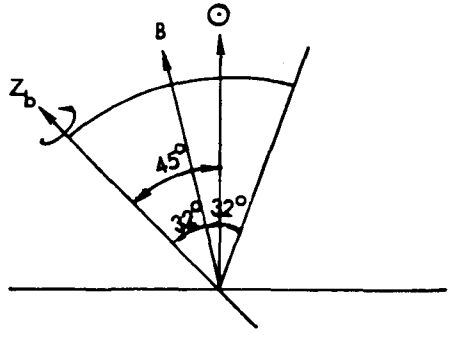

A) 0-96 DAYS. OMNI LINK - EARTH POSITION NOT CRITICAL

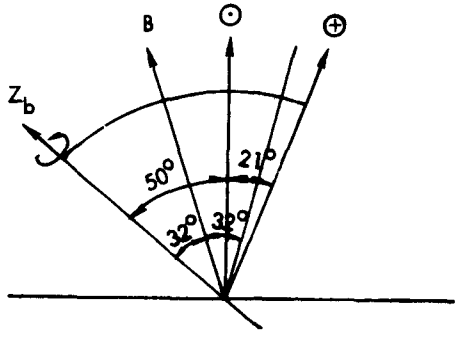

B) 96-128 DAYS. OPTIMIZE MEDIUM-GAIN LINK WITH 5-DEGREE MANEUVER

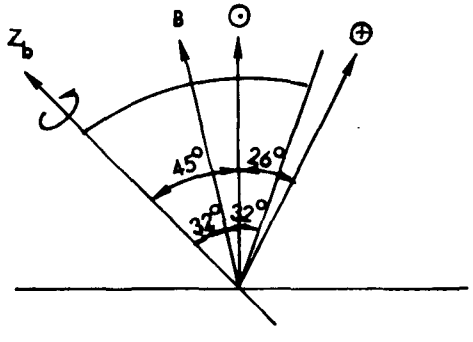

C) 128-200 DAYS. OPTIMIZE MEDIUM-GAIN LINK WITH RETURN 5-DEGREE MANEUVER

Z_b - SPIN AXIS
B - SAS NULL
⊙ - SUN
⊕ - EARTH

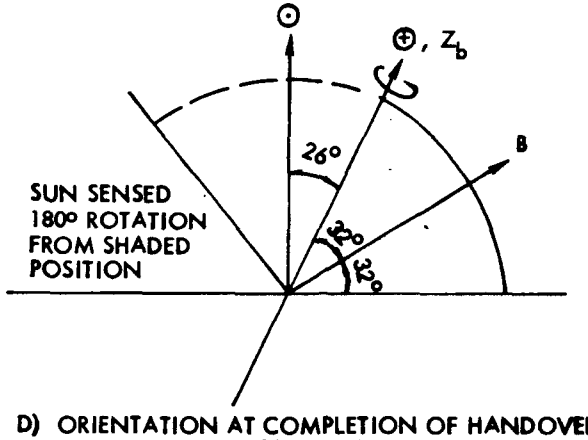

D) ORIENTATION AT COMPLETION OF HANDOVER TO HIGH-GAIN, 200 DAYS

Figure 5-18. Solar Aspect and Spacecraft Orientation Geometry

d) Downlink telemetry dedicates 16 bps to the sensor output.

e) 18-bit resolution (1 part in 260,000) which corresponds to 5 arc seconds.

With these assumptions, the probability of detection of the comet could be computed and, equally important, the probability of false alarm. A false alarm occurs when a nearby star produces a pulse that is falsely interpreted as a pulse from the comet. Figure 5-19 presents the probability of detection, P_D and the probability of false alarm, P_{FA}, versus range from probe to comet. With the pulse threshold adjusted to 80 percent of the comet brightness, the P_d asymptotically approaches 0.99. The effect of adjusting the threshold is to selectively discriminate against the background and thereby reduce the false alarm rate as the comet is approached. In actual hardware, the threshold would not be maintained at 80 percent but would be adjusted in a binary progression. The telemetered data would be selectively analyzed on the ground and the "false alarm" pulses can be removed utilizing comparison of previous data and pattern predictions. Complete simulations of the sensor output signal were not performed in the scope of this study but would be accomplished in a hardware development program.

In this study, a detailed analysis of error sources was made to determine the accuracy of a star mapper sensor and to ascertain whether it could meet mission requirements. The results of this analysis are summarized in Table 5-4. The rss errors in clock and cone angle (azimuth and elevation, respectively, in spacecraft coordinates) are 27 and 37 degrees, respectively, for a 22.5 degree conical sweep angle. This accuracy is more than adequate for the mission requirements.

5.2.4 Guidance Capability

A key consideration of the terminal guidance sensor on the electric propulsion Pioneer is the ability of the spacecraft to perform corrective maneuvers within the time interval from detection of the comet or other target by the terminal guidance sensor and the encounter or actual rendezvous. From the nominal trajectory of the Tempel II mission the distance and days to rendezvous were obtained as shown in Figure 5-20.

Table 5-4. Star Mapper Error Sources (1σ)

	ERROR SOURCE HALF-CONE ANGLE	CLOCK ANGLE ERROR (ARC SEC) 90°	CLOCK ANGLE ERROR (ARC SEC) 22.5°	CONE ANGLE ERROR (ARC SEC) 90°	CONE ANGLE ERROR (ARC SEC) 22.5°
1	RANDOM JITTER	11	18	19	31
2	SKY BACKGROUND	7	7	8	8
3	ELECTRONIC FILTER VARIATION	3	3	4	4
4	THRESHOLD CIRCUIT VARIATION	5	5	4	4
5	RETICLE GEOMETRY	3	3	3	3
6	THERMAL STABILITY	3	3	3	3
7	ALIGNMENT/CALIBRATION ERRORS	10	10	10	10
8	CLOCK STABILITY	1	1	1	1
9	OFFSET DUE TO FINITE IMAGE SIZE	15	15	15	15
	RSS	23	27	28	37

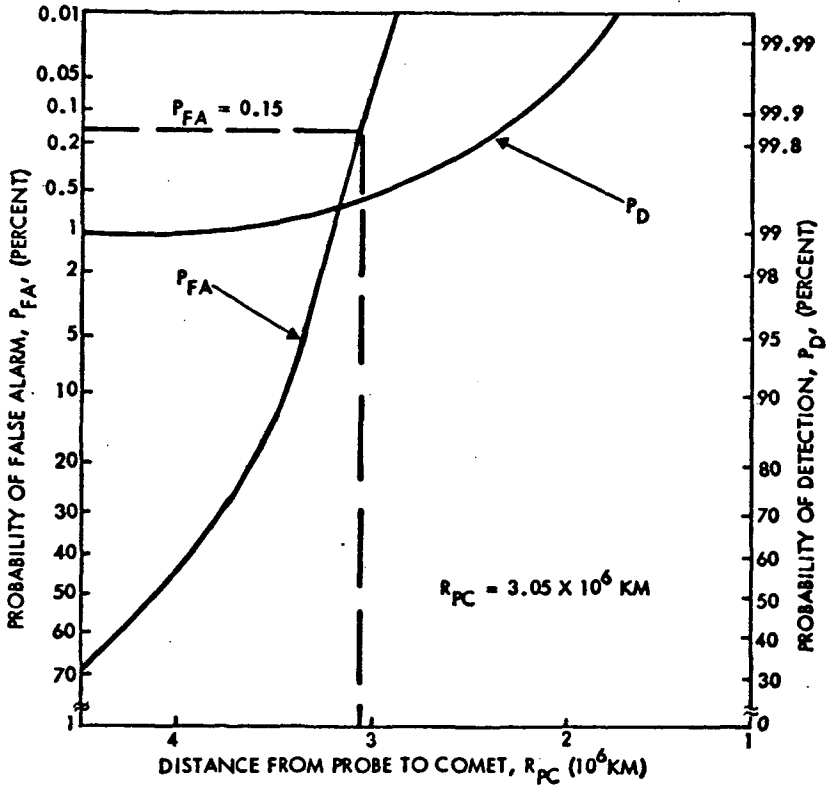

Figure 5-19. Probability of Detection and False Alarm as a Function of Range to Comet

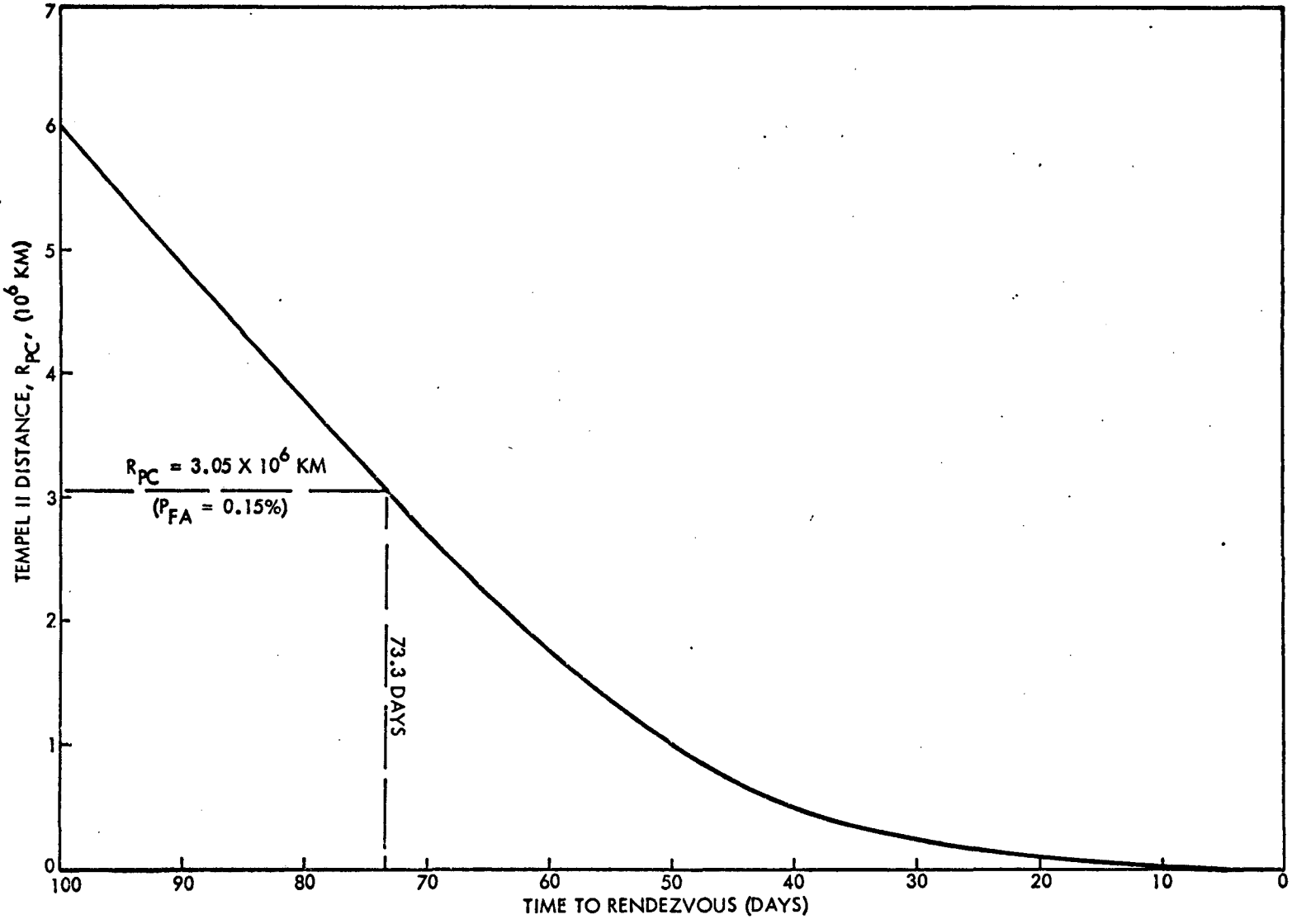

Figure 5-20. Probe/Comet Distance versus Days to Rendezvous

Detection of the comet Tempel II then occurs at a distance of about 3×10^6 km, corresponding to 73 days from encounter.

The terminal guidance is accomplished by deviating the thrust vector from its nominal position and thereby achieving an accelerating force component normal to the trajectory. The key question in the terminal guidance phase is the ability of the solar electric propulsion system to perform a corrective maneuver within the time interval from acquisition of the target until the actual encounter.

Related studies have determined that a miss distance of 30,000 km is likely based on optical telescope observation of the target objects and tracking accuracies of the spacecraft. This value is used in asteroid rendezvous studies and is the upper bound position uncertainty of the majority of asteroids. The uncertainty in comet position is at least this large due to planetary perturbations and the fact that the launch trajectory must be some 1000 days in advance of the comet rendezvous. During the last 70 days of the rendezvous mission, the average thrust level of the 5 kw configuration is 24 m/sec/day accelerating force, equivalent to 2.074×10^3 km/day^2. If the thrust vector is deivated from the nominal by an angle δ, the decelerating force component normal to the nominal thrust line is A sin δ where A is the accelerating force and magnitude. The maximum displacement in the trajectory (ΔY) that can be achieved with an angle of deviation δ, thrusting for a period T is

$$\Delta Y = \frac{AT^2 \sin \delta}{2}$$

This displacement, as a function of δ for a 70-day thrust, is shown in Figure 5-21. With a 3-degree change in thrust direction, a corrective displacement of 2.7×10^5 km could be achieved. This is well in excess of anticipated miss distance, providing a reserve capability of the terminal guidance.

It can be concluded then, that a star mapper with fifth magnitude detection capability provides more than adequate terminal guidance maneuvering capability for rendezvous with the comet Tempel II.

The analysis above of a star mapper capability was based on 4-inch optics. The sensor has had some preliminary design work but has not

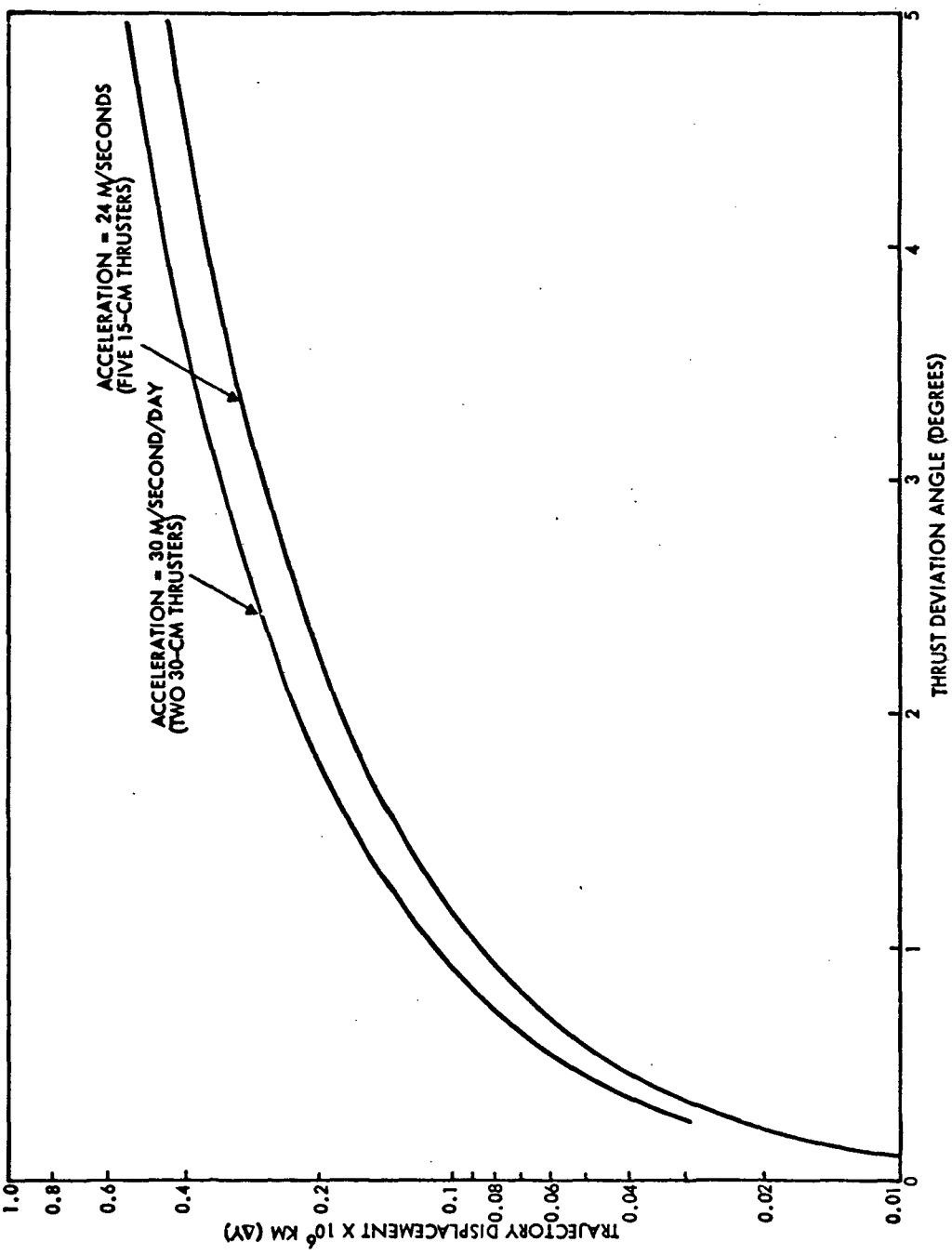

Figure 5-21. Tempel II Rendezvous Trajectory Displacement Capability versus Thrust Deviation Angle for the 70-Day Thrust Period

been developed to the prototype hardware stage. A star mapper which has been developed and flight proven is shown in Figure 5-22 with its basic specifications. Present units have a sensitivity of nearly fourth magnitude. This sensor would detect the comet head about 45 days before rendezvous, still adequate for terminal guidance maneuvers.

5.2.5 Conclusions

Satisfactory attitude determination and control can be provided for the missions evaluated using a sun aspect sensor with the present Pioneer F and G stellar reference assembly. Where terminal guidance is required, as in the case of a comet rendezvous, a star mapper makes possible the intercept and rendezvous. This star mapper also accomplishes the attitude control function and therefore makes the sun aspect sensor and stellar reference assembly unnecessary. In summary:

- For all missions, addition of spinner type solar aspect sensor is required to measure angle between spin axis and sunline.
- For Jupiter swingby mission, requirement for stellar reference assembly is dependent on payload requirements.
- Solar pressure attitude drifts are minimal precluding need to measure angle between spin axis and ecliptic plane unless otherwise required.
- For comet rendezvous and asteroid flyby mission, stellar reference assembly replaced by V-slit mapper terminal guidance sensor.
- With good probability of detection and tolerable false alarm rate, comet (Tempel II) angular position determined approximately 3×10^6 km before rendezvous.
- At 3×10^6 km distance, 3×10^4 km cross range error correctable with small angular offset (~2 degrees) of thrust vector.

5.3 ELECTRICAL POWER SUBSYSTEM

General requirements on the electrical power subsystem design include:

- Utilize a lightweight, flexible rollout solar array as the primary source of power.

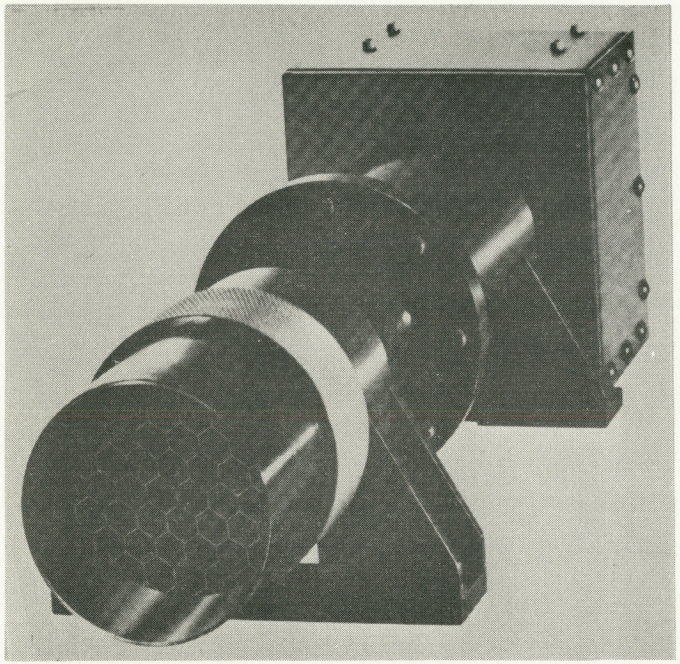

SPECIFICATIONS:

SENSITIVITY	THIRD MAGNITUDE OR BETTER
FIELD OF VIEW	20 DEGREES
RESOLUTION	BETTER THAN 1 ARC MINUTE
POWER REQUIRED	1.5 WATTS AT +28 VDC
WEIGHT	2.6 POUNDS
SIZE	10.62 X 3.75 X 3.31 INCHES
OUTPUT SIGNALS	0 TO 5 VDC
OUTPUT IMPEDANCE	5K OHMS

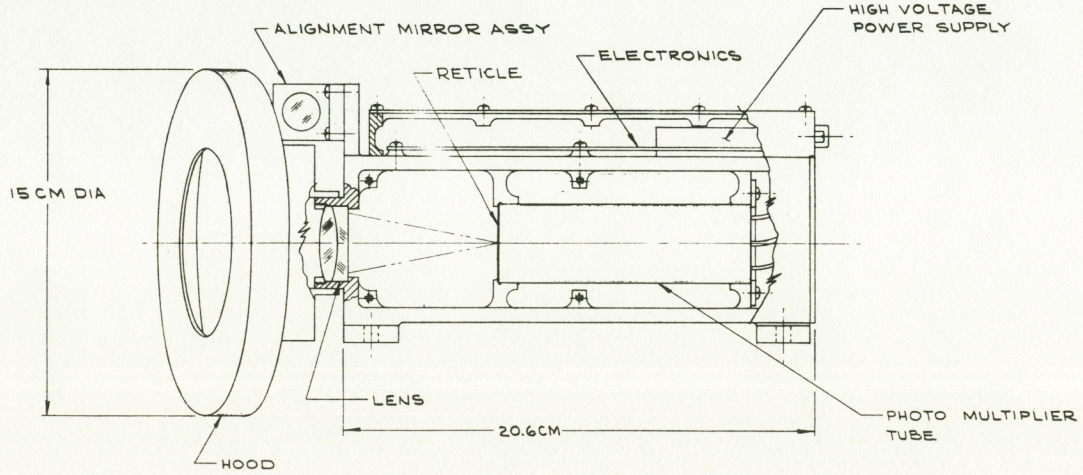

Figure 5-22. Flight-Proven Star Mapper

- Utilize existing Pioneer F and G units to a maximum extent.
- Retain present F and G bus-voltages for experiments and subsystems.
- Utilize prototype thruster power processor characteristics in solar array interface design.
- Minimize costs.
- Minimize weight.

In this report the solar array design criteria will be presented followed by the subsystem design and power budgets. The centrifugally deployed solar array design will be presented along with a modification of an existing design by General Electric.

Critical phases of the mission are predeployment when the spacecraft is operating on battery and the thrust phase when the ion thrusters are throttled to utilize all available power.

5.3.1 Solar Array Design Criteria

The output power profile as a function of solar distance from the solar array was generated by JPL and was supplied to TRW in December 1970 as an input to a previous electric propulsion study. A log-log plot of that function is presented in Figure 5-23 in terms of relative power at 1 AU distance. For this curve to be applicable to the spinning solar electric spacecraft, three additional factors must be considered:

1) Reduced solar intensity due to 45-degree angle of incidence.
2) Reduced operating temperature due to lower angle of solar incidence.
3) Degradation due to energetic electron and proton irradiation.

The reduction in solar intensity per unit area of the solar array is simply the cosine factor of 0.707 for the 45-degree orientation. This factor is used only during the thrust phase of the mission after which the spacecraft is oriented to an earth-pointing position. Consequently the solar incidence angle is less and is time variant.

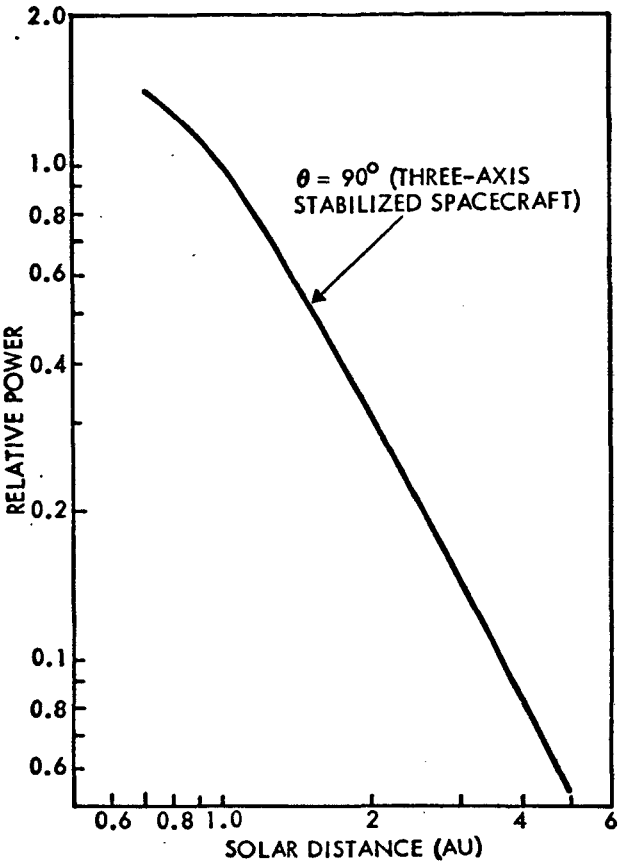

Figure 5-23. Relative Solar Array Power Available versus Solar Distance for 90-degree Solar Incidence Angle

The reduction in operating temperature that results from the off 90-degree incidence angle increases the operating voltage of the array and thereby increases the output power. Figure 5-24 presents a log-log plot of the predicted operating temperature for the array at 90 degrees and 45-degree array operates 30 degrees cooler at 1 AU and 20 degrees cooler at 2 AU. The effects of this cooler temperature on the open circuit voltage (V_{oc}) and maximum power voltage (V_{mp}) is seen in Figure 5-25. The maximum power voltage is 80 percent of the open circuit voltage. This is valid throughout the range of interest, however it falls lower than 80 percent at very high and low illumination levels.

A composite plot of the available power from the solar array is shown in Figure 5-26 for both the 45-degree and 90-degree orientation. The third factor of radiation degradation must be considered to arrive at a final value for available power.

A ten percent degradation in solar array power capability due to solar flare exposure is allowed for in the solar array sizing. This magnitude has been used previously by JPL and is a conservative value and incorporates degradation due to solar flare activity and the decreased cell efficiency at low illumination and temperature conditions.

The desired output voltage from the solar array bus has a direct bearing on the number and arrangement of solar cells on the deployable solar array. The power processor is designed for an input voltage range of 100 to 200 volts. The minimum voltage per solar cell (n on p silicon)

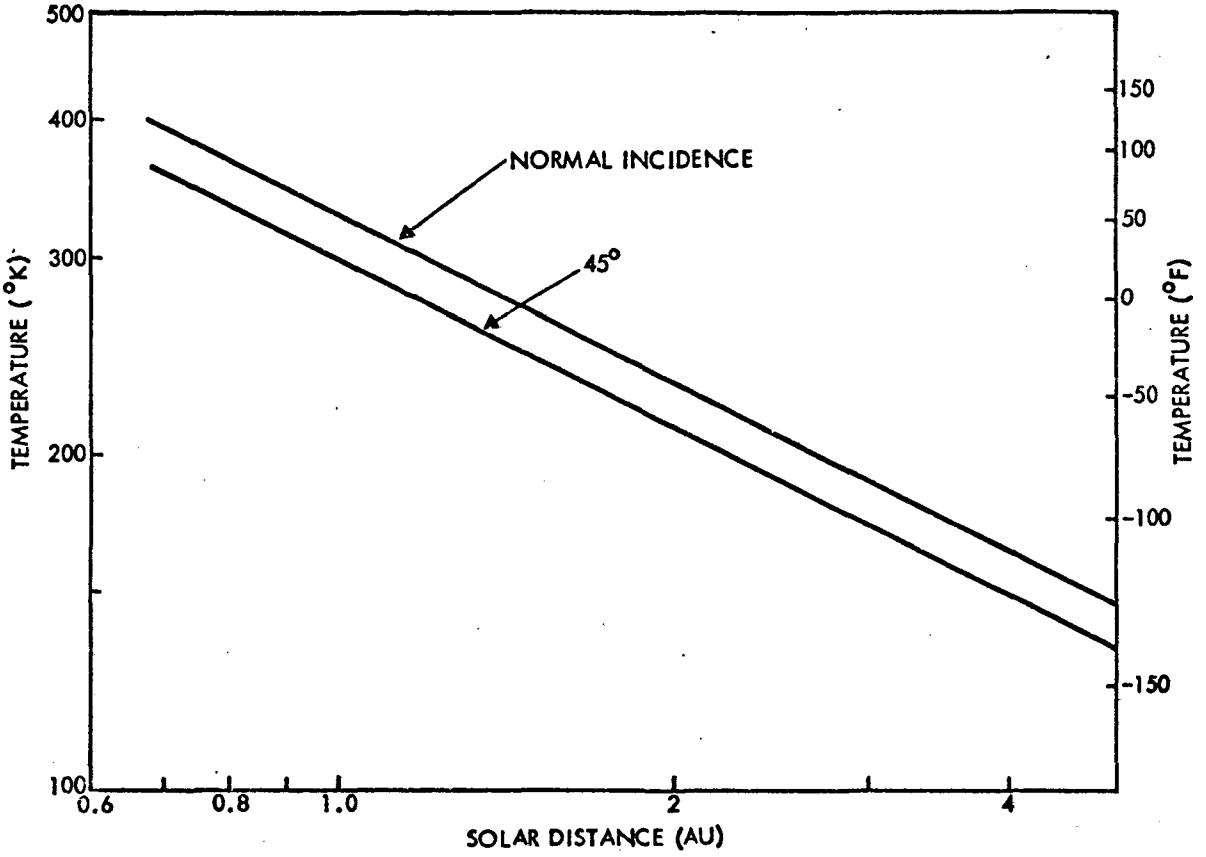

Figure 5-24. Solar Array Operating Temperature versus Heliocentric Distance for Normal and 45-Degree Incidence

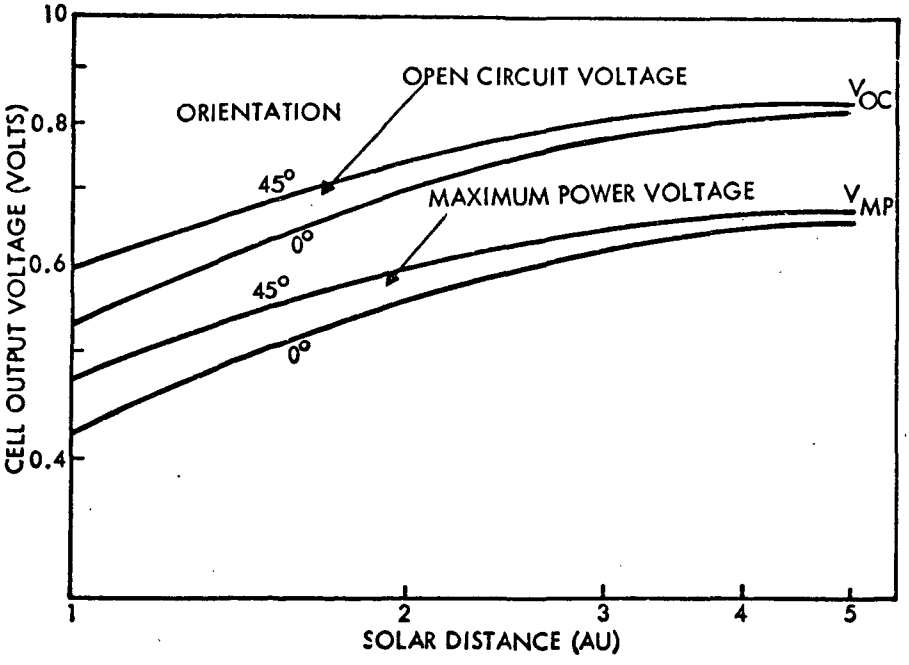

Figure 5-25. Solar Cell Open Current Voltage (V_{oc}) and Maximum Power

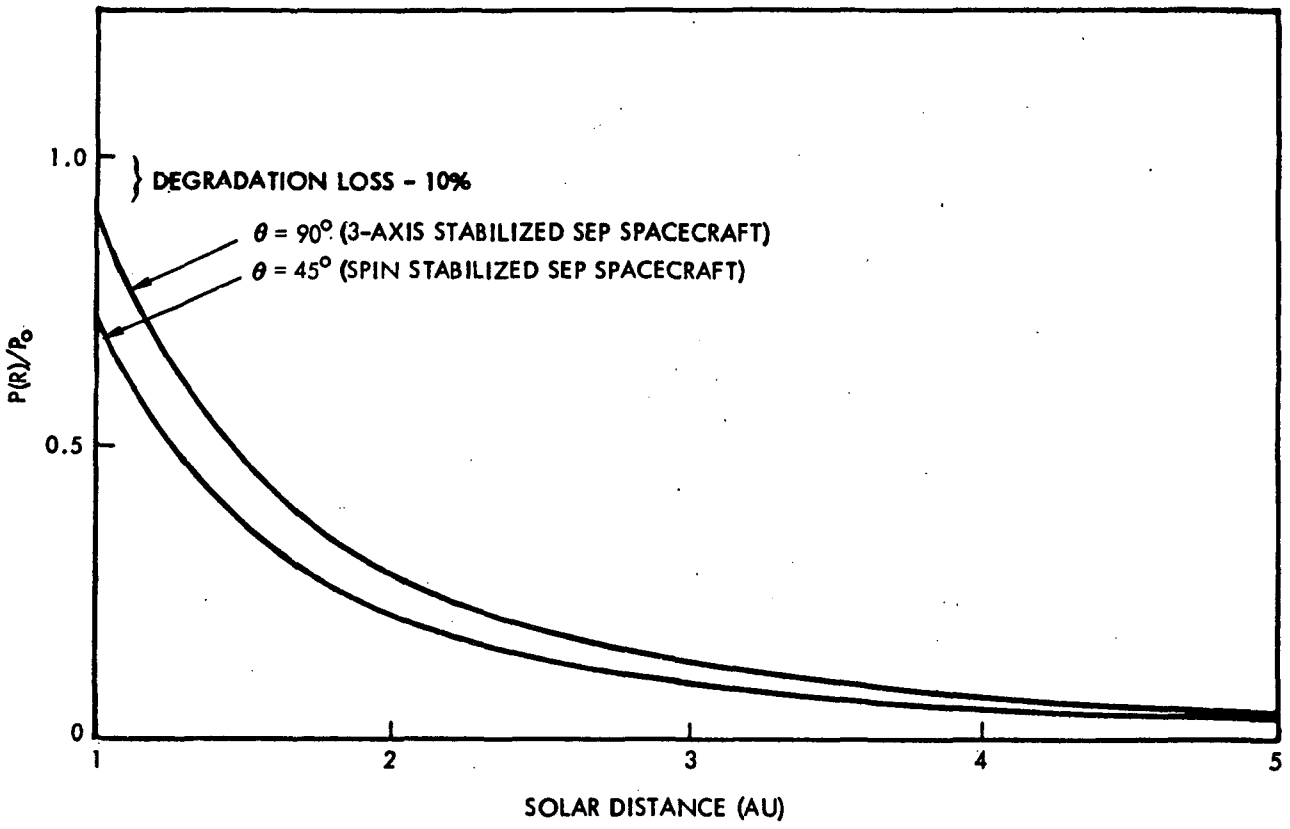

Figure 5-26. Relative Solar Array Power Available from Three-Axis and Spin-Stabilized Spacecraft

is the maximum power point of 0.42 volts when the spacecraft is normal to the sun at 1 AU (although this orientation is not in the mission profile, allowance must be made for this temperature condition at 1 AU). The maximum bus voltage is the open circuit voltage at 5 AU of 0.825 volts The approximate number of solar cells in a series string necessary to achieve 100 volts is $100/0.42 \simeq 238$. This number is rounded to 240 which is more factorable to accommodate various geometric arrangements on the solar cell substrate. The 240 cells times the maximum cell voltage of 0.825 volt is less than 200 volts, thus the maximum voltage of the processor is not exceeded.

The solar array can be readily sized by computing the solar array peak design power required for each watt of conditional power consumed. Table 5-5 presents this computation.

The design factor of 1.525 is used to size the solar array by multiplying the total conditional (PPU output) power to obtain the peak design

power on the solar array at standard conditions (140 mW/cm^2 at 28°C). Thus each watt of conditional power requires 1.525 watts of solar array design power at standard conditions (i.e., normal incidence at 1 AU).

Table 5-5. Compensation Factors for Solar Array Design

	Factor	Product
Power conditioner output	Unity	1.00
Power conditioner loss compensation	1.10	1.10
Compensation factor for 10 percent degradation	1.10	1.21
Temperature compensation for 45-degree orientation	0.893	1.08
Compensation for illumination at 45-degree incidence	1.414	1.525
Design factor for 45-degree solar array orientation		1.525

Figure 5-27 presents a block diagram of the electrical power subsystem. This configuration represents the simplest approach to the power subsystem design. Compared to the Pioneer F/G configuration, the following changes are noted.

- RTG's are replaced by the solar arrays as the primary power source
- The two inverter assemblies are removed
- The power conditioner unit is modified to accept the 100-200 Vdc solar array bus
- The shunt radiators are removed
- A modified inverter assembly is added to convert the 28 Vdc PCU output to 61 Vrms for input to the central transformer rectifier filter

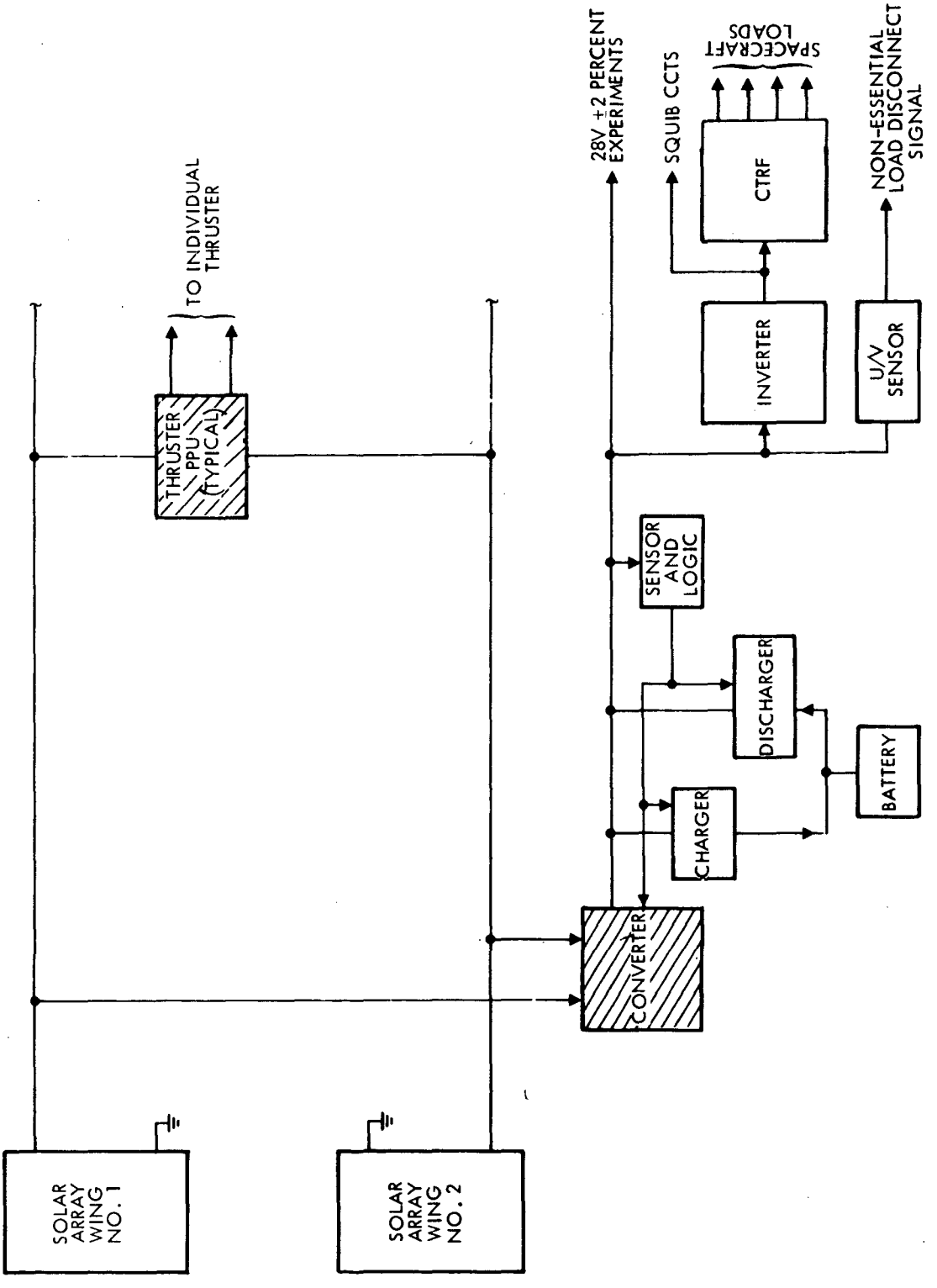

Figure 5-27. Pioneer Electric Propulsion Block Diagram (with Battery)

The power system design is composed of a solar array which generates primary energy, a converter which regulates array power, an inverter, central transformer rectifier filter (CTRF), and a power control unit. The inverter generates ac power to fire squibs and to energize the central transformer rectifier filter assembly which provides conditioned and regulated voltage to individual spacecraft loads and fault limitation and isolation provisions to meet long-life, high-reliability requirements. This is identical to the existing Pioneer F and G system except for the solar array converter.

The solar array may be either of two versions. The General Electric rollout array developed for NASA is the prime selection because of its stage of development, the TRW centrifugally deployed array designed under this contract is approximately 40 pounds lighter than the GE array. Solar arrays are discussed in considerably more detail at the end of this section.

The converter provides conditioning of solar array voltage to 28 volts (as required for the main bus) and uses the same design as the thruster converters except for the following minor changes:

- The power output is sized to match the full load maximum power level of the 28-volt bus
- The output is at the 28-volt bus level only (not multiple voltage outputs)
- The output current is controlled in response to an input signal voltage to meet bus voltage regulation requirements.

The battery is a silver cadmium type and is included to provide support for transient loads in excess of converter rating and to provide power prior to array deployment and orientation. The battery consists of eight 5-AH cells connected in series with each cell protected against excessive overcharge or discharge by electronic bypass circuitry. The battery is identical with the Pioneer F and G battery. Physical characteristics of the battery are shown in Table 5-6.

Table 5-6. Battery Characteristics

Elements	Characteristics
Number of cells	8
Capacity (rated)	5 AH
Nominal voltage	8.2 volts at 70°F
Nominal voltage	6.4 volts at 30°F
Weight (including cell protection)	5.2 pounds
Size	10.0 x 8.2 x 2.7 inches

The battery has an actual energy at launch of 48-watt/hours but must be conditioned for use at the regulated main bus. Pioneer F and G ripple, transient, load sharing, and standby loss requirements resulted in a PCU discharge efficiency of 50 percent. Battery energy available at the bus during the launch phase is therefore 24 watt-hours.

Battery capacity degrades with mission time and with cyclic usage. The present Pioneer battery is conservatively estimated for 900 days at 50 percent capacity.

Because of limited experience and test data this battery performance is now difficult to analyze and predict. It is anticipated that following Pioneer F and G experience less degradation can be assumed. The greatest confidence in meeting this performance is provided by maintaining battery temperatures in the range of 20°F to 30°F throughout the duration of the mission.

The power control unit is identical with the Pioneer F and G unit except for the deletion of rectifying diodes and filter components that were required for the Pioneer F and G system configuration.

The inverter assembly converts regulated 28V±2 percent bus power into ac power for the central transformer rectifier filter (CTRF) assembly and for squib firing circuits in the command distribution unit. It contains

two individual inverters, each of which can supply the required lower power. Fault sensing and isolation switching provisions are included. The unit is identical with the Pioneer F and G unit except that the input voltage change from 4. 1 vdc to 28 vdc requires a small design change. All fault isolation and telemetry circuitry are unaffected.

The CTRF assembly generates the several regulated voltages required by each of the subsystems. Since the loads on the CTRF are the Pioneer F and G loads the CTRF is identical with the Pioneer F and G unit. All individual voltage regulator/current limiter circuits, fault protection/load control switching, and redundancy functions remain unchanged.

The solar array performance curves include power degradation as a result of increasing solar distance and increasing cell efficiency with decreasing illumination. Array performance is evaluated for normal sun illumination and resultant thermal effects. It is then modified downward by the cosine of 45 degrees to account for average thrust vector pointing losses. This decreased illumination also decreases panel temperature from the normal sun condition resulting in an increase in the array output voltage at any given current. Variable thrust operation (throttling) of the thrusters is controlled from the ground such that the intersection of the solar array and thruster I-V curves is at, or near, the array maximum power voltage shown in Figure 5-28. This allows utilization of the array power increase caused by the lower temperature of the solar off-axis incidence angle.

Maximum possible use has been made of existing Pioneer F and G equipment and thus hardware design, analysis, test and cost are minimized while satisfying the requirements. The use of the newly designed thruster converter (modified to accept an input from the maximum power point sensor) minimizes power processing equipment design and costs while meeting the requirement of mating with either of the two-array configurations and being compatible with the several mission profiles and array voltages. Use of Pioneer equipment technology meets the magnetic cleanliness requirement.

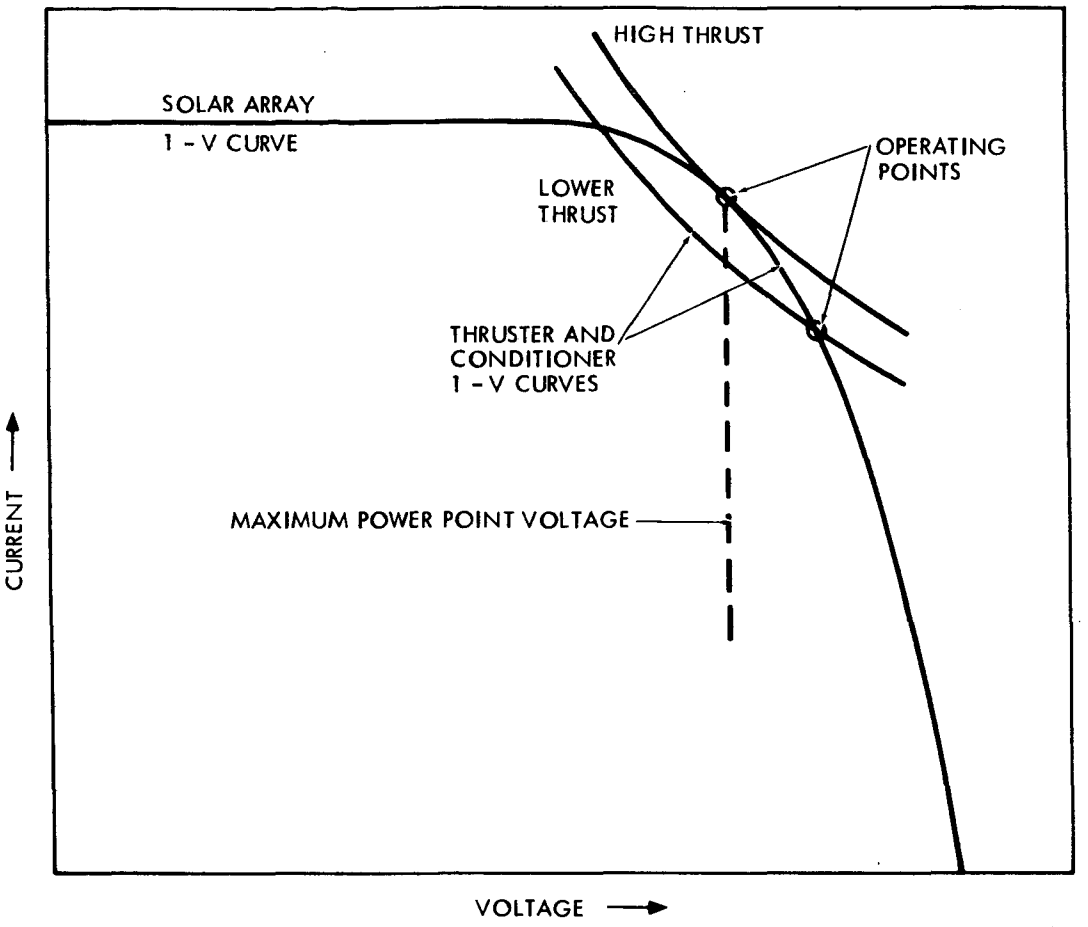

Figure 5-28. Solar Array I-V Curve

A nickel cadmium battery was considered due to the improved knowledge of its life characteristics but the magnetic criteria requires compensation equipment and weight that is unacceptable. In addition, the Pioneer F and G program should prove life and performance data for this unit which will further justify acceptability.

During the study other configurations (1 to 30 AU missions) were devised to allow the use of RTG's as a source of prime power or in parallel with the array. Figure 5-29 shows such a system. This system also uses many of the Pioneer F and G components and makes use of a converter to process high-voltage array power to a level consistent with the electrical parameters of the main bus. This converter then replaces the Pioneer F and G battery functions of transient support and load sharing if RTG degradation is in excess of anticipated values. All other equipment remains as in the Pioneer F and G program except the power control unit which has its battery charger function deleted.

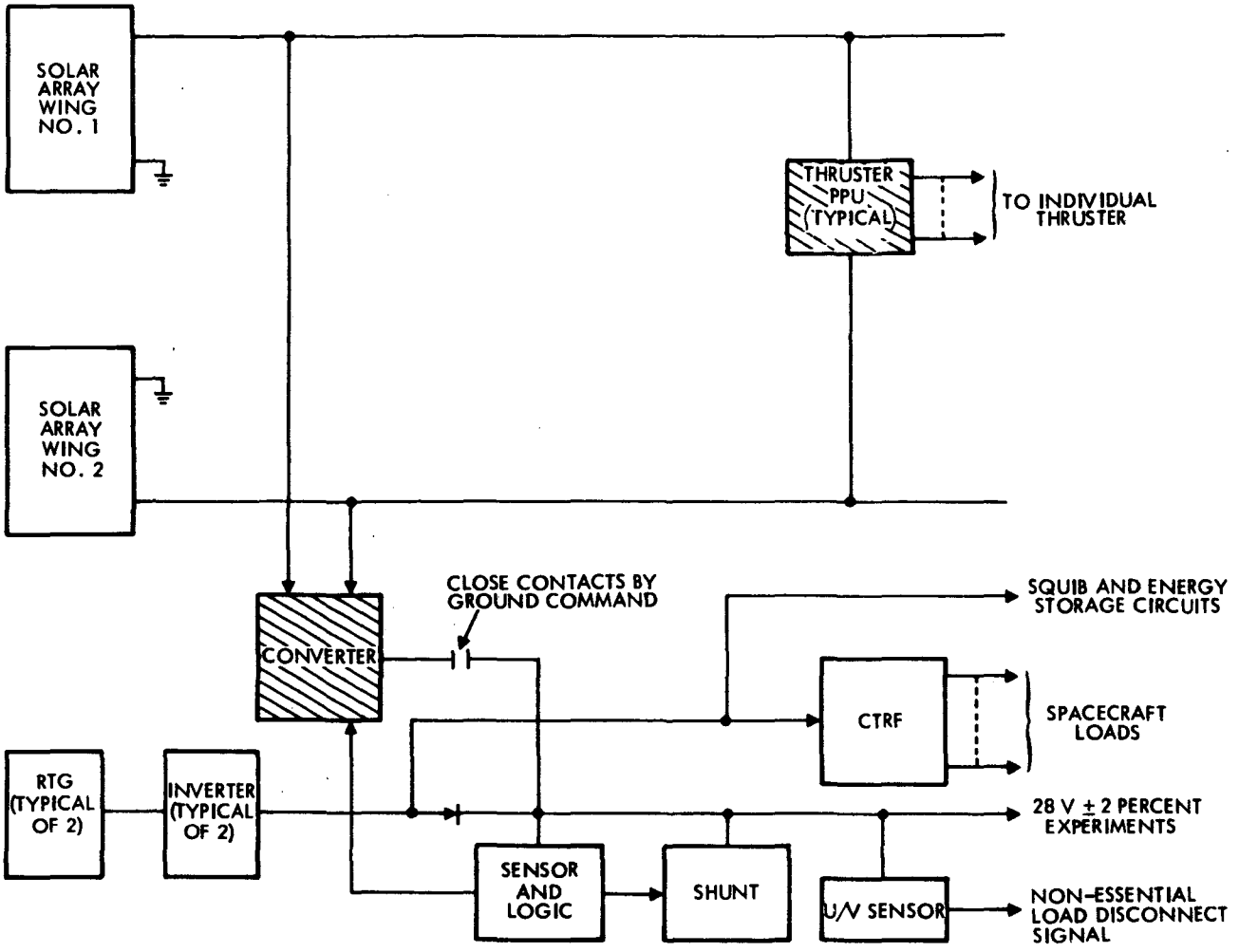

Figure 5-29. Solar Array/RTG Power Subsystem

A summary of the spacecraft power requirements is given in Table 5-7. This summary is based on the subsystem diagram of Figure 5-27 and the solar array curve of Figure 5-28. During the thrust phase of the mission, the spacecraft requires 103.4 watts of power from the solar array. Using the design factor of 1.525 obtained earlier the solar array must be sized 158 watts larger than that required for the electric propulsion system.

The configuration with two 30-cm ion thrusters requires 5718 watts to operate the electric propulsion system, plus 103 watts for the spacecraft. The solar array is sized to 1.525 (5718 + 103) = 8877 watts. The five 15-cm thruster configuration requires 1.525 (3770 + 103) = 5906 watts. Present state of the art in deployable solar arrays produces a nominal

Table 5-7. Power Requirements Summary
(8 kw Three 30-cm Engines, No RTG's)

	Predeployment	Thrust	Cruise	Encounter (Commanding)
Data Handling				
DTU	3.725	3.725	3.725	
DSU	0.425	0.425	0.592	1.163
DDU (2)	0.290	0.290	0.290	1.264
Attitude Sensing/Control				
CEA	2.210	0.910	0.910	2.685
SAS (2)	0.500	0.500	0.500	0.500
*SMA	0.0	0.0	1.500	1.500
Propulsion				
Transducers	0.238	0.238	0.238	0.238
Heaters	2.0	2.0	2.0	2.0
ACS	0.454	0.269	0.269	0.454
Command and Distribution				
CDU	0.215	0.215	0.215	0.215
Communications				
Receivers (2)	3.400	3.4	3.4	3.4
Drivers (2)	1.352	1.352	1.352	1.352
TWTA (8 W)	27.8	0	27.8	27.8
TWTA (24 W)	0.0	67.2	0	0
Conscan	0.0	0	0	1.2
Electrical Power				
Inverter loss	3.10	3.10	10.33	11.15
CTRF loss	8.58	8.58	8.58	9.86
PCU loss	5.5	10.5	7.23	7.30
Cable loss (spacecraft)	0.6	0.6	0.6	0.6
Cable loss (solar array)	0.0			
Battery electronics	0.1	0.1	0.1	0.1
Spacecraft total		103.41		
Electric Propulsion				
PPU losses	0.0	514	0	0
Thruster power	0.0	5204	0	0
		5718		
Experiments				
F/G complement	0	0	24.0	24.0

*On rendezvous missions only

10 watts per square foot of active solar array area. Thus the active areas of solar arrays must be 880 and 590 square feet respectively for the two 30-cm and five 15-cm thruster configurations.

At completion of the thrust phase the spacecraft is oriented to an earth pointing position and the solar array is approximately normal to the

sun line. On the Jupiter flyby out-of-ecliptic mission, the power available at maximum solar distance is 4.9 percent of the initial design power or 290 watts for the five 15-cm thruster configuration.

This provides ample power for the spacecraft at maximum solar distance. The outer planet missions to Uranus and beyond utilize the RTG's and existing Pioneer F/G power subsystem beyond the thrust phase, thus no consideration is given to solar array performance beyond 5 AU.

As previously mentioned, a preliminary design of a centrifugally deployed solar array was accomplished during the study. The goal of this new solar array design was to achieve a significant savings in weight by using centrifugal force to deploy the array rather than a powered boom for deployment.

The design consists of a mylar sheet containing solar cells and substrate wrapped on a cylindrical drum. The array is released on command and allowed to deploy outward under the control of restraint cables. This concept has the desirable feature of being extremely lightweight since the structural requirements are minimal. The deployment control device can be a lightweight pair of cables with a simple governor control. The initial concept consists of the drum with the array, a strongback beam with releasable end fittings to grasp the drum, and a deployment control device to limit the rate of deployment. One method of deployment control considered was to pass a pair of belts which are anchored at one end over the drum and allow the belts to pay out under the control of an escapement mechanism or centrifugal governor. This approach was abandoned for two reasons:

1) The restraining belts would have to be jettisoned after completion of deployment, requiring pyrotechnic cutters and the risk of the jettisoned belts getting fouled on the solar array.

2) The force of the belts against the array could be great enough to displace cracked, or break solar cells.

A design which avoids these problems and which enables the deployment to be controlled is shown in Figure 5-30. This design features the cylindrical drum wrapped with the solar array and held by two end

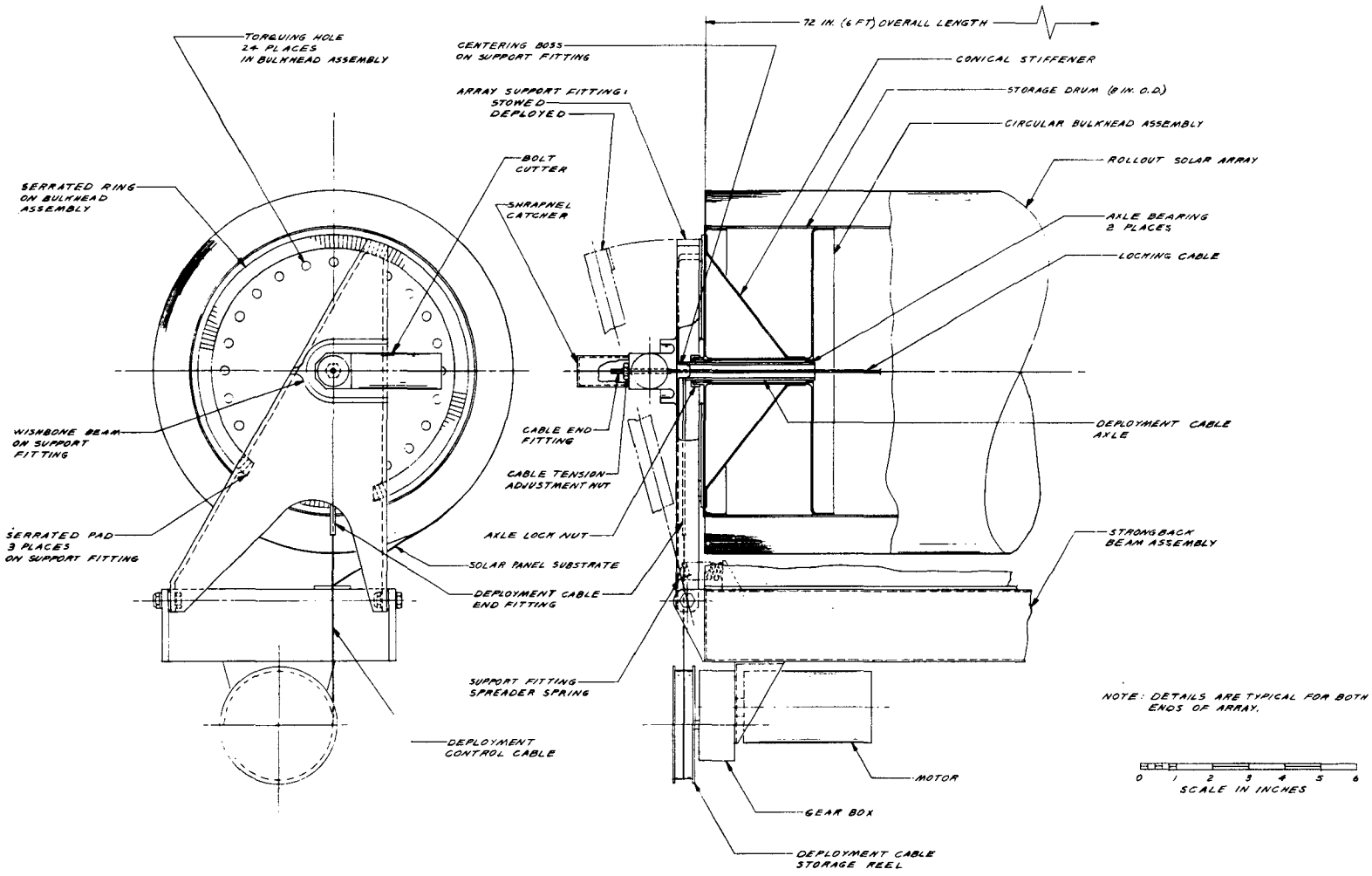

Figure 5-30. TRW Centrifugal Deployment Solar Array

fittings with a cable passing through the axle of the cylinder. The end fittings are attached on pivots to the strongback beam which in turn provides a means for attachment to the spacecraft. The drum is held to the end fittings by the axial cable held in tension through the drum axle. The drum is released for deployment by cutting this cable at each end thereby allowing the end fittings to spring outward from the drum ends. The drum is restrained from free deployment by two deployment control cables attached at each end of the drum axle. The deployment control cables are payed out by a constant speed spool whose rate is controlled by a small motor and gear train. Alternative methods of speed control were considered, including electrical pulse driven escapement mechanism similar to a clock escapement with a solenoid driver for synchronous deployment, or a centrifugal governor similar to the speed control on a telephone dial or mechanical phonograph. Centrifugal governors can control speed of rotation to within 3 to 5 percent and would be the simplest approach.

The dynamics analysis subsequently revealed the requirement that the solar array be stiffened, at least on the inboard section. To solve this problem, stiffening tubes were added as shown in Figure 5-31.

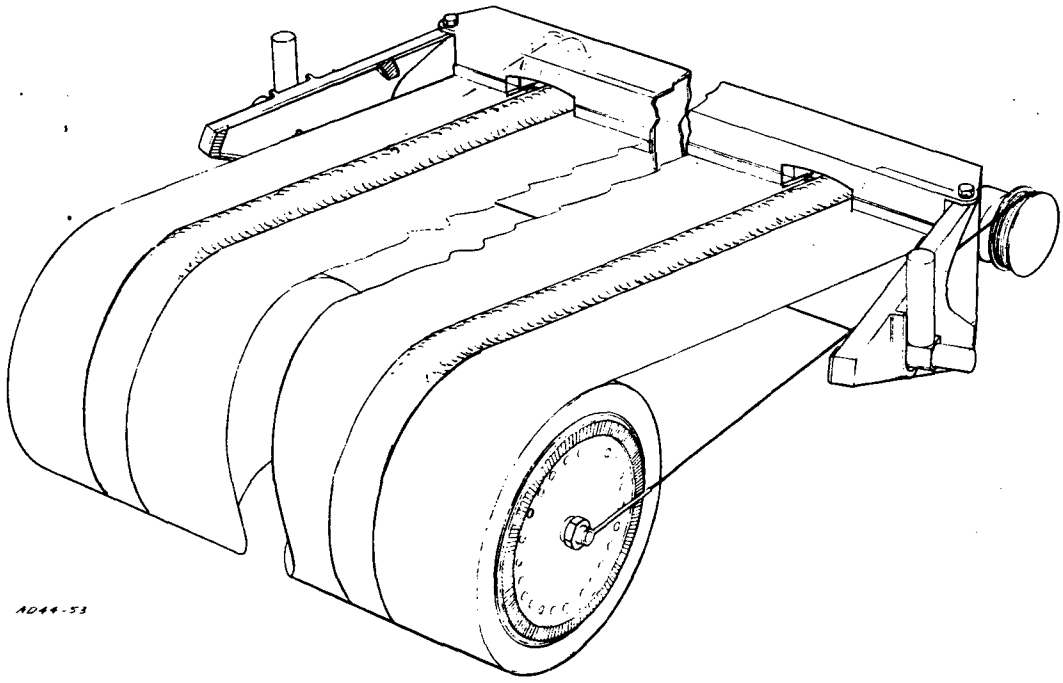

Figure 5-31. TRW Centrifugally Deployed Solar Array Concept

The stiffeners consist of two halves of pre-formed beryllium-copper strip, each strip shaped in cross section approximately like a Gausian curve and bonded together to form a hallow tube. The tube can be flattened easily and rolled onto the drum. The ends of the stiffeners are attached to the strongback beam by means of a hinge and damper. This allows the array to flex at the attachment point with damped motion.

As the design effort for the centrifugally deployed array progressed to more detail and the dynamics analysis imposed more requirements for stiffened solar arrays with damped hinge points, the centrifugally deployed array became less attractive:

a) The requirement for stiffening and hinge dampers defeated some of the weight advantage.

b) Stiffening of only the inboard section of the array created the problem of mating the outboard ends of the stiffeners with the solar array substrate while retaining a thin cover section that can be wrapped on the drum.

c) Testing the centrigugally deployed array under a realistic simulation of actual conditions on the ground appeared to be a formidable problem.

Because of these problem areas and a careful review of the design developed by General Electric it was decided that the GE design would be the most cost effective approach to the solar array problem. A sketch of the GE design is shown in Figure 5-32. This design features a bi-stem motor-powered boom to deploy the array from a fixed drum. The principal difference in the two designs is that the GE design, with a fixed rotating drum, must use slip ring contacts to transfer electrical power from the rotating drum to the spacecraft. A weight comparison (see Table 4-8 shows approximately a 40-pound difference in total weight for the two assemblies. In view of the testing problems of the TRW design, this weight penalty will probably have to be sacrificed to avoid extensive development costs of the centrifugally deployed design.

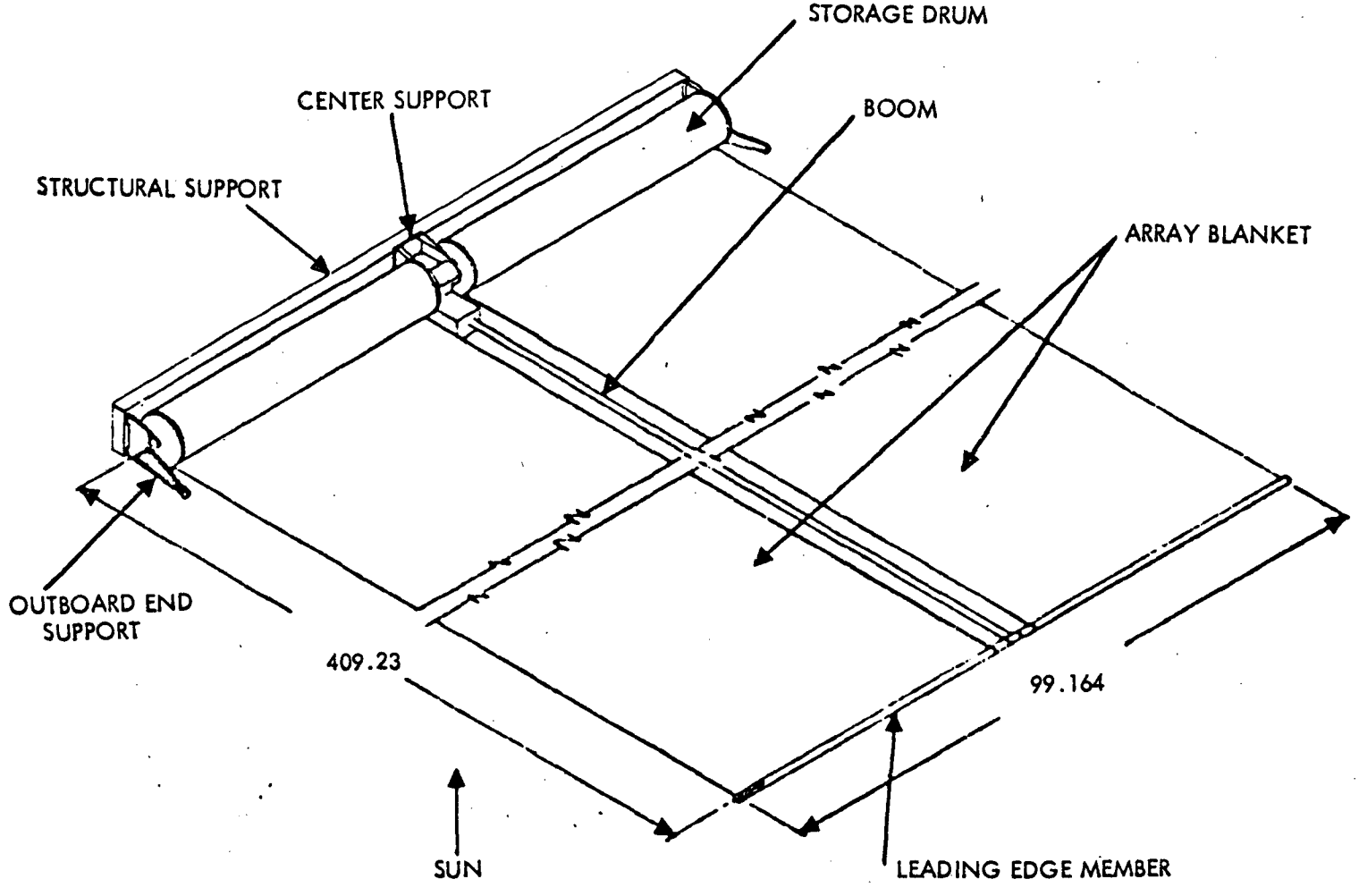

Figure 5-32. GE Boom Deployed Prototype Design

APPENDIX A

ELECTRIC PROPULSION THRUSTER RELIABILITY

1. FAILURE RATE OF ELECTRIC PROPULSION ENGINES

The electric propulsion engines now being developed have not accumulated sufficient historical data by which to establish an operational failure rate. Therefore, we have established a failure rate by considering the manufacturing, electrical and thermal similarities between electric engines and high-level travelling wave tubes (TWT's), the latter of which have known failure rates ($\lambda = 3025 \times 10^{-9}$/hour.

Table A-1 gives the approximate historical proportions of TWT failure attributable to each of their various failure modes and also allocates the TWT failure rate to each mode. Table A-2 identifies design factors relating to each physical element and intangible characteristic of the TWT and the electric engines, and assigns a failure rate factor to each, relating the relative sensitivity of the devices' design. From this exercise, the random failure rate of the electric engine is estimated at $\lambda = 5900 \times 10^{-9}$. Engine wear occurs at 400 days.

Table A-1. Allocation of the Failure Rate of a High-Level Travelling Wave Tube ($\lambda = 3025 \times 10^{-9}$/hour, exclusive of Power Supply) to its Contributing Failure Modes.

Failure Modes	Percent of 3025×10^{-9} Failure Rate Allocated To Each Failure Mode	Failure Rate
Heater - Related	20	605
Cathode - Related	30	907
Helix (Geometry) - Related	20	605
Vacuum Related	25	756
Plate Related	5	151

Table A-2. Impact of TWT and Thruster Design Factors on Failure Rate

Factor	Impact on TWT	Impact on Thruster	Relative Severity On Thruster Versus TWT	Thruster Failure Rate Impact	Cumulative Failure Rate
HEATERS - Baseline λ				λ = 605	
Number (Cathode)	One	Two	More	2.0 x	
Temperature	Lower	Higher	More	1.1 x	
Rigidity and Construction	Sleeve inserted	Firmly wrapped on cathode	Less	0.75 x	
Thermal Cycling	Few cycles	~10 cycles	More	1.25 x	
Net				2.06 x	1250
Number (Vaporizer)	One	Four	More	4.0 x	
Temperature	Higher	Lower	Less	0.75 x	
Rigidity and Construction	Sleeve inserted	Firmly wrapped on cathode	Less	0.75	
Thermal Cycling	Few cycles	~10 cycles	More	1.25	
Net				2.11	1700
CATHODE - Baseline λ				λ = 907	
Number	One	Two	More	2.0 x	
Temperature	700°C	1000°C	More	1.25 x	
Current Density			Lower	0.6 x	

Table A-2. Impact of TWT and Thruster Design Factors on Failure Rate - Continued

Factor	Impact on TWT	Impact on Thruster	Relative Severity On Thruster Versus TWT	Thruster Failure Rate Impact	Cumulative Failure Rate
Emissivity Requirements			Lower	0.5 x	
Net				.75	680
GEOMETRY - Baseline λ				λ = 605	
Helix or Electrode Alignment	Very sensitive, for any interception of the beam by the helix causes burnout.	Sensitive, for build-up of debries between electrodes can cause shorting-particularly after a long operational time.	Slightly Less	0.9 x	
Rigidity and Manufacturability	Fine wires; high geometrical precision required, not supported entirely around periphery.	Sturdier material; geometry less critical during most of life; well supported around periphery.	Less	0.8 x	
Net				0.72 x	435
Vacuum Related	Good vacuum must be maintained during handling, launch, etc., or the cathode will be poisoned and electron stream will be obstructed by gas molecules.	Because of low-emissivity requirements, cathode is not generally susceptible to atmospheric poisoning; atmosphere in the plasma		λ = 756 0.2 x	

Table A-2. Impact of TWT and Thruster Design Factors on Failure Rate - Continued

Factor	Impact on TWT	Impact on Thruster	Relative Severity On Thruster Versus TWT	Thruster Failure Rate Impact	Cumulative Failure Rate
		chamber is no problem.			
Net				0.2 x	
FACTORS WITH DIRECT CORRELATION					
Electromagnet and Windings		Because of size, judged 5 x transformer.			60
Baffles, Collars, Plumbing and Other Structural Members					150
Isolators					100
Vaporizers					300
SUBTOTAL					4890
Intangible-Experience		Clogging of parts, Mercury condensation, geometry	More	1.20 x	
Net				1.20 x	1000
Total, Constant λ Period					λ = 5890

2. PROPULSION SUBSYSTEM RELIABILITY ANALYSIS

In accordance with the objectives of this Pioneer Electric Propulsion study, analyses of mission reliability for solar electric propulsion systems of various configurations have been performed. Results of mission reliability analyses presented in this Appendix are applicable to configuration data based on a maximum thruster burn time of 400 days and a maximum mission duration of 550 days. Probability of mission success is presented as a function of nominal mission duration for alternate configurations exploying four, five, and six thrusters, for the nominal case (nominal solar flares, and all thrusters working at the beginning of the mission, and the worst case (worst case solar flare conditions, and one engine out at the beginning of the mission).

2.1 Conclusions

Conclusions formulated from results presented in this Appendix are summarized below. The reliability results are based on mission reliability analyses performed as described in Section 3.2, using a Monte Carlo simulation program.

- For the nominal case (nominal solar flares, all engines working at the beginning of the mission), mission probability of success asymptotically approaches a value close to one (~0.9981) for missions of less than 250 days duration.

- Beyond a 250-day mission duration, mission probability of success decreases rapidly as mission duration approaches maximum thruster burn time. For all configurations studied, the probability of success decreases to zero prior to the 550-day maximum mission time.

- **Beyond a 250-day nominal mission duration, a five thruster configuration provides a higher probability of success than a four thruster configuration, with six thrusters providing a higher probability of success than five.**

- **For a worst case mission of 150 days duration, either a 4, 5, or 6 thruster configuration yields reasonably high reliability, although not as high as the predicted reliability of 0.9981 for each of the nominal cases. The four thruster worst case configuration reliability (.8877) exhibits a rapidly decreasing trend compared to the five thruster and six thruster reliabilities (.9711 and .9745, respectively).**

- The maximum attainable figure of merit for the test program tradeoffs considered is < 0.8845 (the conditional probability of success for a 150-day mission, given that the thruster design life equals 150 days). Figure of merit, interpreted as an interaction between propulsion subsystem reliability and demonstrated test confidence level, is defined as the confidence that the thruster design life exceeds a given value x, times the conditional probability of subsystem success, given that the thruster design life equals x.

- The maximum cost-effective risk reduction is achieved by a test program which provides for testing four thrusters 180 days each. The figure of merit associated with this test program is 0.8786 for a 150-day mission.

2.2 Mission Reliability Estimates

2.2.1 Nominal Case (4, 5, 6 thrusters for various mission durations)

The probability of mission success as a function of nominal mission duration for the nominal case (nominal solar flares, and all thrusters working at the start of the mission) is presented in Figure A-1. Table A-3 is a tabulation of input data used in generating these results. The thruster failure rate of 59×10^{-6} is roughly 20 times the failure rate for a TWT, a device with which the thruster exhibits many engineering commonalities. This assumed failure rate is felt to be highly conservative.

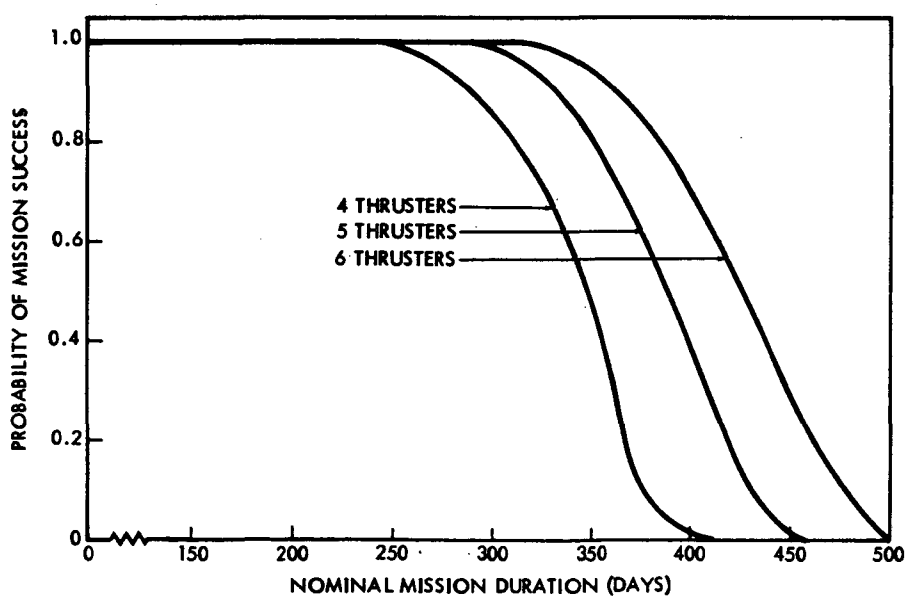

Figure A-1. Probability of Mission Success vs Nominal Mission Duration

Table A-3. Input Data for Propulsion Subsystem Reliability Analysis

Parameter	Program Symbol	Value Used
Failure Rate of Thrusters	L7	59×10^{-6}
Maximum Thruster Burn Time in Days	T7	400
Number Thrusters, Number Power Supplies, Number Required at Start of Mission	M6, N6, M7	4, 4, 4 or 5, 5, 5 or 6, 6, 6
Thruster Startup Probability	P2	0.999
Nominal Mission Duration, Maximum Mission Duration (Days)	T, T5	(0, 500), 550
Maximum Thrust Level, Minimum	A5, G	1.25%, .50%
Power Supply Failure Rate	L9	3.6×10^{-6}
Standby Failure Rate	K1	0.1
Injection Error Adjustment Factor	K2	72
AU Distance Adjustment Factor	K3	.00027
Worst Case or Nominal Case Solar Flare Run	S4	0 or 1
Thruster Out Run or All Operating	E	0 or 1
Power Supplies Cross-Strapped or not Cross-Strapped with Thrusters	F	1
Solar Flare Magnitude Factor	N3	8.76
Coefficient of Fourth Degree Term of Thruster Power Curve Versus Time Equation (For Time Expressed in Days)	J1	9E-11
Coefficient of Third Degree Term of Thruster Power Curve	J2	17E-07
Coefficient of Second Degree Term of Thruster Power Curve	J3	13E-04
Coefficient of First Degree Term of Thruster Power Curve	J4	53E-02
Constant Term of Thruster Power Curve	J5	0.98
Solar Flare Distribution Parameters	D1, D2, D3, D4 P5, P6, P7, P8	1, 2, 4, 8, .2, .4, .2, .2

Separate curves are plotted for propulsion subsystems employing 4, 5, and 6 thruster configurations, and are based on a maximum mission duration of 550 days. It is noted that for missions of less than 250 days duration, the curves are approximately coincidental, with the reliability asymptotically approaching one (~.9981). As the mission duration increases beyond 250 days and approaches the maximum thruster burn time, the reliability decreases rapidly, although slower for a five thruster configuration than for the four thruster case, and slower for the six thruster case than for the five thruster case. For all cases, the reliability has decreased to zero prior to the maximum mission duration.

The analysis technique employed to obtain the results plotted in Figure A-1 uses a computerized Monte Carlo simulation procedure (see attachment for program listing) which accepts as input basic configuration data, mission operational requirements data, and data relating to certain environmental variables which affect operational procedures and probability of success of the mission. Specifically, the assessment techniques include the effects of solar flares, injection errors, and thruster operational flexibility on the mission probability of success. The computer program accepts basic input data relating to the above described variables and simulates a specified number of missions (300 missions was used for the cases run in this analysis), with the precision of the results depending on the number of missions simulated. The basic output data generated from running the program includes mission probability of success versus mission time, and results showing the effect on mission duration of injection errors, solar flares, and failure contingencies. These results can be plotted in various ways, depending on the emphasis desired in their utilization. For example, probability of mission success can be plotted as a function of thruster design life for a fixed mission duration, or as a function of mission duration with the design life held fixed. In this analysis emphasis was given to the probability of success versus mission duration for a fixed thruster design life of 400 days.

2.2.2 Worst Case (4, 5, 6 thrusters for worst case solar flare, one engine out, 150-day mission)

To assess the impact on mission reliability of worst case conditions (worst case solar flares, one engine not working at the beginning of the mission), a reliability analysis was performed based on these conditions, using values of input data in the area of interest. A nominal mission duration of 150 days for four, five, and six thruster configurations was selected as the desired input value. The thruster burn time and the maximum mission duration were held fixed at 400 days and 550 days, respectively, and the computer program was run using built-in input options for worst case conditions.

Results of the worst case mission reliabilities are compared with the nominal case results in Table A-4.

Table A-4. Propulsion Subsystem Reliability (Based on a 150-day mission)

Number Thrusters	Nominal Case	Worst Case
4	0.998	.888
5	0.998	.971
6	0.998	.974

It is concluded that for missions of up to 150 days duration, all three configurations yield an acceptable worst case reliability value, although the four thruster configuration reliability, .8877, indicates that the reliability versus mission duration curve starts to decrease sharply at 150 days, while the five thruster and six thruster configuration reliabilities, 0.9711 and .9745, respectively, appear to be close to the asymptotic value for a worst case condition. The reliability for the corresponding nominal cases, 0.9981, which has approached the asymptotic value, is clearly slightly higher than the worst case asymptotic value.